



**$^1\text{H}$  Magnetic Resonance Spectroscopy of  
 $\gamma$ -Aminobutyric Acid:  
Methodological Development and  
Multimodal Application**

**Mark Mikkelsen**

*A Thesis Submitted to the Senate of Cardiff University  
in Partial Fulfilment of the Requirements for the Degree of  
Doctor of Philosophy*

**School of Psychology  
Cardiff University**

**April 2016**



## *The Wonder Physical*

*It is the light that unveils the soul  
Dispelling darkness of the unknown  
Elevating worlds of the quantum  
That whirl in magic and momentum*

~ ♀ ~



---

## SUMMARY

---

The topic of this doctoral thesis is the magnetic resonance spectroscopy (MRS) of the neurotransmitter  $\gamma$ -aminobutyric acid (GABA). Its scope encompasses areas of MRS of GABA that currently require material methodological improvement and further empirical investigation. Thus, the work presented herein has two overarching objectives. Firstly, to develop MRS of GABA by addressing outstanding methodological limitations of the technique, namely (i) contamination of the GABA signal by signals from macromolecules and (ii) issues regarding the absolute quantification of MRS-measured GABA concentration. Secondly, this thesis describes an investigation of the role of GABA in the haemodynamic response as measured with functional magnetic resonance imaging. This multimodal study both brings together the methodological developments described earlier in the thesis into practical implementation and attempts to address certain unresolved issues with respect to associating GABA concentration with the haemodynamic response.

In Chapter 1, the basic physical principles and methodology of MRS are detailed. In Chapter 2, the neurobiology of GABA and the detection of the GABA signal by MRS are discussed. A new method for absolutely quantifying GABA in volumes composed of heterogeneous brain tissue compartments is introduced and validated in Chapter 3. This is followed by an investigation of how much error is introduced into the absolute quantification of GABA from tissue segmentation procedures in Chapter 4. In Chapter 5, the repeatability of MRS of GABA with and without contamination from macromolecules is assessed. Chapter 6 describes the multimodal study of the role of GABA in the saturation of the haemodynamic response through so-called haemodynamic contrast tuning with the use of a graded visual contrast stimulus. Numerical simulations of the editing efficiency of and the impact of frequency drift on MRS of GABA with and without macromolecule signal suppression are then presented in Chapter 7. Finally, in Chapter 8, this thesis concludes with a general discussion of the empirical findings of the research described in the earlier chapters and a commentary on the current and future advances of MRS of GABA in addition to what inferences can be appropriately made when using measures of GABA concentration.





---

## ACKNOWLEDGEMENTS

---

Both the scientific content and the mental, physical and emotional labour that was poured into the work presented in this doctoral thesis would not have been possible without the continuous guidance and support of the following individuals. I wish to extend my eternal gratitude and immense thanks to each and every one of you for having helped me achieve the greatest personal accomplishment of my life.

To my doctoral supervisors Prof. Krish Singh, Prof. Petroc Sumner and Dr. John Evans—this thesis, and the science it describes, just would not have been possible without you, simple as that.

Krish, I would like to thank you for your role as “captain at the helm”. I am indebted to your wise direction and invaluable supervision. Your wealth of years pushing neuroimaging forward has granted this work the opportunity to place it amongst the repertoire of high-calibre NMR research.

Petroc, your steering towards a rigorous approach to statistical analysis has given me a fresh outlook of what modern science should be. My philosophy and approach toward doing good research have definitely changed for the better because of you.

John, you have truly instilled in me the laudable characteristics of an MR physicist. Speaking from the perspective of someone who began his career in science as a psychologist, I would not have been able to complete such methodologically rigorous research into NMR spectroscopy without you. Only now at the end have I realised just how much physics I have come to understand! This is how you have made my PhD both intellectually satisfying and, just as importantly, downright fun! I have no doubt whatsoever that your inimitable tuition and practical guidance will stay with me for the rest of my professional life.

To Jemma Sedgmond—although I have never told you this, you have been my anchor, the one person who I have relied upon, overtly or otherwise, for companionship, for laughter and for well-being. With you I have been able to just be myself—quirks, cracks and all! Thank you so much for putting up with all my complaining about getting this thesis written up. And most importantly of all, you were instrumental in finally allowing me to bring some long overdue Light to my

Darkness. You are my best friend, my sister, my blood. And you have my love forevermore.

To Claire Hanley, my sister-in-arms and fellow metalhead—we each had our own mountains to climb but we got there in the end, making our first firm steps into what I hope will be long and prolific academic careers. I am so proud to call you my friend and colleague. There ain't no stopping the GABAndwagon! Horns up!

To Dr. Jessica Steventon—I can say quite confidently that I have looked up to you as a role model throughout my PhD. I esteem you highly for your sharp mind and for your natural attributes of a leader. All the after-hours chats about matters both academic and personal did me a world of good. (I still find it amusing that we never really spoke in my first year...and we even sat next to each other...). You supported me both motivationally and emotionally in such a way that I will forever remain in your debt. I make the promise to always repay you in kind.

To Dr. Esther Warnert, my General—your no-nonsense attitude and uplifting humour really got me through the hard times. You kept me grounded, helping me keep the big picture in frame. Thank you also for your expertise in all things vascular! Your soldier will continue to follow your example as a top-class scientist and all-around excellent human being.

To Hannah Furby—thank you for being you! I very much will miss having you sat across from me, sharing in a giggle or three. Perhaps more than you will ever know just your being there brought a little sunflower-sunshine to my otherwise MATLAB-filled days. I will do my level best to always remember that “life is like a bagel: holy and circular”. You are truly a remarkable, one-of-a-kind person, with a spirit that lights up even the darkest night. So shine on evermore, Star.

And to all my officemates in the Analysis Room, past and present—these three-and-a-bit years that I have shared with you have been an utter joy, though difficult at times they may have been. I will keep with me till the end of my days the many happy memories.

There are also a number of scientists whose contribution to this thesis, in one form or another, is deserving of acknowledgement. Dr. Kevin Murphy (Cardiff University), Dr. Molly Bright (University of Nottingham) and Dr. Alan Stone (University of Oxford)—thanks go to you for sharing your knowledge about, your

analysis scripts for and your advice on a multitude of topics and projects (even those that never made it into this thesis!). Dr. Jamie Near (McGill University)—thank you for providing your expertise on numerical simulations and for your wonderful FID-A toolkit. Dr. Richard Edden (Johns Hopkins University)—if Gannet had not been around when I started this PhD I have no idea how much harder the analysis side of things would have been(!), so thank you for the software and for your help received with it. To all of you—I have valued and will continue to value your collaboration in my scientific endeavours.

Finally, to my family and all my friends, who are far too numerous to thank individually—a resounding THANK YOU! You all played a part in my reaching this point. So let the good times roll; it only gets better from here!

*Bloodied yet unbowed.*

M. M.



# Contents

<b>Abbreviations and Symbols .....</b>	<b>xvii</b>
<b>Preface .....</b>	<b>xxi</b>
<b>1. <sup>1</sup>H Magnetic Resonance Spectroscopy: Principles and Methods.....</b>	<b>1</b>
1.1 Summary .....	1
1.2 Basic Principles .....	2
1.2.1 Nuclear Magnetic Resonance.....	2
1.2.2 Magnetic Resonance Spectroscopy.....	11
1.3 Data Acquisition.....	17
1.3.1 Free Induction Decay and Fourier Transform NMR .....	18
1.3.2 Techniques and Pulse Sequences .....	20
1.3.3 <i>B</i> <sub>0</sub> Field Homogeneity .....	25
1.3.4 Chemical Shift Displacement.....	26
1.3.5 Water Suppression .....	27
1.3.6 Outer Volume Suppression .....	28
1.4 Data Processing .....	29
1.4.1 Apodization.....	29
1.4.2 Zero Filling .....	31
1.4.3 Residual Water Filtering .....	32
1.4.4 Phase and Frequency Correction.....	32
1.5 Quantification.....	35
1.5.1 Brain Metabolites .....	35
1.5.2 Basic Principles of Quantification .....	37
1.5.3 Prior Knowledge .....	42
<b>2. <math>\gamma</math>-Aminobutyric Acid: From Neurobiology to Applications in <sup>1</sup>H MRS.....</b>	<b>45</b>
2.1 Summary .....	45
2.2 Neurobiology and Neurophysiology .....	46
2.2.1 GABA: Neurotransmitter, Metabolite and More .....	46
2.2.2 GABAergic Inhibition.....	49
2.3 Magnetic Resonance Spectroscopy of GABA .....	53
2.3.1 The GABA Spin System.....	53

2.3.2	Detection of the GABA Signal .....	55
2.4	Applications and Correlates: A Concise Review .....	61
2.4.1	Clinical Applications .....	62
2.4.2	Correlates with Cognition and Behaviour.....	67
2.4.3	Haemodynamics.....	69
2.4.4	Pharmacology .....	69
<b>3.</b>	<b>Absolute Quantification of GABA in Spectroscopic Volumes Composed of Heterogeneous Tissue Compartments.....</b>	<b>73</b>
3.1	Abstract .....	73
3.2	Introduction .....	74
3.3	Theory .....	76
3.4	Methods.....	80
3.4.1	Estimation of GABA in GM and WM.....	80
3.4.2	Sensitivity Analysis .....	80
3.4.3	Empirical Validation.....	82
3.5	Results .....	84
3.6	Discussion .....	87
3.7	Conclusions .....	91
<b>4.</b>	<b>Contribution of Error from Tissue Segmentation to the Absolute Quantification of GABA Concentration.....</b>	<b>93</b>
4.1	Abstract .....	93
4.2	Introduction .....	94
4.3	Theory and Methods.....	94
4.3.1	Tissue Water Correction in Absolute Quantification.....	94
4.3.2	Estimation of Error .....	96
4.4	Results and Discussion.....	98
4.5	Conclusions .....	102
<b>5.</b>	<b>Comparison of the Repeatability of GABA-Edited MRS with and without MM Suppression.....</b>	<b>103</b>
5.1	Abstract .....	103
5.2	Introduction .....	104
5.3	Methods.....	104
5.3.1	Phantom Experiments .....	104
5.3.2	In Vivo Experiments .....	105

5.3.3	MRS Analysis .....	107
5.3.4	Statistical Analysis .....	107
5.4	Results .....	108
5.4.1	Phantom Experiments .....	108
5.4.2	In Vivo Experiments .....	109
5.5	Discussion .....	112
5.6	Conclusions .....	116
<b>6.</b>	<b>Endogenous GABA Concentration and Individual Differences in Haemodynamic Contrast Tuning .....</b>	<b>117</b>
6.1	Abstract .....	117
6.2	Introduction .....	118
6.3	Methods .....	120
6.3.1	Participants .....	120
6.3.2	Visual Paradigm .....	120
6.3.3	Imaging Protocol .....	121
6.3.4	MR Analysis .....	122
6.3.5	Contrast Response Function .....	124
6.3.6	Statistical Analysis .....	125
6.4	Results .....	126
6.5	Discussion .....	131
6.6	Conclusions .....	135
<b>7.</b>	<b>Numerical Simulations of GABA-Editing Efficiency and the Impact of Frequency Drift .....</b>	<b>137</b>
7.1	Abstract .....	137
7.2	Introduction .....	138
7.3	Methods .....	140
7.3.1	Simulations .....	140
7.3.2	Phantom Experiments .....	141
7.4	Results .....	141
7.4.1	Effect on Spectral Lineshape .....	141
7.4.2	Editing Efficiency .....	143
7.4.3	Impact of Frequency Drift .....	145
7.5	Discussion .....	148
7.6	Conclusions .....	152

<b>8. General Discussion.....</b>	<b>153</b>
8.1 Summary of Findings .....	153
8.2 <sup>1</sup> H MRS of GABA: The Current and Future State of the Art .....	154
8.3 GABA Concentration as a Correlate: How Much Can Really Be Inferred? 156	
8.4 Closing Remarks .....	158
<b>References.....</b>	<b>161</b>
<b>Appendix A: Supplementary Material .....</b>	<b>193</b>
<b>Appendix B: Product Operator Formalism .....</b>	<b>197</b>
<b>Appendix C: Published Work .....</b>	<b>201</b>

# Abbreviations and Symbols

<b>Abbreviation</b>	<b>Description</b>
AC	Anterior cingulate
AFNI	Analysis of Functional NeuroImages
BET	Brain Extraction Tool
BOLD	Blood oxygenation level dependent
CBF	Cerebral blood flow
CI	Confidence interval
CSD	Chemical shift displacement
CSF	Cerebrospinal fluid
CSI	Chemical shift imaging
CV	Coefficient of variation
CV <sub>bs</sub>	Between-subject coefficient of variation
CV <sub>ws</sub>	Within-subject coefficient of variation
DIFF	The difference between the ON and OFF MEGA-PRESS scans
DLPFC	Dorsolateral prefrontal cortex
FAST	FMRIB's Automated Segmentation Tool
FID	Free induction decay
fMRI	Functional magnetic resonance imaging
FOV	Field of view
FSL	FMRIB Software Library
FSPGR	Fast spoiled gradient echo
FT	Fourier transform
FWHM	Full width at half maximum
GABA	$\gamma$ -Aminobutyric acid
GABA'	Macromolecule-suppressed $\gamma$ -aminobutyric acid
GABA+MM	Macromolecule-contaminated $\gamma$ -aminobutyric acid
GABA'+MM	Macromolecule-contaminated $\gamma$ -aminobutyric acid
GABA-T	GABA transaminase
GAD	Glutamate decarboxylase
GAT	GABA transporter

GLM	General linear model
Gln	Glutamine
Glu	Glutamate
Glx	Glutamate + glutamine
GM	Grey matter
ICC	Intraclass correlation coefficient
i.u.	Institutional units
MEGA-PRESS	Mescher-Garwood point resolved spectroscopy
MM	Macromolecule(s); macromolecular
mM	Millimolar
MNI	Montreal Neurological Institute
MR	Magnetic resonance
MRI	Magnetic resonance imaging
MRS	Magnetic resonance spectroscopy
MRSI	Magnetic resonance spectroscopy imaging
NMR	Nuclear magnetic resonance
OCC	Occipital lobe
OFF	The spectral editing MEGA-PRESS experiment where 180° frequency-selective refocusing RF pulses do not refocus the scalar evolution of <i>J</i> -coupled resonances
ON	The spectral editing MEGA-PRESS experiment where 180° frequency-selective refocusing RF pulses refocus the scalar evolution of <i>J</i> -coupled resonances
OVS	Outer volume suppression
ppm	Parts per million
PRESS	Point resolved spectroscopy
PSF	Point spread function
RF	Radiofrequency
ROI	Region of interest
SM	Sensorimotor
SNR	Signal-to-noise ratio
SPM	Statistical Parametric Mapping
SVS	Single voxel spectroscopy
T	Tesla

TCA	Tricarboxylic acid
TE	Echo time
TI	Inversion time
TR	Repetition time
VOI	Volume of interest
WM	White matter

<b>Symbol</b>	<b>Description</b>
$B_0$	External magnetic field (T)
$B_{10}, B_{01}$	Default Bayes factor
$B_1$	Magnetic radiofrequency field (T or $\mu\text{T}$ )
$\text{CH}_2$	Methylene
$f_0$	Larmor frequency (Hz)
$f_A$	Frequency of sample nucleus A (Hz)
$f_{\text{CSF}}$	Fractional voxel volume of CSF
$f_{\text{GM}}$	Fractional voxel volume of GM
$f_{\text{WM}}$	Fractional voxel volume of WM
$G_x, G_y, G_z$	Magnetic field gradients in the x, y and z directions
$\text{H}_2\text{O}$	Water
$J$	Scalar coupling constant (Hz)
$M$	Macroscopic magnetisation
$M_0$	Equilibrium magnetisation
$M_x, M_y, M_z$	Orthogonal magnetisation components
$M_{\text{GM}}$	Basis metabolite concentration in grey matter
$M_{\text{WM}}$	Basis metabolite concentration in white matter
$r_{\text{M}}$	Ratio of intrinsic GABA concentration in GM and WM
$R$	Time-bandwidth product for an RF pulse ( $T\Delta f$ )
$R^2$	Coefficient of determination
$R_{\text{max}}$	Modelled response at maximum contrast
$t_{\text{GM}}$	Fractional GM volume per unit tissue
$S$	Time-domain signal (ms)
$T$	RF pulse duration (ms)
$T_1$	Longitudinal relaxation time (ms or s)
$T_2$	Transverse relaxation time (ms or s)

$s$	Scale factor of the Cauchy distribution of a continuous mixture of normals
$\delta$	Chemical shift (ppm)
$\Delta f$	Spectral resolution (Hz)
$\Delta f_{\text{edit}}$	Frequency bandwidth of an RF editing pulse (Hz)
$\Delta\omega$	Frequency offset or rotational frequency ( $\text{rad s}^{-1}$ )
$\epsilon_{\text{fit}}$	Fit error (%)
$\gamma$	Gyromagnetic ratio ( $\text{rad T}^{-1} \text{s}^{-1}$ )
$\gamma$	Response saturation rate
$\sigma$	Magnetic shielding constant
$\sigma$	Signal noise
$\sigma^2$	Variance
$\tau$	Echo time (ms)
$\tau_n$	RF pulse timing (ms)
$\omega$	Frequency of sample compound ( $\text{rad s}^{-1}$ )
$\omega_0$	Larmor frequency ( $\text{rad s}^{-1}$ )
$\phi$	Phase (rad)
[ ]	Concentration (i.u., mM, $\text{mmol L}^{-1}$ or $\mu\text{mol g}^{-1}$ )

# Preface

Magnetic resonance imaging (MRI) as it is known today has come a long way since its beginnings in the 1970s. It may go without saying that its application in both medicine and neuroscience has truly revolutionised both fields. This doctoral thesis focuses on one particular modality of magnetic resonance, that of  $^1\text{H}$  magnetic resonance spectroscopy (MRS). Although historically older than MRI, MRS has not attained the same level of popularity as MRI. Consequently, there is at present a pressing need for methodological development and optimisation of this imaging technique.

Ever since its advent MRS has provided invaluable insight into the molecular workings of living systems. As a technique that is based on the physical principles of nuclear magnetic resonance, MRS detects the signals that arise from specific molecules when they are placed in a strong magnetic field and perturbed by radiofrequencies. Since the electromagnetic radiation of radiofrequencies does not harm living tissue, MRS has found a strong footing in basic and clinical neuroimaging. To this day it continues to be unmatched in its ability to noninvasively probe the signatures of chemicals in the living human brain.

More recently, MRS has been increasingly employed as a tool to measure the biochemical concentration of the major inhibitory neurotransmitter  $\gamma$ -aminobutyric acid (GABA). GABA is one of the most important neurochemicals, playing an integral part in a multitude of functions in the brain. In the last few years it has become apparent that MRS is the neuroimaging modality of choice for *in vivo* investigations of GABA and its role in behaviour, cognition, neurophysiology, neuropsychiatric disorder and neurological pathology, so much so that its methodological improvement and optimal application have become strongly active areas of research.

The work presented in this doctoral thesis consists of several theoretical investigations, experimental studies and simulations aimed at advancing the methodology of the MRS of GABA. In particular, attempts were made to address outstanding methodological issues concerning the absolute quantification of GABA concentration as well as the significant problem of contamination by macromolecules in the GABA signal. On the whole, much of the work in this thesis

was geared towards dealing with this latter problem. The methodological developments were then incorporated into a multimodal imaging study that investigated how GABA is associated with neurovascular signals measured by functional magnetic resonance imaging (fMRI).

# **1. $^1\text{H}$ Magnetic Resonance Spectroscopy: Principles and Methods\***

## **1.1 Summary**

In this introductory chapter, an overview of  $^1\text{H}$  MRS is presented. First, the basic physical principles of this imaging technique are described, starting with the phenomenon of nuclear magnetic resonance (NMR) and moving towards principles relevant to MRS. From here the chapter continues onto the techniques, acquisition sequences and protocols by which the MRS signal is optimally detected. The standard data processing steps that are taken to unambiguously resolve NMR resonances of interest are then discussed. This chapter concludes with a discussion of the theoretical principles and general methodologies of signal quantification.

---

\* The content in this chapter is based on various printed and electronic sources, including de Graaf (2007), de Graaf and Rothman (2001) and many other scientific articles.

## 1.2 Basic Principles

### 1.2.1 Nuclear Magnetic Resonance

Since its discovery by Isidor Isaac Rabi (1937), the phenomenon of NMR has forever changed the state of imaging science. Subsequent pioneering work by scientists such as Edward Mills Purcell (1946), Felix Bloch (1946), Paul Lauterbur (1973) and Peter Mansfield (1973) vastly extended the application of NMR in both physics and medicine. Indeed, the application of NMR, and later of magnetic resonance imaging (MRI), in the basic and clinical sciences has provided incomparable insight into the natural world. This has made NMR one of the most important discoveries and MRI one of the most important inventions in modern science. At its basic core, NMR can be summarised as the scientific study of the magnetic and energetic properties of atomic nuclei (de Graaf, 2007). The frequencies that are studied lie within the radiofrequency (RF) range of 10–800 MHz. Since the energy changes that occur when nuclei are perturbed by magnetic fields do not involve ionising radiation, NMR has been extremely useful for medicine, in particular diagnostic medicine. In the same fashion, its use in the neurosciences has propelled human understanding of the brain considerably, including how it is structured, how it functions and how it is disrupted by pathologies and disorders. This chapter first begins by laying out the basic physical principles of NMR, after which certain principles of NMR highly relevant to MRS are considered.

#### 1.2.1.1 Larmor precession

In classical physics, atomic nuclei can be described as having an angular momentum  $L$ , which is dependent on their mass and velocity of rotation about a fixed point in space. Rotating nuclei are also associated with a given electrical charge that gives rise to a current loop, and consequently a magnetic field. The magnetic field can be quantified by measuring the magnetic dipole moment  $\mu$ , which has magnitude and direction. The angular momentum and magnetic moment of a given nucleus are intrinsically related, summarised as

$$\mu = \gamma L \quad [1.1]$$

where  $\gamma$  is the gyromagnetic ratio: the relation between an object's magnetic moment and its angular momentum. When placed in an external magnetic field  $B_0$ , the magnetic moment will alter its orientation according to the differential equation

$$\frac{d\mu}{dt} = \gamma\mu \times B_0 \quad [1.2]$$

As the magnetic moment is constant, Eq. [1.2] shows that  $\mu$  rotates about  $B_0$  over time  $t$ . This can also be described as follows:

$$\frac{d\mu}{dt} = \mu \times \omega_0 \quad [1.3]$$

This is known as the Larmor precession of nuclei (named after the physicist and mathematician Joseph Larmor). Combining Eqs. [1.2] and [1.3] gives the well-known Larmor equation:

$$\omega_0 = \gamma B_0 \quad [1.4]$$

where  $\omega_0$  is the angular precessional frequency, or more commonly, the Larmor frequency of an atomic nucleus (in  $\text{rad s}^{-1}$ ), which is proportional to  $B_0$ , the strength of the external magnetic field (in T). The gyromagnetic ratio  $\gamma$  is expressed in  $\text{rad T}^{-1} \text{s}^{-1}$ . For  $^1\text{H}$  protons,  $\gamma$  is  $26.752 \times 10^7 \text{ rad T}^{-1} \text{ s}^{-1}$ . However, it is conventional to express the Larmor frequency in  $\text{MHz T}^{-1}$ . Eq. [1.4] can then be rewritten giving

$$f_0 = \frac{\gamma}{2\pi} B_0 \quad [1.5]$$

The gyromagnetic ratio of  $^1\text{H}$  protons by this convention equals  $42.57 \text{ MHz T}^{-1}$ . Larmor precession is the fundamental physical basis of NMR.

### 1.2.1.2 Quantum mechanical description

The classical description of the precession of atomic nuclei as mathematically represented in Eq. [1.4] is useful for understanding the relation between angular momentum, magnetic moment and the Larmor frequency. However, to fully understand the origin of the NMR signal with respect to spectroscopy it is necessary to provide a quantum mechanical description of NMR.

Through quantization of the elementary particles involved in spin precession (i.e.,  $^1\text{H}$  protons), it is shown that, firstly, the amplitude of angular momentum  $L$  is limited to discrete values according to

$$L = \left(\frac{h}{2\pi}\right) \sqrt{I(I+1)} \quad [1.6]$$

where  $h$  is Planck's constant and  $I$  is the spin quantum number, which can only be integral or half-integral. Hydrogen nuclei have a spin quantum number of  $1/2$ . Secondly, the direction of the angular momentum is characterised by the magnetic quantum number  $m$ , which is also limited to discrete values. This is given by

$$L = \left(\frac{h}{2\pi}\right) m \quad [1.7]$$

where  $m$  can have  $2I + 1$  values, such that

$$m = I, I - 1, I - 2, \dots, -I \quad [1.8]$$

As in classical physics, in quantum mechanics the angular momentum is directly proportional to the magnetic moment, as defined by the gyromagnetic ratio. For a given discrete orientation (e.g., along the longitudinal axis  $z$ ), the quantized magnetic moment is given by

$$\mu_z = \gamma \left( \frac{h}{2\pi} \right) m \quad [1.9]$$

When elementary particles are placed in an external magnetic field, they acquire magnetic energy  $E$ . In the context of the quantum mechanical description of NMR, the associated energy of atomic nuclei is given by

$$E = -\mu_z B_0 = -\gamma \left( \frac{h}{2\pi} \right) m B_0 \quad [1.10]$$

As described previously, the number of values ascribed to an elementary particle's magnetic quantum number is  $2I + 1$ . This means <sup>1</sup>H nuclei only have two energy levels, equal to  $-1/2$  and  $+1/2$ . The difference between energy levels can then be formulated as follows:

$$\Delta E = \gamma \left( \frac{h}{2\pi} \right) B_0 \quad [1.11]$$

Nuclear transitions between energy levels are caused by the absorption or emission of radiation with energy  $\Delta E$ . Thus, this gives the fundamental quantum mechanical basis for NMR spectroscopy, expressed as

$$\Delta E = hf_0 \quad [1.12]$$

Eq. [1.12] is known as Bohr's frequency condition and states that the frequency of emitted radiation  $f_0$  is equal to the difference in energy levels divided by  $h$ . Finally, it can be seen that by combining Eqs. [1.11] and [1.12] the Larmor equation is once again derived:

$$f_0 = \frac{\gamma}{2\pi} B_0 \quad [1.13]$$

The quantum mechanical description of NMR is the only way to fully understand the origin and physical manifestation of NMR spectroscopy, and describes the basis of certain spectral characteristics described later in this chapter.

This image is copyrighted. It can be found at its original source.

**Figure 1.1** *a: Larmor precession of the magnetic moment  $\mu$  of an atomic nucleus in an external magnetic field  $B_0$  in the non-rotating laboratory frame of reference. The amplitude ( $\mu_z$ ) and orientation of rotation ( $\theta$ ) are quantized. b: Rotating frequency frame of reference displaying the quantized magnetic moments of 1/2-spin hydrogen nuclei precessing parallel ( $\alpha$ ) or antiparallel ( $\beta$ ) to  $B_0$ . Reproduced from de Graaf (2007).*

### 1.2.1.3 Macroscopic magnetisation and $B_1$ excitation

The Larmor precession of  $^1\text{H}$  protons is classically illustrated with a schematic of the so-called non-rotating laboratory frame of reference (Figure 1.1a). This succinctly describes spin precession for a single magnetic moment. However, in actuality the NMR signal arises from the sum of all detected magnetic moments. The difference in energy levels for atomic nuclei as described in Eq. [1.12] means that the spins will have different spin states. The two spin states for  $^1\text{H}$  nuclei ( $m = +1/2$  and  $m = -1/2$ ) lead to magnetic moments being either parallel or antiparallel with  $B_0$ . These are respectively called the  $\alpha$  and  $\beta$  spin states. The quantized magnetic moments parallel or antiparallel with  $B_0$  are represented in Figure 1.1b, using the rotating frequency frame of reference. Moreover, the small difference in energy levels of the atomic nuclei leads to a slightly larger population of spins in the lower energy (parallel)  $\alpha$  state than in the higher energy (antiparallel)  $\beta$  state.

The net magnetic moment, or the macroscopic magnetisation  $M$ , will be equal to the sum of all individual magnetic moments  $\mu_z$  in the macroscopic sample. At thermal equilibrium there is no phase coherence of spins (in the xy plane) leading to a net macroscopic magnetisation  $M$  along the longitudinal direction of the rotating frame. Phase ( $\phi$ ) refers to the orientation of spins (in rad) in the xy plane of the frame, while coherence refers to a uniform orientation that is parallel to a given vector in this plane. The population difference in  $\alpha$  and  $\beta$  spins means that the net component of  $M$  will be parallel with  $B_0$  along the +z axis (denoted  $M_z$ ). There is therefore no

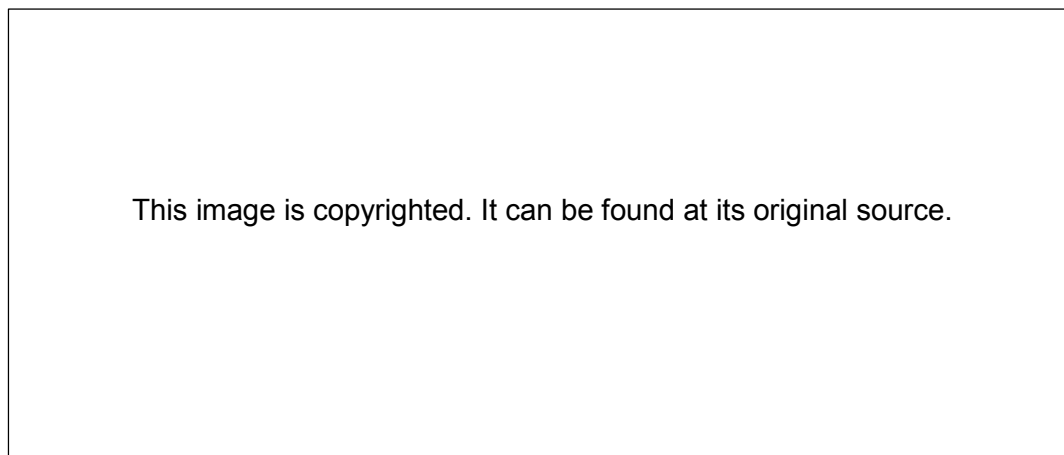


**Figure 1.2** *Transverse excitation of nuclear spins in the rotating frequency frame of reference. a: At thermal equilibrium the spins are randomly distributed about the z axis. On the macroscopic scale this leads to a net magnetisation along +z. That is, the longitudinal magnetisation component  $M_z$  is equal to the magnetisation at thermal equilibrium ( $M_0$ ). b: When a second magnetic field ( $B_1$ ) is applied in form of an RF pulse along  $-x$ , the spins begin to orient towards  $+y$ . The transverse magnetisation component  $M_y$  then begins to increase in amplitude as  $M_z$  proportionally decreases. c: If the  $B_1$  field is appropriately calibrated and applied for long enough the nuclear spins will achieve complete coherence along  $+y$ . This achieves complete transverse magnetisation on the macroscopic scale where  $M_y$  is maximal and  $M_z$  is nulled. Reproduced from de Graaf (2007).*

net magnetisation along the transverse plane. The magnitude of the longitudinal magnetisation at thermal equilibrium ( $M_0$ ) is given by

$$M_0 = \sum_{i=1}^n \mu_i = n_\alpha \mu_z + n_\beta \mu_z = \gamma \left( \frac{h}{4\pi} \right) (n_\alpha - n_\beta) \quad [1.14]$$

where  $n_\alpha$  is the number of spins parallel to  $B_0$  and  $n_\beta$  is the number of spins antiparallel to  $B_0$ .

In order to detect the NMR signal, the magnetisation must be transferred to the transverse plane. This is achieved by applying RF energy at the resonant frequency of nuclear spins. This is termed  $B_1$ . In NMR, the applied  $B_1$  energy is generated by an oscillating RF pulse defined as  $B_{1\max} \cos(\omega t)$ , where  $B_{1\max}$  is the amplitude of the pulse,  $\omega$  is the resonant frequency (from the Larmor equation) and  $t$  is the length of time the pulse is turned on. When the RF pulse is applied the nuclear spins will precess about both the static  $B_0$  field and the irradiating  $B_1$  field. When the frequency of the  $B_1$  pulse is equal to Larmor frequency  $\omega_0$  and the pulse is applied along  $-x$  for a sufficient length of time, the spins will attain phase coherence (i.e., the spins will be non-randomly distributed in the rotating frame) and the net magnetisation is rotated onto the transverse plane along the vector  $+y$  (Figure 1.2). The net magnetisation component is now denoted  $M_y$ . This excitation of  $M_0$  will generate an electromotive force that is detected by RF receiver coils placed parallel

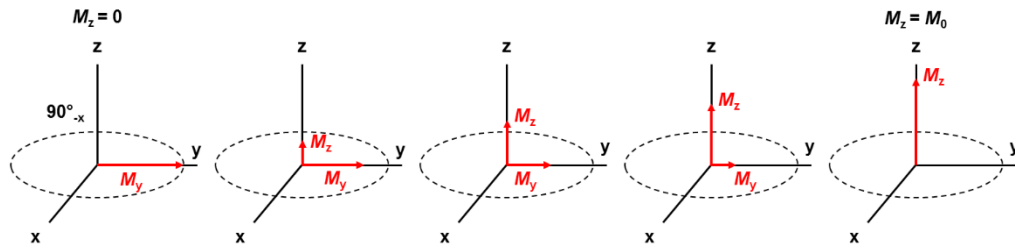


**Figure 1.3** Longitudinal (or spin–lattice) relaxation of macroscopic magnetisation. Following excitation by the  $B_1$  field the longitudinal magnetisation returns to thermal equilibrium in an exponential manner.

to the transverse plane in the MRI scanner. This is then processed by the MR hardware into an interpretable signal (see Sections 1.3 and 1.4).

### 1.2.1.4 Longitudinal and transverse relaxation

Excitation of the magnetisation of nuclear spins by an applied  $B_1$  field is not a static process; once the  $B_1$  field is no longer applied (i.e., the RF pulse is switched off), the spins will over time return to the net macroscopic magnetisation vector  $M_0$ . This phenomenon has two characteristics with respect to  $M$ : a return of the net magnetisation to the longitudinal axis  $+z$  and the dephasing of spin coherences in the  $xy$  plane. These are respectively denoted longitudinal relaxation and transverse relaxation.

As explained previously, to detect the NMR signal nuclear spins must be rotated onto the transverse plane. In a simple pulse-acquire experiment the  $B_1$  magnetic field is applied in the form of a  $90^\circ$  excitation pulse—that is, the  $B_1$  field is calibrated such that the spins are rotated perpendicularly to  $B_0$ . Once the pulse is switched off the longitudinal magnetisation component  $M_z$  begins to return to  $M_0$  (Figure 1.3). This occurs because the energy from the excited spins is lost to the surrounding environment, the so-called “lattice”, eventually returning the magnetisation to thermal equilibrium. Thus, longitudinal relaxation is also called spin–lattice relaxation. The rate of this recovery is defined as

$$M_z(t) = M_0(1 - e^{-t/T_1}) \quad [1.15]$$

where  $T_1$  is a constant denoting the longitudinal relaxation time of the nuclear spins, or in other words, the length of time it takes for the transversely magnetised spins to return to thermal equilibrium. When considering a pulse-acquire experiment that is

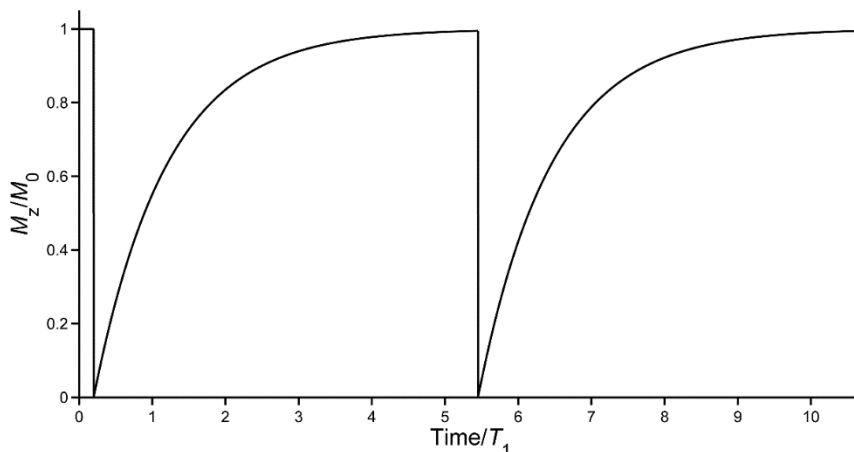


**Figure 1.4** Illustration of  $T_1$  relaxation following transverse excitation by a  $90^\circ$   $B_1$  pulse in a repeated pulse-acquire acquisition. After complete transverse magnetisation  $M_z$  is reduced to zero, which then exponentially recovers over time  $TR$  at rate equal to  $1/T_1$ , where  $T_1$  is the relaxation time constant. When  $TR > 5T_1$ , the signal per unit of time is optimal and saturation of the longitudinal magnetisation is avoided.

repeated (as shown in Figure 1.4), enough time must be given before the next acquisition to prevent saturation of the longitudinal magnetisation. Here,  $TR$  is the time to the repetition of the excitation pulse. For a  $90^\circ$  excitation RF pulse,  $TR$  is optimal when  $TR > 5T_1$ . Should it be desired that the  $TR$  be shortened, the flip angle of the excitation pulse must also be reduced to obtain sufficient signal per unit of time. The optimal flip angle is equal to

$$\alpha_{opt} = \cos^{-1}(e^{-TR/T_1}) \quad [1.16]$$

where  $\alpha_{opt}$  is the optimal flip angle (called the Ernst angle) required to obtain maximum signal per unit of time in the acquisition. Using Eq. [1.16] one can show that a  $90^\circ$  excitation pulse is the optimum flip angle for transverse magnetisation when the  $TR$  is five times the  $T_1$  time constant.

After ideal transverse magnetisation is achieved by  $B_1$  excitation, the phase of spins that were previously coherent begin to decohere. Simply put, the net phase of spins in the transverse plane begins to become random until the transverse magnetisation has completely dissipated. This arises from the fact that the spins exchange energy with each other through a process of entropy as dictated by the laws of thermodynamics. Transverse relaxation is therefore also called spin-spin relaxation. The rate of decay can be calculated as

$$M_{xy}(t) = M_{xy}(0)e^{-t/T_2} \quad [1.17]$$

where  $T_2$  is a constant denoting the transverse relaxation time of the nuclear spins, or in other words, the length of time it takes for coherent spins to fully decohere. It

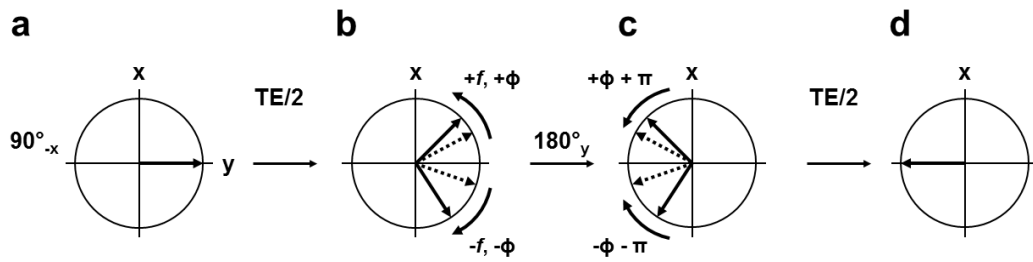


**Figure 1.5** Vector diagram of the evolution of phase coherences in the spin echo experiment. **a:** The spins are completely in-phase and aligned along the +y vector following excitation by a 90° excitation pulse along -x. **b:** The spins will begin to lose their phase coherence during the first time delay of the echo time (TE) as a result of intrinsic  $T_2$  relaxation and  $B_0$  inhomogeneity that causes shifts in the nominal Larmor frequency of the spins. **c:** A second 180° pulse is applied at time TE/2, which inverts the spins along the y axis such that their phase is reset. **d:** After a second delay TE/2 the spins regain phase coherence at the top of the spin echo at time TE. Note that the signal will have decayed because of  $T_2$  relaxation.

is possible to measure  $T_2$  by modifying the pulse-acquire sequence. After the initial 90° excitation pulse the spins begin to lose coherence. In the rotating frame this is visualised as the magnetic moments of all spins randomly deviating away from +y (if the  $B_1$  field was set perpendicularly along -x). Using a vector diagram to illustrate this effect shows that some spins will precess slightly faster than the Larmor frequency, while others will precess slightly slower (Figure 1.5). These differences in precessional frequency will lead to the spins having vectors with different phases. By applying a second RF pulse that rotates the spins through a 180° inversion (a “180° pulse”) after a delay equal to TE/2, the phase of the spins is changed, such that  $\phi \rightarrow \phi + \pi$ . After a second period equal to TE/2 the spins will now refocus. This leads to what is termed a spin echo than is detected by RF receiver coils. The interval between the onset of excitation and the top of the spin echo is called the echo time (TE). Performing multiple experiments at various echo times shows that the transverse magnetisation  $M_{xy}$  decays exponentially according to Eq. [1.17] (Figure 1.6).

Transverse relaxation originates from two sources of dephasing: the intrinsic  $T_2$  relaxation of spins and the additional dephasing caused by spatial inhomogeneities in the  $B_0$  magnetic field. For the latter, differences in  $B_0$  throughout a sample will lead to spins precessing at different frequencies (as dictated by the Larmor equation), leading to the spins having different phases. This difference in phase contributes to the decay in transverse magnetisation. Thus, the observed rate of transverse relaxation is equal to

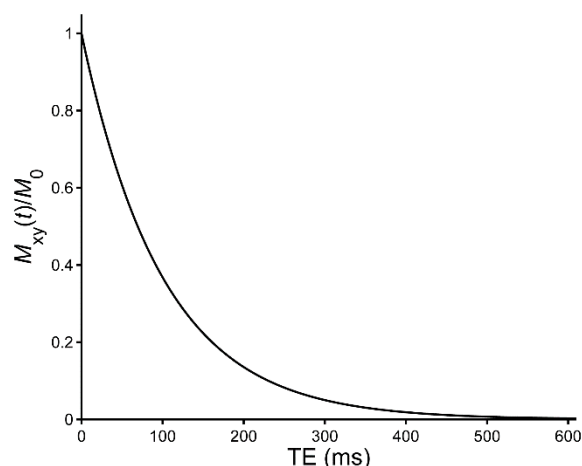


**Figure 1.6** Exponential decay of transverse magnetisation ( $M_{xy}$ ) as a function of echo time (TE). In this example the  $T_2$  relaxation time is 100 ms.

$$\frac{1}{T_2^*} = \frac{1}{T_2} + \frac{1}{T_2'} \quad [1.18]$$

where  $T_2^*$  is the observed relaxation time,  $T_2$  is the intrinsic relaxation time and  $T_2'$  is the relaxation time of nuclear spins ascribed to  $B_0$  inhomogeneity. Whereas  $T_2$  is a random process arising from the laws of thermodynamics,  $T_2'$  is dependent on the external magnetic field such that  $1/T_2' = \gamma\Delta B_0(r)$ , where  $\Delta B_0(r)$  is the difference between the nominal magnetic field of the sample ( $B_{\text{nom}}$ ) and the magnetic field at position  $r$ ,  $B_0(r)$ . The dephasing caused by  $B_0$  inhomogeneities leads to a more rapid decay in transverse magnetisation because spins begin to precess at slightly different frequencies, meaning that the  $T_2^*$  relaxation time will be shorter than  $T_2$ . As will be discussed in Section 1.3,  $T_2^*$  relaxation has an important effect on the NMR signal when it is digitally processed.

The physical mechanisms behind relaxation are numerous and complex. Those relevant to NMR spectroscopy include molecular motion, scalar coupling, dipolar coupling, chemical shift anisotropy, spin rotation interactions and quadrupole interactions. Common to all is the generation of fluctuations in the magnetic field. The intricacies of these processes are beyond the scope of this thesis, and although most will not be discussed here, the principles of scalar coupling and chemical shift will be explored in the next section as they are fundamental to NMR spectroscopy. Finally, it should be mentioned that when NMR data is acquired in vivo, the biological environment from where the signal originates has a substantial effect on relaxation.

Molecules visible to NMR spectroscopy will have a range of  $T_1$  and  $T_2$  relaxation times. It is, therefore, a matter of importance that these times are known before conducting an MRS study, or at the very least that their differences and how they will be affected by the NMR acquisition is adequately taken into account. This allows for the optimal choice in parameters for a given acquisition method. Additionally, understanding  $T_1$  and  $T_2$  relaxation effects is especially crucial in signal quantification when measurements are to be treated in absolute terms. This will be revisited in Section 1.5 and Chapter 3.

## 1.2.2 Magnetic Resonance Spectroscopy

### 1.2.2.1 Chemical shift

The Larmor equation describes the precessional frequency of a <sup>1</sup>H proton, which for water nuclei would resolve as a single spectral peak if represented as function of frequency and magnitude. However, molecules will differ in their observed magnetic  $B_0$  field as their nuclei are shielded by a surrounding covalent electron structure. These electrons produce their own magnetic moment  $\mu_e$ , which is in opposition to the  $B_0$  field and reduces the magnetic field experienced at the nucleus. Thus, the precessional frequency of the protons within the molecular structure of individual metabolites will differ depending on the degree of electron shielding. As such, the Larmor equation is then modified to give

$$f_0 = \frac{\gamma}{2\pi} B_0 (1 - \sigma) \quad [1.19]$$

where  $\sigma$  is a shielding constant that is dependent on the chemical environment encompassing the atomic nuclei. This is known as chemical shift, which was first discovered independently by Proctor and Yu (1950) and Dickinson (1950), and is the key property of NMR that distinguishes MRS from MRI. Each molecule will have a different degree of electron shielding, leading to a different shielding constant and thus a different chemical shift.

Eq. [1.19] shows that the chemical shift of metabolites will be dependent on the external magnetic field. This is undesirable when one wishes to compare data across MRI scanners of differing field strengths. Additionally, there is no substance in nature with a chemical shift equal to 0. To overcome this issue, the chemical shift scale is standardised using a reference according to Eq. [1.20]:

$$\delta = \frac{f_s - f_{ref}}{f_{ref}} \times 10^6 \quad [1.20]$$

where  $\delta$  is the chemical shift,  $f_s$  is the frequency of the sample substance and  $f_{\text{ref}}$  is the frequency of the reference substance. In NMR spectroscopy,  $f_{\text{ref}}$  is typically based on tetramethylsilane (TMS), which is assigned an arbitrary chemical shift of 0. Chemical shift is a dimensionless quantity and is represented in parts per million (ppm). This scale is known as the ppm scale.

### 1.2.2.2 *J*-coupling

An interesting characteristic of NMR resonances is the phenomenon of single peaks splitting into multiple peaks. This occurs because nuclei with magnetic moments can interact with each other either directly through space (dipolar coupling) or through electrons in the chemical bonds that bind molecules (scalar coupling, also called *J*-coupling). The effect of dipolar coupling can be overlooked because in a liquid dipolar interactions will average out to zero, leaving no net effect on the nuclear energy levels. This is not the case with scalar coupling, where the interactions of electrons through chemical bonds leads to a nonzero interaction between magnetic moments and, therefore, observed splitting of peaks.

*J*-coupling can potentially lead to quite complex interactions between nuclei and, as with the physical principles of NMR spectroscopy, can only be truly understood through quantum mechanics. To begin simply, an uncoupled single-spin system A has two energy levels ( $\alpha$  and  $\beta$ ) that are separated according to Bohr's frequency condition  $\Delta E_{\alpha\beta} = hf_A$ . Since there is only one possible energy level transition, the nucleus will have a single resonance at frequency  $f_A$  (Figure 1.7a). In the case of two coupled nuclei A and X of a two-spin system, each of the single resonances at frequencies  $f_A$  and  $f_X$ —which would resolve as single peaks if they were not coupled—will split into two equal but smaller peaks, referred to as a doublet (Figure 1.7b). Here, the  $\alpha$  and  $\beta$  spins of nucleus A will interact with the  $\alpha$  and  $\beta$  spins of nucleus X by virtue of the electrons in the chemical bond (i.e., by scalar coupling). The Pauli exclusion principle dictates that the chemically bonded electrons of the two molecules must be antiparallel to each other. For uncoupled nuclei the nuclear and electronic spins would normally be antiparallel, meaning that in scalar coupling, because of the Pauli exclusion principle, some of the nuclear spins will become parallel to each other. This leads to some of the spins having two

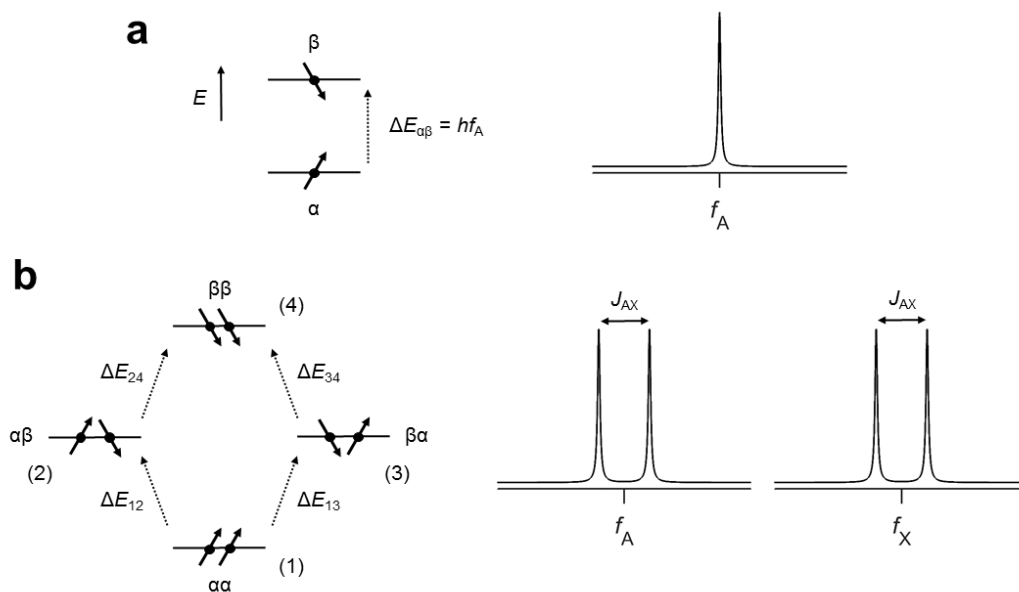


**Figure 1.7** Energy level diagrams and corresponding NMR resonances for (a) an uncoupled spin system A and (b) a coupled two-spin system AX. Since only one energy level transition is possible for the uncoupled spin system, there is correspondingly only a single resonance line with frequency  $f_A$  in the frequency-domain spectrum based on Bohr's frequency condition  $\Delta E_{\alpha\beta} = hf_A$ . For a scalar-coupled AX spin system four energy levels are apparent due to the mixture of the  $\alpha$  and  $\beta$  spins of the A and X resonances in virtue of their chemical bonding. Thus, there are four possible energy level transitions. This leads to characteristic peak-splitting of the A and X resonances at frequencies  $f_A$  and  $f_X$ , respectively. Four spectral peaks now appear, with each of the two pairs of split peaks separated by the  $J$ -coupling constant  $J_{AX}$ . See text for details.

energetically less favourable states:  $\alpha\alpha$  and  $\beta\beta$ . The other nuclear spins are able to maintain the energetically more favourable antiparallel states  $\alpha\beta$  and  $\beta\alpha$ . Thus, four energy level transitions are now possible:  $\Delta E_{12}$ ,  $\Delta E_{34}$ ,  $\Delta E_{13}$  and  $\Delta E_{24}$ . More importantly, these discrete transitions mean that each of the single resonance peaks separate into two proportionally smaller peaks, forming a doublet as previously stated. The peaks of the two nuclei have a frequency equal to  $f_A \pm J_{AX}/2$  and  $f_X \pm J_{AX}/2$ , where  $J_{AX}$  is the difference in frequency between the split peaks known as the  $J$ -coupling constant. An illustration of the quantum mechanical principles of scalar coupling based on energy levels is given in Figure 1.7b.

Unlike chemical shift, the  $J$ -coupling constant is independent of the external magnetic field and so is expressed in units of Hz. Values range from 1–15 Hz for  $^1\text{H}$ – $^1\text{H}$  bonds and 100–200 Hz for  $^1\text{H}$ – $^{13}\text{C}$  bonds. Both of these features of spin systems have fundamental roles in determining how NMR resonances are resolved in frequency-domain spectra. In order to fully understand the spectral patterns of all types of spin systems a numerical analysis using the principles of quantum mechanics is required; this is beyond the scope of this thesis, however.

Another fundamental characteristic of  $J$ -coupling is the effect that arises from chemically equivalent and magnetically equivalent nuclear spins. Chemical equivalence refers to resonances with the same chemical shift coupled to a separate resonance of a different chemical shift with a different  $J$ -coupling constant. Magnetic equivalence refers to resonances with the same chemical shift coupled to a separate resonance of a different chemical shift with an identical  $J$ -coupling constant. Thus, magnetically equivalent nuclei are also chemically equivalent. Certain rules apply to the spins of such nuclei. Firstly, isolated magnetically equivalent nuclei such as the methyl compound ( $\text{CH}_3$ ) do not exhibit any splitting of peaks. Secondly, when there are magnetically equivalent scalar-coupled spins within a molecule, the phenomenon of successive peak splitting is observed. A typical example is that of lactic acid, which is an  $\text{AX}_3$  molecule composed of two coupled nonequivalent spins (A and X) and three magnetically equivalent spins ( $\text{X}_3$ ). (In NMR spectroscopy, the purpose of assigning letters as identifiers of nuclear spins in covalently bonded molecules is to symbolically represent their chemical shift; the alphabetical order denotes the difference in frequency for each resonance. Thus, an AX spin system contains nuclei with frequencies that are comparatively further apart than those of an AB spin system.) If the spins A and  $\text{X}_3$  of lactic acid were not coupled they would resolve as single peaks (including the  $\text{X}_3$  spins as they are magnetically equivalent). The presence of coupling, however, means that the A spins interact with the  $\text{X}_3$  spins leading, successively, from a doublet to a triplet and eventually to a quartet (Figure 1.8). The magnetically equivalent  $\text{X}_3$  spins will interact with the A spins and split into a doublet only. For both resonances the frequency difference between each of the split peaks is equal to the coupling constant  $J_{\text{AX}}$ . A third rule is that the spectral pattern (i.e., the total number of peaks and the amplitude ratio) of a resonance containing magnetically equivalent spins whose peaks successively split can be predicted by  $\text{AX}_n$ , where  $n$  is the number of magnetically equivalent nuclei in X. For instance, for lactic acid, which has an  $\text{AX}_3$  spin system, the A spins will resolve as a quartet with amplitude ratio 1:3:3:1. This is because the peaks successively split according to binomial theorem.

This image is copyrighted. It can be found at its original source.

**Figure 1.8** Successive splitting of the spectral peaks of the coupled  $AX_3$  spin system of lactic acid. The A spins successively split from a singlet to a quartet as they are coupled to three X nuclei. The X spins resolve as a doublet because the three nuclei in X are magnetically equivalent, which do not display peak-splitting behaviour. The number of peaks and their amplitude ratio can be predicted as splitting occurs according to binomial theorem. The A quartet has an amplitude ratio of 1:3:3:1. The relative integrals of each peak can also be derived from the number of protons that give rise to the signal: one and three. Reproduced from de Graaf (2007).

The physical phenomenon of successive splitting of spectral peaks applies to the coupled GABA spin system, which will be discussed in detail in Chapter 2. Moreover,  $J$ -coupling is the most important phenomenon of NMR that is exploited in the MRS to unambiguously detect the GABA signal, which will be demonstrated later in this chapter and directly or indirectly referred to throughout this thesis.

### 1.2.2.3 $J$ -evolution

When scalar-coupled spin systems are perturbed by RF pulses such as those in the spin echo experiment, the spins will be rotated as described in Section 1.2.1.3. They will then evolve following the principles of relaxation. However, because of  $J$ -coupling the dephasing of spin coherences will be more complicated than that of an uncoupled nucleus (the example used in Section 1.2.1.4 was based on such a nucleus). By investigating the  $AX_3$  spin system of lactic acid, it can be seen that excitation by a  $90^\circ_{-x}$  pulse rotates the  $X_3$  spins such that at  $t = 0$  (or when  $TE = 0$ ) the magnetisation is aligned with the +y direction (Figure 1.9a). The spins then begin to lose phase coherence as a result of transverse relaxation. In the case of scalar-

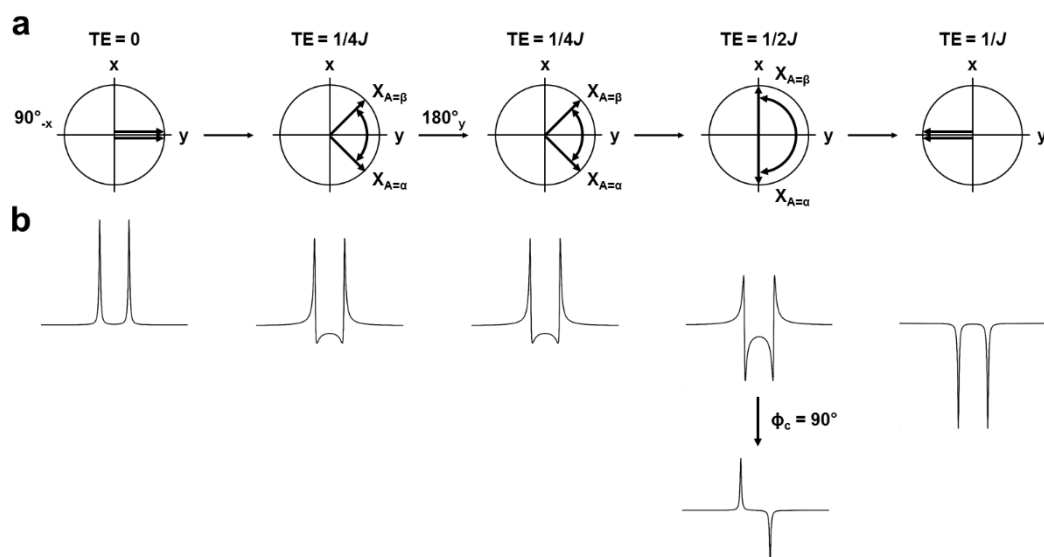


**Figure 1.9 a:**  $J$ -evolution of the  $X$  spins of the  $AX_3$  spin system of lactic acid during the spin echo experiment. Following transverse magnetisation, the coherences begin to dephase as a result of transverse relaxation. Two phase coherences rotate at different frequencies because of the frequency offsets of spins caused by  $J$ -coupling. After time delay  $TE = 1/4J$  the broadband  $180^\circ$  pulse inverts the  $A$  spins, leading to a simultaneous rotation of the  $X$  spins and a resetting of their phase. Therefore, the coherences are not refocused. At times  $TE = 1/2J$  and  $TE = 1/J$  the phase coherences are anti-phase and in-phase, respectively. **b:** The corresponding NMR resonances display predictable phase changes at each time delay in the spin echo experiment as shown. At  $TE = 1/2J$  a  $90^\circ$  phase correction leads to the peaks being anti-phase.

coupled spins the changes in phase will be influenced not only by  $B_0$  inhomogeneities but also by chemical shift and  $J$ -coupling. Since the  $X_3$  spins resolve as a doublet according to the principals of  $J$ -coupling, each of the resonances will have a different Larmor frequency according to  $f_X \pm J/2$ . The spins will therefore precess at different frequencies, leading to a difference in phase shifts at the end of the first delay in the spin echo experiment. As explained in the previous section, this arises from energy level transitions (Figure 1.7b): whereas the  $X_3$  spins resonating at a lower frequency ( $f_X - J/2$ ) are coupled to the  $A$  spins in the lower-energy  $\alpha$  spin state, the  $X_3$  resonating at the higher frequency ( $f_X + J/2$ ) are coupled to the  $A$  spins in the higher-energy  $\beta$  spin state. Using vector diagrams this can be visualised as two rotating vectors  $X_{A=\alpha}$  and  $X_{A=\beta}$  in antiphase to each other (Figure 1.9a). By applying a broadband  $180^\circ_y$  pulse (i.e., affecting both spin species) at  $TE/2$ , two effects occur. Firstly, the phase of the spins is inverted, such  $\phi = \pi(f_X \pm J/2)TE \rightarrow \phi = -\pi(f_X \pm J/2)TE$ , as expected. Secondly, the non-selectivity of the refocusing pulse means that it excites all frequencies in the sample, causing the coupled  $A$  spins to simultaneously be inverted. The lower-frequency  $X$  spins that were coupled with the

$A_\alpha$  spins at the lower-energy level are now attached to the  $A_\beta$  spins at the higher-energy level and begin to resonate at the higher frequency, and vice versa. Thus, the phase rotation is reversed. At the top of the spin echo after the second delay  $TE/2$  the spins are not refocused and have acquired a net phase shift of  $2\phi$ . The dual effect of the refocusing pulse on phase coherence in scalar-coupled spins systems is of great relevance to the detection of the NMR resonances of molecules such as GABA. In Section 1.3.2.3 it will be shown how  $J$ -evolution and the spin echo experiment can be advantageously exploited to unambiguously discriminate between uncoupled and coupled resonances.

The lineshape of the spectral peaks of scalar-coupled spin systems when detected in the spin echo experiment is dependent on the echo time, and how these peaks evolve throughout the experiment will depend on the phases of the spin coherences and on how the spin system is coupled. For this reason, the phenomenon just described is termed  $J$ -evolution. Furthermore, the spectral pattern of the split peaks of scalar-coupled resonances can be straightforwardly predicted based on the  $J$ -coupling constant. This is possible as the spins will rotate at their nominal Larmor frequency, which for scalar coupled resonances will depend on their coupling constant. For instance, a resonance with  $J = 10$  Hz that resolves as a doublet will have both its peaks completely positively in-phase at  $TE = 0$  s,  $TE = 0.2$  s,  $TE = 0.4$  s, etc., completely negatively in-phase at  $TE = 0.1$  s,  $TE = 0.3$  s,  $TE = 0.5$  s, etc. and anti-phase (when  $90^\circ$  out of phase with the RF receiver) at  $TE = 0.05$  s,  $TE = 0.15$  s,  $TE = 0.25$  s, etc. This generalises to the following rules of thumb for AX spin systems: when  $TE$  is a multiple of  $1/2J$  the peaks will be in-phase or anti-phase; when  $TE$  is a multiple of  $1/J$  the peaks will be in-phase (either positively or negatively). At all other echo times the peaks will display a mixture of phases. Examples of these rules and their corresponding phase shifts in vector diagrams are displayed in Figure 1.9b. Changes in lineshape become increasingly more complex with increasing numbers of coupled nuclei such that numerical simulations based on quantum mechanics must be used in order to fully evaluate the spectral pattern.

### 1.3 Data Acquisition

From an MR hardware perspective, the acquisition of MRS data is relatively straightforward. Any MR scanner can in principle detect the <sup>1</sup>H NMR spectral signal

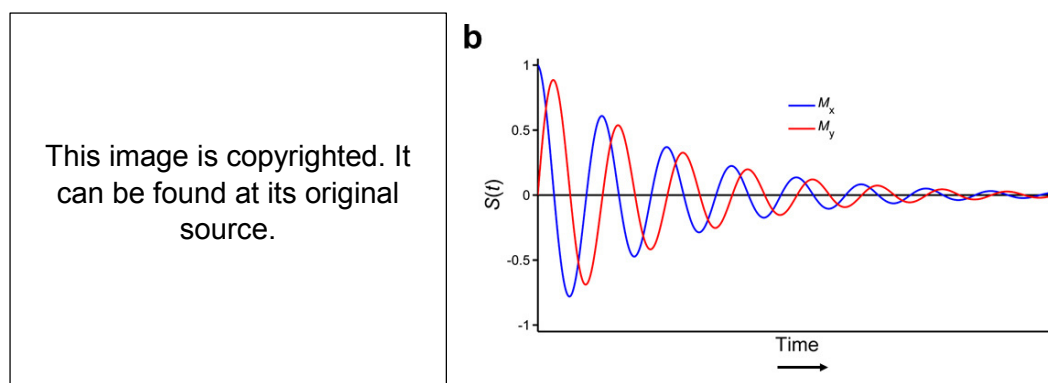


**Figure 1.10 a:** Three-dimensional view of the complex damped exponential signal of the free induction decay (FID). The magnetisation components  $M_x$  and  $M_y$  are orthogonal to each other and decay according to the  $T_2^*$  time constant. Reproduced from de Graaf (2007). **b:** A two-dimensional view of the real ( $M_{x,t}$ ) and imaginary ( $M_{y,t}$ ) components of the FID.

since all that is required is a superconducting magnet, a gradient coil system, an RF transmitter/receiver system and a computer to control the hardware and store the data.

### 1.3.1 Free Induction Decay and Fourier Transform NMR

Following excitation by a  $90^\circ$  RF pulse, the magnetisation components  $M_x$  and  $M_y$  of a given  $^1\text{H}$  proton will decay over time according to the  $T_2^*$  time constant. This decay of the NMR signal is called the free induction decay (FID). The FID is mathematically represented as exponentially decaying time-domain functions according to:

$$M_x(t) = M_0 \cos[(\omega_0 - \omega)t + \phi] e^{-t/T_2^*} \quad [1.21]$$

$$M_y(t) = M_0 \sin[(\omega_0 - \omega)t + \phi] e^{-t/T_2^*} \quad [1.22]$$

where the rotational frequency (or frequency offset) of the FID is represented by  $\omega_0 - \omega$ , that is, the difference between the Larmor frequency and the frequency of the sample compound (sometimes denoted as  $\Omega$  or  $\Delta\omega$ ); and  $\phi$  (in rad) is the phase at the beginning of the decay (when  $t = 0$ ). It is useful to combine  $M_x(t)$  and  $M_y(t)$  into a complex damped exponential signal, given by

$$S(t) = S_0 \exp\{i[(\omega_0 - \omega)t + \phi] - t/T_2^*\} \quad [1.23]$$

where  $S_0$  is the signal amplitude at  $t = 0$ .  $S(t)$  contains both real and imaginary components that correspond to the  $M_x(t)$  and  $M_y(t)$  transverse magnetisation decays. Two- and three-dimensional representations of the FID are shown in Figure 1.10.

The time-domain signal is not very human-interpretable, however. Interpretation is more straightforward in the frequency domain. Thus, the time-

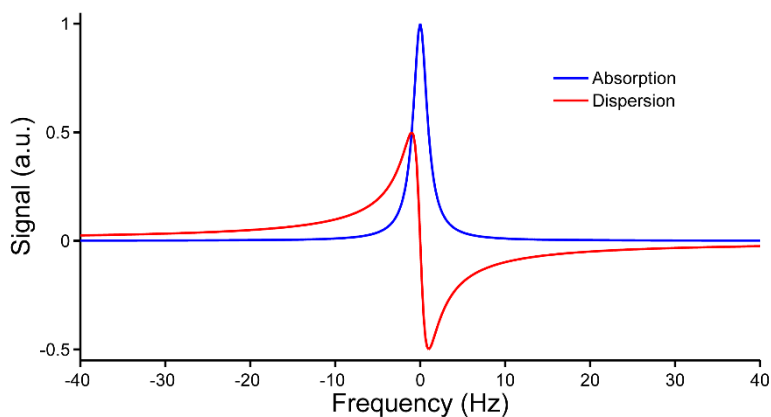


**Figure 1.11** Fourier transformation of the time-domain FID results in two Lorentzian peaks in the frequency domain. The real ( $M_{x,t}$ ) component has an absorption lineshape while the imaginary ( $M_{y,t}$ ) component has a dispersion lineshape.

domain signal can be converted into the frequency domain by a Fourier transform (FT) according to

$$F(f) = \int_{-\infty}^{+\infty} S(t) \exp(-i2\pi ft) dt \quad [1.24]$$

The FT produces real and imaginary frequency-domain signals, which again correspond to the  $M_x$  and  $M_y$  magnetisation components of the FID, respectively.

These are represented as

$$R(f) = A(f) \cos \phi - D(f) \sin \phi \quad [1.25]$$

$$I(f) = A(f) \sin \phi + D(f) \cos \phi \quad [1.26]$$

where

$$A(f) = \frac{S_0 T_2^*}{1+(f_0-f)^2 T_2^{*2}} \quad [1.27]$$

$$D(f) = \frac{S_0(f_0-f)T_2^{*2}}{1+(f_0-f)^2 T_2^{*2}} \quad [1.28]$$

$A(f)$  and  $D(f)$  refer to the absorption and dispersion mode spectral lineshapes of the frequency-domain NMR signal (Figure 1.11). The absorption lineshape has a full width at half maximum (FWHM) equal to  $1/(\pi T_2^*)$ . In a spectrum acquired in vivo, spectral peak separation and metabolite quantification is reliant on the linewidth of the Lorentzian absorption peak, which itself is dependent on both the intrinsic  $T_2$  of a given metabolite and the magnetic field homogeneity. As a rule, a metabolite with a relatively short  $T_2$  will have a relatively broad spectral linewidth whereas a metabolite with a relatively long  $T_2$  will have a relatively narrow spectral linewidth. In terms of the FID, the rate of decay is directly related  $T_2^*$  as described in Eq. [1.23].

### 1.3.2 Techniques and Pulse Sequences

As discussed in the previous sections, the NMR signal can be detected by RF receiver coils in the MRI scanner when transverse magnetisation is achieved by  $B_1$  excitation. Both the pulse-acquire and spin echo pulse sequences are able to achieve this. However, it is invariably desired that spatial specificity is obtained should meaningful experiments be conducted either in vitro or in vivo. Moreover, localising the detection of the NMR signal to a prescribed volume of interest (VOI) has several benefits on spectral data. Firstly, contamination from extracranial lipids can be greatly reduced when the detected signal is restricted to a volume of the brain that excludes tissue that may contain lipids such as fats (e.g., in the scalp). Lipid contamination is particularly problematic for MRS as it will lead to substantial distortion in the spectrum baseline. Secondly, suppression of the water resonance (which would dominate the spectrum if not removed) is considerably more effective when a prescribed VOI is used. Thirdly, achieving  $B_0$  homogeneity is easier when only a smaller area of the magnetic field is adjusted.

Localised NMR spectroscopy is by and large the most dominant method used. Localisation is made possible by the combined use of magnetic field gradients that modulate the  $B_0$  field and slice-selective RF pulses that selectively excite the necessary frequencies to obtain the desired VOI. Magnetic field gradients make it possible to achieve 2D or 3D single volume localisation or, if phase encoding is incorporated, multivolume localisation. The exact manner in which localisation is achieved is dependent on the pulse sequence of the MRS acquisition. Since localised MRS was first introduced a number of sequences have been developed, each with their own approach to localisation. These are now discussed with respect to single volume localisation. It will then be briefly described how these pulse sequences can be modified to achieve multivolume localisation.

#### 1.3.2.1 Single voxel spectroscopy

Single voxel spectroscopy (SVS) is a technique whereby a single, spatially prescribed cuboid VOI is defined. The spatial position in the x, y and z directions in the MRI scanner are determined by magnetic field gradients that linearly modulate the  $B_0$  field. The frequencies within the spatially defined magnetic field are then

This image is copyrighted. It can be found at its original source.

**Figure 1.12** Localisation in single voxel spectroscopy is achieved by exciting the magnetisation of spins in three orthogonal planes. This is possible by simultaneously applying slice-selective excitation RF pulses and magnetic field gradients in each plane. Unwanted coherences that originate from outside the volume of interest (black cube) can be dephased by using crusher gradients in the localising pulse sequence. Reproduced from Jung (1996).

selectively excited by frequency-selective RF pulses to produce a spatial slice. When both are used in unison, a so-called 3D voxel can be localised (Figure 1.12). Two of the most popular SVS pulse sequences that take advantage of 2D and 3D localisation are point resolved spectroscopy (PRESS) and stimulated echo acquisition mode spectroscopy (STEAM). Both are similar in the fact that they both are variants of the spin echo sequence described in Section 1.2.1.4.

#### ***Point resolved spectroscopy (PRESS)***

PRESS (Bottomley, 1987) is what is called a double spin echo sequence made up of a 90° slice-selective excitation pulse and two 180° slice-selective refocusing pulses (Figure 1.13a). A spin echo is produced following the first 180° refocusing pulse at time  $2t_1$  that is then refocused by the second refocusing pulse. A second spin echo is formed, the top of which occurs at time  $2t_2$ . Data is acquired from this second spin echo. The excitation and refocusing pulses are applied at the same time as magnetic field gradients  $G_x$ ,  $G_y$ ,  $G_z$ , respectively, leading to 3D localisation. Only frequencies originating from the intersection of all three planes are detected after time  $2t_1 + 2t_2$  (which equals the TE of the PRESS sequence).

#### ***Stimulated echo acquisition mode (STEAM)***

STEAM (Frahm et al., 1987) is a multi-spin echo sequence that employs, in addition to magnetic field gradients, three 90° slice-selective excitation pulses, which will generate, three FIDs, four spin echoes and one stimulated echo (Figure 1.13b). The

This image is copyrighted. It can be found at its original source.

**Figure 1.13** Pulse sequence diagrams for (a) point resolved spectroscopy (PRESS) and (b) stimulated echo acquisition mode spectroscopy (STEAM). Time delays and nominal flip angles for each of the excitation and refocusing sinc pulses are indicated. Magnetic field gradients for spatial localisation are displayed as ramped rectangles. Echo time (TE) crusher gradients are highlighted in light grey and the mixing time (TM) crusher gradient in STEAM is highlighted in dark grey. In the STEAM sequence refocusing field gradients (indicated by the dotted boxes) can be placed to either side of the TM delay. Reproduced from de Graaf (2007).

first two 90° pulses are separated by a delay TE/2 and produce a spin echo at time TE. The third excitation pulse is applied after the second pulse after a second delay called the mixing time (TM). The second spin echo is formed at time 2TM followed shortly thereafter by the stimulated echo. The two remaining spin echoes form at times TE/2 + 2TM and TE + 2TM, respectively.

Several other SVS pulse sequences have been developed since PRESS and STEAM were first introduced, including localisation by adiabatic selective refocusing (LASER) (Garwood and Delabarre, 2001) and spin echo, full intensity acquired localised spectroscopy (SPECIAL) (Mlynárik et al., 2006). These have their own advantages over PRESS and STEAM but they will not be discussed here.

### 1.3.2.2 Chemical shift imaging

Much like conventional techniques in fMRI, MRS is also able to acquire data over multiple voxels. Chemical shift imaging (CSI), or MRS imaging (MRSI), is a multi-voxel technique whereby the spatial distribution of the spectral signal of metabolites can be distinguished. This is achieved by incorporating phase-encoding gradients into a standard localised MRS sequence.

### 1.3.2.3 Spectral editing

As it was demonstrated earlier, *J*-coupling has a distinctive effect on scalar-coupled spin systems in the spin echo experiment. If the pulse sequence is modified to include frequency-selective pulses it is possible to selectively perturb the

This image is copyrighted. It can be found at its original source.

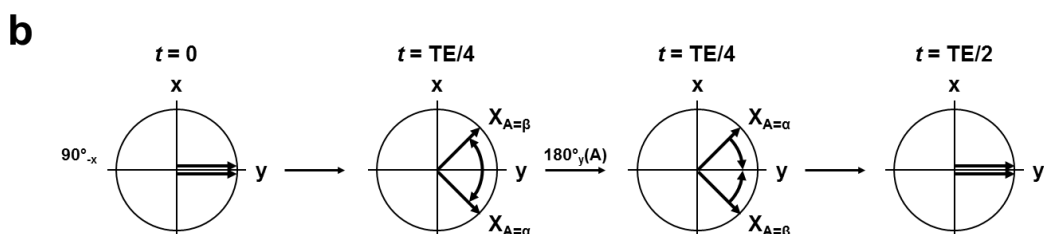


**Figure 1.14 a:** In the *J*-difference editing experiment, two  $180^\circ$  frequency-selective refocusing (editing) pulses are added to the standard spin echo sequence. The editing pulses selectively excite the A spins in the ON scan, whereas they are not applied or are applied far off resonance in the OFF scan. Reproduced from de Graaf (2007). **b:** Vector diagrams illustrate the behaviour of spin coherences in the ON scan. When the  $180^\circ$  pulse is applied after a time delay  $TE/4$ , the A spins are selectively inverted, which causes the X spins to reverse in rotation. However, their phases are not reset as would occur in a typical spin echo experiment. Thus, after a second time delay  $TE/4$  the coherences are refocused along  $+y$ , eventually becoming in-phase at time  $TE/2$ .

magnetisation of specific coupled spins, in virtue of the principles of *J*-coupling. This technique is termed spectral editing, which is defined as any NMR technique that exploits the scalar couplings of a spin system in order to distinguish it from all other uncoupled resonances. By exploiting the couplings of spin systems it possible to unambiguously detect resonances that are normally overlapped by more intense peaks. There are two main forms of spectral editing: *J*-difference editing and multiple quantum coherence editing. Since the former constitutes the principle MRS technique used in this thesis, the latter will not be discussed.

### *J*-difference editing

The *J*-difference editing experiment is a spin echo sequence that includes two  $180^\circ$  frequency-selective refocusing pulses placed symmetrical about the  $180^\circ$  slice-selective pulse (positioned in time at  $TE/2$ ) (Figure 1.14a). These frequency-selective pulses are termed editing pulses as they will selectively invert scalar-coupled spins based on their chemical shift while leaving all other uncoupled spins unaffected. As the name suggests, *J*-difference editing involves the subtraction of two scans: in the first the editing pulses are applied on resonance (the “ON” scan),

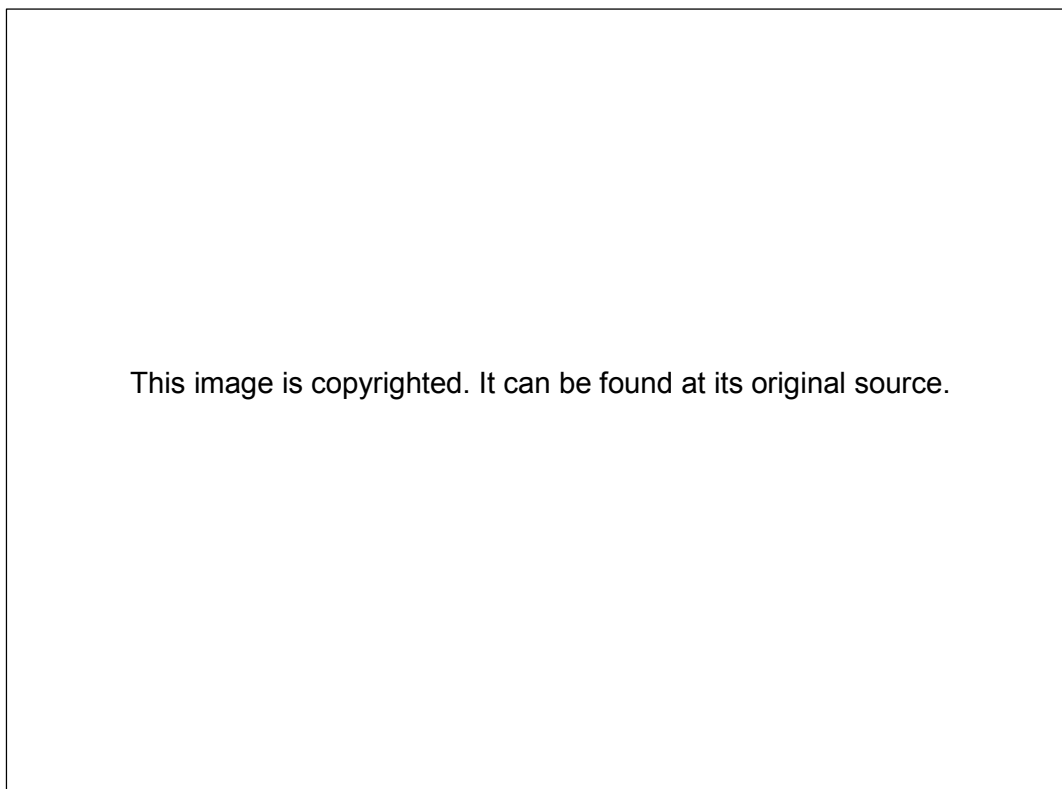


**Figure 1.15** *J*-difference editing of a generic AX two-spin system. **a:** A simulated spectrum showing how the A and X resonances of interest (grey lines) are overlapped by more intense signals originating from lipids and water. **b:** In the OFF scan, the X spin evolves as normal becoming inverted at  $TE = 1/J$  since the frequency-selective  $180^\circ$  editing pulses do not affect the A spin. Spin A is not shown as it has been removed during water suppression. **c:** When the editing pulses are applied in the ON scan, the X spin is selectively refocused, becoming in-phase with all other uncoupled resonances at  $TE = 1/J$ . **d:** Subtraction of the ON and OFF scans will remove the uncoupled resonances while unambiguously resolving the edited X spin. **e:** Adding the two scans will give the uncoupled resonances only. Adapted from de Graaf (2007).

while in the second the editing pulses are either not applied or are applied far off resonance (the “OFF” scan). In the OFF scan the coherences of the scalar-coupled spins evolve as they would in a typical spin echo experiment, with the broadband slice-selective  $180^\circ$  pulse simultaneously resetting their phase and changing their rotation (as described in Section 1.2.2.3 and Figure 1.9). When the editing pulses are applied in the ON scan the behaviour of the coherences is different. Using  $AX_3$  spin system of lactic acid once more, if the selective  $180^\circ$  pulses are set to selectively excite the A spins, the effect will be that the A spins will be inverted. This will cause the X spins to reverse in their rotation. That is, and as stated before, the slower rotating X spins linked to the  $A_\alpha$  spins are now linked to the  $A_\beta$  spins and begin to resonate at a higher frequency, and thus rotate faster. Therefore, the nonselective  $180^\circ$  pulse will end up refocusing the phase evolution leading to the X spins being completely in-phase after delays that are multiples of  $TE/2$ . This is more easily

understood using vector diagrams (Figure 1.14b). Using two symmetrically placed 180° editing pulses in the pulse sequence ensures that the phase coherences are fully refocused. When the difference between the ON and OFF scans is taken, only the coupled spins that were affected by the editing pulses remain. A graphical illustration of a spectrally edited generic AX two-spin system is provided in Figure 1.15 to more concretely demonstrate the elegance of *J*-difference editing and how it can unambiguously detect resonances that are typically overlapped by other resonances.

Note that *J*-difference editing can be applied to any scalar-coupled spin system; for the remainder of this thesis, however, this technique is treated strictly in relation to editing of the GABA spin system (hereafter denoted GABA-editing or GABA-MRS). The *J*-difference editing experiment as it applies specifically to the detection of the GABA signal will be discussed in detail in Chapter 2. Finally, it should be pointed out that there are other MRS techniques that can also unambiguously resolve the GABA resonances (e.g., multiple quantum coherence editing and 2D spectroscopy), but these are beyond the scope of this thesis.

### 1.3.3 $B_0$ Field Homogeneity

The practical applications of MRS in modern brain imaging tend to be dominated by investigations of local areas of interest in the brain. As such, SVS is arguably the most popular implementation of MRS in neuroscience. The acquisition of data from a single VOI, and therefore metabolite concentration quantification (see Section 1.5), relies quite heavily on a homogenous magnetic field. This becomes even more critical, and challenging, *in vivo* given the marked non-uniformity of brain structures. The homogeneity of the magnetic field of an object, be it a phantom or a brain, depends on the object's magnetic susceptibility  $\chi$ , which denotes the degree of magnetisation an object will experience in the presence of an applied magnetic field. Ferromagnetic materials have a  $\chi \gg 1$  and MR-compatible materials have a  $\chi \ll 1$ . The macroscopic magnetisation of a given object or sample can then be approximated as

$$M \approx \frac{\chi}{\mu_0} B_0 \quad [1.29]$$

where  $\mu_0$  is the magnetic permeability in a vacuum. Recalling the Larmor equation, Eq. [1.29] demonstrates that interactions between magnetic susceptibility and  $B_0$  will shift the Larmor frequency of nuclear spins.

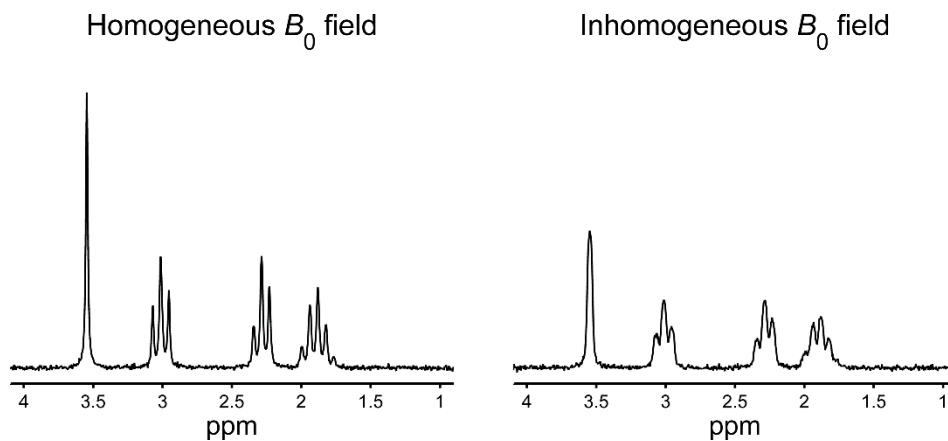


**Figure 1.16** Simulated  $^1\text{H}$  MRS data displaying the glycine (Gly) and GABA resonances. When the  $B_0$  field is homogeneous, the peaks display excellent spectral resolution and a high signal-to-noise ratio (SNR). In the presence of  $B_0$  inhomogeneity, spectral resolution is lost and SNR is decreased. Increased line-broadening is also seen.

The impact of differences in the magnetic susceptibility of brain tissue compartments on the NMR signal can now be illustrated. It is useful to consider the brain as a composition of  $n$  small volumes, each with a constant but differential homogeneous  $B_0$  field. Given that the head contains air- and liquid-filled cavities and sinuses, which will adversely affect magnetisation, the total NMR signal from the summed  $n$  volumes will arise from a heterogeneous mixture of magnetic fields, each with different frequencies. This is given by

$$S(t) = S_0 \exp(ift - t/T_2) \sum_{n=1}^N \exp(i\Delta f_n t) \quad [1.30]$$

where  $N$  equals the total number of volumes and  $\Delta f_n$  is the frequency difference between the Larmor frequency  $f_0$  and frequency  $f$  in volume  $n$ . In a homogeneous  $B_0$  field  $\Delta f_n = 0$ , which will lead to each  $n$  volume having an identical Lorentzian absorption peak. In other words, the FWHM of the frequency-domain signal will equal  $1/(\pi T_2^*)$ . If each  $n$  volume has a different frequency, due to the differences in magnetic susceptibility of the tissue compartment in question, the Lorentzian peaks will not add coherently, leading to broadening of the summed signal and a reduction in spectral resolution and signal sensitivity. Figure 1.16 illustrates the effect of  $B_0$  inhomogeneity using simulated spectral data.

### 1.3.4 Chemical Shift Displacement

Localised spectroscopy is reliant on spatial slice selection using magnetic field gradients and RF pulses. As discussed in Section 1.3.2.1, a volume of tissue from which the NMR signal is detected can be localised by exciting orthogonal slices using frequency-selective RF pulses. Since the slice selection is not only spatially

dependent but frequency-dependent as well, the frequencies that are excited will be influenced by their chemical shift. Consequently, a frequency-dependent spatial displacement in detected metabolite signals will occur. This is known as chemical shift displacement (CSD). The CSD of a given metabolite based on a given gradient strength can be calculated as

$$\Delta x = \frac{\Delta\omega}{\gamma G_x} \quad [1.31]$$

where  $\Delta x$  is the CSD in the  $x$  direction,  $\Delta\omega$  is the difference in frequency between two compounds (e.g., between water and lipids) and  $G_x$  is the strength of the magnetic field gradient. This spatial–frequency displacement phenomenon requires attention by spectroscopists as the majority of given metabolite signals may not necessarily originate in the volume of tissue prescribed at acquisition. CSD is potentially problematic for volumes prescribed close to the scalp, skull and air cavities. One can reduce CSD by altering the direction or sequence order of the gradients, increasing the gradient strength, increasing the bandwidth of the frequency-selective RF pulses or changing the frequency of the RF pulses such that  $\Delta\omega$  is decreased (e.g., offsetting the transmitter frequency to match the 2.0 ppm *N*-acetylaspartate resonance instead of water).

### 1.3.5 Water Suppression

The NMR signal of water ( $\delta = 4.7$  ppm) is of an order of magnitude 10,000 times greater than the majority of metabolites in the human brain. Consequently, the water peak greatly dominates the <sup>1</sup>H NMR spectrum, obscuring the peaks of metabolites of all other brain metabolites. Suppression of the water signal then becomes a requisite for unambiguous detection of metabolite peaks. A multitude of water suppression techniques are available and they can be classed into four categories: frequency-selective excitation methods, relaxation-based methods, spin echo-based methods and subtraction methods. For the purpose of this thesis, only an example of a technique that combines the principles behind frequency-selective and relaxation-based water suppression will be discussed.

Suppression by variable pulse power and optimised relaxation delays (VAPOR) (Tkáč et al., 1999) can achieve efficient suppression of the water signal while minimising unwanted suppression of resonances near the water peak. VAPOR makes use of seven frequency-selective asymmetric RF pulses that selectively excite the water resonance, each of which are followed by a crusher gradient to dephase all

coherences in the transverse plane. The delay between each pulse is optimally varied such that recovery of the water signal by  $T_1$  relaxation is eventually nullified by the seventh pulse. A primary advantage of VAPOR is its ability to optimally suppress the longitudinal magnetisation of water in spite of the recovery experienced through  $T_1$  relaxation. Secondly, by varying the  $B_1$  power of the frequency-selective pulses by a factor of 1.78 a wide range of nominal flip angles can be accommodated that can still achieve excellent water suppression. Thus, VAPOR is relatively insensitive to  $T_1$  and  $B_1$  variations. It is a trivial task to incorporate VAPOR into other localised MRS sequences such as PRESS and STEAM.

### 1.3.6 Outer Volume Suppression

Contamination of spectral data by outer volume lipids occurs as a result of CSD. Significant contamination will lead to large distortions in the spectral baseline in addition to obscuring the resonances of other molecules. While crusher gradients applied during water suppression and localisation work to dephase outer volume resonances, imperfect slice profiles will allow some degree of lipid signal to bleed into the VOI. Therefore, it is necessary to incorporate a technique to eliminate the signals arising from these resonances.

The methodology of outer volume suppression (OVS) is very similar to water suppression. Slices (or slabs) are spatially localised along the edges of the VOI and magnetised by slice-selective excitation using magnetic field gradients. A crusher gradient is applied subsequent to slice selection to dephase excited coherences. As with water suppression, repetitions of OVS modules will lead to improved suppression. When applied in an optimal fashion all signals arising from outside the VOI (e.g., from muscle, lipids, the eyes and the scalp) can be prevented from contaminating the localised MRS signal.

While OVS will reduce lipid contamination, in vivo spectra will still contain a prominent macromolecular contribution arising from large molecules naturally occurring in living tissue. As stated in the Preface, addressing the significant issues posed by macromolecules to GABA-edited MRS constitutes a key aim of the research presented in this thesis. Macromolecular contamination and techniques to deal with this are addressed in Chapters 2 and 5.

## 1.4 Data Processing

Acquisition of the raw MRS data requires a certain degree of signal processing in order for it to be interpretable, useful and applicable to specific research questions. The FT of the time-domain signal into the frequency domain allows certain mathematical manipulations to be performed on the FID to improve both spectral resolution and signal sensitivity. Spectral resolution (also termed spectral dispersion) describes the degree of separation of spectral peaks while sensitivity equates to the signal-to-noise ratio (SNR) of the signal. Both properties are crucial for unambiguous and accurate detection of metabolite resonances and for quantification of concentration levels. The next few sections describe standard data processing steps that are typically applied to raw MRS data prior to quantification.

### 1.4.1 Apodization

Unprocessed FIDs contain a significant degree of high-frequency noise. This will have a detrimental effect on detecting spectral peaks throughout the frequency-domain spectrum. To improve spectral resolution and sensitivity of the signal, the FID can be filtered prior to FT. This processing step is known as apodization or time-domain filtering. Since the FID is a time-domain signal, certain mathematical manipulations in the form of time-varying weighting functions can be used to enhance the data.

An example of a simple weighting function applies an exponential weighting to the FID. This monoexponential decaying function improves the SNR of the frequency-domain signal by attenuating the amplitude of the noisy data points towards the end of the acquisition. This function is expressed as

$$W(t) = e^{-t/T_w} \quad [1.32]$$

where  $T_w$  is a rate constant that determines the rate of decay of the function. An example of exponential filtering applied to an unprocessed FID is shown in Figure 1.17. Although exponential weighting will enhance signal sensitivity by filtering the high-frequency noise, it will also increase the linewidths of the spectral peaks and decrease their amplitudes. This occurs because the exponential filter increases the decay of the FID, which will broaden the linewidths of spectral peaks in the frequency-domain data after FT. In other words, the observed  $T_2^*$  of the NMR

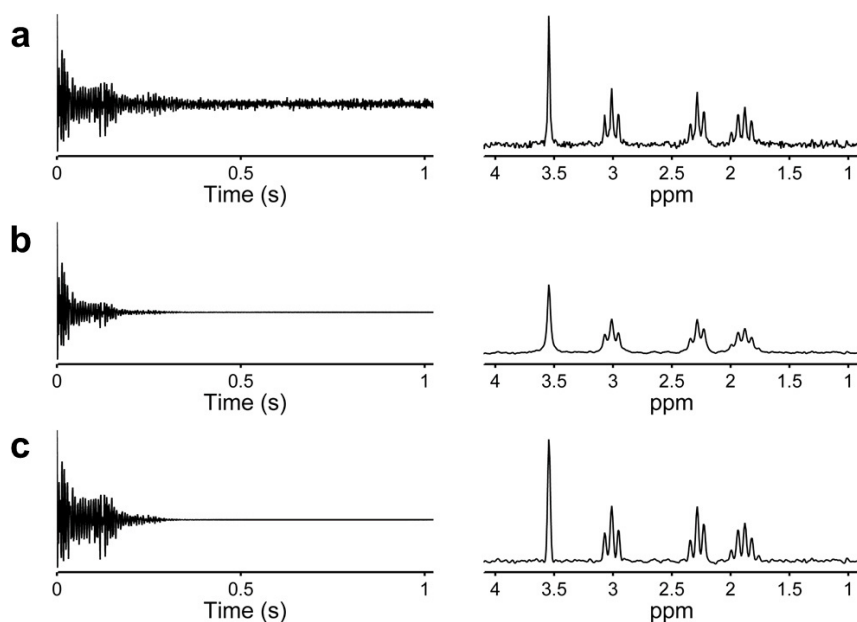


**Figure 1.17** **a:** A simulated unprocessed FID (left panel) and the corresponding frequency-domain spectrum (right panel) showing Gly and GABA resonances. **b:** Application of a match-weighted exponential filter function to the FID increases signal sensitivity (by filtering out high-frequency noise towards the end of the acquisition) but at the expense of line-broadening and decreased spectral resolution, as shown in the frequency spectrum. **c:** If appropriate weighting parameters are selected, a Lorentz-Gaussian filter function can increase signal sensitivity while maintaining spectral resolution.

resonances is reduced as a consequence of the exponential weighting. For this reason, the optimum amount of filtering when using exponential weighting is a matched filter, where the rate constant in Eq. [1.32] is equal to the original decay rate of the unprocessed FID (i.e.,  $T_W = T_2^*$ ). This achieves an optimum SNR without excessive line-broadening.

An alternative weighting function uses a Lorentz-Gaussian function. This is given by

$$W(t) = e^{+t/T_L} e^{-t^2/T_G^2} \quad [1.33]$$

where  $\exp(+t/T_L)$  is the Lorentzian component of the function, which is multiplied by  $\exp(-t^2/T_G^2)$  to give the function a Gaussian shape. The Gaussian component works to cancel out the comparatively longer tails of the Lorentzian component, thereby narrowing the base of the function but maintaining its linewidth. In this way, and by careful choice of the  $T_L$  and  $T_G$  weighting factors, both spectral resolution and sensitivity can be improved simultaneously. An example of Lorentz-Gaussian filtering is given in Figure 1.17.

In the end, the choice of an appropriate weighting function to filter, and the amount of weighting applied, is dependent on the quality of the raw data. In cases

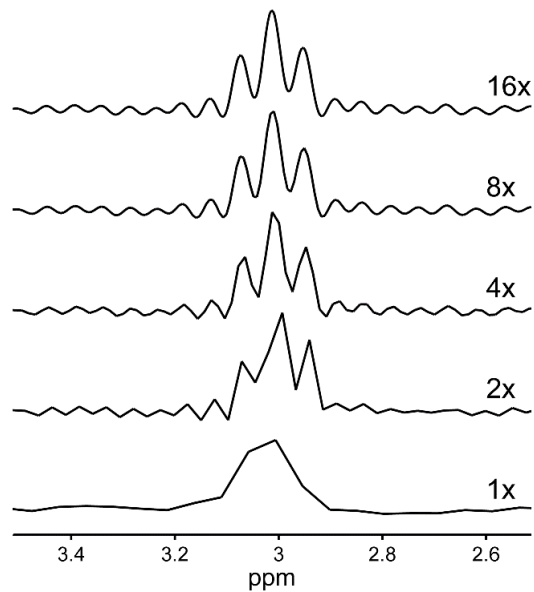


**Figure 1.18** Zero filling of data with a relatively coarse spectral resolution ( $\Delta f = 6.67$  Hz) can dramatically improve spectral resolution with even a low zero-filling factor. No observable benefit comes after four times zero filling.

where data with a high SNR are acquired, simple exponential filtering with a matched filter can be applied, whereas in other cases where maintaining reasonably fine spectral resolution is paramount will dictate that a more sophisticated weighting function be used. There are a number of possible weighting functions available to spectroscopists beyond the functions described above but in most instances exponential filtering is the default apodization method.

#### 1.4.2 Zero Filling

Zero filling involves appending zeros to the end of the FID. This processing step is applied in the analysis pipeline of MRS data as it can greatly improve spectral resolution. Figure 1.18 shows how an acquisition with relatively poor spectral resolution can be zero-filled sufficiently in order to better define a given spectral peak. The unprocessed data, which was sampled at 2000 Hz, has a relatively coarse spectral resolution ( $\Delta f = 6.67$  Hz) due to the number of data points acquired ( $N = 300$ ). Since the intermediate frequencies of the peak are stored in the time-domain data (because they fall within the frequency bandwidth) but are not displayed in the frequency-domain spectrum after FT because of the discrete nature of the transformation, appending zeros to the FID allows more points to be transformed into the frequency domain and therefore improved spectral resolution. Zero filling has diminishing returns, however. Only the frequencies stored in the FID can be

displayed; it cannot show data that was not acquired at the outset. This is illustrated in Figure 1.18 by the manifold increases in zero filling on the original data.

The primary advantage of zero filling is that it does not increase data size as it does not add more information—it is simply a mathematical transformation of the discrete digital data—but can enhance spectral resolution several fold.

### 1.4.3 Residual Water Filtering

Even with the application of water suppression techniques during acquisition, the 4.7 ppm water peak may likely still leave some degree of residual signal in the frequency spectrum. This may occur due to inefficient water suppression (e.g., non-ideal flip angles), poor  $B_0$  field homogeneity or frequency drift. Removing the residual water peak is an important step in processing raw MRS data for two reasons: (i) if the residual water signal is large enough it may introduce a distortion in the baseline, causing artefactual line-broadening, phase shifts or changes in lineshapes of metabolite peaks; (ii) spectral fitting procedures are constrained by the assumption that peaks have an approximately linear baseline, which will lead to poor fitting if a residual water signal distorts the baseline. The most popular method for removing residual water is by Hankel Lanczos singular value decomposition (HLSVD). This algorithm estimates the full parameters of the time-domain model used to fit an exponential damped sinusoidal function to acquired FIDs (Cabanes et al., 2001). The frequencies of the time-domain signal that correspond to the frequencies within and about the water frequency range are then selected and subsequently removed from the original FID. This so-called “black box” method requires no user input, allowing for automated water removal when incorporated into software packages for the processing and quantification of MRS spectra.

### 1.4.4 Phase and Frequency Correction

The FID and absorption and dispersion mode spectra of the NMR signal shown in Figure 1.10 and Figure 1.11 represent a signal with zero phase. However, the phase of the signal at  $t = 0$  will not remain constant throughout a given experiment. Magnetic field gradients and head motion will both contribute to errors in the phase of nuclear spins. When  $\phi \neq 0$ , the Lorentzian peak appears as a mixture of the absorption and dispersion mode components (Figure 1.19a). Over a series of excitations in an MRS experiment, each FID will have a certain degree of phase

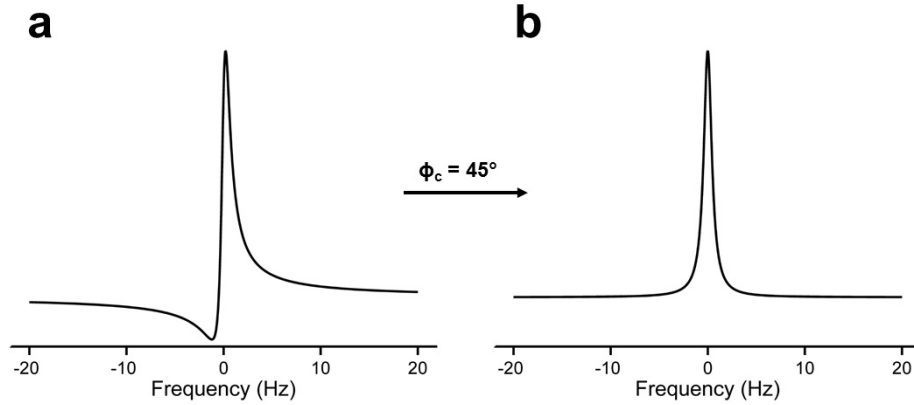


**Figure 1.19** **a:** Phase shifts will cause observable distortions in NMR spectra. In this example, the peak is 45° out of phase. **b:** A corresponding phase correction restores the peak to its ideal in-phase Lorentzian lineshape.

shift. Since these FIDs are usually averaged, phase errors in the signal will lead to a loss in SNR. This can be rectified by “phasing” the absorption and dispersion mode components of each individual FID according to

$$A(f) = R(f) \cos \phi_c + I(f) \sin \phi_c \quad [1.34]$$

$$D(f) = I(f) \cos \phi_c - R(f) \sin \phi_c \quad [1.35]$$

By simply adjusting  $\phi_c$ , the Lorentzian absorption and dispersion peaks can be shifted into the correct phase (Figure 1.19b). Eqs. [1.34] and [1.35] will phase the entire spectrum (i.e., at all frequencies), which is called zero-order phasing.

Phase shifts will also occur on a frequency-dependent basis. This occurs because of off-resonance effects of RF pulses or when the RF field strength is not strong enough to optimally excite all the relevant frequencies. Since the shift in phase is most extreme at the opposite ends of the frequency spectrum, such that the phase is  $\phi - \phi_e$  at one end of the spectrum and  $\phi + \phi_e$  at the other end, the error is linearly dependent. To correct for these phase shifts, frequency-dependent, first-order phasing can be applied. The phase correction parameter  $\phi_c$  then becomes

$$\phi_c = \phi_0 + (f_0 - f)\phi_1 \quad [1.36]$$

where  $\phi_0$  is the constant, zero-order phase correction and  $\phi_1$  is the linear, first-order phase correction.

During an MRS acquisition, the transmitter frequency is centred on a particular frequency; usually this is the water resonance. All frequency offsets of RF pulses can then be considered relative to the centre frequency  $f_0$ . Instabilities in the  $B_0$  magnetic field will cause shifts in  $f_0$ , however. Over time these instabilities will

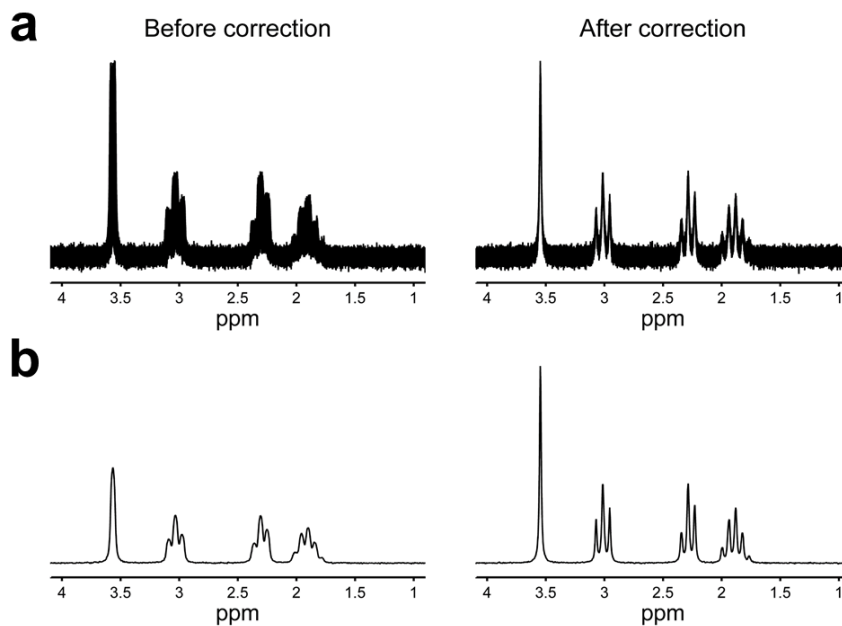


**Figure 1.20** Demonstration of phase and frequency correction by spectral registration using simulated spectral data. **a:** Individual spectra from 128 FIDs prior to correction display frequency and phase shifts (left panel). Simulated normally distributed random phase shift (zero mean, 2 deg random error) and linear frequency drift (5 Hz total drift, 0.2 Hz random error) were applied to the data. Following spectral registration, the individual spectra are aligned and phased based on the frequency and phase of the first FID (right panel). **b:** Averaging the 128 uncorrected acquisitions leads to loss in SNR and line-broadening. After correction the average spectrum has a much improved SNR and excellent spectral resolution.

lead to approximately linear drift in the centre frequency. This typically arises from heating of gradient coils that will alter the magnetisation of passive shim coil elements. Increases in thermal energy lead to decreases in the strength of  $B_0$ , causing  $f_0$  to drift negatively. Participant motion can also contribute to changes to the external magnetic field. Given that frequency offsets of RF pulses are fixed, frequency drift will adversely affect MRS data, leading to signal reduction, artefactual line-broadening and decreased spectral resolution. Drift is particularly problematic for spectral editing as the efficiency of this technique relies quite heavily on the frequency selectivity of narrowband pulses.

A number of frequency correction methods using different approaches have been published in the literature. Note that because of the inextricable relationship between frequency and phase errors, these methods simultaneously correct for frequency and phase. Some use the residual water peak as a reference resonance to estimate the correct frequency and phase (Helms and Piringer, 2001; Star-Lack et al., 2000), while others use a water-based navigator scan interleaved in the MRS acquisition (Thiel et al., 2002). It is also possible to use a predefined resonance that

is usually well-defined in in vivo data (e.g., creatine) as a reference (Evans et al., 2013; Waddell et al., 2007). A recent approach has proposed using a spectral registration method similar to motion correction in fMRI (Near et al., 2015). An example of spectral registration using simulated MRS data is given in Figure 1.20.

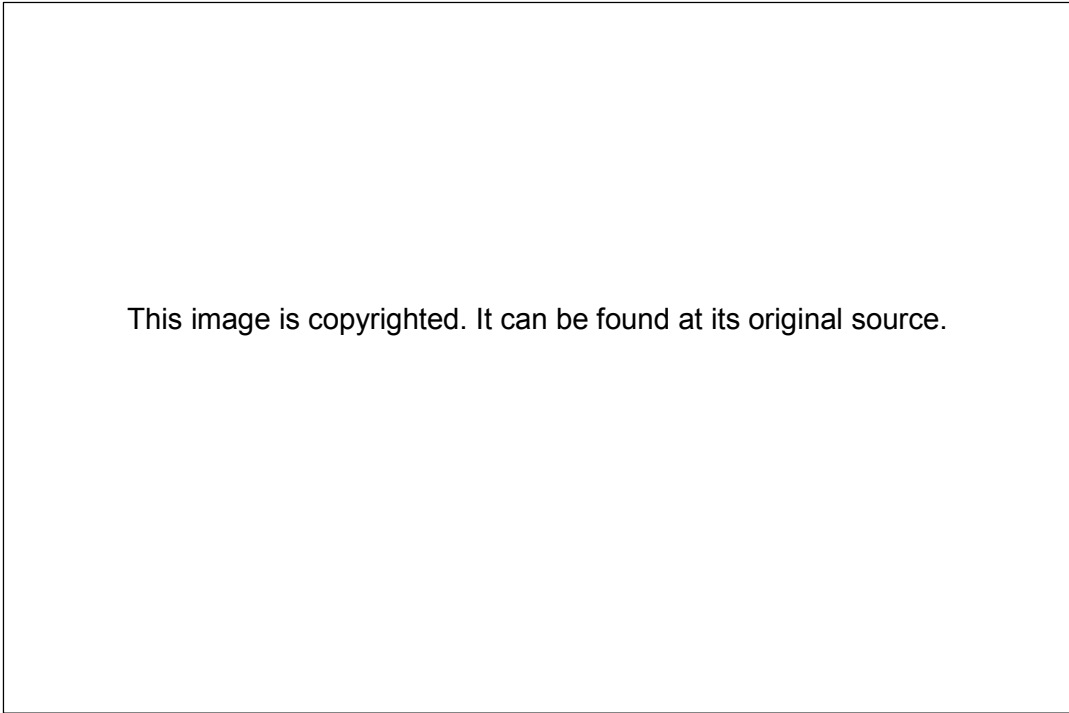
## 1.5 Quantification

A standard <sup>1</sup>H MRS spectrum acquired in the human brain using straightforward localisation sequences at short TE contains a significant amount of biochemical information. Once the raw data has been appropriately and sufficiently processed and has passed quality control metrics (up until this point in the experiment pipeline), it can then be used for the quantification of the concentration of the molecules that were successfully detected by the acquisition. Historically, quantification involved manually estimating the area underneath spectral peaks. Modern computing has significantly simplified and optimised this process, however. In this section the theoretical principles of spectral quantification will be laid out. Firstly, however, the molecules detectable by <sup>1</sup>H MRS in the brain will be briefly discussed.

### 1.5.1 Brain Metabolites

One of the chief advantages and unique aspects of MRS in comparison to other neuroimaging modalities is its ability to detect, noninvasively, the chemical signatures of a number of molecules in the living brain. These molecules have a plethora of functions in mammalian physiology but it is standard to refer to all resonances detectable by MRS as metabolites (even though not all are involved in metabolism in the strictest sense). Approximately 18+ metabolites can be detected in the in vivo rodent brain using short-echo <sup>1</sup>H MRS at ultra high-field. An example of the resonances of these metabolites acquired in vivo in the rat brain at 14.1 T and their role in brain function is shown in Figure 1.21. Assuming good  $B_0$  homogeneity and the employment of optimised acquisition protocols, a similar number of metabolites can be detected in the living human brain with short-echo methods. A list of human brain metabolites detectable by <sup>1</sup>H MRS and their typical in vivo concentration levels are provided in Table 1.1. Although a large number of molecules make up the typical in vivo neurochemical profile, with each providing an insight into animal physiology or biochemistry, the sensitivity of <sup>1</sup>H MRS is limited to the detection of metabolites with intrinsic concentrations greater than 0.5–

1 mM. In addition, certain molecules are invisible to MRS due to their spins being rotationally immobile, which causes their transverse relaxation times to be very short. Thus, molecules such as serotonin, dopamine, DNA and molecules bound to macromolecular structures cannot be detected by <sup>1</sup>H MRS.



This image is copyrighted. It can be found at its original source.

**Figure 1.21** *In vivo* <sup>1</sup>H MRS spectrum acquired at 14.1 T in the rat hippocampus. Individual brain metabolites are numbered and their role in brain physiology is indicated. Reproduced from Duarte et al. (2012).

**Table 1.1** Prototypical neurochemical profile of human brain metabolites with corresponding *in vivo* concentrations (mM). Adapted from Duarte et al. (2012).

Alanine (Ala)	0.3
Ascorbate (Asc)	1.4
Aspartate (Asp)	2.1–3.1
Phosphorylcholine (PCho)	–
Glycerophosphorylcholine (GPC)	–
PCho + GPC <sup>a</sup>	0.9–1.1
Creatine (Cr)	3.2–5.8
Phosphocreatine (PCr)	2.2–4.5
$\gamma$ -Aminobutyric acid (GABA)	1.3–2.5
Glutamine (Gln)	1.6–2.2
Glutamate (Glu)	8.9–12.8
Glutathione (GSH)	1.1–1.4
Glycine (Gly)	1.2
Glucose (Glc)	1.4–2.2
<i>myo</i> -Inositol (mI)	4.9–5.7
<i>scyllo</i> -Inositol (sI)	0.3–0.4
Lactate (Lac)	0.5–0.7
<i>N</i> -Acetylaspartate (NAA)	11.0–13.5
<i>N</i> -Acetylaspartylglutamate (NAAG)	1.0–1.1
Phosphorylethanolamine (PE)	1.6–2.8
Taurine (Tau)	1.3–3.3

<sup>a</sup>The choline-containing compounds PCho and GPC are typically grouped together into a single concentration measurement.

### 1.5.2 Basic Principles of Quantification

The magnitude of the NMR signal is determined by the macroscopic magnetisation at thermal equilibrium  $M_0$ . Since macroscopic magnetisation is proportional to the number of spins in the sample as defined by Eq. [1.14], and the number of spins corresponds to the number of detected molecules,  $M_0$  is therefore directly proportional to the concentration of the species in question. For this reason NMR spectroscopy can in principle be called a quantitative imaging method. Taken

together it can be said that in theory the signal for a metabolite M ( $S_M$ ) is proportional to the number of nuclear spins such that

$$S_M = kn_M \quad [1.37]$$

where  $S_M$  is the signal originating from the metabolite in question,  $k$  is a global constant of proportionality that reflects several complex factors that modulate  $S_M$ , such as RF coil loading and receive gain, and  $n_M$  is the number of spins belonging to the metabolite (or the number of moles of the molecule). From this the molar concentration of the metabolite ( $C_M$ ) is given by

$$C_M = \frac{n_M}{V} \quad [1.38]$$

where  $V$  is the volume of the tissue being sampled (i.e., the size of the VOI). When expressing concentration in terms of signal units Eq. [1.38] becomes

$$C_M = \frac{S_M}{kV} \quad [1.39]$$

These seemingly straightforward equations are in actuality a grand simplification of the actual relationship between the NMR signal and the biochemical concentration of a given metabolite. This is because the signal that is detected by the MRI scanner is only an indirect measure. The detected NMR signal is not a direct measurement of  $M_0$  but is rather a measurement of transverse magnetisation in the form of an induced current (electromotive force) detected by the RF receiver coils. Various signal amplification steps (e.g., receiver amplifier gains) performed by the RF receiver hardware mean that a number of factors alter the metabolite signal  $S_M$  before it can be used offline for data processing and spectral quantification. Thus, the detected signal of a metabolite cannot be directly used to quantify the molar concentration as suggested by Eq. [1.39]. As will be discussed in the next section, the signal must first be calibrated in one manner or another to be able to derive a meaningful biochemical measurement.

### 1.5.2.1 Signal calibration

When metabolite concentrations are described in biochemical units such as mmol L<sup>-1</sup>, mM (which refer to molarity) or  $\mu\text{mol g}^{-1}$  (which refers to molality), the quantified concentration is taken to be absolute. In truth, concentrations quantified in this manner are not absolute in the true sense of the term. This is because certain factors that modulate the NMR signal are either very challenging to measure (e.g., the physical and electrical characteristics of the RF coils) or virtually impossible to

directly measure in vivo (e.g., the amount of RF energy that is able to enter the VOI located in the brain or the proportion of nuclear spins that are invisible to detection). Hence, to be truly defined in absolute terms,  $S_M$  would be properly expressed as

$$S_M = k_G(p, s, \psi)k_T(p, s, \psi, r, f_M)k_S(p, s, r)R_M(T_{1,M}, T_{2,M}, \psi)N_{AV}VC_M \quad [1.40]$$

This complex equation expands the global proportionality constant  $k$  into more meaningful factors (Alger, 2010). The term  $k_G$  refers to the arbitrary receive gain that the MRI scanner applies to the RF signal for the purposes of converting the analogue signal into a digital format. Receive gains will be dependent on the participant ( $p$ ), the scanner system ( $s$ ) and the pulse sequence ( $\psi$ ).  $k_T$  is a factor relating to how efficiently the transmitter coil and pulse sequence are at exciting the spins of metabolite  $M$ . This will of course be determined by the features of the pulse sequence  $\psi$ , including characteristics of the RF pulses (waveform,  $B_1$  amplitude, phase, etc.), localisation strategy, OVS and water suppression. In addition, since the metabolite will have a particular frequency ( $f_M$ ) that the transmitter frequency must excite,  $k_T$  is also dependent on influences from frequency offsets caused by spatial variations in  $B_0$  homogeneity ( $r$ ). All these influences will also vary from participant to participant and from scanner to scanner.  $k_S$  represents the sensitivity of the scanner RF coils to detect the NMR signal in the brain. The origin of the signal, the location of the RF coils in relation to this and the build details of the coil system all have an influence on this. An additional factor that will modulate  $S_M$  is the longitudinal and transverse relaxation of the metabolite ( $R_M$ ). Signal attenuation by relaxation effects remains one of the most active areas of research in absolute spectral quantification. The difficulties arise from the fact that  $T_1$  and  $T_2$  relaxation values should ideally be measured on a per-subject basis using the pulse sequence employed to collect the data of interest. Accounting for relaxation is important in absolute quantification given that individual metabolites will differ in their  $T_1$  and  $T_2$  time constants. Moreover, the pulse sequence used will complicate things due to modulation in transverse magnetisation by the RF pulses and by the effects of  $J$ -evolution (in the case of scalar-coupled metabolites). Finally, the number of FID averages acquired ( $N_{AV}$ ) is an important consideration in signal quantification as it directly affects the SNR of the signal. Increasing the number of averages will reduce the noise in the signal, which would otherwise hamper the robustness of spectral quantification.

Obtaining values for every variable just described is, of course, unreasonable, particularly in a clinical setting. Clearly, then, the aim of quantification is far more complex in practice than in principle. Nevertheless, the determination of some of the factors in Eq. [1.40] can be avoided by the use of a concentration reference. Such a reference refers to a species of known concentration that is detected either external or internal to the VOI. Internal and external concentration referencing is now described.

### 1.5.2.2 Internal concentration reference

Internal concentration referencing refers to the use of an endogenous concentration reference such as tissue water, *N*-acetylaspartate (NAA) or creatine (Cr). Since the reference signal is acquired in the exact same way as the metabolites of interest, the signal attenuation factors  $k_G$ ,  $k_T$  and  $k_S$  are exactly the same. Therefore, many of the factors described in the previous section will cancel out upon division of the two signals. Eq. [1.40] then becomes

$$\frac{S_M}{S_{ref}} = \frac{R_M(T_{1,M}, T_{2,M}, \psi) N_{AV,M} C_M}{R_{ref}(T_{1,ref}, T_{2,ref}, \psi) N_{AV,ref} C_{ref}} \quad [1.41]$$

where  $S_{ref}$ ,  $R_{ref}$ ,  $N_{AV,ref}$  and  $C_{ref}$  are the signal, relaxation attenuation factor, number of signal averages and concentration of the reference, respectively. When the concentration of the reference is known or assumed, Eq. [1.41] can be rearranged to give the concentration of the metabolite:

$$C_M = \frac{S_M R_{ref}(T_{1,ref}, T_{2,ref}, \psi) N_{AV,ref}}{S_{ref} R_M(T_{1,M}, T_{2,M}, \psi) N_{AV,M}} C_{ref} \quad [1.42]$$

When using an internal reference such as NAA or Cr,  $C_M$  can be expressed in absolute terms if the concentration of NAA or Cr is assumed from literature values. This approach can be simplified even more by expressing the measurement in relative terms instead of absolute terms. That is, by simply measuring the signal area (or integral) of, for example, choline (Cho) and dividing it by the signal area of NAA (i.e., Cho/NAA), the (nominal) concentration of Cho then becomes relative to the (nominal) concentration of NAA. Relative quantification has the advantage of being the most straightforward of quantification approaches, dispelling the need to make complicated corrections. Note, however, that strictly speaking separate corrections for relaxation for the metabolite and the reference must still be made given that relaxation times will differ between the two. For scalar-coupled resonances that experience *J*-evolution this becomes even more crucial. Nonetheless, there are also

some disadvantages. While in theory NAA and Cr are stable in their intrinsic concentration, this may not necessarily be true in disease states. Additionally, a change in a relative concentration could mean that the metabolite concentration has altered, the reference concentration has altered or both have altered. Alternatively, the relaxation of either may have changed. An inappropriate conclusion could therefore lead to incorrect theoretical interpretations of research results or, more seriously, incorrect clinical diagnosis. Moreover, relative quantification may be less reliable than absolute quantification (Schirmer and Auer, 2000).

Unlike referencing using endogenous metabolites, internal tissue water can be used for more robust absolute quantification. The water resonance can be easily detected by removing the water suppression modules that precede the localisation pulse sequence. The intrinsic water concentration is then assumed to be ~55,000 mM, replacing  $C_{ref}$  in Eq. [1.42]. The advantages of using water for absolute quantification include its very high SNR (only a few unsuppressed water scans need to be acquired), the ease with which water  $T_1$  and  $T_2$  relaxation times can be determined and its well-characterised intrinsic content in cerebral tissue (Christiansen et al., 1997; Ernst et al., 1993; Kreis et al., 1993). However, caution must be taken when using internal tissue water in disease states as pathology may have a dramatic effect on either the intrinsic tissue water content and/or relaxation times. Another issue is that of partial volume effects. This refers to the fact that a spectroscopic VOI is not composed of homogenous tissue compartments. Longitudinal and transverse relaxation times and MR visibility of tissue water differ markedly between grey and white matter (de Graaf et al., 2006; Ernst et al., 1993; Stanisiz et al., 2005; Wansapura et al., 1999). Thus, the water resonance detected in a VOI composed of certain fractions of grey and white matter will have observed  $T_1$  and  $T_2$  relaxation times and visible water content weighted by the composition of the VOI's tissue content. The effect of partial voluming on the absolute quantification of GABA is dealt with more extensively in Chapters 3 and 4. Despite the methodological considerations that need to be taken into account, calibrating the spectral signal using an internal tissue water reference remains one of the most popular quantification approaches in <sup>1</sup>H MRS.

### 1.5.2.3 External concentration reference

There are in general two approaches to calibrating the NMR signal using an external concentration reference. The first is where a phantom or vial with a solution of known concentration is placed within scanner bore with the participant near or within the RF receiver coil during data acquisition. Since the RF coils are loaded in the same manner for both the metabolite and reference scans, many of the factors due to the physical and electrical characteristics of the coils are assumed to be equal for both signals. The second approach is called the phantom replacement method. Like the aforementioned approach, here a phantom with known concentration is used as a reference. The key difference is that the reference signal is detected before or after the participant's scan using a spherical phantom with a volume equal in size and position to the VOI.

In the end, the choice of which quantification method or which endogenous reference to use lies on several factors, including the necessity for unambiguous differentiation between two concentrations (such as between healthy and disease states or between two groups), available time and expertise (absolute quantification requires more time spent on acquiring a well-defined reference signal and a sufficient degree of knowledge regarding appropriate methodology and potential pitfalls) and the kinds of data that can be reliably used. In certain instances simple relative quantification is perfectly valid and sufficient, whereas in others the validity of the experiment or clinical diagnosis is critically reliant on obtaining measurements in absolute biochemical units. The approach chosen in this thesis was that of absolute quantification using an internal tissue water reference as this allows <sup>1</sup>H MRS to be considered a truly distinctive quantitative imaging modality.

### 1.5.3 Prior Knowledge

The previous sections illustrate the non-trivial nature of signal quantification in MRS. Fortunately, the core methodology of quantification can be aided by the fact that many of the physical and biochemical properties of NMR resonances and metabolites are known or can be predicted prior to data acquisition. For instance, quantum mechanics imposes well-understood rules regarding *J*-coupling constants, peak splitting and the number of peaks per resonance. Moreover, properties such as transverse relaxation rates will be virtually identical for each resonance corresponding to the nuclear spins in a given molecule and can be measured as part

of the data acquisition process or assumed from literature values. Such prior knowledge can for example be used to detect metabolites of lower concentration that are usually overlapped by the more intense signals of metabolites of higher concentration (such as by distinguishing the known chemical shift of each). Prior knowledge is used to create basis sets of every metabolite that is theoretically detectable by conventional MRS. Basis sets that include more available information regarding the physical and biochemical characteristics of a given dataset invariably improve signal quantification (Hofmann et al., 2002; Mierisová et al., 1998; Ratiney et al., 2005; Slotboom et al., 1998; Vanhamme et al., 1997). It is important, however, to avoid biasing the mathematical procedure that is used to fit model functions to data. Therefore, hard or soft constraints on prior knowledge are usually placed on the model parameters to minimise bias. The use of prior knowledge has become a norm in spectral quantification partly thanks to the implementation of product operator formalism—a quantum mechanical method of numerical simulation that very accurately characterises nuclear spin systems (see Chapter 7 and Appendix B)—in many of the common analysis software tools. Programmes that can simulate NMR spectra include GAMMA (Smith et al., 1994), QUEST (Ratiney et al., 2005) and FID-A (Simpson et al., 2015).



## **2. $\gamma$ -Aminobutyric Acid: From Neurobiology to Applications in $^1\text{H}$ MRS**

### **2.1 Summary**

In this chapter, overviews of the neurobiology and biosynthesis of GABA are given. It will be shown how GABA has various roles beyond those concerned with synaptic neurotransmission. GABAergic inhibition, the most important function of GABA, is discussed at length. Following these overviews, the MRS of GABA is discussed, with the focus set on the detection of the GABA NMR signal by *J*-difference editing. The major issue of signal contamination by macromolecules is laid out. Finally, a concise review of the applications of  $^1\text{H}$  MRS of GABA in basic and clinical neuroimaging is presented. This review will attempt to demonstrate how GABA has been identified as a correlate in a wide variety of behavioural, cognitive, neurophysiological, neuropsychiatric and neurological domains.

## 2.2 Neurobiology and Neurophysiology

$\gamma$ -Aminobutyric acid (GABA) is the major inhibitory neurotransmitter in the mammalian brain that was first discovered by Eugene Roberts and Sam Frankel (1950). Although chemically it is an amino acid, it is neither considered an  $\alpha$ -amino acid nor is it involved in the formation of proteins. Along with the excitatory neurotransmitter L-glutamic acid (or glutamate, Glu), GABA's traditional function is in maintaining the excitation–inhibition balance of neuronal synaptic transmission (McCormick, 1989). This is a simplification, however. In actuality GABA's major functions can be separated into functions involved with neurotransmission (tonic and phasic GABAergic inhibition, hyperpolarisation) and functions involved with metabolism (GABA to Glu/glutamine cycling, neuronal energy consumption). The latter will be discussed first, followed by an overview of the former.

### 2.2.1 GABA: Neurotransmitter, Metabolite and More

Beginning in the presynaptic GABAergic neuron (Figure 2.1), GABA is first synthesised through decarboxylation of Glu by the enzyme glutamate decarboxylase (GAD), which exists in two isoforms: GAD<sub>65</sub> and GAD<sub>67</sub>. GAD<sub>65</sub> is predominantly found in axon terminals while GAD<sub>67</sub> is more widely distributed in the neuronal environment (Esclapez et al., 1994; Kaufman et al., 1991). It has been shown that both isoforms are generated by two distinct genes (Erlander et al., 1991). GABA is then transported in vesicles by vesicular GABA transporter (VGAT) (Jin et al., 2003; McIntire et al., 1997) and released into the synapse via exocytosis. Once in the synaptic cleft GABA either binds to GABA receptors in the postsynaptic neuron or is reuptaken by high-affinity sodium- and chloride-dependent protein GABA transporters (GAT) back into the presynaptic neuron or into neighbouring astrocytes. Four homologous types of GAT are known to exist, namely GAT-1, GAT-2, GAT-3 and BGT-1 (Borden, 1996; Guastella et al., 1990). A lot of interest has been placed on GAT as their function is not simply to just clear GABA from the synaptic cleft but to also maintain the dynamic equilibrium of neuronal excitability, thus making their function important to tonic inhibition (which is further discussed in the next section) (Bernstein and Quick, 1999; Richerson and Wu, 2003). This is achieved by the ability of GAT to spontaneously reverse its reuptake of GABA from the extracellular environment (Wu et al., 2003; Y. Wu et al., 2007). Moreover,

This image is copyrighted. It can be found at its original source.

**Figure 2.1** Biosynthesis of GABA in the presynaptic GABAergic neuron and a neighbouring astrocyte (glial cell). See text for details. GAD = glutamate decarboxylase. VGAT = vesicular GABA transporter. GAT = GABA transporter. GABA-T = GABA transaminase. TCA = tricarboxylic acid cycle. PAG = phosphate-activated glutaminase. GABA(A)R = GABA<sub>A</sub> receptor. GABA(B)R = GABA<sub>B</sub> receptor. Reproduced from Rae (2014).

exogenous increases in GABA uptake by facilitation of GAT activity by GABA analogues has been shown to lead to a higher degree of anticonvulsant activity (Bolvig et al., 1999).

When reuptaken into astrocytes, GABA is not directly available for synaptic neurotransmission but instead undergoes further catabolism, whereby it enters the so-called GABA shunt (Balázs et al., 1970). Here in the astrocytic mitochondria the enzyme GABA transaminase (GABA-T) converts GABA into succinic semialdehyde (SSA) while stoichiometrically converting  $\alpha$ -ketoglutarate to Glu (Martin and Rinvall, 1993). GABA-T activity is aided by the cofactor pyridoxal phosphate, which is also involved in the enzymatic mechanisms of GAD in presynaptic neurons (Tillakaratne et al., 1995). SSA is then further oxidised by the enzyme succinic semialdehyde dehydrogenase to become succinic acid. From here succinic acid enters the tricarboxylic acid cycle. This particular step is significant because it shows that GABA biosynthesis is directly involved in the energy

metabolism of neurons. Although a full discussion of this is beyond the scope of this thesis, it will be noted that <sup>13</sup>C MRS has provided *in vivo* evidence that GABAergic neurons account for ~18% of total neuronal oxidative metabolism (Hyder et al., 2006; Patel et al., 2005). Since GABA cannot be synthesised in the astrocytes due to a lack of GAD, Glu is catabolised into glutamine (Gln) by another enzyme, glutamine synthetase, which is found only in astrocytes (Martinez-Hernandez et al., 1977; Norenberg and Martinez-Hernandez, 1979). Gln is subsequently exported into the extracellular environment and uptaken by the presynaptic GABAergic neuron. Here it is converted back into Glu by phosphate-activated glutaminase (Curthoys and Watford, 1995), thereby completing the metabolic cycle. The preceding summary of GABA biosynthesis succinctly demonstrates that GABA is not just a classical neurotransmitter but also acts as a metabolite in a strict biological sense (as opposed to in the nonspecific spectroscopic sense), having a role in both GABA/Glu/Gln cycling and brain energy metabolism.

It is believed that only a fraction of total GABA in neurons is available for synaptic activity (Rae, 2014). The transient of concentration change of synaptic GABA is incredibly brief, estimated to be on the order of < 500 μs (Farrant and Nusser, 2005; Mozrzymas, 2004; Mozrzymas et al., 2003). The rest of GABA is dedicated to metabolism and is likely found in large concentration in metabolic pools within the neuronal and astrocytic cytoplasm (Dericicoglu et al., 2008; Hanstock et al., 2002; Rae et al., 2009). Moreover, the two isoforms of GAD appear to have distinct roles in GABA synthesis. Synaptically localised GAD<sub>65</sub> is theorised to preferentially synthesise vesicular GABA (Asada et al., 1996; H. Wu et al., 2007), while the more widespread GAD<sub>67</sub> isoform is possibly more directly involved with non-vesicular GABA synthesis and release (Asada et al., 1997; Mason et al., 2001; Soghomonian and Martin, 1998). Approximately half of total GABA concentration is hypothesised to be produced by GAD<sub>67</sub> activity (Patel et al., 2006), with GAD<sub>65</sub> displaying a much quicker turnover (Battaglioli et al., 2003). Thus, pharmacologically challenging GAD activity represents an interesting avenue to pursue with *in vivo* <sup>1</sup>H MRS in humans in order to better understand the biochemical origin of the GABA NMR signal. Indeed, one recent study has shown that inhibition of GAD activity by 3-mercaptopropionate resulted in decreased GABA concentration as measured by 9.4 T <sup>1</sup>H MRS in rat brain (Waschkies et al., 2014).

Further examples of the integration of neuropharmacology and MRS of GABA are given in Section 2.4.4.

At the heart of neurotransmission and GABAergic synaptic activity are the major GABA receptors GABA<sub>A</sub> and GABA<sub>B</sub>. GABA<sub>A</sub> is an ionotropic receptor that acts upon GABA binding through a ligand-gated chloride ion channel. GABA<sub>A</sub> receptors have at least five known subunits— $\alpha$ ,  $\beta$ ,  $\gamma$ ,  $\delta$  and  $\epsilon$  (Olsen, 2002)—and have binding sites for benzodiazepines, barbiturates and picrotoxin (Olsen, 1982). It has also been noted that a proportion of GABA<sub>A</sub> receptors are found extrasynaptically (Belelli et al., 2009). Furthermore, synaptically localised GABA<sub>A</sub> receptors are believed to mediate phasic inhibition, while extrasynaptic GABA<sub>A</sub> receptors give rise to persistent tonic inhibition (Mody, 2001). GABA<sub>B</sub> receptors are distinct from their GABA<sub>A</sub> counterparts in that they are metabotropic in nature, meaning that they are coupled to G-protein receptors. Activation of GABA<sub>B</sub> receptors leads to the release of G $\beta\gamma$  subunits that inhibit calcium ion channels and activate potassium ion channels (Gähwiler and Brown, 1985; Mintz and Bean, 1993). Similar to the subunits of GABA<sub>A</sub> receptors, GABA<sub>B</sub> receptors are known to exist as two heteromeric subtypes: GABA<sub>B1</sub> and GABA<sub>B2</sub> (Kaupmann et al., 1998). There is also evidence to suggest that they play a role in modulating the calcium ion signals of the Glu receptor *N*-methyl-D-aspartate (NMDA) (Chalifoux and Carter, 2011). Importantly, this demonstrates that GABA has an additional role as a neuromodulator.

### 2.2.2 GABAergic Inhibition

As already stated, GABA's chief role is that of an inhibitory neurotransmitter that regulates the excitation–inhibition balance. The exact mechanisms of GABAergic inhibition are significantly complex. Indeed, even defining GABAergic inhibition proves to be problematic. As Bernard et al. (2000) rightly highlight, GABAergic inhibition is a term difficult to define for three reasons. First, GABA activity does not only reduce the firing of an inhibited neuron; there is also strong evidence that GABA can have an excitatory role (Gulledge and Stuart, 2003; Marty and Llano, 2005; Stein and Nicoll, 2003). Second, the degree of GABA activity (as measured by the hyperpolarisation of the postsynaptic neuron) is dependent on a multitude of variables, primarily as a result of the different subunits and properties of the aforementioned GABA receptors and the manner in which they release GABA.

Third, there are many different classes of GABAergic interneurons that are characterised by distinct neuroanatomical pathways and electrophysiological patterns (for reviews see Gupta et al., 2000; Markram et al., 2004). In addition to these points, GABAergic inhibition is further complicated by the apparent functional divergence of interneurons into feedforward and feedback microcircuits that are distinct in the net effect they have on postsynaptic activity (Tepper et al., 2008, 2004).

That said, however, GABAergic inhibition can still be classed into two complementary types: phasic and tonic (for a review see Farrant and Nusser, 2005). Generally speaking, phasic inhibition refers to GABAergic activity that is initiated by synaptic transmission that comes about by the propagation of electrochemical action potentials from presynaptic terminals. This leads to the vesicular transport of GABA by VGAT and eventual exocytosis into the synaptic cleft. Near synchronous binding with ionotropic GABA<sub>A</sub> receptors on the postsynaptic dendrite results in the influx of chloride ions, (usually) causing hyperpolarisation in the postsynaptic neuron. This hyperpolarisation is characterised by inhibitory postsynaptic currents that last for 10–100 ms (Edwards et al., 1990; Mody et al., 1994). These currents are followed by the classical inhibitory postsynaptic potential. Arguably, this type of inhibition is the inhibition one thinks of when talking about GABAergic control of neuronal responses. However, it is now known that GABAergic activity also results from neurotransmission outside of the synapse. It is believed that GABA release and uptake that occurs extrasynaptically via high-affinity ionotropic GABA<sub>A</sub> and metabotropic GABA<sub>B</sub> receptors is responsible for so-called tonic inhibition (Brickley et al., 1996; Mann et al., 2009; Semyanov, 2002; Wall and Usowicz, 1997). This form of inhibition is characterised by a slower but continuous current (Semyanov et al., 2004). Through “spillover” effects during multivesicular release, a degree of GABA will remain in the extracellular space (Rossi and Hamann, 1998; Telgkamp et al., 2004). This ambient GABA, found in nano- to micromolar concentrations (Lerma et al., 1986), is thought to contribute to persistent activation of extrasynaptic GABAergic receptors.

What are the functional properties of phasic and tonic inhibition? Aside from preventing pathological over-excitation, there is considerable evidence that phasic GABAergic inhibition is the mechanistic source of synchronous neuronal oscillations, predominately in the gamma frequency band (30–90 Hz) (Bartos et al.,

2007; Buzsáki and Wang, 2012). GABAergic interneurons work to synchronise the firing rates of large populations of interconnected neurons through active hyperpolarisation of action potentials and refined modulation of the corresponding spatiotemporal properties of excitatory and inhibitory neurons (Cobb et al., 1995; Jonas et al., 2004; Somogyi and Klausberger, 2005). While a full discussion of gamma oscillatory activity and its relation to GABA is beyond the scope of this thesis, it will be noted that the prevailing theory behind the purpose of these oscillations is in the critical step of the encoding of information (Mann and Paulsen, 2007; Singer, 1996). This would mean that GABA plays a far more important role than simply in preventing over-excitation. The functional importance of tonic inhibition is distinct from phasic inhibition. Firstly, it appears that decreasing the tonic conductance, or the “holding current”, of a given GABAergic neuron by pharmacological perturbation reduces the current necessary to achieve a certain firing rate, thereby increasing the neuron’s overall excitability (Brickley et al., 1996; Chadderton et al., 2004; Hamann et al., 2002). This can be described as a leftward shift in the input–output function of the relationship between current input and firing rate frequency. Secondly, it has been shown that tonic inhibition depends on the level of excitatory input, which leads to a multiplicative modulation in the input–output function (Chance et al., 2002; Mitchell and Silver, 2003). Thus, the function of tonic inhibition appears to be in gain control of global neuronal excitability (Semyanov et al., 2004). Given these mechanisms, tonic inhibition has also been shown to directly impact on the robustness of synchronous oscillations (Mann and Mody, 2010; Vida et al., 2006). The presence of such a relationship suggests that phasic and tonic inhibition act interdependently. Perhaps this is unsurprising given the close biosynthetic relationship between the synaptic and metabolic GABA pools described in the previous section.

The effect of GABAergic inhibition, and GABAergic activity in general, on global neuronal responses is important to consider as they are tightly intertwined with brain energy consumption (Buzsáki et al., 2007), making them key components in the origin of a host of neuroimaging signals, including the blood oxygenation level-dependent (BOLD) signal and cerebral blood flow (CBF) (Lauritzen et al., 2012). As stated earlier, GABA metabolic turnover is known to contribute to approximately 20% of total neuronal oxidative metabolism (Hyder et al., 2006; Patel

This image is copyrighted. It can be found at its original source.

**Figure 2.2** *The neurophysiological origin of the BOLD signal. The model shows that the BOLD signal comes about from contributions from both excitatory and inhibitory neuronal activity. These respectively lead to neuronal energy metabolism in the form of glycolysis, the glycogen shunt and oxidative phosphorylation. CBF is assumed to arise independently of glucose and oxygen consumption. Adapted from Sotero and Trujillo-Barreto (2007).*

et al., 2005). There is also strong evidence that GABAergic interneurons release vasoactive substances that directly modulate the vasodilation and vasoconstriction of microvessels (Cauli and Hamel, 2010; Lecrux and Hamel, 2011), further demonstrating that GABA is integral to neurovascular coupling. Since the commonly detected BOLD signal is understood to arise from a complex dependency on CBF, glucose consumption and oxidative phosphorylation (Buxton et al., 2004; Raichle and Mintun, 2006), the fact that GABA appears to contribute to several of these underlying components of the neurovascular response makes properly understanding its function quite important to neuroimaging in general. However, the contribution of inhibitory activity to neurovascular signals remains an area of controversy as at least one prominent report showed that GABA does not appear to have a direct impact on the metabolic components of these signals (Chatton et al., 2003). Nonetheless, when taken as a whole there is sufficient evidence that naturally leads to the argument that (noninvasive) imaging of GABAergic activity (alongside

glutamatergic activity) constitutes a more mechanistically appropriate target for understating brain function. Indeed, it has become clear that the mechanistic pathways that lead to the formation of the BOLD signal should include both excitatory and inhibitory contributions alongside those from glucose and oxygen consumption (Figure 2.2). Although  $^1\text{H}$  MRS does not (yet) come with the same technical ease with which to capture the functional changes that occur in the brain in comparison to modern fMRI, there is sufficient rationale for further developing and exploiting the unique capabilities of MRS given that it is able to directly detect the molecular constituents of neuronal activity and energy metabolism.

## 2.3 Magnetic Resonance Spectroscopy of GABA

### 2.3.1 The GABA Spin System

The GABA molecule ( $\text{NH}_2\text{-}^4\text{CH}_2\text{-}^3\text{CH}_2\text{-}^2\text{CH}_2\text{-}^1\text{COOH}$ ) is traditionally described as having a weakly coupled  $A_2M_2X_2$  spin system with three pairs of magnetically equivalent nuclei.  $A_2$  denotes the 3.01 ppm GABA-H4 methylene ( $\text{CH}_2$ ) resonance,  $M_2$  denotes the 1.89 ppm GABA-H3  $\text{CH}_2$  resonance and  $X_2$  denotes the 2.28 ppm GABA-H2  $\text{CH}_2$  resonance (Figure 2.3). The subscripts refer to the two  $^1\text{H}$  nuclei that are attributed to each resonance. The carbonyl ( $\text{COOH}$ ) and amide ( $\text{NH}_2$ ) compounds are not MR-visible. The H4 and H3 and the H3 and H2 resonances are coupled, respectively. Thus, the rules of  $J$ -coupling dictate that the GABA-H4 and -H2 resonances each split into triplets since both are coupled to the GABA-H3 resonance. Theoretically, the GABA-H3 should split into a “quartet of doublets” because of its coupling to the four  $^1\text{H}$  nuclei in GABA-H4 and -H2. However, the  $J$ -coupling constants of the latter two are magnetically equivalent (i.e.,  $J_{AM} = J_{MX}$ ). Therefore, the quartet of doublets collapses into a quintet lineshape. This description is a simplification, however, as will now be explained.

The scalar coupling of the GABA  $\text{CH}_2$  groups gives rise to complex multiplet patterns. The simulated spectrum of the GABA spin system in Figure 2.3 shows that the GABA-H4 resonance at 3.0 ppm resolves as a triplet, as previously described. Strictly speaking, this is not true: this resonance is more properly two “doublet of doublets” rather than a triplet. This is because the two coupled vicinal<sup>†</sup> pairs of the

---

<sup>†</sup> In chemistry, vicinal is a term that refers to nuclei that are coupled by virtue of their bond with two atoms that are adjacent to each other (three total chemical bonds).

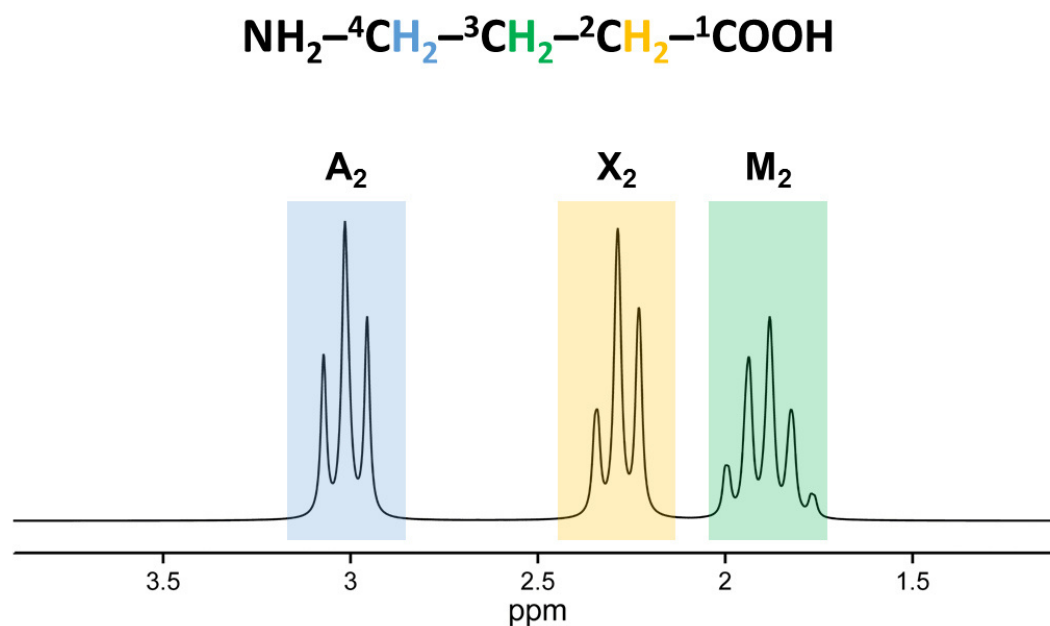


**Figure 2.3** The weakly coupled  $A_2M_2X_2$  NMR spin system of GABA. GABA's molecular structure is shown above the spectrum. The colours indicate the  $CH_2$  group that gives rise to its corresponding resonance in the spectrum.

<sup>1</sup>H nuclei in GABA-H4 and GABA-H3 are magnetically nonequivalent; that is,  $J_{AM} \neq J_{AM'}$  (see Near et al., 2012). The prime in  $J_{AM'}$  refers to the second <sup>1</sup>H nucleus in  $M_2$ . Therefore, GABA is more accurately described as having an  $AA'MM'XX'$  spin system, where each pair of letters denotes chemically (but not magnetically) equivalent nuclei (Kreis and Bolliger, 2012). By this notation the corresponding  $J$ -coupling constants should then include values for both the vicinal and geminal<sup>‡</sup> chemical bonds within the molecular structure. A complete table of the chemical shifts and  $J$ -coupling constants of the GABA  $CH_2$  resonances is provided in Table 2.1. In terms of the successive splitting of the GABA-H4 peak, because of the magnetic nonequivalence of its coupled nuclei, the resonance is in fact a superposition of two doublet of doublets. This distinction is important because assuming accurate  $J$ -coupling constants as part of the prior knowledge used in signal quantification may significantly improve the model fit (Near et al., 2012). For the sake of the simplicity, however, the GABA-H4 peak will be referred to as a triplet for the remainder of this thesis.

The lineshape of the GABA-H4 multiplet is made even more complex in the  $J$ -difference editing experiment as a result of the transition width, refocusing bandwidth and flip angle of the slice-selective refocusing pulses (Near et al., 2013b).

<sup>‡</sup> Geminal nuclei are coupled by one atom (two total chemical bonds).

**Table 2.1** Chemical shifts and coupling constants of the GABA spin system. From Near et al. (2013).

Spin	Chemical shift (in ppm)	Scalar couplings (in Hz) to:				
		H2'	H3	H3'	H4	H4'
H2	2.2840	-15.938	7.678	6.980		
H2'	2.2840		6.980	7.678		
H3	1.8880			-15.000	8.510	6.503
H3'	1.8880				6.503	8.510
H4	3.0130					-14.062
H4'	3.0130					

Moreover, it can be seen from Figure 2.3 that the GABA multiplets are asymmetric, with their outer peaks having different amplitudes. This demonstrates that strong coupling effects are present when the GABA spin system is detected at 3 T. These complexities in lineshape indicate that the GABA multiplets can only be adequately described by numerical simulations that take into account the quantum states of the GABA proton spins as well as the physical parameters of the RF pulse sequence. These simulations are based on a time-dependent density matrix that describes the physical state of proton spins in relation to chemical shift, scalar coupling and the interaction with external magnetic RF fields according to product operators (Sørensen et al., 1984). (See Appendix B for an overview of product operator formalism.) Through density matrix formalism, appropriate prior knowledge of  $J$ -coupling and predefined parameters of a given pulse sequence, the GABA spin system can be very accurately simulated (de Graaf and Rothman, 2001; Kaiser et al., 2008; Near et al., 2013b; Snyder et al., 2009). An implementation of density matrix formalism used in the FID-A toolbox was used to simulate the spectrum in Figure 2.3.

### 2.3.2 Detection of the GABA Signal

Detecting GABA with conventional NMR spectroscopy is challenging at field strengths below 7 T. In addition to being found in relatively low concentrations in the brain (~1–2 mM), the GABA resonances are overlapped by peaks of higher intensities, in particular the 3.0 ppm Cr resonance that has a chemical shift similar to the GABA-H4 resonance. Nevertheless, as a weakly coupled spin system GABA

can be detected in vivo through localised *J*-difference spectral editing. This was seminally demonstrated by Rothman et al. (1993). In the basic GABA-editing experiment two scans are performed. In the ON scan, spectrally selective editing pulses are applied to the 1.9 ppm GABA-H3 resonance. This has the effect of refocusing all the spins that are coupled to this resonance, in particular the 3.0 ppm GABA-H4 resonance as noted in the previous section. Any uncoupled resonances are unaffected and evolve as normal. In the OFF scan, the editing pulses are placed in such a fashion that they act as symmetric counterparts to the ON editing pulses, whereby the ON and OFF pulses are symmetrical about the water resonance at 4.7 ppm. In other words, the OFF editing pulses are placed far off resonance at 7.5 ppm. This symmetrical placement ensures that any magnetisation transfer effects that may occur on the water peak are nullified (see de Graaf et al., 1999; Leibfritz and Dreher, 2001). The GABA-H3 resonance and any spins coupled to it evolve as normal in this scan. The GABA-H4 peak at 3.0 ppm is then unambiguously resolved in the spectrum obtained from the difference between the ON and OFF scans, the so-called DIFF spectrum. Any peaks unaffected by the *J*-refocusing of the editing pulses, such as the high-intensity 3.0 ppm Cr resonance that overlaps the GABA-H4 peak, will be removed. Since the GABA-H4 and -H3 CH<sub>2</sub> resonances constitute a coupled A<sub>2</sub>M<sub>2</sub> spin system, the principles of *J*-coupling and *J*-evolution dictate that the centre peak of the GABA-H4 triplet will not experience any phase modulation in the spin echo experiment. Instead, partial editing can be achieved when the TE of the GABA-editing experiment is set to  $1/2J$ . This means that during the OFF scan the GABA-H4 triplet will display a “W” lineshape, with the two outer peaks being antiphase with the centre peak. The difference between the two scans will lead to a pseudo-doublet. In in vivo experiments, this pseudo-doublet will most often appear as a single-lobe Gaussian peak as a result of  $B_0$  inhomogeneity and line-broadening. A visualisation of the GABA-editing procedure is given in Figure 2.4.

The foregoing approach is most popularly implemented in localised SVS using a combination of PRESS and Mescher-Garwood (MEGA) frequency-selective refocusing, which can simultaneously suppress water and edit the GABA spin system by using double-banded Gaussian 180° frequency-selective refocusing pulses that selectively excite the 4.7 ppm water and 1.9 ppm GABA-H4 resonances (Mescher et al., 1998, 1996). A schematic of the MEGA-PRESS sequence is given in Figure 2.5. Although MEGA provides excellent water suppression, being

This image is copyrighted. It can be found at its original source.

**Figure 2.4** *J*-difference editing of GABA. **a:** In the ON scan, editing pulses are applied at 1.9 ppm to refocus the coupled GABA-H3 and -H4 resonances. All other resonances evolve as normal. In the OFF scan, the editing pulses are applied far off resonance, leading the coupled GABA resonances to evolve as normal. Subtracting the two scans removes all unwanted resonances and leaves the GABA-H4 peak at 3.0 ppm unambiguously resolved. Co-edited Glu + Gln (Glx), NAA and an MM resonance will also remain in the difference (DIFF) spectrum. **b:** Visualisation of the effect of GABA-editing on the 3.0 ppm GABA resonance lineshape in the ON, OFF and DIFF spectra. The Cr signal is not affected by the editing pulses and so is removed during subtraction. Reproduced from Mullins et al. (2014).

relatively insensitive to  $B_1$  inhomogeneities, MEGA-PRESS can also be successfully employed with the VAPOR sequence. Thanks to the efficiency of spectral editing by the MEGA method and the comparatively high SNR of PRESS, it has been relatively straightforward to detect GABA in vivo. This is in large part due to the more-or-less simple technical implementation of MEGA-PRESS and increasing standardisation of relevant methodology (for a review see Mullins et al., 2014).

Although conceptually simple, GABA-MRS methodology comes with a number of special challenges and considerations, on top of those that apply to MRS in general. Perhaps most important to the success of the experiment is the efficiency of the spectral editing procedure. Broadly speaking, editing efficiency refers to how much signal is resolved following spectral editing. For instance, the efficiency of

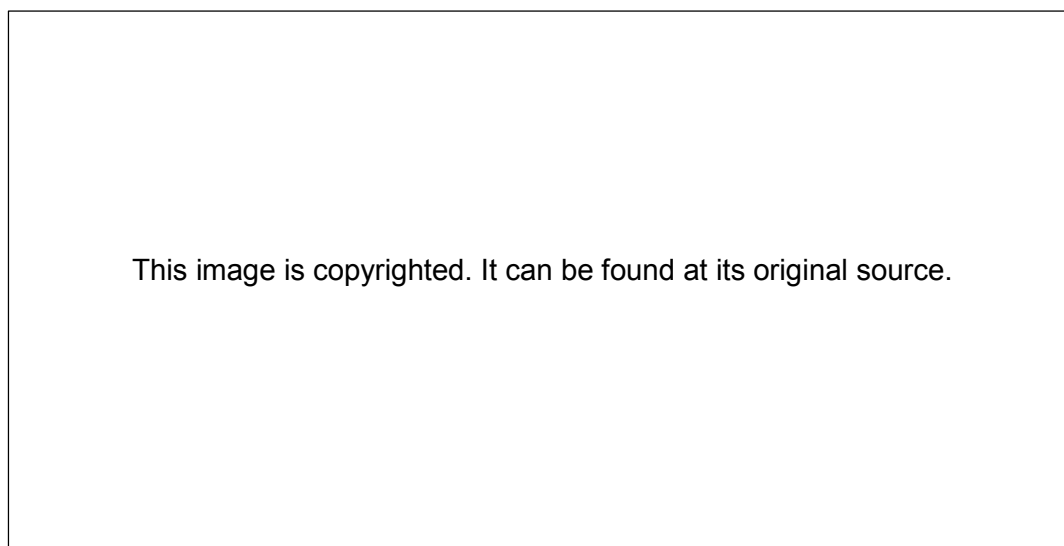


**Figure 2.5** Pulse sequence diagram for MEGA-PRESS. Two Gaussian frequency-selective  $180^\circ$  refocusing pulses are placed about the second PRESS  $180^\circ$  slice-selective refocusing pulse. These editing pulses selectively excite the GABA spins at 1.9 ppm, which are coupled to the GABA spins at 3.0 ppm. Magnetic field gradients for localisation are shown in white. Crusher gradient waveforms are in black. The  $G_1$ ,  $G_2$  and  $G_3$  gradient waveforms are used for MEGA-editing in this particular implementation. Reproduced from Mescher et al. (1998).

GABA-editing using the  $J$ -difference approach is theoretically 50% because only half of the total GABA signal in the NMR spectrum is present in the difference spectrum. This is result of the subtraction of the ON and OFF scans, where in the former the GABA-H4 peak is completely refocused, displaying an in-phase triplet, while in the latter the peak resolves as a W-like triplet with the outer peaks being anti-phase with the centre peak (Figure 2.4). The centre peak is removed during subtraction, meaning the pseudo-doublet in the DIFF spectrum constitutes only 50% of the total available signal (de Graaf and Rothman, 2001). Note that the 0.5 editing efficiency factor of GABA-edited MRS is only a theoretical approximation. Precise determination of the editing efficiency of a given sequence can only be determined through phantom experiments or with numerical simulations (Near et al., 2013b; Oeltzschner and Bhattacharyya, 2015). In Chapter 7, numerical simulations are used to determine the editing efficiency of GABA-MRS following specific modifications and modulations of the  $J$ -difference editing experiment.

### 2.3.2.1 Macromolecule contamination

In another sense, editing efficiency also refers to the specificity of the selective refocusing of coupled spins. A major limitation with GABA-editing is that a macromolecular (MM) resonance at 1.7 ppm (M4) coupled to another MM

This image is copyrighted. It can be found at its original source.

**Figure 2.6** *a: In vitro spectrum of the GABA spin system. b: In vivo spectrum of the macromolecular (MM) baseline with each of the nine MM resonances indicated. This was acquired using an inversion recovery method to null metabolite resonances. c: In vivo  $^1\text{H}$  NMR spectrum acquired at 9.4 T. The inversion frequency profile for a Gaussian frequency-selective editing pulse (grey) placed at 1.9 ppm shows that partial co-editing of the M4 resonance at 1.7 ppm will lead to contamination of the GABA signal at 3.0 ppm by signal from the coupled M7 resonance also at 3.0 ppm. Reproduced from de Graaf (2007).*

resonance also at 3.0 ppm (M7) is partially excited by the ON editing pulses that selectively excite the GABA-H3 spins at 1.9 ppm, leading to co-editing of the 3.0 ppm MM resonance. This is directly a result of the frequency bandwidth of the Gaussian editing pulses (Figure 2.6). To illustrate, at 3 T the frequency distance between the GABA-H3 and M4 resonances is  $\sim 22$  Hz. Typically, Gaussian MEGA-editing pulses are 16–20 ms long (given the limited available time in the MEGA-PRESS sequence); assuming a time-bandwidth product ( $R$ ) of 1.53, the corresponding frequency bandwidth is 76–95 Hz. This demonstrates that the ON editing pulses that excite the GABA-H3 spins when on-resonance will additionally excite the M4 spins to some extent. Thus, the GABA-H4 peak at 3.0 ppm in the difference spectrum contains a degree of MM contamination from the partially refocused M7 peak, which may account for up to 60% of the total GABA signal

(Aufhaus et al., 2013; Kegeles et al., 2007; Rothman et al., 1993). This significant problem of MM contamination remains one of the biggest flaws of GABA-MRS given that the quantified “GABA” concentration is not solely GABA but includes a large fraction of MM<sup>§</sup>, constituting a major confound in any study seeking to correlate GABA concentration with another measure or to observe differences in GABA levels between groups. This thesis seeks to address this perennial issue by the development of methodology to remove MM contamination in the GABA-edited signal, as now discussed.

One method that can be implemented to account for this contamination involves measurement of the MM baseline by nulling metabolites of interest through an inversion recovery technique (Behar et al., 1994; Hofmann et al., 2001; McLean et al., 2004). The method behind metabolite-nulling is based on the  $T_1$  relaxation differences between MM and metabolites. Since MM have substantially shorter  $T_1$  times in comparison to metabolites (de Graaf et al., 2006), an inversion pulse can be applied prior to excitation by conventional localised spectroscopy that will invert the longitudinal magnetisation of all excited spins. The transverse relaxation is then detected after a delay (the inversion time, TI). The MM spins return to  $M_0$  more quickly such that the signals from metabolites are nulled when their longitudinal magnetisation is zero. By performing several inversion recovery experiments where the TI is sufficiently varied, the optimal TI can be determined and used for measuring the MM baseline devoid of any metabolite resonances. In GABA-editing, this baseline can then be subtracted from a conventional difference-edited spectrum to remove residual MM (Terpstra et al., 2002). The disadvantages of this technique, however, include assumptions of  $T_1$  relaxation times of metabolites and MM (unless determined by direct measurement) and increased total acquisition time (both non-nulled and MM-only spectra need to be acquired, effectively doubling scanning time). In addition, subtraction of the MM baseline from the non-nulled spectrum will add noise to the MM-subtracted spectrum.

Alternatively, the issue with MM can be mitigated by using a symmetric editing-based suppression method (Henry et al., 2001). By simply placing OFF

---

<sup>§</sup> The GABA spectral peak also contains a fraction of signal arising from homocarnosine, a dipeptide of GABA and histidine that contains a GABA moiety. Thus, any concentration of GABA is strictly speaking an amalgam of GABA, homocarnosine and MM, unless steps are taken to separate the NMR signals from each.

editing pulses at 1.5 ppm instead of at 7.5 ppm, and keeping ON pulses at 1.9 ppm, the MM signal at 1.7 ppm is equally excited in both scans and thus the coupled MM resonance at 3.0 ppm is removed from the difference spectrum. Since hypotheses relating the measured GABA concentration to behaviour or pathology relate specifically to the GABA molecule, rather than to loosely defined “macromolecules”, a more specific measure of GABA is required for proper interpretation. The elegant symmetric suppression method has not been widely adopted as it requires editing pulses to be sufficiently selective so that the pulses placed at 1.5 ppm do not undesirably excite the GABA resonance at 1.9 ppm. This partial excitation of the GABA resonance in OFF sub-spectra would lead to a reduction in GABA signal in the difference spectrum. However, by increasing TE from the widely used 68 ms to 80 ms, more time is available in the acquisition sequence and the duration of editing pulses can be increased to 20 ms (Edden et al., 2012b). On some platforms it is possible to employ longer editing pulses whilst maintaining a TE of 68 ms (Aufhaus et al., 2013). This alteration provides better frequency selectivity of editing pulses, preventing unwanted suppression of the resolved GABA signal, while still correcting for MM. Symmetric MM suppression comes with its own set of challenges, however. In particular, the issue of the selectivity of the editing pulses arguably presents an even bigger concern than for standard editing given the proximity of the ON and OFF pulses to the M4 resonance at 1.7 ppm. This will be compounded by frequency drift in the  $B_0$  field. As noted earlier, this falls under the domain of editing efficiency. Frequency selectivity of the editing pulses and the problems that frequency drift cause with regard to the editing efficiency of symmetric suppression will be touched upon in Chapter 5 and investigated in detail in Chapter 7.

## **2.4 Applications and Correlates: A Concise Review**

It has been suggested that because of its fundamental role in the excitatory–inhibitory balance of neurotransmission, and because it is either present in or somehow indirectly associated with almost all neurons in the brain, GABA can be said to be involved in nearly every function of the central nervous system (Olsen, 2002). Perhaps, then, it should not be surprising that in recent years  $^1\text{H}$  MRS of GABA has brought a unique perspective to understanding the relationships between

brain function, behaviour, cognition and pathology. Thus, the focus of the following concise review will be on how MRS has contributed evidence to the specific hypotheses that state that GABAergic function underlies or is at least partly involved with particular aspects of psychiatric dysfunction, neuropathology, cognition, behaviour and haemodynamics in humans. Pharmacological interventions in MRS studies will also be discussed to highlight the role that GABAergic drugs have in elucidating the biochemical origins of the GABA NMR signal.

## **2.4.1 Clinical Applications**

### **2.4.1.1 Anxiety disorders**

There has been a theoretical drive towards a GABAergic hypothesis of anxiety disorders. Specifically, amounting evidence suggests that anxiety disorders are characterised by abnormalities surrounding benzodiazepine binding sites located on the GABA<sub>A</sub> receptor (Chang et al., 2003; Nutt and Malizia, 2001). Although there is more evidence of such abnormalities from other molecular imaging modalities, <sup>1</sup>H MRS has also contributed empirical evidence. Goddard et al. (2001) were the first to show that in unmedicated patients with panic disorder occipital GABA concentration was reduced. The group followed this up with a later study where they showed that patients had a blunted response to acute administration of the benzodiazepine clonazepam (Goddard et al., 2004). Healthy controls, on the other hand, showed a reduction in GABA levels. MRS-measured GABA deficits in panic disorder are also apparent in the anterior cingulate cortex (ACC) and the basal ganglia (Ham et al., 2007) but not the prefrontal cortex (Hasler et al., 2009). These results are somewhat contradicted by the findings by Long et al. (2013) who also found reductions in GABA in the ACC but not in the occipital lobe.

Currently, only one publication has reported an investigation of GABA levels in social anxiety disorder. Using CSI, Pollack et al. (2008) found that GABA was reduced in the thalamus of patients compared to controls, and that this difference was reduced following eight weeks of pharmacotherapy. More recently, groups have begun to inspect GABA abnormalities in obsessive compulsive disorder (OCD). A GABA-editing study from Simpson et al. (2012) reported that GABA was significantly reduced in the medial prefrontal cortex of patients with OCD but that this deficit did not extend to the dorsolateral prefrontal cortex (DLPFC). Moreover, it appears that infusion of the Glu NMDA receptor antagonist ketamine increases

GABA concentration in OCD patients over time (Rodriguez et al., 2015). Finally, in vivo GABA also appears to be abnormal in posttraumatic stress disorder based on several very recent MRS studies (Meyerhoff et al., 2014; Michels et al., 2014; Pennington et al., 2014; Rosso et al., 2014).

#### **2.4.1.2 Developmental disorders**

GABAergic dysfunction is thought to be a possible explanation for the social, cognitive and sensory deficits seen in autism spectrum disorder (ASD). This forms part of the excitation/inhibition balance theory of ASD (Pizzarelli and Cherubini, 2011; Rubenstein and Merzenich, 2003), whereby either over-excitation or under-inhibition leads to a hyperexcitable, poorly synchronised neural system. Although only a few studies have investigated in vivo GABA abnormalities with GABA-MRS, the consistent finding is of reduced GABA concentration in autistic individuals (Gaetz et al., 2014; Harada et al., 2011b; Kubas et al., 2012; Rojas et al., 2014). Moreover, a recent high-impact publication has demonstrated that GABA but not Glu is associated with perceptual dysfunction in ASD (Robertson et al., 2016).

In a similar vein, GABA-MRS has been able to detect GABAergic deficits in Tourette syndrome. Tinaz et al. (2014) found that GABA levels in the sensorimotor (SM) cortex of adults with Tourette syndrome were related to motor-related synchronous oscillatory activity in the same region, while Draper et al. (2014) reported that excitability of the supplementary motor area correlated with GABA concentration. Finally, there is also evidence that GABA is tied to vibrotactile sensory deficits in individuals with this syndrome (Puts et al. 2015). It was also demonstrated in this study that motor tic severity was strongly associated with SM GABA levels. GABA-MRS has also been employed in other neurodevelopmental disorders such as attention deficit/hyperactivity disorder (Edden et al., 2012a; Ende et al., 2016), complex motor stereotypy (Harris et al., 2015d) and Down's syndrome (Śmigielska-Kuzia et al., 2010).

#### **2.4.1.3 Epilepsy**

Of all neurological disorders epilepsy is perhaps the most tightly linked to the GABA system (Bradford, 1995), which arguably is not surprising given the anticonvulsant effects of many GABAergic drugs. Soon after the seminal publication by Rothman et al. (1993) demonstrating the use of localised *J*-difference–editing for in vivo

detection of GABA, several studies soon followed where GABA abnormalities in epilepsy were investigated using MRS. This has typically been in conjunction with modulation of GABA levels by pharmacological interventions using antiepileptics. The Rothman et al. study showed that administration of the antiepileptic vigabatrin increased GABA levels in epileptic patients, thereby demonstrating the effect of such drugs on endogenous GABA. This finding was replicated by Verhoeff et al. (1999) using the same drug and by Doelken et al. (2010) using levetiracetam. There is indication that the level of GABA is associated with both recency and frequency of seizures, and that epileptic patients with better seizure control have more GABA (Petroff et al., 1996c). This, however, does not appear to be the case with juvenile myoclonic epilepsy (Petroff et al., 2001a). For idiopathic generalised epilepsy, although no difference in endogenous GABA is apparent in the frontal lobe when using conventional MRS (Simister et al., 2003a), GABA-editing recently has revealed that there are significant differences in frontal GABA (Chowdhury et al., 2015). Additionally, GABA is increased in the occipital lobe in this type of epilepsy (Simister et al., 2003b). Abnormal levels are also found in patients with malformations of cortical development that cause epilepsy (Simister et al., 2007) but not in those with temporal lobe epilepsy (Simister et al., 2009). Finally, the degree of responsiveness to antiepileptic medication has been demonstrated to depend on baseline GABA concentration before treatment (Mueller et al., 2008).

#### **2.4.1.4 Mood disorders**

Similar to anxiety, GABAergic mechanisms have been proposed to partly underlie the pathogenesis of mood disorders such as major depressive disorder (MDD) and bipolar disorder. This is supported by the antidepressant effects of anxiolytic GABAergic drugs, highlighting that the GABA system is involved in both anxiety and depression (Kalueff and Nutt, 2007). A <sup>1</sup>H MRS study by Sanacora et al. (1999) provided the first evidence of a reduction in endogenous GABA concentration in patients with MDD. This finding was replicated in a later study by the authors using a larger sample (Sanacora et al., 2004) and independently by separate groups (Bhagwagar et al., 2008, 2007; Hasler et al., 2007). Furthermore, treatment-resistant MDD has also been shown to exhibit more prominent reductions in GABA (Price et al., 2009). Interestingly, both pharmacotherapy using antidepressants (Bhagwagar et al., 2004; Sanacora et al., 2002) and electroconvulsive therapy (Sanacora et al.,

2003) lead to increases in GABA in depressed patients but cognitive behavioural therapy does not (Abdallah et al., 2014; Sanacora et al., 2006). The former finding is also apparent when the hypnotic zolpidem is given to patients who are currently on antidepressants (Licata et al., 2014). It has also been shown that individuals with remitted depression have normal GABA levels (Hasler et al., 2005), further supporting that GABA is associated with the pathogenesis of depression. Going further, Gabbay et al. (2012) reported that scores of anhedonia in adolescents with MDD negatively correlated with ACC GABA concentration. Nevertheless, not all studies have been able to find differences in GABA between depressed patients and healthy controls (Godlewska et al., 2015; Shaw et al., 2013).

GABAergic deficits in bipolar disorder have also been investigated with  $^1\text{H}$  MRS, but to a lesser extent. Unfortunately, findings remain ambiguous. For instance, whereas Wang et al. (2006) and Brady et al. (2013) found that bipolar patients had significantly higher GABA concentration in the occipital lobe, ACC and parieto-occipital cortex compared to controls, Bhagwagar et al. (2007) found the opposite to be the case in their study. To complicate things further, some reports have shown no differences in GABA levels (Godlewska et al., 2014; Kaufman et al., 2009; Soeiro-de-Souza et al., 2015). It is possible, however, that the medication patient volunteers were on at the time of scanning could have affected these results.

#### **2.4.1.5 Neurodegeneration**

There is strong evidence that disruption of GABAergic inhibition in the basal ganglia is a principal component of the neuropathology of Parkinson's disease (Calabresi et al., 2014). Thus, GABA has the potential to be a useful and much-needed noninvasive molecular biomarker for this disease. However, at present only two human  $^1\text{H}$  MRS studies have attempted to probe GABA abnormalities in subcortical brain regions. Öz et al. (2006) reported a proof of concept study that showed increased GABA in the substantia nigra of Parkinson's patients compared to healthy controls, but there was no statistical difference. On the other hand, a later 7 T study conducted by Emir et al. (2012) provided evidence of significantly greater pontine and putaminal GABA concentration in patients compared to controls. It is likely that the increasing use of ultra-high field MRS and continued methodological improvements of acquisition techniques will allow for further investigations of GABA in Parkinson's disease in subcortical brain areas.

MRS has also been used to detect GABA abnormalities in other neurodegenerative diseases such as Alzheimer's disease/mild cognitive impairment (Bai et al., 2015; Mandal, 2007; Riese et al., 2015), amyotrophic lateral sclerosis (Foerster et al., 2014) and multiple sclerosis (Bhattacharyya et al., 2013; Cawley et al., 2015).

#### **2.4.1.6 Schizophrenia and psychosis**

In the last 15 years the dopamine hypothesis has become less held as the sole neurobiological explanation for the cause of schizophrenia. In its place the Glu/GABA hypothesis has gained traction (Benes and Berretta, 2001; Carlsson et al., 2001; Lewis et al., 2005, 1999). Specifically in relation to GABA, the hypothesis points toward a key dysfunction in GABAergic interneurons and GABA neurotransmission. Evidence suggests that deficits in the GABA system lead to abnormal cognitive function. From this has come the belief that disruptions to synchronised neuronal oscillations, to which GABAergic inhibition is critical (Bartos et al., 2007; Brunel and Wang, 2003; Traub et al., 2003), leads to the cognitive symptoms seen in schizophrenia (Gonzalez-Burgos and Lewis, 2008). In vivo assessments of GABA concentration using <sup>1</sup>H MRS aim to elucidate the purported pathogenetic role of GABA in schizophrenia (for a review see Wijtenburg et al., 2015). Goto et al. (2009) were amongst the first to use *J*-difference-edited MRS to examine GABA deficits in schizophrenia. They found that GABA was significantly lower in individuals with early-stage schizophrenia compared to controls but only in the basal ganglia. A second study by this group showed that GABA levels did not alter after six months of antipsychotic treatment (Goto et al., 2010a). In one high-impact report, it was shown that not only was occipital GABA decreased in schizophrenics, but GABA also correlated with a perceptual measure of visual stimulus orientation-specific surround suppression (Yoon et al., 2010). This particular result supports the hypothesis that there may be a dysfunction in GABAergic inhibition in schizophrenia, which has been backed up by two later studies investigating the relationship between neuronal oscillations and GABA concentration in schizophrenics (Chen et al., 2014; Rowland et al., 2013a). It has furthermore been shown recently that individuals at ultra-high risk for psychosis display lower levels of GABA in the medial prefrontal cortex and dorsal caudate compared to healthy controls (de la Fuente-Sandoval et al., 2015). Reductions have

also been found in the visual cortex (Kelemen et al., 2013) and medial prefrontal cortex (Marsman et al., 2014).

However, findings have not consistently shown this pattern of reduced GABA concentration. Some studies have observed increased GABA levels, for instance (Öngür et al., 2010), while other groups have failed to find any differences (Marenco et al., 2016; Stan et al., 2015; Tayoshi et al., 2010). This could be explained by medication effects as Kegeles et al. (2012) showed that increased prefrontal GABA was observed in unmedicated patients versus controls but not in medicated ones. However, this was true only in the medial prefrontal cortex and was not seen in the DLPFC. Recently, Rowland et al. (2016) reported that medial prefrontal GABA was significantly lower in older patients with schizophrenia compared to controls, but this was not the case in younger patients. This suggests that GABA levels are much more reduced when individuals have had schizophrenia for an extended period of time, replicating an earlier finding published by the same authors (Rowland et al., 2013b). Interestingly, the authors used symmetric MM suppression in their GABA-editing acquisition, possibly hinting towards better discrimination of GABA deficits when the MM contaminant is removed from the GABA signal.

#### **2.4.1.7 Other disorders**

Examples of  $^1\text{H}$  MRS being used to quantify GABA levels in other disorders can be found with regard to fibromyalgia (Foerster et al., 2012), migraine (Aguila et al., 2015; Bigal et al., 2008), insomnia (Morgan et al., 2012; Winkelman et al., 2008), neurofibromatosis type 1 (Ribeiro et al., 2015; Violante et al., 2013), hearing disorders (Gao et al., 2015; Sedley et al., 2015) and premenstrual dysphoric disorder (Epperson et al., 2002; Liu et al., 2015).

#### **2.4.2 Correlates with Cognition and Behaviour**

Viewing GABA as a correlate for cognition and behaviour forms part of the much greater objective of linking overt human nature with the infinitely complex molecular mechanisms that take place in the cerebral cortex. More specifically, GABA can theoretically serve as a neurochemical substrate for a host of cognitive processes and behaviours. Such being the case, the MRS of GABA has increasingly been employed to test the relationship between GABA concentration and cognitive

and behavioural measures. Kim et al. (2009) were among the first to document interindividual differences in harm avoidance temperament that were dependent on ACC GABA concentration. Following suit, several recent studies have demonstrated that GABA is a potential neurochemical predictor of executive function (de la Vega et al., 2014; Fujihara et al., 2015; Haag et al., 2015; Jocham et al., 2012; Kühn et al., 2015), emotional empathy (Wang et al., 2014), cognitive failures (Sandberg et al., 2014) and interoceptive awareness (Wiebking et al., 2014). Another domain of interest has been that of impulsivity. Boy et al. (2011) reported that DLPFC GABA in men was inversely associated with trait measures of urgency. Importantly, this finding was replicated in an independent cohort of males. A similar study examined impulsivity in adolescents and reported decreased GABA levels in adolescents compared to emerging adults, with GABA also being associated with impulsivity measures (Silveri et al., 2013). Furthermore, Goto et al. (2010b) were able to show that frontal GABA levels were related to questionnaire measures of extroversion. As discussed earlier, GABA appears to be an important component in anxiogenesis. Consequently, in a unique randomised controlled study it was shown that sessions of yoga asana not only led to reductions in trait anxiety, but also to increases in thalamic GABA concentration (Streeter et al., 2010). GABA also correlated with mood and anxiety scores. Further supporting a role for GABA in anxiety, Hasler et al. (2010) were able to demonstrate GABA-related changes during a threat-of-shock task.

A paramount feature of GABAergic inhibition is the manner in which it fine-tunes synaptic responses during processing of sensory stimuli (Isaacson and Scanziani, 2011). Consequently, a fair number of studies have explored whether GABA concentration can serve as a neurochemical predictor of sensory processing. Early on, Floyer-Lea et al. (2006) demonstrated that GABA-MRS could be used to track functional decreases during a motor learning task. This has since been followed by several studies showing associations between GABA and motor or oculomotor control (Boy et al., 2010; Kim et al., 2014; Long et al., 2014; Quetscher et al., 2014; Sampaio-Baptista et al., 2015; Stagg et al., 2011a; Sumner et al., 2010). Furthermore, a number of studies have shown that there are individual differences when it comes to the level of GABA concentration and the ability to discriminate between two stimuli. In a landmark study, Edden et al. (2009) found that occipital GABA levels correlated with discrimination thresholds for obliquely oriented

stimuli, with participants with higher levels having lower thresholds. The incorporation of  $^1\text{H}$  MRS of GABA in psychophysical experiments to study the molecular underpinnings of perception is an emerging field that has so far produced several high-impact findings (e.g., Heba et al., 2016; Puts et al., 2015, 2011; Rowland et al., 2013; Terhune et al., 2014; van Loon et al., 2013; Yoon et al., 2010).

### **2.4.3 Haemodynamics**

One of the most relevant areas of GABA-MRS research to functional neuroimaging in general is the investigation of the role that GABA levels play in haemodynamics and neurovascular coupling. In Section 2.2.2, an overview of the contribution of GABAergic inhibition to the neurovascular response was given. The earliest known  $^1\text{H}$  MRS study that examined the relationship between GABA concentration and the BOLD signal was that of Chen et al. (2005). The authors used the GABA-T inhibitors vigabatrin and gabaculine to increase endogenous levels of GABA and subsequently observed a concomitant, linear decrease in BOLD signal amplitude. This landmark study laid the foundations for many subsequent investigations of the GABA–BOLD relationship. Most studies have used simple tasks to elicit a task-related change in the BOLD signal, which have for the most part supported the observation of an inverse relationship between GABA concentration and signal change (Bednařík et al., 2015; Donahue et al., 2010; Muthukumaraswamy et al., 2012, 2009; Northoff et al., 2007; Stagg et al., 2011a). Separate studies have shown that resting CBF also appears to correlate with endogenous GABA levels (Donahue et al., 2014, 2010). However, the relationship between MRS-measured GABA and haemodynamics is perhaps the most contentious of areas in applied GABA-MRS research. For example, Harris et al. (2015a) failed to find a significant association between GABA levels and the BOLD signal in several different brain regions. In other cases the relationship is not inverse as most studies have shown. These controversies contribute to the rationale of the experiment described in Chapter 6 and so will be described in detail there.

### **2.4.4 Pharmacology**

Another highly active area of research in  $^1\text{H}$  MRS has been that of studying the effects of GABAergic and non-GABAergic drugs on endogenous GABA concentration in healthy and clinical populations. Using GABAergic drugs to

challenge the GABA system is advantageous as their actions are typically focal, perturbing metabolism or synaptic transmission in a very particular manner. Moreover, the complexity of the GABA system means there are many different sites to target, including GABA<sub>A</sub> and GABA<sub>B</sub> receptors, GABA-T, GAT and GAD (Froestl, 2011; Sivilotti and Nistri, 1991; Sytinsky et al., 1978). As with noninvasive neurostimulation modalities (e.g., see Stagg, 2014), performing pharmacological studies with <sup>1</sup>H MRS has the potential to better define the biochemical origin of the NMR signal of GABA.

The vast majority of GABAergic drugs currently available were designed or are exploited for their anticonvulsant effect in the treatment of epilepsy. For example, gabapentin, levetiracetam, pregabalin, tiagabine, topiramate and vigabatrin are all antiepileptics. Of course, this should not be surprising given the very direct role GABAergic inhibition plays in the generation of epileptiform neuronal activity. As mentioned in Section 2.4.1.3, the advent of GABA-edited MRS swiftly led to several investigations into epilepsy, particularly with regards to the effect of GABAergic anticonvulsants on endogenous GABA levels. The highly selective GABA-T inhibitor vigabatrin was first shown by Rothman et al. (1993) to increase GABA concentration in the occipital lobe in healthy and epileptic volunteers. This has since been followed by many reports describing similar and consistent results (Hanstock et al., 2002; Mueller et al., 2008; Petroff et al., 1999, 1998, 1996a, 1996d; Verhoeff et al., 1999; Waschkes et al., 2014; Weber et al., 1999). The sheer number of publications reporting an increase in MRS-measured GABA following vigabatrin administration is strong evidence that the GABA NMR signal is more than likely linked to the metabolic GABA pool. Nonetheless, there has also been success in observing GABA level increases with the GABA<sub>A</sub> receptor agonist topiramate (Kuzniecky et al., 2002, 1998; Petroff et al., 2001b).

A number of studies have examined the effects of tiagabine, which selectively inhibits GABA reuptake by blocking GAT-1, on total GABA concentration. Although Myers et al. (2014) recently failed to observe any differences in occipital and limbic GABA concentration following dosage of tiagabine, Waschkes et al. (2014) were able to observe a significant increase in rat striatal GABA at 9.4 T with a dosage of 20 mg/kg. Tiagabine's effects may be more related to perturbation of GABA metabolic flux (Patel et al., 2015) or facilitation of synaptic binding (Stokes et al., 2014) rather than affecting total concentration levels.

Gabapentin, an antiepileptic that is commonly used to treat neuropathic pain, is believed to bind to voltage-dependent calcium ion channels. Like tiagabine, gabapentin elevates endogenous GABA in epilepsy patients (Petroff et al., 2000, 1996b) and healthy individuals (Kuzniecky et al., 2002), and raises cellular GABA in human neocortical slice preparations (Errante et al., 2002). Moreover, a more recent 7 T study reported that the percentage of GABA increase following gabapentin administration was inversely correlated with participants' baseline GABA levels (Cai et al., 2012). Preuss et al. (2013), however, showed that a low dosage did not lead to significant changes in GABA.

As alluded to earlier, the selective serotonin reuptake inhibitors citalopram and fluoxetine have been shown to increase GABA levels in patients with depression (Bhagwagar et al., 2004; Sanacora et al., 2002). More recently, ketamine has been gaining substantial interest given its theorised anti-depressant effects. A handful of  $^1\text{H}$  MRS studies have attempted to investigate concentration changes in GABA follow ketamine infusion but with mixed results (Milak et al., 2015; Perrine et al., 2014; Rodriguez et al., 2015; Stone et al., 2012; Valentine et al., 2011). Although the incredibly popular benzodiazepines are known to bind to the interface between the  $\alpha$  and  $\gamma$  subunits of the GABA<sub>A</sub> receptor, only a few  $^1\text{H}$  MRS studies have investigated the effect of these drugs in human. Goddard et al. (2004) found that occipital GABA levels decreased after clonazepam administration in healthy volunteers but there was no change in patients with panic disorder. Although not a benzodiazepine, the hypnotic zolpidem binds at benzodiazepine binding sites on GABA<sub>A</sub> receptors. Results are equivocal regarding the effects of zolpidem as it has been shown to either decrease (Licata et al., 2009) or increase (Licata et al., 2014) endogenous GABA.

Whether MRS is appropriate for studying the pharmacological effects on the GABA system, or indeed whether it is even capable of doing so, remains an ongoing issue. The equivocality of the findings from some of the previously mentioned studies continues to fuel questions as to whether the (non-)specificity of MRS-detected GABA concentration can discriminate acute changes in GABAergic function or whether it simply can only be used for measurements of bulk GABA content in a given VOI (Stagg et al., 2011b).



# 3. Absolute Quantification of GABA in Spectroscopic Volumes Composed of Heterogeneous Tissue Compartments

## 3.1 Abstract

Quantification of GABA using localised MRS suffers from partial volume effects related to differences in the ratio of intrinsic GABA concentration in GM and WM ( $r_M$ ). Thus, individual differences in the GM tissue fraction could drive apparent GABA concentration differences. Here, a quantification method to correct for these effects is formulated and validated. Absolute quantification using internal tissue water as a concentration reference while correcting for voxel CSF content has previously been described. GM tissue fraction effects can be normalised by incorporating into this established method a multiplicative correction factor based on measured or literature values of  $r_M$  relative to the proportion of GM and WM within tissue-segmented volumes. Simulations were performed to test the sensitivity of this correction using different assumptions of  $r_M$ . The tissue correction method was then validated by applying it to an independent dataset of in vivo GABA measurements using an empirically measured value of  $r_M$ . It is shown that incorrect assumptions of  $r_M$  can lead to overcorrection and inflation of quantified GABA in volumes composed predominantly of WM. For the independent dataset, GABA concentration was linearly related to GM volume when only the water reference was corrected for partial volume effects. Correcting for partial volume effects ascribed to  $r_M$  successfully removed this dependency. With appropriate assumptions of the intrinsic ratio of GABA in GM and WM, GABA measurements can be corrected for partial volume effects, potentially reducing between-subject variance.

### 3.2 Introduction

An outstanding problem in the absolute quantification of GABA concentration is the issue of partial volume effects, which arise from signal detection in heterogeneous spectroscopic voxels composed of GM, WM and CSF. Partial volume effects will lead to differences in apparent GABA concentration (across regions either within or between participants) that are dependent on differences in tissue content and not necessarily on differences in intrinsic concentrations of GABA. This also has implications for the SNR of detected spectral peaks, where variations in tissue content will lead to differences in signal intensity.

Early post-mortem studies have indicated that GABA content is heterogeneous across the mammalian cerebrum. Fahn and Côté (1968) reported large variability in concentration in rhesus monkeys, with highest GABA levels found in subcortical regions (e.g., basal ganglia) and lowest in pure WM (centrum semiovale). Petroff et al. (1988) measured GABA concentrations in biopsied rabbit brains, revealing two times greater levels in GM compared to WM. Comparatively higher GABA in GM has also been seen in the monkey brain (Sytinsky and Think, 1964). The use of <sup>1</sup>H MRS has also revealed regional differences of in vivo GABA across the brain in rats (Hong et al., 2011) and humans (Dou et al., 2013; Durst et al., 2015; Harada et al., 2011a; Veen and Shen, 2013; Waddell et al., 2011).

A number of studies have reported a positive linear dependence of MRS-measured GABA measurements on GM volume, where the amount of GABA in pure GM and WM can be estimated by linear regression given sufficient variability in tissue content (Hetherington et al., 1996). GABA detection using CSI has been particularly useful in characterizing this relationship given the large range in fractional GM volume sampled across the acquisition slab. CSI studies have shown two- to eight-fold increases in GABA in GM compared to WM (Choi et al., 2006; Jensen et al., 2005; Zhu et al., 2011). SVS experiments have also shown a similar finding within more regionally specific volumes (Bhattacharyya et al., 2011; Choi et al., 2007; Ganji et al., 2014; Geramita et al., 2011).

This GM dependency has implications for studies including systematic differences in fractional GM volume either between experimental groups or across individual participants. For instance, in an extreme case one set of GABA values has been acquired from predominantly WM volumes (such as where significant atrophy

has occurred) and is compared to another dataset from a control cohort. A difference will likely be apparent but this may not be due to intrinsic differences in GABA concentration but rather to differences in tissue content between the two cohorts. Confounds will also occur where GABA is correlated with a behavioural measure (e.g., impulsivity) or a functional imaging signal (e.g., the BOLD response) when these other variables also show a dependency on GM volume. Positive relationships between GABA, GM and a variable of interest will lead to overestimation of the correlation between GABA and the variable of interest. In contrast, a negative relationship between GM and a variable of interest will lead to underestimation of the positive correlation between GABA and this variable. Accounting for heterogeneous tissue content is, therefore, an important step for accurate quantification of *in vivo* GABA concentration.

A hindrance to the implementation of such an approach is the assumed value of the ratio of concentration of GABA in pure GM to the concentration of GABA in pure WM,  $r_M$ . Harris et al. (2015c) have recently detailed a comprehensive method that corrects for intrinsic GABA signal differences due to partial volume effects. Crucially, their method relies on assuming the ratio of GABA in pure GM and WM (i.e.,  $r_M$ ). The effect of various ratios on simulated data was investigated, where an  $r_M$  value of 2 was shown to be the most appropriate. This value was then used to correct *in vivo* data for differences in voxel volume fractions across participants, where it did not lead to increased variance in corrected GABA concentration values between-subjects.

Here, a correction method mathematically similar to Harris et al. (2015c) is presented. However, a slightly different approach is taken in that the intrinsic ratio of region-specific GABA in pure GM and WM is empirically estimated in a large reference dataset. Additionally, the aim is to show how various assumptions of  $r_M$  taken from previous studies influence the correction. Thus, this study's objectives were threefold: Firstly, to estimate  $r_M$  in the occipital lobe (OCC) of a large reference cohort. Secondly, to simulate the effect of altering the assumed value of  $r_M$  (based on literature values) when correcting GABA concentration in heterogeneous volumes. Thirdly, to validate this tissue correction method by applying it to OCC GABA measurements quantified in an independent dataset.

### 3.3 Theory

As was introduced in Section 1.5.2, the NMR signal of a metabolite is proportional to its concentration scaled by constants related to the scanner system and the chemical sample:

$$S_M = kR_M C_M \quad [3.1]$$

where  $S_M$  is the observed signal,  $k$  is a complex global proportionality constant containing numerous system scaling factors (e.g., receive gain, coil loading, pulse sequence design, TR, TE, etc.) and  $C_M$  is the metabolite concentration (equal to the number of moles of the molecule that is visible). The signal attenuation factor  $R_M$  accounts for the longitudinal and transverse relaxation of the metabolite:

$$R_M = \exp\left(-\frac{TE}{T_{2,M}}\right) \left[1 - \exp\left(-\frac{TR}{T_{1,M}}\right)\right] \quad [3.2]$$

where  $TE$  and  $TR$  are the echo and repetition times of the acquisition and  $T_{1,M}$  and  $T_{2,M}$  are the  $T_1$  and  $T_2$  of the metabolite. It is assumed that the relaxation times of metabolites do not differ substantially across GM and WM (Choi et al., 2006; Ethofer et al., 2003; Mlynárik et al., 2001; Träber et al., 2004).

For a given localised spectroscopic voxel, the metabolite concentration will be equal to a weighted sum of the intrinsic concentration of the metabolite in each MR-visible tissue compartment in the brain (Hetherington et al., 1996; Wang and Li, 1998). This can be formulated as follows:

$$C_M = \alpha x + \beta y + \gamma z \quad [3.3]$$

where  $\alpha$ ,  $\beta$  and  $\gamma$  are the volume fractions of GM, WM and CSF within the voxel and  $x$ ,  $y$  and  $z$  represent the basis concentrations of the metabolite in pure GM, WM and CSF. It is important to note that Eq. [3.3] assumes that the basis metabolite concentration for each compartment does not change throughout the cerebrum.

The GM, WM and CSF volumes in the voxel can be estimated by tissue segmentation algorithms available in widely used MRI analysis packages (e.g., FSL, SPM or FreeSurfer), such that the terms  $\alpha$ ,  $\beta$  and  $\gamma$  equate to the fractional voxel volumes for each tissue compartment:  $\alpha = f_{GM}$ ,  $\beta = f_{WM}$ ,  $\gamma = f_{CSF}$ . The basis concentrations can now be represented as:  $x = M_{GM}$ ,  $y = M_{WM}$ ,  $z = M_{CSF}$ . Rewriting Eq. [3.1] gives

$$S_M = kR_M (f_{GM}M_{GM} + f_{WM}M_{WM} + f_{CSF}M_{CSF}) \quad [3.4]$$

The intrinsic concentration of most metabolites in CSF is considered to be negligible (Glaeser and Hare, 1975; Petroff et al., 2006); therefore, the CSF terms can be removed from the equation. This then requires that the GM and WM voxel volume terms be normalised by the amount of tissue in the voxel. Eq. [3.4] then becomes

$$S_M = kR_M \left[ \frac{f_{GM}M_{GM}}{1-f_{CSF}} (1 - f_{CSF}) + \frac{f_{WM}M_{WM}}{1-f_{CSF}} (1 - f_{CSF}) \right] \quad [3.5]$$

$f_{GM}$  and  $f_{WM}$  are normalised by the degree of tissue in the voxel by

$$t_{GM} = \frac{f_{GM}}{1-f_{CSF}} \quad [3.6]$$

$$t_{WM} = \frac{f_{WM}}{1-f_{CSF}} \quad [3.7]$$

where  $t_{GM}$  and  $t_{WM}$  are the fractional GM and WM volumes per unit tissue volume.

This obtains

$$S_M = kR_M [t_{GM}M_{GM}(1 - f_{CSF}) + t_{WM}M_{WM}(1 - f_{CSF})] \quad [3.8]$$

$$S_M = kR_M (t_{GM}M_{GM} + t_{WM}M_{WM})(1 - f_{CSF}) \quad [3.9]$$

Since the tissue volumes are based in terms of GM and WM, the basis concentrations of the metabolite can be interpreted as a ratio of  $M_{GM}$  to  $M_{WM}$ , as so:

$$r_M = \frac{M_{GM}}{M_{WM}} \quad [3.10]$$

Eq. [3.9] can be rewritten, giving

$$S_M = kR_M (t_{GM}r_M M_{WM} + t_{WM}M_{WM})(1 - f_{CSF}) \quad [3.11]$$

The basis concentrations are now relative to the concentration of the metabolite in pure WM. Consequently, when  $r_M = 1$ ,  $M_{GM} = M_{WM}$ .

It is common practice when quantifying metabolite concentrations to standardise to an internal reference, the signal of which will also be dependent on the tissue composition of the voxel. In such a case, Eq. [3.11] can be written as

$$\frac{S_M}{S_N} = \frac{R_M(t_{GM}r_M M_{WM} + t_{WM}M_{WM})}{R_N(t_{GM}r_N N_{WM} + t_{WM}N_{WM})} \times (1 - f_{CSF}) \quad [3.12]$$

where  $k$  is cancelled out and the  $N$  terms are treated in the same manner as the  $M$  terms.

While the choice of a reference is important for a multitude of reasons, such as for being certain any possible effect of a metabolite of interest is due to the metabolite itself and not the reference, correcting for heterogeneous tissue content adds another layer of complexity. From Eq. [3.12] it can be seen that assuming inappropriate basis concentrations for either the metabolite of interest or the

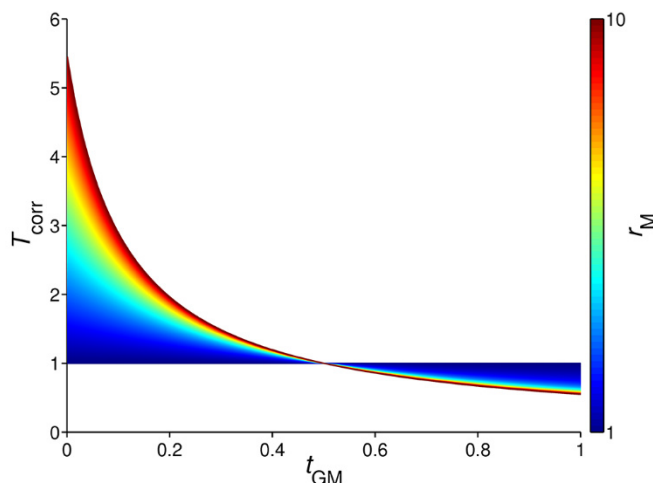


**Figure 3.1** The modelled multiplicative tissue correction factor ( $T_{corr}$ ) for assumed  $r_M$  values ranging from 1 to 10 as a function of fractional GM volume per unit tissue volume ( $t_{GM}$ ). Assumption of a large  $r_M$  necessitates a greater correction for volumes composed predominately of WM, leading to inflation of concentration measurements. The model assumes that there is no metabolite in CSF, that  $f_{CSF} = 0$  and that there are no relaxation differences for the metabolite between GM and WM.

reference will adversely affect the quantified metabolite concentration. It is useful to frame this potential problem by considering the normalisation factor needed to correct for partial volume effects. This is a multiplicative tissue correction factor derived from Eq. [3.11] and is formulated as follows:

$$T_{corr} = (t_{GM}r_M M_{WM} + t_{WM}M_{WM})^{-1} \quad [3.13]$$

It is important to note that the purpose of this normalisation is to scale measured concentrations to the concentration that would have been measured if the volume in which the signal was acquired were 50% GM and 50% WM. Therefore, the basis concentrations  $M_{GM}$  and  $M_{WM}$  must each be divided by the mean of  $M_{GM}$  and  $M_{WM}$ . In this way,  $T_{corr}$  will equal 1 (i.e., no correction) if  $t_{GM} = 0.5$ . Figure 3.1 displays  $T_{corr}$  as a function of  $t_{GM}$  based on a range of assumptions of  $r_M$ . It can be clearly seen that incorrectly assuming a large  $r_M$  value will lead to inflation of concentrations measured in voxels composed predominately of WM. Thus, inappropriate assumptions of the ratio of the intrinsic metabolite concentration in pure GM and WM could significantly bias measurements when there is large variability in fractional voxel volumes across participants or groups.

For relative quantification (referencing to another metabolite), the basis concentration values for the reference are typically assumed from previous studies in the literature. However, when absolute concentration values are desired, a common method is to use tissue water as an internal concentration reference. The

use of tissue water as a standard reference has been described extensively (Barker et al., 1993; Christiansen et al., 1993; Ernst et al., 1993; Gussew et al., 2012; Knight-Scott et al., 2003; Kreis et al., 1993). The major advantages of quantitative water referencing over relative metabolite referencing include the ability to compare data across sites, high SNR of the water peak and relative ease of acquisition (Alger, 2010). The observed water signal is not homogenous throughout brain tissue, however; tissue-dependent water relaxation and visibility differences have to be taken into account. Gasparovic et al. (2006) have described a metabolite quantification method that accounts for the differential density and relaxation times of water in volumes comprised of heterogeneous tissue compartments, formulated as follows:

$$C_M = \frac{S_M(f_{GM}\rho_{H_2O,GM}R_{H_2O,GM} + f_{WM}\rho_{H_2O,WM}R_{H_2O,WM} + f_{CSF}\rho_{H_2O,CSF}R_{H_2O,CSF})}{S_{H_2O}R_M(1-f_{CSF})} \times \frac{\#H_{H_2O}}{\#H_M} \times C_{H_2O} \quad [3.14]$$

where  $S_{H_2O}$  is the observed water signal,  $\rho_{H_2O,y}$  is the relative density of MR-visible water in compartment  $y$ ,  $\#H_{H_2O}$  and  $\#H_M$  are the number of protons that give rise to the water and metabolite peaks and  $C_{H_2O}$  is the molar concentration of water (55,000 mM). The differential longitudinal and transverse relaxation times of water in each tissue compartment are corrected for by the attenuation factor  $R_{H_2O,y}$  (see Eq. [3.2]). In similar fashion, the metabolite of interest could be referenced to internal tissue water according to Eq. [3.12], where the signal ratio is

$$\frac{S_M}{S_{H_2O}} = \frac{R_M(t_{GM}r_M^{M_{WM}} + t_{WM}^{M_{WM}})(1-f_{CSF})}{R_{H_2O}(f_{GM}H_{2O_{GM}} + f_{WM}H_{2O_{WM}} + f_{CSF}H_{2O_{CSF}})} \quad [3.15]$$

Finally, the equation can be now rearranged to determine the absolute concentration of the metabolite while additionally accounting for tissue-dependent signal weightings of the metabolite and the water reference:

$$C_M = \frac{S_M(f_{GM}\rho_{H_2O,GM}R_{H_2O,GM} + f_{WM}\rho_{H_2O,WM}R_{H_2O,WM} + f_{CSF}\rho_{H_2O,CSF}R_{H_2O,CSF})}{S_{H_2O}R_M(t_{GM}r_M^{M_{WM}} + t_{WM}^{M_{WM}})(1-f_{CSF})} \times \frac{\#H_{H_2O}}{\#H_M} \times C_{H_2O} \quad [3.16]$$

Eq. [3.16] quantifies the absolute concentration of the metabolite of interest corrected for relative water and metabolite signal weightings due to signal relaxation and partial volume effects dependent upon given proportions of GM, WM and CSF in a localised spectroscopic volume, which is represented in institutional units (i.u.).

## 3.4 Methods

### 3.4.1 Estimation of GABA in GM and WM

Basis concentrations of GM and WM GABA in the OCC were estimated in a reference cohort of 95 participants (62 females;  $23.98 \pm 4.48$  years), the “100 Brains” cohort. This dataset was collected and analysed prior to and separately from the present investigation. Briefly, GABA'+MM was detected in the medial OCC using MEGA-PRESS at 3 T (TE/TR = 68/1800 ms, voxel size =  $30 \times 30 \times 30$  mm<sup>3</sup>, 332 averages). Tissue water was used as an internal concentration reference, which was corrected for relative signal contributions from GM, WM and CSF according to Eq. [3.14]. The GABA'+MM measurements were normalised by the amount of CSF in the voxel. Tissue volume fractions were calculated from within the voxel, which was co-registered with a high-resolution 1-mm isotropic  $T_1$ -weighted 3D fast spoiled gradient echo (FSPGR) structural image (TE/TI/TR = 3.0/450/7.9 ms). A linear regression analysis was then employed to test the relationship between  $t_{GM}$  and GABA'+MM concentration (Hetherington et al., 1996). The uncertainty of the gradient of the regression model was estimated by calculating a 95% confidence interval (CI) for the slope parameter.

### 3.4.2 Sensitivity Analysis

To evaluate the sensitivity of applying Eq. [3.13] to GABA measurements, the impact of various assumptions of  $r_M$  on simulated data was assessed. A scatterplot of 10,000 randomly generated, normally distributed data points was created where each point was a coordinate of a  $t_{GM}$  by GABA'+MM linear function. The mean and standard deviation (SD) of each variable and the slope of the best-fit line were based on the 100 Brains cohort. The simulated GABA'+MM measurements were then corrected for partial volume effects based on values of  $r_M$  estimated from basis concentrations reported in the literature (Table 3.1). The selection of prior assumptions was restricted to in vivo spectroscopic studies to avoid differences between MRS-measured GABA concentration and “gold standard” quantification through histological or ex vivo methods.

**Table 3.1** Basis concentrations of GABA in pure GM and WM taken from previous empirical studies.

	Technique	Region	$M_{GM}$	$M_{WM}$	$r^M$
100 Brains cohort	SVS	Occipital	2.32 [1.67, 2.97] <sup>a</sup> i.u.	1.16 i.u.	2.00 [1.44, 2.56] <sup>a</sup>
Bhattacharyya et al. (2011)	SVS	Sensorimotor	2.87 mM	0.33 mM	8.70
C. Choi et al. (2007)	SVS	Prefrontal	1.10 mM	0.40 mM	2.75
I.-Y. Choi et al. (2006)	CSI	Posterior	1.30 $\mu$ mol/g	0.16 $\mu$ mol/g	8.13
Evans et al. (2011)	SVS	Multiple	1.37 i.u.	0.87 i.u.	1.57
Ganji et al. (2014)	SVS	Occipital	1.00 mM	0.15 mM	6.67
Geramita et al. (2011)	SVS	Cingulate	$1.91 \times 10^{-4}$ i.u.	$1.29 \times 10^{-4}$ i.u.	1.48
Jensen et al. (2005)	CSI	Posterior	0.96 mM	0.44 mM	2.18
Zhu et al. (2011)	CSI	Posterior	4.67 i.u.	3.16 i.u.	1.48

<sup>a</sup> Based on the 95% confidence interval of the slope.

SVS: single voxel spectroscopy; CSI: chemical shift imaging.

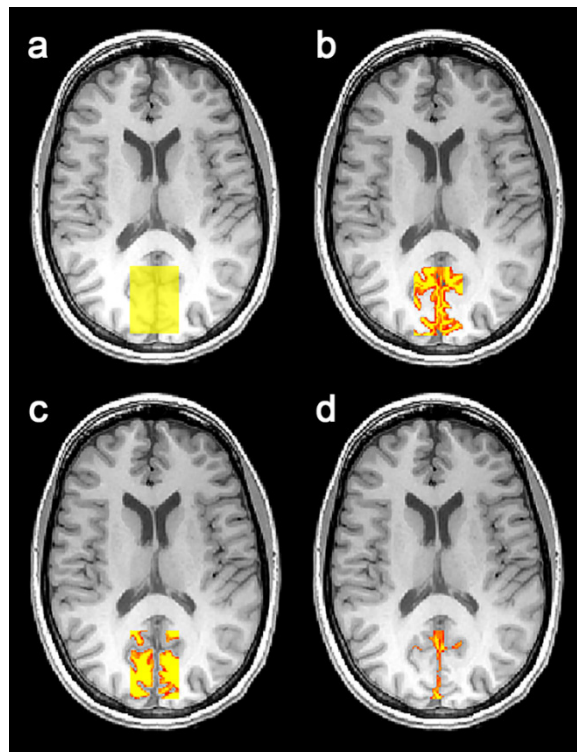


**Figure 3.2** High-resolution  $T_1$ -weighted structural image for one participant with co-registered MRS voxel mask displayed in yellow (a). Corresponding probabilistic partial volume voxel maps following FAST segmentation are shown for GM (b), WM (c) and CSF (d).

### 3.4.3 Empirical Validation

#### 3.4.3.1 In vivo GABA detection

Endogenous GABA concentration was quantified in an independent cohort of 32 volunteers (17 females;  $26.9 \pm 3.9$  years). Participants consented to taking part in scanning, which was approved by the local institutional ethics committee.

A  $30 \times 30 \times 30 \text{ mm}^3$  voxel was positioned medially in the OCC with the ventral face of the voxel aligned with the cerebellar tentorium (Figure 3.2). GABA concentration was measured with two 15-min MEGA-PRESS acquisitions. A standard acquisition ( $TE = 68 \text{ ms}$ ) was used where two editing pulses (16-ms duration) were placed at either 1.9 ppm (ON) or 7.5 ppm (OFF), which leads to an MM-contaminated GABA signal (GABA'+MM). A second acquisition ( $TE = 80 \text{ ms}$ ) using the symmetric suppression method (Henry et al., 2001) was also employed. Here, the editing pulses (20-ms duration) were placed symmetrically about the 1.7 ppm MM resonance (ON = 1.9 ppm, OFF = 1.5 ppm). The MM resonance is in this way excited equally in both ON and OFF scans, and the coupled 3.0 ppm MM resonance, which is present to the same extent in both ON and OFF scans, is absent

from the difference spectrum (GABA'). Other scan parameters for both acquisitions were as follows: TR = 1800 ms, 512 averages, 4096 data points, 5 kHz spectral width. Eight water-unsuppressed scans were acquired in each acquisition to act as an internal concentration reference.

A high-resolution  $T_1$ -weighted 3D FSPGR structural image (TE/TI/TR = 3.0/450/7.9 ms, flip angle =  $20^\circ$ , voxel resolution =  $1 \text{ mm}^3$ , FOV =  $256 \times 256 \times 168 \text{ mm}^3$ , matrix size =  $256 \times 256$ ) was acquired for voxel co-registration and tissue segmentation.

### 3.4.3.2 Voxel co-registration and segmentation

MRS voxels were co-registered with the FSPGR image using in-house software created in MATLAB (release R2012b; Natwick, NA), producing a binary voxel mask in individual structural space. Structural images were segmented into probabilistic partial volume maps corresponding to GM, WM and CSF using the automated segmentation tool FAST (Zhang et al., 2001) following removal of non-brain tissue using BET (Smith, 2002). Each partial volume map was then multiplied by the binary voxel mask to give probabilistic partial volume voxel maps (Figure 3.2). The volume of each tissue compartment was calculated by multiplying the volume (in voxels) of the partial volume map by the mean partial volume estimate.  $f_{\text{GM}}$ ,  $f_{\text{WM}}$  and  $f_{\text{CSF}}$  were then calculated by dividing the voxel volume of each tissue compartment by the sum of the voxel volumes.  $t_{\text{GM}}$  was calculated by dividing  $f_{\text{GM}}$  by the sum of  $f_{\text{GM}}$  and  $f_{\text{WM}}$ .

### 3.4.3.3 Absolute quantification

Spectra were processed and GABA was quantified in Gannet (Edden et al., 2014). Three-hertz exponential line broadening was applied to time-domain data prior to Fourier transformation. Frequency-domain data were then automatically corrected for frequency and phase using spectral registration (Near et al., 2015). Using a nonlinear least-squares fitting procedure, the GABA integral was calculated by fitting a Gaussian function to the GABA peak in the difference spectrum. The water integral was calculated by fitting a Lorentzian-Gaussian function to the water peak in the unsuppressed water spectrum. GABA concentrations were then standardised to internal tissue water in three separate ways: (i) by only applying a global absolute concentration scaling factor to the GABA to water integral ratio (i.e.,  $\#H_{2O} /$

$\#H_{\text{GABA}} \times C_{\text{H}_2\text{O}}$ ), (ii) by correcting the water signal for relative signal contributions from GM, WM and CSF (Eq. [3.14]) or (iii) by correcting the water signal and normalising the GABA signal to the relative metabolite signal contributions from GM and WM (Eq. [3.16]). For absolute GABA concentrations quantified using GABA-editing it is necessary to correct for the estimated degree of MM contamination and editing efficiency ( $MM / \kappa$ ).  $MM$  is the estimated amount of GABA in the MM-contaminated GABA signal (0.45) and  $\kappa$  is the editing efficiency of GABA-editing (0.5). The relative water proton densities in CSF, GM and WM were set to 1.00, 0.78 and 0.65 (Ernst et al., 1993). The  $T_1$  and  $T_2$  of water in GM were set to 1.33 s and 0.11 s, the  $T_1$  and  $T_2$  of water in WM were set to 0.83 s and 0.08 s (Wansapura et al., 1999) and the  $T_1$  and  $T_2$  of water in CSF were set to 3.82 s (Lu et al., 2005) and 0.50 s (Piechnik et al., 2009). The  $T_1$  and  $T_2$  of GABA were set to 0.80 s and 0.088 s (Harris et al., 2015c). Two protons give rise to the water and the 3.0 ppm GABA peaks.  $M_{\text{WM}}$  and  $r_{\text{M}}$  were estimated from the 100 Brains dataset. Given the uncertainty in the regression slope as determined by the 95% CI, the optimal  $r_{\text{M}}$  value was selected from 100 values calculated by linearly interpolating between the upper and lower bounds of the CI for  $M_{\text{GM}}$  (at  $t_{\text{GM}} = 1$ );  $M_{\text{WM}}$  (i.e., the intercept) was kept fixed (at  $t_{\text{GM}} = 0$ ) (see Table 3.1). The optimal  $r_{\text{M}}$  was that which produced the smallest possible coefficient of determination ( $R^2$ ) when GABA concentration was regressed against  $t_{\text{GM}}$ .

### 3.5 Results

The mean ( $\pm$  SD) [GABA'+MM] and  $t_{\text{GM}}$  in the 100 Brains cohort was  $1.71 \pm 0.25$  i.u. and  $0.47 \pm 0.07$ , respectively. The two variables were positively related ( $R^2 = 0.118$ ,  $p < 0.001$ ) (Figure 3.3). The slope parameter equalled 1.16, and the 95% CI of this was [0.51, 1.81]. Extrapolating from the regression,  $M_{\text{GM}}$  and  $M_{\text{WM}}$  were estimated to be 2.32 i.u. and 1.16 i.u., respectively ( $r_{\text{M}} = 2.00$ ).

The outcome of the simulated sensitivity analysis is displayed in Figure 3.4. As expected, the assumption of  $r_{\text{M}}$  taken from the 100 Brains cohort resulted in the largest reduction in the variance shared by  $t_{\text{GM}}$  and [GABA'+MM] ( $R^2 < 0.001$ ). This was followed by the assumptions taken from studies that estimated a ratio of approximately 1.5–3:1 ( $R^2 \leq 0.02$ ). The assumptions of  $r_{\text{M}}$  above 6 introduced more shared variance into the regression model ( $R^2 > 0.16$ ). This led to overcorrection,

demonstrated by the inflation of GABA measurements in predominantly WM voxels. Correcting for tissue volume using appropriate assumptions of  $r_M$  also reduced the amount of variance within the GABA dataset ( $\sigma^2$ ) compared to the original uncorrected dataset. Overcorrection resulted in increased variance within the GABA dataset.

Thirty-one pairs of good quality spectra were acquired in the validation experiment. One participant's data were excluded because of a large linewidth as a result of poor  $B_0$  shimming. Mean ( $\pm$  SD) [GABA'+MM] was  $2.22 \pm 0.14$  i.u. and mean ( $\pm$  SD) [GABA'] was  $1.06 \pm 0.16$  i.u. (global scaling only). Tissue segmentation showed an average  $t_{GM}$  of  $0.41 \pm 0.06$  across voxels. Regression models of the dependence of [GABA] on  $t_{GM}$  for MM-contaminated and MM-suppressed measures are displayed in Figure 3.5. Correcting the water signal alone revealed a dependence of [GABA'+MM] on  $t_{GM}$  ( $R^2 = 0.12$ ). This dependence was weaker for GABA' ( $R^2 = 0.04$ ). [GABA'+MM] in pure GM was estimated to be 1.89 i.u. and 1.29 i.u. in pure WM. For [GABA'], this was 0.97 i.u. (GM) and 0.58 i.u. (WM).

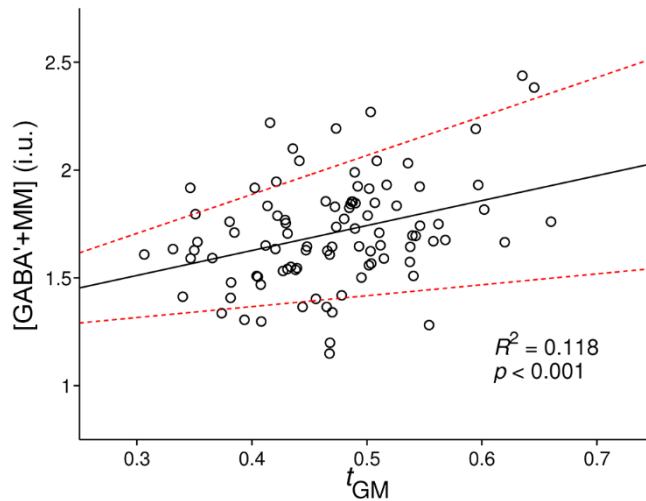


**Figure 3.3** Linear dependence of [GABA'+MM] on  $t_{GM}$  in the 100 Brains cohort ( $n = 95$ ). The solid black line is the line of best fit for the regression model. The dashed red lines represent the 95% CI for the upper and lower bound of the slope parameter.

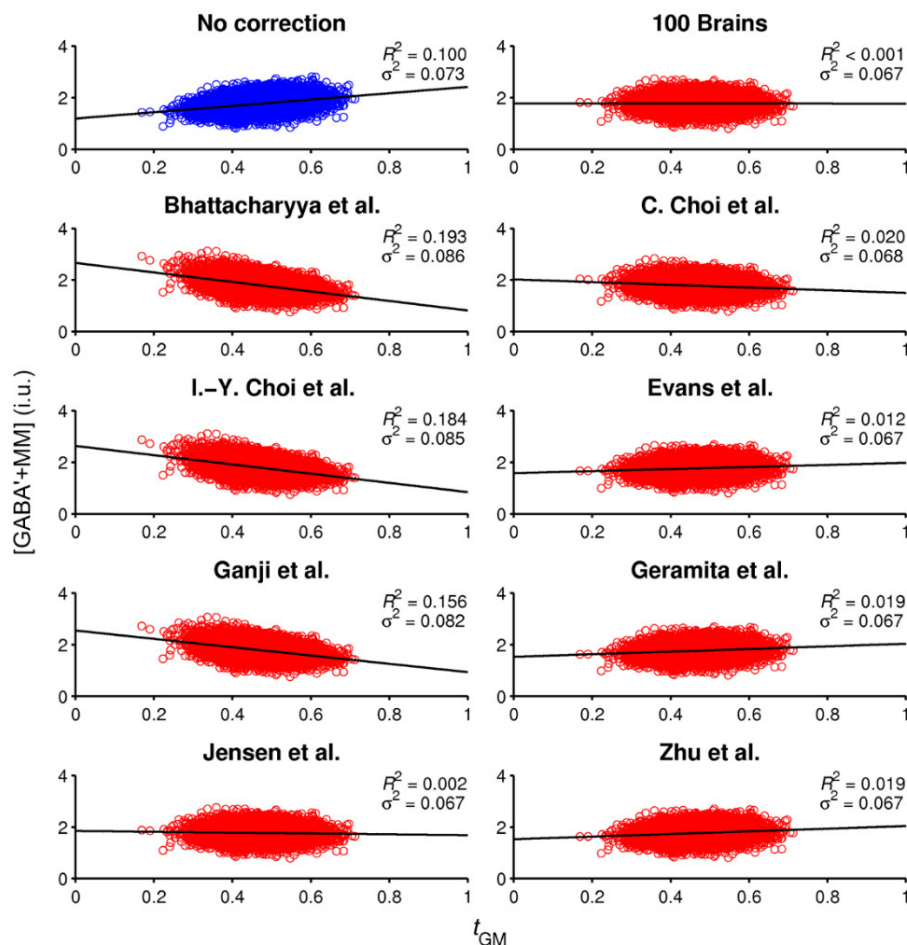


**Figure 3.4** Simulated sensitivity analysis of normalising the linear dependence of  $[GABA'+MM]$  on  $t_{GM}$  (blue scatterplot) assuming various assumptions of  $r_M$  based on literature values (red scatterplots). The coefficient of determination of each regression model ( $R^2$ ) and the variance within each simulated GABA dataset ( $\sigma^2$ ) are displayed.

Performing a combined water and GABA tissue correction led to a substantial reduction in  $R^2$  in the regression model for both  $GABA'+MM$  and  $GABA'$  compared to only correcting the water signal. The optimal  $r_M$  taken from the range of interpolated ratios was 1.45 for  $GABA'+MM$  and 1.57 for  $GABA'$ . Additionally, using this correction method did not introduce more variance into the GABA datasets in comparison to the water-only correction.  $F$ -tests for equality of variances showed that the variances of the two tissue-corrected datasets were not significantly different from each other for either  $GABA'+MM$  ( $F(30, 30) = 1.05$ ,  $p = 0.90$ ) or  $GABA'$  ( $F(30, 30) = 0.97$ ,  $p = 0.93$ ).

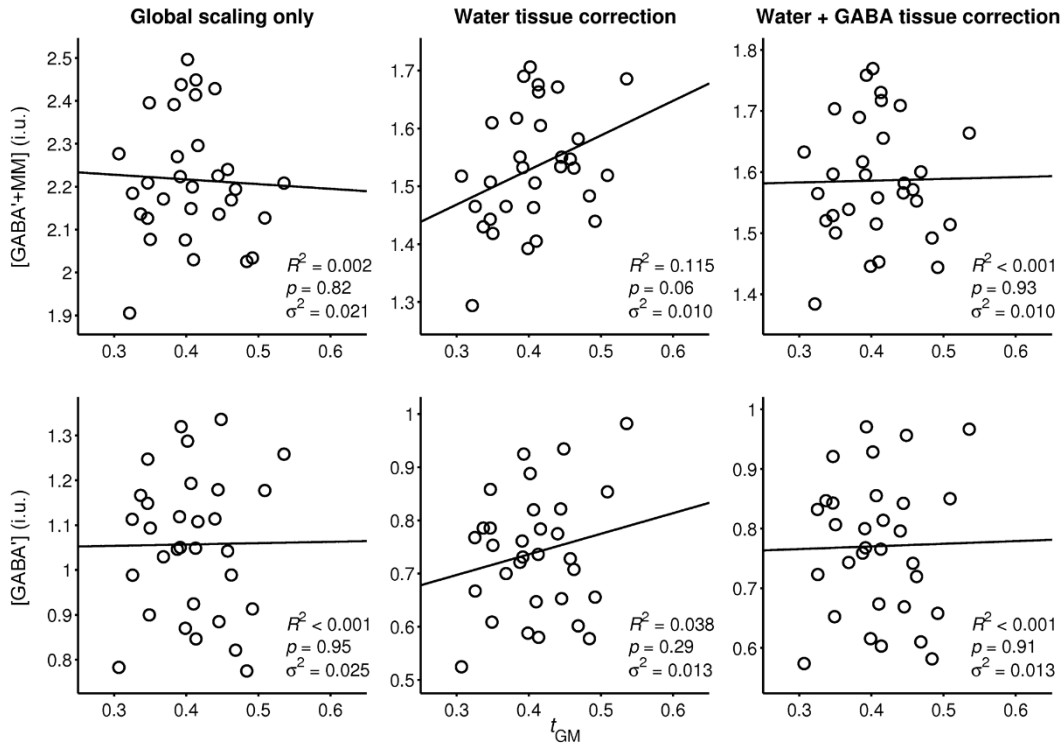


**Figure 3.5** Scatterplots of  $t_{GM}$  versus [GABA] acquired *in vivo* with standard GABA-editing (top row) and symmetric MM suppression (bottom row). The leftmost column displays the relationship between  $t_{GM}$  and GABA without any correction for partial volume effects. The middle column displays the same relationship following correction of the water signal only. The rightmost column shows the relationship when both water and GABA are tissue-corrected.  $R^2$  = coefficient of determination;  $p$  =  $p$ -value;  $\sigma^2$  = variance within GABA datasets.

### 3.6 Discussion

The simulations on the sensitivity of correcting for heterogeneous tissue content demonstrate that significant care needs to be taken when assuming the ratio between the basis metabolite concentration in pure GM and WM. An inappropriately large ratio will lead to overcorrection and introduction of a negative correlation with GM tissue fraction. This would be particularly detrimental with concentrations quantified from data acquired in predominately WM volumes as these values will be greatly inflated. When an appropriate assumption of the basis concentration ratio  $r_M$  is used, however, correction for partial volume effects can substantially reduce the variance shared between quantified GABA and fractional GM volume and potentially can decrease the between-subject variance within the GABA dataset itself.

These findings largely mirror the results from Harris et al. (2015c). The intrinsic ratio of GABA in GM and WM in the OCC was found to be approximately 2 in the reference dataset, which is equal to the ratio they recommend for partial

volume correction (the ratio term used here is the inverse of what they call  $\alpha$  in Eq. (2)). In addition, by having access to a large cohort, not only was it possible to estimate  $r_M$  in a region specific to an independent cohort using the same acquisition technique but the degree of uncertainty of the gradient of the regression model of GABA against GM tissue volume could also be gauged. These methodological differences from Harris et al.'s investigation corroborate their approach, further supporting the assumption of the intrinsic ratio of GM and WM GABA as a method to account for partial volume effects.

A linear dependence of GABA concentration on fractional GM was observed in both the reference dataset and the independent validation dataset. This relationship was only apparent after correcting the internal tissue water reference for differential water density and relaxation time based on tissue content in the voxel. By assuming the basis concentrations of GABA in GM and WM, this dependence was successfully attenuated by the normalisation procedure. A valid concern is that normalising GABA measurements in this way may potentially be counterproductive and could increase error, especially if incorrect basis concentrations are assumed. However, tests for equality of variances demonstrated that this additional correction did not add significantly more variance to the GABA datasets. Therefore, it is demonstrated that normalising GABA concentration for heterogeneous tissue content is a straightforward and viable step in quantification methodology in MRS.

To account for the possibility that group or individual differences are attributed to differences in GM volume, it is sometimes usual to treat  $t_{GM}$  as a covariate of no interest (e.g., by analysis of covariance). Intuitively, this appears to be a sensible approach, given that the aim of an experiment is to demonstrate that the variance of a dependent variable (e.g., differences in GABA concentration) is mostly explained by the independent variable (e.g., younger vs. older participants) alone, independent of the variance explained by a covariate, such as  $t_{GM}$ . However, it is a common misconception to attempt to control for a covariate when the covariate (in this case,  $t_{GM}$ ) is related to both the dependent and independent variables. Covarying out a covariate that correlates with both of these variables will not just remove some of the unexplained variance, it will also remove variance that would have been attributable to the predicted effect (Miller and Chapman, 2001). This makes interpreting the outcome of the analysis problematic and reduces the ability to observe true effects that may otherwise have been evident prior to partialling out

the variance attributed to the covariate. The alternative method of normalising GABA concentration for partial volume effects presented here obviates this issue as any variance of a covariate shared with GABA concentration and another variable is removed from the GABA measurements only. Notably, this approach can be implemented regardless of whether GM volume is associated with GABA and another variable of interest or with GABA alone.

Whether or not GABA measurements should be corrected for heterogeneous tissue content should be considered. It is clear from the simulated data that when there is large variability in GM volume across the dataset, the variance shared between  $t_{GM}$  and GABA concentration is predicted to be relatively large ( $\sim 10\%$ ). In the context of the relevant literature, this dependency could potentially contribute a significant amount to the effect sizes of relationships between MRS-measured GABA and other variables of interest. Therefore, as an initial step in analysis it is recommended that researchers investigate whether or not GM volume correlates with both quantified GABA measurements and any variables of interest in a given study.

The estimations of the basis concentrations of GABA in pure GM and WM from previous MRS studies reveal a considerable range in ratios ( $\sim 1.5\text{--}8:1$ ). This discrepancy is problematic as it adds uncertainty to the appropriate assumption of  $r_M$ . It is unclear why such a range of estimations exists, but one possible explanation is that this is down to the variety of spectroscopy techniques that have been employed. The majority have employed SVS, where the acquisition approach has included double quantum filtering (Choi et al., 2007), ultra-high field unedited spectroscopy (Ganji et al., 2014) and  $J$ -difference editing (Bhattacharyya et al., 2011; Evans et al., 2011; Geramita et al., 2011). Approaches in CSI experiments have also varied from employing multiple quantum filtering (Choi et al., 2006) to 2D  $J$ -resolved (Jensen et al., 2005) or  $J$ -difference edited imaging (Zhu et al., 2011). All of these methods have their own advantages and disadvantages with regard to resolving the GABA signal (Puts and Edden, 2012), which may play a factor in the inconsistent estimations of  $M_{GM}$  and  $M_{WM}$ . There is also the problem of different tissue segmentation algorithms and how much they contribute to quantification error. There is already some indication that some of the major toolboxes result in more error than others (Gasparovic et al., 2006; Klauschen et al., 2009). This particular issue is explored in the next chapter. The choice of reference in previous

studies will also be an important factor in explaining the variance of these estimates. Tissue water and Cr are the most commonly used internal references and both require assumptions about their respective intrinsic concentration in the sample prior to conversion to absolute concentration values, adding uncertainty to estimates of intrinsic concentrations. Another plausible explanation is that the sample size in most of these previous investigations has been relatively small (typically three to 10 participants). Even for CSI, where the number of voxels allows for a better estimation of intrinsic concentration across tissue type, a small sample size limits the generalisability of estimated intrinsic concentrations. Finally, MM contamination in MEGA-edited spectroscopy will add some variance to the relationship between GABA measurements and GM volume. At least one CSI study has reported a relationship between GM and the MM baseline (McLean and Barker, 2006). Given these discrepancies, it is recommended that research groups use reported values of  $M_{GM}$  and  $M_{WM}$  from previous studies that implemented a similar acquisition technique, sequence parameters, concentration reference and/or region of interest. Ideally, a reference dataset acquired from a sufficiently large sample at the local research site should be used, but this may not be practical in some settings.

Aside from inconsistency in  $r_M$  for GABA in the literature, a major limitation with the approach described here is the assumption that this ratio is constant throughout the cerebrum. Given the variation in GABA levels in different cortical and subcortical regions (Dou et al., 2013; Durst et al., 2015; Fahn and Côté, 1968), it is plausible that there are regional differences in the basis concentrations of GABA in pure GM and WM. Additionally, the correction also assumes that  $r_M$  is the same for all participants, which is unlikely to be the case. To overcome these limitations,  $r_M$  would need to be estimated within the region of interest on a per-participant basis, such as by using CSI. Methodological limitations and time constraints make this impractical, however, particularly in a clinical setting. Alternatively, and as previously stated, a sufficiently large, independent reference dataset that matches the technique and region of interest would circumvent these issues to a certain extent.

Although accounting for the basis concentration of GABA in GM and WM will normalise tissue-dependent signal heterogeneity across participants within a given study, other factors influencing absolute quantification will affect measurements both within and across datasets. For instance, spatial effects of the MEGA-PRESS experiment will lead to signal loss in particular compartments of

localised volumes (Edden and Barker, 2007; Kaiser et al., 2008), which can only be assessed through simulated or in vitro experiments. Related to this, the resolved difference-edited 3.0 ppm GABA multiplet profile will vary depending on the transition width, refocusing bandwidths and flip angles of the slice-selective refocusing pulses (Near et al., 2013b). These will differ across acquisition protocol, platform and research site, leading to subtle differences in absolute measures. Finally, it is assumed that the relaxation times of the metabolite of interest are equal or at least similar between GM and WM. Although the  $T_1$  and  $T_2$  of GABA have been determined in vivo, relaxation differences across tissue type have yet to be characterised and must be taken into account in quantification steps. This applies equally to other metabolites and especially to tissue water (Gasparovic et al., 2009; Gussew et al., 2012; Lecocq et al., 2015; Yamamoto et al., 2015). These issues highlight some of the difficulties of absolute quantification in MRS, and in particular the quantification of GABA.

### 3.7 Conclusions

A method to correct GABA concentration measurements for partial volume effects in single spectroscopic volumes has been presented. This approach is a simple extension of an established method that quantifies metabolite concentration using tissue water as an internal reference while correcting for differential water signal contributions across tissue type. Although care must be taken when assuming the basis concentration of GABA in pure GM and WM, appropriate assumptions will remove the tissue dependence and potentially reduce variance within the dataset of GABA measurements.



# **4. Contribution of Error from Tissue Segmentation to the Absolute Quantification of GABA Concentration**

## **4.1 Abstract**

In the previous chapter, a comprehensive tissue correction method was introduced. An important source of error was not evaluated, however: the error due to tissue segmentation procedures. The degree of partial voluming in an MRS voxel is determined through tissue segmentation algorithms such as FSL's FAST, SPM and FreeSurfer. Here, the contribution of error from tissue segmentation to the correction of partial volume effects in MRS voxels is investigated. One hundred FSPGR images from ten participants (ten FSPGRs per participant) were used in the error analysis. All structural images were registered to standard MNI space and segmented into CSF, GM and WM using FAST. A sample MRS voxel mask was also registered to standard space and segmented into the aforementioned tissue compartments. CSF, GM and WM volume fractions were quantified for each tissue compartment in each voxel for each participant. These volume fractions were then used to calculate tissue correction factors for a theoretical concentration of GABA. Both the volume fractions and the tissue-corrected GABA values were assessed for inter- and intrasubject variation. Based on the small variation of the tissue-corrected GABA values, it is concluded that tissue segmentation contributes a small degree of error to the absolute quantification of GABA in MRS.

## 4.2 Introduction

As discussed extensively in Chapter 3, there is ample evidence that GABA concentration is linearly related to the GM tissue fraction in a given localised volume. The robustness of any method to normalise or correct for this dependency will of course depend in large part on how well the volume of the principal tissue compartments in the brain (i.e., GM, WM and CSF) are estimated. It is not clear, however, how much error from tissue segmentation procedures is introduced into the correction for partial volume effects. In this chapter, the contribution of error from tissue segmentation to the absolute quantification of GABA is investigated. Firstly, the combined effect of scaling the water signal for different proportions of tissue content and accounting for the degree of CSF in a given VOI is modelled. Secondly, the error on absolute quantification of GABA concentration due to the use of the FAST segmentation algorithm using default parameters is estimated. This is based on the registration of a sample MRS voxel individually onto a large selection of  $T_1$ -weighted structural images that were tissue-segmented in a standard manner. These segmented images were then used to calculate theoretical measurements of GABA concentration for each brain in the sample. Measures of repeatability and reliability were calculated to statistically estimate the error.

## 4.3 Theory and Methods

### 4.3.1 Tissue Water Correction in Absolute Quantification

As introduced in Chapter 3, the concentration of a given metabolite quantified in a localised spectroscopic volume can be expressed in absolute terms by referencing the observed metabolite signal to an internal standard. Tissue water can be used as such a standard to convert arbitrary GABA concentration values into molar units (Eq. [3.14]). This equation can be rewritten as

$$C_G = \frac{S_G \#H_{H_2O} C_{H_2O} MM}{S_{H_2O} \#H_G \kappa} \quad [4.1]$$

where  $C_G$  is the measured concentration of GABA,  $S_G$  and  $S_{H_2O}$  are the measured NMR signals of the GABA and water resonances,  $\#H_{H_2O}$  and  $\#H_G$  are the number of protons that give rise to the water and GABA peaks (2),  $C_{H_2O}$  is the molar concentration of water (55,000 mM),  $MM$  is a correction factor for the estimated degree of co-edited MM in the GABA signal (0.45) and  $\kappa$  is the efficiency of the

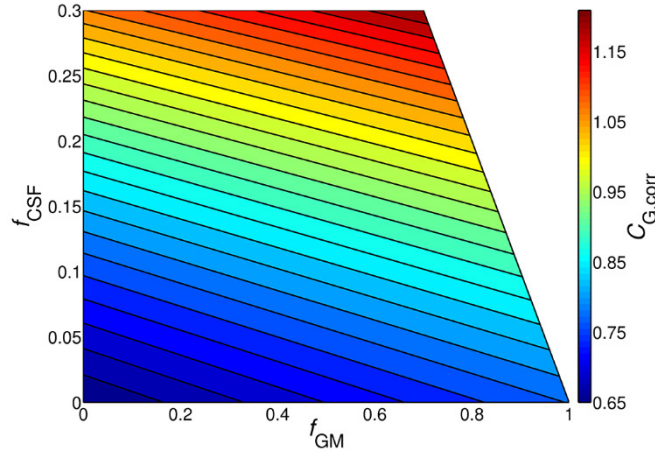


**Figure 4.1** The modelled effect of  $W_{corr}$  and  $CSF_{corr}$  on the absolute quantification of GABA ( $C_G$ ) assuming a theoretical concentration of 1 i.u. The fraction of CSF ( $f_{CSF}$ ) and GM ( $f_{GM}$ ) range from 0 to 0.3 and 0 to 1, respectively. The colour bar indicates the value of  $C_{G,corr}$ .

editing sequence (0.5). Eq. [4.1] represents the signal ratio of GABA and water scaled by a global absolute concentration scaling factor (as used in Chapter 3). The observed signals are assumed to have been detected in the absence of relaxation effects (i.e.,  $TE = 0$  and  $TR = \infty$ ).

This formula does not take into account partial volume effects on the water signal or of the amount of CSF volume in the voxel (which is assumed to contain negligible GABA). As detailed in the previous chapter, the tissue-dependent signal weighting of water content can be accounted for using the following formula:

$$W_{corr} = f_{GM}\rho_{H2O,GM} + f_{WM}\rho_{H2O,WM} + f_{CSF}\rho_{H2O,CSF} \quad [4.2]$$

and CSF volume in the voxel can be corrected by

$$CSF_{corr} = (1 - f_{CSF})^{-1} \quad [4.3]$$

Combining Eqs. [4.2] and [4.3] with Eq. [4.1] gives the molar concentration of GABA weighted by tissue-dependent water content and differential CSF volume in the voxel:

$$C_{G,corr} = C_G W_{corr} CSF_{corr} \quad [4.4]$$

For the sake of simplicity, the intrinsic concentration of GABA in GM and WM was assumed to be equal. If assuming  $C_G$  is equal to 1 i.u., then the effect of  $W_{corr}$  and  $CSF_{corr}$  on  $C_G$  can be modelled by assuming a full range of  $f_{GM}$  and  $f_{WM}$  values, with  $f_{CSF}$  ranging from 0 to 0.30. It can be seen from the change in the colour gradient of the contour plot in Figure 4.1 that the tissue correction is more sensitive to differences in the amount of CSF in the voxel than to differences in the amount of tissue content (GM/WM).

### 4.3.2 Estimation of Error

A schematic of the study protocol is shown in Figure 4.2. A sample of 10 participants that had previously been scanned at the Cardiff University Brain Research Imaging Centre (CUBRIC) were selected from a repository of  $T_1$ -weighted FSPGR structural images. These participants had the largest number of stored structural images in the repository. For each individual participant, a random subsample of 10 of their structural images was selected for analysis. Non-brain tissue was removed from each image using BET and the brain-only image was linearly registered to MNI space using a  $T_1$ -weighted 1-mm isotropic standard brain as a reference (Mazziotta et al., 2001). Registration was performed in FLIRT (Jenkinson and Smith, 2001; Jenkinson et al., 2002) using an affine transformation model with 12 degrees of freedom (rigid body + scaling + skewing). Each MNI-registered brain image was then segmented into probabilistic GM, WM and CSF partial volume maps using FAST. A randomly chosen binary MRS voxel mask localised in the OCC was selected to serve as a representative VOI; this was co-registered with the MNI brain. This MNI-registered sample voxel mask was then multiplied by the GM, WM and CSF partial volume maps for each participant giving probabilistic partial volume voxel maps for each tissue compartment. Fractional voxel volumes ( $f_{GM}, f_{WM}, f_{CSF}$ ) were calculated as in Section 3.4.3.2. Default parameters were used in BET, FLIRT and FAST.

The voxel volume fractions were used to calculate theoretical tissue-corrected GABA concentrations according to Eq. [4.4].  $C_G$  was set to 1 i.u. for all participants. In this way, the contribution of error from tissue segmentation to the absolute quantification of GABA was specifically assessed.

Coefficients of variation (CV) were calculated to represent the error within participants (within-subject coefficient of variation,  $CV_{ws}$ ) and the error across participants (between-subject coefficient of variation,  $CV_{bs}$ ) for the estimated voxel volume fractions and theoretical tissue-corrected GABA values.

If  $\sigma_{ij}$  is the standard deviation of participant  $i$ 's voxel volume fractions for tissue compartment  $j$ , and  $\mu_{ij}$  is the mean of their respective volume fractions, then the CV is given by

$$CV_{ij} = 100 \frac{\sigma_{ij}}{\mu_{ij}} \quad [4.5]$$

and the  $CV_{ws}$  for tissue compartment  $j$  is defined as

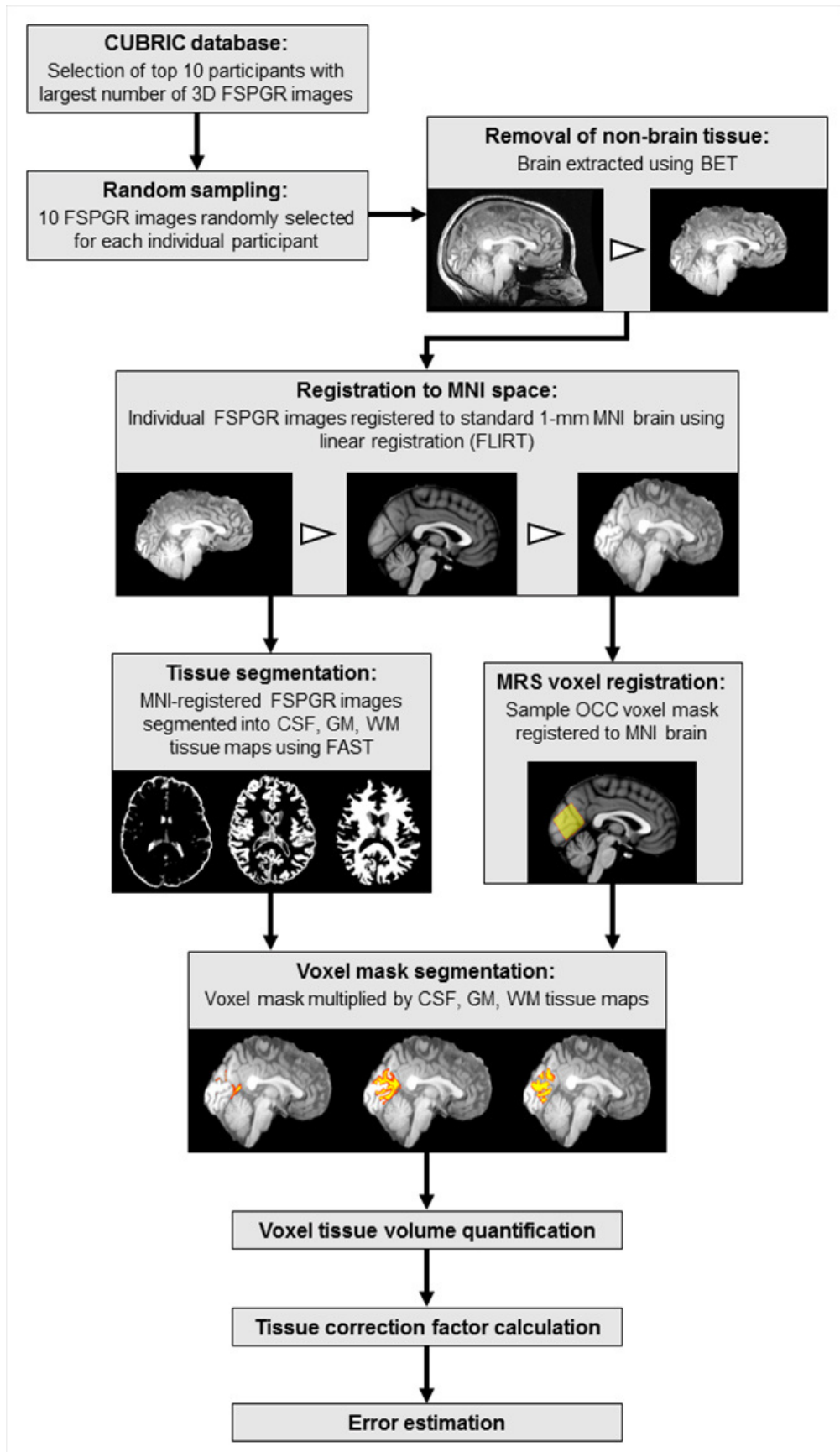


Figure 4.2 Analysis pipeline for the estimation of error from tissue segmentation.

$$CV_{ws,j} = \frac{\sum CV_{ij}}{n} \quad [4.6]$$

Similarly, if  $\mu_j$  is the mean of all volume fractions for compartment  $j$  then the  $CV_{bs}$  is

$$CV_{bs,j} = 100 \sqrt{\frac{\sum (\mu_{ij} - \mu_j)^2}{n-1}} \mu_j^{-1} \quad [4.7]$$

Intraclass correlation coefficients (ICCs) were calculated in SPSS (version 20.0; IBM, Armonk, NY) using a two-way random effects model with measures of consistency. Whereas the CV characterises measurement variability in one dimension (either within or between participants) and is useful for comparing the variability of measurements with different means, the ICC represents a ratio between between-subject variance and total variance and is a more informative statistic of the test–retest reliability of a measurement.

#### 4.4 Results and Discussion

Mean ( $\pm$  SD) voxel volume fractions and CVs for each participant are listed in Table 4.1. The corresponding overall average volume fractions for each tissue compartment and respective  $CV_{ws}$ ,  $CV_{bs}$  and ICCs are shown in Table 4.2. As can be seen, CSF content in the voxel had the greatest amount of variability both within and between participants ( $CV_{ws} = 39.4\%$ ;  $CV_{bs} = 63.8\%$ ). This is despite a very high ICC (0.97).

Each participant's theoretical tissue-corrected [GABA] in each tissue-segmented MRS voxel is given in Table A.1. The average concentration value was  $0.71 \pm 0.01$  i.u. The degree of variability in these values, and therefore the error attributed to tissue segmentation, was minimal ( $CV_{ws} = 0.96\%$ ;  $CV_{bs} = 1.31\%$ ). The ICC was also very high (0.96). It can be concluded then that tissue segmentation and tissue correction only contributes a small degree of error to absolute quantification.

To illustrate the distribution of  $C_{G,corr}$  with respect to the tissue composition of the sample MRS voxel, for each participant fractional GM volume was plotted against the respective fractional CSF volume (Figure 4.3). The scatterplot demonstrates that the variability of the GABA values, and therefore the variability of the tissue correction factors, is greater across  $f_{CSF}$  than  $f_{GM}$ . This can be further illustrated by calculating the percentage difference between  $C_{G,corr}$  corresponding to

**Table 4.1** Mean ( $\pm$  SD) fractional voxel volume of GM, WM and CSF for each participants and corresponding coefficients of variation.

	$f_{GM}$		$f_{WM}$		$f_{CSF}$	
	M $\pm$ SD	CV (%)	M $\pm$ SD	CV (%)	M $\pm$ SD	CV (%)
S01	0.38 $\pm$ 0.03	7.2	0.59 $\pm$ 0.03	5.9	0.028 $\pm$ 0.007	26.0
S02	0.39 $\pm$ 0.03	6.9	0.61 $\pm$ 0.03	5.0	0.008 $\pm$ 0.004	49.2
S03	0.37 $\pm$ 0.02	4.6	0.62 $\pm$ 0.02	3.1	0.008 $\pm$ 0.003	36.0
S04	0.34 $\pm$ 0.01	3.8	0.65 $\pm$ 0.01	2.3	0.009 $\pm$ 0.002	19.0
S05	0.35 $\pm$ 0.02	5.1	0.65 $\pm$ 0.02	3.2	0.008 $\pm$ 0.003	41.0
S06	0.33 $\pm$ 0.03	10.2	0.66 $\pm$ 0.04	5.6	0.006 $\pm$ 0.003	59.1
S07	0.30 $\pm$ 0.04	14.4	0.69 $\pm$ 0.05	7.2	0.008 $\pm$ 0.005	72.6
S08	0.31 $\pm$ 0.02	6.2	0.68 $\pm$ 0.02	3.1	0.007 $\pm$ 0.002	27.6
S09	0.32 $\pm$ 0.02	7.1	0.66 $\pm$ 0.03	4.1	0.011 $\pm$ 0.005	42.6
S10	0.35 $\pm$ 0.01	3.4	0.64 $\pm$ 0.01	2.1	0.009 $\pm$ 0.002	21.1

**Table 4.2** Mean ( $\pm$  SD) fractional voxel volume of GM, WM and CSF across all participants and corresponding within- and between-subject coefficients of variation.

	Mean $\pm$ SD	CV <sub>ws</sub> (%)	CV <sub>bs</sub> (%)	ICC
$f_{GM}$	0.35 $\pm$ 0.03	6.9	8.0	0.94
$f_{WM}$	0.64 $\pm$ 0.03	4.2	4.8	0.94
$f_{CSF}$	0.01 $\pm$ 0.006	39.4	63.8	0.97

the voxels composed of the maximum and minimum fraction of GM and the maximum and minimum fraction of CSF across all voxels (triangles in Figure 4.3). This difference was 5.2% for the former and 9.5% for the latter. Furthermore, performing linear regressions of  $C_{G,corr}$  versus  $f_{GM}$  and  $f_{CSF}$  reveals that the concentration value increases more per unit of  $f_{CSF}$  than per unit of  $f_{GM}$  as evidenced by the slopes of the two regression models (Figure 4.4). These findings signify that the tissue correction procedure is more sensitive to  $f_{CSF}$  than  $f_{GM}$ , which supports the model represented in Figure 4.1.

The CV for the estimation of CSF volume is likely to have been driven in large part by error due to the linear registration procedure. Given that the fraction of CSF in the voxel is substantially smaller compared to the fraction of GM and WM, even small deviations in the location of co-registered CSF voxels from the gold

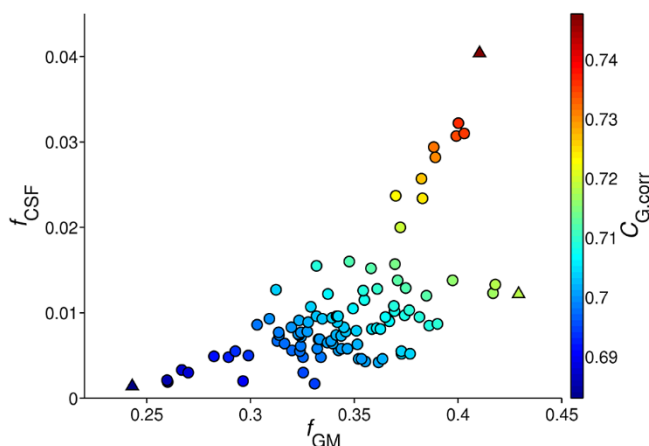


**Figure 4.3** Scatterplot of fractional GM volume versus fractional CSF volume for each participant's tissue-segmented sample MRS voxel. The colour of each data point indicates the corresponding  $C_{G,corr}$  value. Triangles indicate data points where the fractions of GM and CSF are maximal and minimal across all participants' sample MRS voxels.

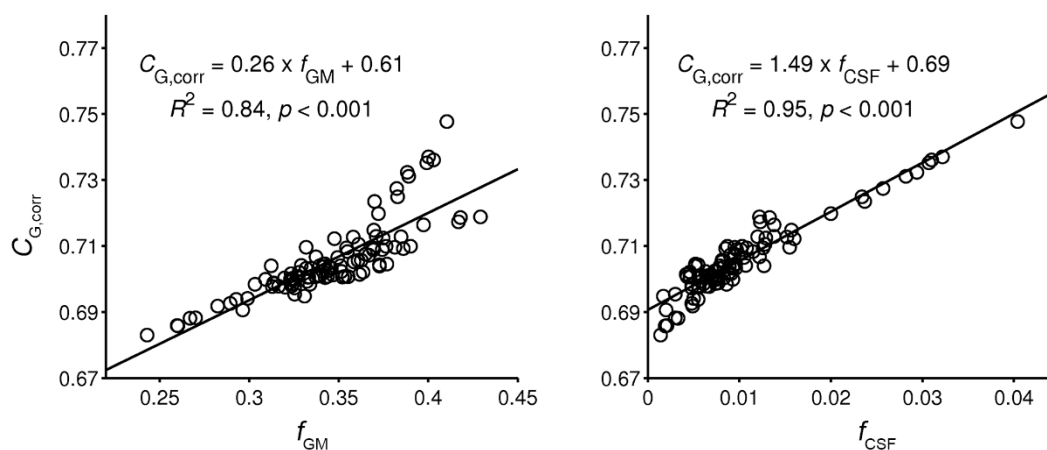


**Figure 4.4** Linear regression models showing the dependence of  $C_{G,corr}$  on either  $f_{GM}$  or  $f_{CSF}$ . The steeper slope of the second model demonstrates that the correction factor is more sensitive to variability in  $f_{CSF}$  than variability in  $f_{GM}$ .

standard base reference voxels will lead to a significant change in the CV. This sensitivity is further compounded by the fact that the CV will be large when the values of the mean and standard deviation are small. For instance, the average  $f_{CSF}$  was 0.01 with a standard deviation of 0.006. The small quantity of these values leads to a large CV. To increase the accuracy of the CV for a measurement with small means and standard deviations requires increased precision of the measurement.

A potential source of error in absolute quantification that has not been addressed here is the error attributed to assumption of the transverse and longitudinal relaxations times of water in GM, WM and CSF. In their seminal paper on using internal tissue water as a concentration reference, Gasparovic et al. (2006) showed

that the greatest degree of variability is due to the assumption of water  $T_2$  relaxation times in GM and WM. Moreover, it appears that this error can be significantly reduced by performing acquisitions at the shortest TE possible. In addition, Harris et al. (2015c) examined the effect of assuming different literature values for relaxation corrections when quantifying GABA concentration. They showed that there were significant differences in concentration estimates when using different values, suggesting that comparison of GABA measurements between different studies using different assumptions should be performed with caution. It would be interesting to see a more thorough investigation of the impact of assuming relaxation parameters in partial volume correction for the absolute quantification of GABA, where the tissue-dependent weighting of the water and GABA signals are both considered.

Only FAST was used in this study to examine the contribution of error from tissue segmentation to absolute quantification. It would be worthwhile to compare against the robustness of other segmentation packages, namely, SPM and FreeSurfer. A few studies have examined and compared the performance of each of these popular algorithms. Clark et al. (2006) conducted a comprehensive investigation of how many sources of variability impact on structural image segmentation. The choice of acquisition, noise reduction algorithm and brain-extraction algorithm all had a differential impact on segmenting structural images into GM, WM and CSF. The choice of tissue segmentation algorithm, however, had the greatest impact. They also note that the problem of partial voluming can be ameliorated by using a priori probability tissue maps, which can benefit segmentation of deep brain structures. It is also worth noting that aside from variation between segmentation algorithms there will be also be variation within and between scanner platforms with regards to volumetric quantification (Huppertz et al., 2010). The overriding message is that the choice of algorithm depends on which factors in segmentation are most important to the user, as each method has its own distinct advantages and disadvantages (Eggert et al., 2012; Klauschen et al., 2009; Tsang et al., 2008). Taking into account these factors would of course be beneficial for absolute quantification in MRS, particularly when using tissue water as an internal concentration reference. Nevertheless, the findings of the present study

suggest the contribution of error from tissue segmentation need not be overly concerning.

#### **4.5 Conclusions**

To conclude, tissue segmentation using the FAST segmentation algorithm appears to only contribute a minimal amount of error to theoretical quantification of GABA concentration. In particular, despite the fact that there was a large amount of inter- and intrasubject variability in the quantification of CSF content in the MRS volumes, the water tissue correction procedure to absolutely quantify GABA concentration did not appear to be adversely affected.

# **5. Comparison of the Repeatability of GABA-Edited MRS with and without MM Suppression\*\***

## **5.1 Abstract**

In this chapter the repeatability of GABA-edited MRS with and without MM suppression is compared. GABA' (non-MM contaminated) and GABA'+MM (MM-contaminated) concentration was measured in the OCC and anterior cingulate (AC) using symmetric and standard editing ( $n = 15$ ). Each method was performed twice in each region. Within-subject coefficients of variation for each technique were 4.0% (GABA'+MM) and 8.6% (GABA') in the OCC and 14.8% (GABA'+MM) and 12.6% (GABA') in the AC. Intraclass correlation coefficients were better for the suppression method than standard editing in both the OCC (0.72 vs 0.67) and AC (0.41 vs 0.16). These findings were replicated in the OCC of a second cohort ( $n = 15$ ). Symmetric suppression is shown to be comparable in repeatability to standard GABA-editing. Measuring a purer quantification of GABA becomes increasingly important as more research is conducted on links between GABA concentration, pathology and healthy behaviour.

---

\*\* The content of this chapter is based on a published peer-reviewed article (Mikkelsen et al., 2016). A copy of this article is provided in Appendix B.

## 5.2 Introduction

Several studies have already reported on the reproducibility of edited spectroscopy used to quantify GABA concentration in the human brain (Bogner et al., 2010; Geramita et al., 2011; O’Gorman et al., 2011). To date, however, no such research has been conducted on symmetric editing. Therefore, the principal aim of this study was to determine, at 3 T, whether the repeatability of the more specific measure of GABA obtained using the symmetric MM suppression technique is comparable to that of the standard GABA-edited MRS technique, which includes a significant MM contribution to the derived GABA concentration.

## 5.3 Methods

All single-voxel <sup>1</sup>H MRS experiments were conducted using a 3 T GE Signa HDx scanner (GE Healthcare, Waukesha, WI) with an eight-channel receive-only head coil and a body coil for transmit.

### 5.3.1 Phantom Experiments

Two phantom experiments were performed in a 20-mM GABA phantom to select the symmetric suppression acquisition to be used in the study. The phantoms were scanned at room temperature and the effect of temperature on chemical shift was accounted for by adjusting the placement of editing pulses accordingly.

#### 5.3.1.1 Effect of partial excitation

The proximity of the OFF editing pulse to the GABA resonance in the MM-suppressed acquisition will lead to partial excitation of the GABA resonance and signal loss. The impact of this on the GABA signal was measured using two variants of the editing acquisition: (i) a “standard” GABA acquisition with TE = 68 ms allowing an editing pulse duration of 16 ms and (ii) an acquisition similar to Edden et al. (2012b) with TE = 80 ms to allow longer 20-ms editing pulses. Other scan parameters were as follows: 20 × 20 × 20 mm<sup>3</sup> voxel, repetition time (TR) = 1800 ms, 128 averages, 4096 data points, 5 kHz spectral width. One editing pulse position was varied from 1.26 ppm to 2.54 ppm in increments of 0.04 ppm over a series of acquisitions, while the other was fixed at 7.5 ppm. The degree of GABA co-editing

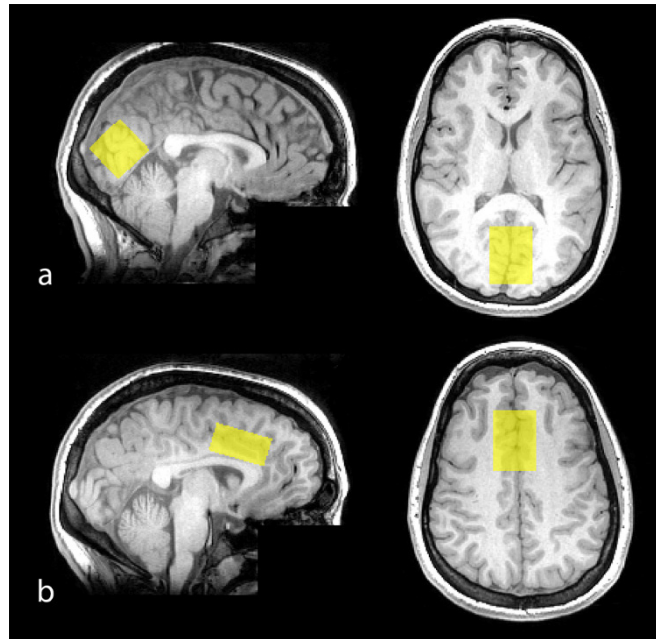


**Figure 5.1** Representative placement of MRS voxels in the occipital lobe (a) and anterior cingulate (b) in one participant.

(and hence signal loss) in the OFF sub-spectra is reflected in the GABA integral when ON editing pulses are placed at 1.5 ppm.

### 5.3.1.2 Effect of increasing TE

To investigate the impact of an increase in TE on the GABA signal, TE was modulated from 60 to 80 ms in 4-ms steps in order to estimate the overall signal loss between the two methods (other scan parameters were as above). ON and OFF editing pulses (16 ms) were placed at 1.9 ppm and 7.5 ppm, respectively.

## 5.3.2 In Vivo Experiments

### 5.3.2.1 Experiment 1

Fifteen healthy participants (mean age =  $26.1 \pm 5.1$  years; eight females) were recruited for two one-hour scan sessions. Participants consented to take part in this research, which was approved by the local institutional ethics committee.

In the first scan session, a  $30 \times 30 \times 30$  mm<sup>3</sup> voxel was prescribed to the medial OCC (Figure 5.1a). The ventral face of the voxel was aligned with the cerebellar tentorium and the volume positioned as posteriorly as possible without including the sagittal sinus. Participants then underwent a second scan, on a separate day, where a  $20 \times 30 \times 40$  mm<sup>3</sup> voxel was positioned medially in the AC (Figure

5.1b). The ventral face of this voxel was aligned parallel to the anterior-dorsal edge of the trunk of the corpus callosum.

For each voxel, two MEGA-PRESS acquisition methods (outlined below) were used to detect GABA. Two scans were performed using each method giving a total of four measurements per session. Scans were interleaved and the order counterbalanced across participants. Participants were not repositioned during the repeated acquisitions in each session. GABA measures including an MM component are denoted GABA'+MM; GABA concentrations acquired using the symmetric suppression method are denoted GABA' (to distinguish it from the molecule GABA).

#### ***Non-suppressed acquisition (GABA'+MM)***

Here, two Gaussian editing pulses (16-ms duration) were placed in an interleaved fashion at either 1.9 ppm (ON) or 7.5 ppm (OFF), resulting in a “standard” measurement of GABA plus co-edited MM. Echo time was set to 68 ms.

#### ***Symmetric MM suppression (GABA')***

In the second acquisition, the OFF editing pulses were placed at 1.5 ppm with the ON pulses kept at 1.9 ppm, thereby suppressing the MM resonance. To ensure editing selectivity, the duration of the editing pulses was increased to 20 ms, with TE increased to 80 ms.

The following parameters were the same for both acquisition methods: TR = 1800 ms, 332 averages, 4096 data points, 5 kHz spectral width, 10-min acquisition time. Eight additional water-unsuppressed scans were acquired as an internal concentration reference.

### **5.3.2.2 Experiment 2**

Repeatability of the two techniques was also assessed in a second cohort of 15 healthy participants (mean age = 27.5 ± 4.1 years; seven females). The scan protocol and acquisition parameters were identical to those in Experiment 1 except spectra were acquired in an OCC voxel only. Additionally, the number of averages used in each acquisition technique was increased to 512 (acquisition time = 15 min) to improve the SNR of GABA'+MM and GABA' measures.

### 5.3.3 MRS Analysis

MRS spectra from the phantom and in vivo experiments were processed in Gannet (Edden et al., 2014), following an analysis pipeline similar to Evans et al. (2013). Line broadening (0.5 Hz for phantom spectra, 3 Hz for in vivo spectra) was applied to raw time-domain data prior to Fourier transformation. Frequency-domain data were then automatically corrected for frequency and phase. Using a nonlinear least squares fit, GABA concentration was quantified from the integral of the difference spectrum with a Gaussian function placed over a range 2.79 ppm to 3.55 ppm. Tissue water was used as an internal concentration reference. The ratio of GABA to water (in i.u.) was multiplied by a scaling factor to account for the  $T_1$  and  $T_2$  of water and GABA, for MR-visible water concentration and for editing efficiency. Concentration values were not corrected for partial volume effects for either the water or GABA signals. Thus, the quantification procedure used here can be considered a global absolute concentration scaling approach as described by Eq. [4.1] but without incorporating tissue-dependent signal weightings. Gannet also produces estimates of fit error for both the GABA and water peak model fits calculated as the standard deviation of the fit residuals normalised to peak height. Overall fit error is then defined as the square root of the sum of the squared GABA and water peak fit errors ( $\epsilon_{\text{fit}}$ ).

### 5.3.4 Statistical Analysis

To quantify the repeatability of the two techniques, coefficients of variation were calculated to represent the measurement error ( $CV_{\text{ws}}$ ) and the population variability ( $CV_{\text{bs}}$ ). These were calculated as in Section 4.3.2. To estimate the error on  $CV_{\text{ws}}$ , a 95% CI was calculated from a bootstrap of the set of  $CV_{ij}$  values, sampling with replacement 100,000 times.

Default Bayes factors ( $B_{10}$ ) were calculated according to the method described by Dienes (2011) in order to assess whether the difference in  $CV_{\text{ws}}$  values between each acquisition technique in each voxel is better explained by the null hypothesis (a difference of 0%) or by the alternative hypothesis (a plausible difference in population means). The plausibility of the alternative hypothesis was predicted based on previous studies investigating the reproducibility of GABA-edited spectroscopy at 3 T using either occipital (a difference of 9%) or frontal (a difference of 7%) voxels. The plausibility of the predicted population differences

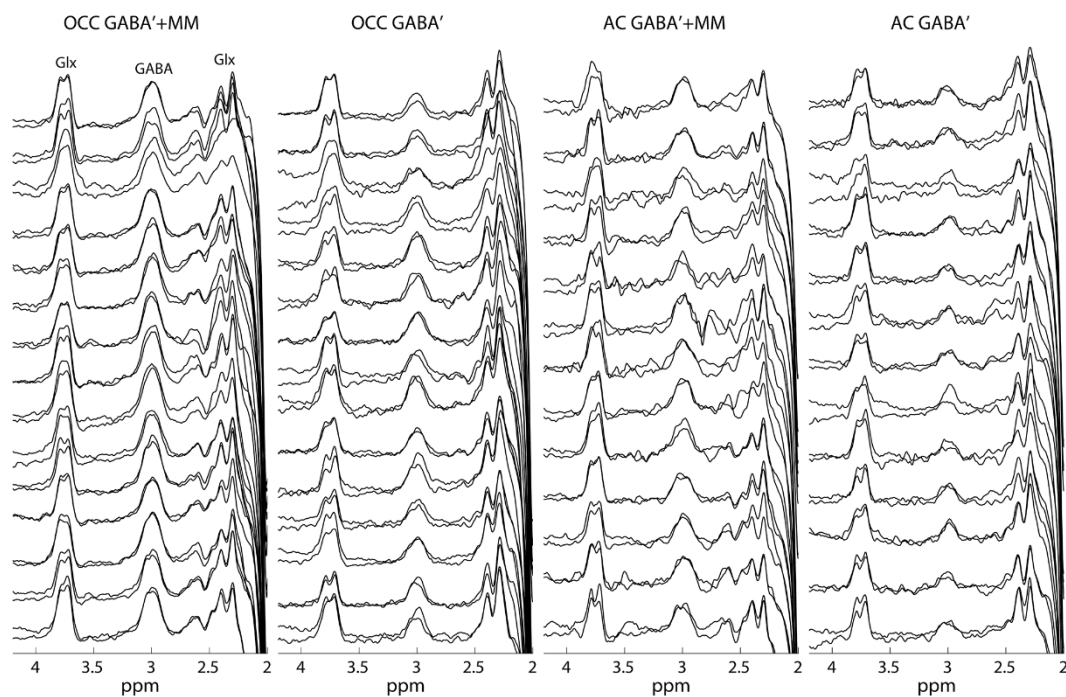


**Figure 5.2** Individual difference spectra acquired in vivo in all participants from Experiment 1 using standard GABA-editing (GABA'+MM) and symmetric MM suppression (GABA') in the occipital lobe (OCC;  $n = 15$ ) and anterior cingulate (AC;  $n = 13$ ). Repeated measurements for each technique are overlain. It can be clearly seen that the amplitude of the 3.0 ppm GABA peak is attenuated in GABA' spectra compared to the same peak in the spectra acquired using standard editing. The composite glutamate + glutamine (Glx) peaks are also shown.

was assumed to follow a normal distribution. A  $B_{10}$  greater than 3 indicates substantial evidence for the alternative hypothesis and a  $B_{10}$  less than 1/3 indicates substantial evidence for the null hypothesis. If  $B_{10}$  is between 1/3 and 3 then the evidence is insensitive and no judgement can be passed.

A one-way analysis of variance (ANOVA) was used to calculate the proportional contribution of measurement and population variance to the total variance in the dataset. In addition, as a test of reliability of the two techniques, ICCs were calculated as in Section 4.3.2.

## 5.4 Results

### 5.4.1 Phantom Experiments

The GABA signal loss for a symmetric editing scheme (reflected in the signal intensity when editing pulses were placed at 1.5 ppm) was 44% for the TE = 68 ms, 16-ms editing pulse acquisition, but only 20% for the TE = 80 ms, 20-ms editing pulse acquisition. This corresponded to a reduction in the editing pulse bandwidth

from 82 Hz to 57 Hz. Increasing TE from 68 to 80 ms resulted in a small increase in the GABA integral (approximately 3%), without correcting for  $T_2$  relaxation effects. These results indicate that, overall, the signal loss due to the increase in TE is small in comparison to the signal improvement by improving the frequency selectivity of the editing pulses.

## 5.4.2 In Vivo Experiments

### 5.4.2.1 Experiment 1

A total of 120 spectra were analysed for Experiment 1. Following visual inspection, two AC spectra (from two different participants) were rejected because of excessive head movement in one and excessive fit error in the other; therefore, only 13 participants' data were included in the AC dataset. As shown in Figure 5.2, there was a clear difference between the GABA'+MM and GABA' peak amplitudes. Mean concentrations ( $\pm$  SD) averaged across scans and participants were as follows: [GABA'+MM]:  $1.13 \pm 0.07$  i.u. (OCC),  $0.99 \pm 0.15$  i.u. (AC); [GABA']:  $0.54 \pm 0.08$  i.u. (OCC),  $0.43 \pm 0.06$  i.u. (AC). The fraction of the total signal retained following MM suppression ( $[GABA'] / [GABA'+MM]$ ) was 0.48 in the OCC voxel and 0.43 in the AC voxel, in good agreement with previous findings (Aufhaus et al., 2013; Kegeles et al., 2007). Mean  $\epsilon_{fit}$  ( $\pm$  SEM) for OCC measures were  $4.0 \pm 0.1\%$  (GABA'+MM) and  $5.2 \pm 0.3\%$  (GABA'), and  $7.7 \pm 0.4\%$  (GABA'+MM) and  $10.4 \pm 0.6\%$  (GABA') for AC measures. Although these were shown to be significantly different for each region ( $t(14) = -3.74$ ,  $p = 0.002$  and  $t(12) = -4.11$ ,  $p = 0.001$ , respectively), these percentages fall in line with previously reported estimates (Evans et al., 2013). The average linewidth ( $\pm$  SD) was  $8.2 \pm 1.4$  Hz for the OCC voxel and  $7.1 \pm 0.5$  Hz for the AC voxel.

The repeatability and reliability results (CV, components of variance and ICCs) are reported in Table 5.1. Paired  $t$ -tests showed that  $CV_{ws}$  values were not significantly different for OCC ( $t(14) = -1.92$ ,  $p = 0.08$ ) or for AC ( $t(12) = 0.58$ ,  $p = 0.57$ ) acquisitions. However, the Bayesian analysis revealed that for both voxels the data were insensitive (OCC:  $B_{10} = 1.64$ ; AC:  $B_{10} = 0.62$ ), meaning there was not enough evidence in Experiment 1 to decide whether the within-participant repeatability of symmetric suppression and standard editing is or is not comparable. Taking voxel and acquisition technique as separate factors, a two-way repeated measures ANOVA demonstrated that there was no significant interaction in  $CV_{ws}$

**Table 5.1** Measures of repeatability and reliability for the standard GABA-edited (GABA'+MM) and MM-suppressed (GABA') acquisition techniques from in vivo Experiment 1.

	OCC ( <i>n</i> = 15)		AC ( <i>n</i> = 13)	
	GABA'+MM	GABA'	GABA'+MM	GABA'
Mean $\epsilon_{\text{fit}}$ ( $\pm$ SEM)	4.0 $\pm$ 0.1%	5.2 $\pm$ 0.3%	7.7 $\pm$ 0.4%	10.4 $\pm$ 0.6%
CV <sub>ws</sub> <sup>a</sup>	4.0%	8.6%	14.8%	12.6%
95% CI <sup>b</sup>	2.4–5.8%	5.3–13.9%	9.6–21.5%	8.9–16.4%
CV <sub>bs</sub>	6.1%	15.0%	14.7%	13.6%
$\sigma^2_{\text{p}}$	38%	53%	13%	27%
$\sigma^2_{\text{e}}$	62%	47%	87%	73%
ICC	0.67	0.72	0.16	0.41

$\epsilon_{\text{fit}}$ , fit error; CV<sub>ws</sub>, within-subject coefficient of variation; CI, confidence interval; CV<sub>bs</sub>, between-subject coefficient of variation;  $\sigma^2_{\text{p}}$ , between-participant component of variance;  $\sigma^2_{\text{e}}$ , measurement error component of variance; ICC, intraclass correlation coefficient.

<sup>a</sup> CV<sub>ws</sub> values were not significantly different between the two acquisition methods for OCC or AC spectra ( $p = 0.08$ ,  $p = 0.57$ , respectively).

<sup>b</sup> 95% CI from the bootstrapping results sampling from the CV<sub>p</sub> dataset.

between voxel and acquisition technique ( $F(1, 12) = 3.10$ ,  $p = 0.10$ ) and no main effect of acquisition technique ( $F(1, 12) = 0.33$ ,  $p = 0.58$ ). However, there was a main effect of voxel ( $F(1, 12) = 9.93$ ,  $p = 0.008$ ), with the AC voxel showing significantly higher CV<sub>ws</sub>. CV<sub>bs</sub> was larger in the suppressed OCC data (15.0%) than in the contaminated data (6.1%) but similar in the AC (13.6% vs 14.7%, respectively).

The component of the variance associated with differences between participants ( $\sigma^2_{\text{p}}$ ) and the component of the variance that is attributed to measurement error ( $\sigma^2_{\text{e}}$ ) are expressed as percentages of the total variance across the whole dataset. For the symmetric suppression method,  $\sigma^2_{\text{p}}$  was greater compared to standard editing in both the OCC (53% vs 38%) and AC (27% vs 13%). It also produced comparatively higher ICCs: 0.72 vs 0.67 (OCC); 0.41 vs 0.16 (AC).

#### 5.4.2.2 Experiment 2

No datasets were rejected as a result of visual inspection of data acquired in Experiment 2, resulting in 60 good quality OCC spectra. Mean concentrations ( $\pm$  SD) were as follows: [GABA'+MM]: 1.15  $\pm$  0.07 i.u.; [GABA']: 0.56  $\pm$  0.08 i.u. The

**Table 5.2** Measures of repeatability and reliability for the standard GABA-edited (GABA'+MM) and MM-suppressed (GABA') acquisition techniques from *in vivo* Experiment 2.

	OCC ( $n = 15$ )	
	GABA'+MM	GABA'
Mean $\varepsilon_{\text{fit}}$ ( $\pm$ SEM)	$3.2 \pm 0.1\%$	$4.2 \pm 0.2\%$
$CV_{\text{ws}}^{\text{a}}$	3.5%	4.6%
95% CI	2.5–4.6%	2.8–7.9%
$CV_{\text{bs}}$	5.8%	14.6%
$\sigma_{\text{p}}^2$	64%	86%
$\sigma_{\text{e}}^2$	36%	14%
ICC	0.78	0.90

<sup>a</sup> $CV_{\text{ws}}$  values were not significantly different between the two acquisition methods ( $p = 0.69$ ).

GABA' to GABA'+MM signal fraction was 0.49. Mean  $\varepsilon_{\text{fit}}$  ( $\pm$  SEM) was  $3.2 \pm 0.1\%$  (GABA'+MM) and  $4.2 \pm 0.2\%$  (GABA') ( $t(14) = -3.92$ ,  $p = 0.002$ ). The average linewidth ( $\pm$  SD) was  $8.6 \pm 1.2$  Hz.

Compared to Experiment 1, there was an overall improvement in both repeatability and reliability for each acquisition technique in the second cohort, particularly for symmetric suppression (Table 5.2). This is likely a consequence of a reduction in measurement noise following increased acquisition time. As the  $CV_{\text{ws}}$  data were shown to be non-normal following a Shapiro–Wilk test ( $W = 0.79$ ,  $p = 0.006$ ), a Wilcoxon signed-rank test was performed. Again, the  $CV_{\text{ws}}$  were not significantly different from each other ( $z = -0.40$ ,  $p = 0.69$ ). Moreover, in this experiment  $B_{10} = 0.21$ , indicating that there was substantial evidence in support of the null hypothesis (a difference of 0%).

Of interesting note is that the MM-suppressed concentrations still revealed increased inter-individual variability compared to contaminated concentrations, reflected in the  $CV_{\text{bs}}$  (14.6% vs 5.8%),  $\sigma_{\text{p}}^2$  (86% vs 64%) and ICC (0.90 vs 0.78).

#### 5.4.2.3 Pooled data

Finally, the OCC data from Experiments 1 and 2 were pooled together and examined. The ICC for standard editing was 0.72 and the ICC for symmetric suppression was 0.81. Figure 5.3 shows the association between GABA'+MM and

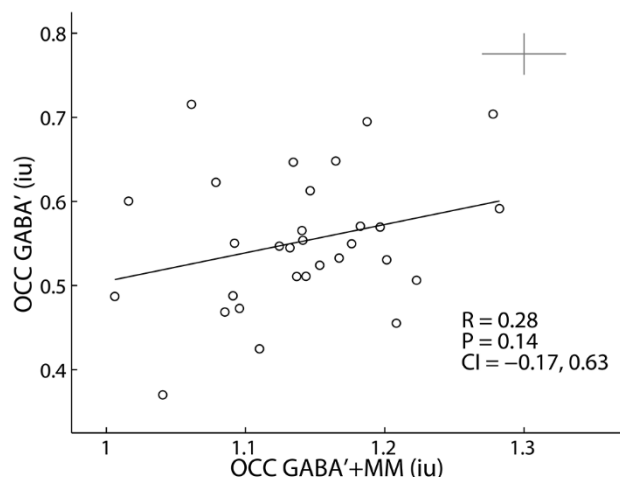


**Figure 5.3** Scatterplot of OCC GABA concentration for participants pooled from Experiments 1 and 2 ( $n = 30$ ) acquired with standard editing (OCC GABA'+MM) and symmetric suppression (OCC GABA'). Each point represents the average of the two repeat measurements. Crosshairs indicate the mean scan–rescan difference between the two repeat measurements for each technique. For GABA'+MM this was  $0.06 \pm 0.05$  i.u.; for GABA' this was  $0.05 \pm 0.05$  i.u. CI: 95% confidence interval of the correlation coefficient calculated by bootstrapping with replacement 10,000 times.

GABA' concentration for participants from both cohorts. There was a weak but non-significant correlation between the two measures ( $r = 0.28$ ,  $p = 0.14$ ,  $CI = [-0.17, 0.63]$ ). Whilst it is surprising that the two measurements were not more strongly related, the expected correlation will have an upper bound based on both the intrinsic correlation and the reliabilities of the two techniques. This can be calculated with the following formula:  $\text{Observed } r_{(\text{variable A, variable B})} = \text{True } r_{(\text{variable A, variable B})} \times \sqrt{(\text{Reliability}_A \times \text{Reliability}_B)}$  (Vul et al., 2009). Assuming an intrinsic correlation of 0.7, and using the ICCs for the two techniques based on the pooled data, the expected correlation between the two measurements would be no higher 0.53. Further to this, a range of possible intrinsic correlations (i.e., a 95% CI) was estimated by firstly taking the ICCs and observed correlation coefficient and bootstrapping with replacement each 10,000 times and then randomly sub-sampling from the distribution of bootstrapped values and running the above formula again 10,000 times. The CI of True  $r$  was shown to be  $-0.18, 0.90$ .

## 5.5 Discussion

The main focus of this research was to compare the repeatability of symmetric MM suppression and standard GABA-editing.  $CV_{\text{ws}}$  was used as an index of measurement repeatability and it was found that there was no significant difference

in  $CV_{ws}$  resulting from the symmetric suppression technique and the non-suppression technique, in either the occipital lobe or anterior cingulate. To further determine whether there was indeed evidence for the hypothesis that the two techniques are comparable in repeatability, Bayes factors were calculated on  $CV_{ws}$  values. Whereas the *in vivo* data in the first cohort was not sensitive enough to make a decision, the second cohort did provide enough evidence in favour of this hypothesis. Therefore, this suggests that symmetric suppression is comparable in repeatability to standard GABA-edited MRS.

Although there was no significant difference between  $CV_{ws}$  for the two techniques in the occipital lobe data, mean  $CV_{ws}$  in Experiment 1 increased from 4.0% to 8.6% and from 3.5% to 4.6% in Experiment 2 when using symmetric suppression. This is consistent with the overall reduction in the GABA' integral when using symmetric suppression due to the exclusion of MM. However, there appears to be an increase in the population variance (reflected in higher  $CV_{bs}$  and higher  $\sigma_p^2$ ), which accounts for the improvement in the ICCs. The increased population variance was also found in the occipital data of the second cohort. Given that  $CV_{ws}$  and mean  $\epsilon_{fit}$  both decreased relative to the first cohort, it is unlikely that this increased sensitivity was due to noise in the acquisition. This also suggests that the symmetric suppression technique may benefit from longer acquisition time than may be typically used in standard GABA-edited experiments.

Only a few studies have reported ICC values for GABA measurements. Muthukumaraswamy et al. (2012) reported an ICC of 0.87 for occipital spectra, whilst Geramita et al. (2011) and Harada et al. (2011) reported ICCs of approximately 0.70 for anterior cingulate measures. The use of ICCs is useful to an extent but does present difficulties for interpretation. Greater between-participant variance will increase ICC scores if other variance components remain stable (Gasparovic et al., 2011). As such, the poorer ICC values for spectra acquired in the AC reported here are likely the result of inherently noisier data. This is supported by the fact that the mean  $\epsilon_{fit}$  was higher in AC spectra for both acquisition methods and that the AC  $CV_{bs}$  percentages were comparable to the  $CV_{bs}$  for the MM suppression technique in the occipital session, despite the latter producing a much higher ICC.

$CV_{ws}$  percentages for acquisitions in the OCC are similar to or better than those in other studies (Bogner et al., 2010; Evans et al., 2010, 2013). Repeatability results for AC spectra, however, are higher than what has been previously reported

for frontal brain regions (Geramita et al., 2011; Harada et al., 2011a; O’Gorman et al., 2011), but do agree with Evans et al. (2013). The higher  $CV_{ws}$  corresponds to the difficulties in acquiring spectra in frontal regions. Although different protocols and analysis methods make comparisons across research groups challenging, on the basis of the findings here, MM suppression by symmetric editing is comparable in repeatability to standard GABA-editing methods.

In vivo quantification of GABA without MM contamination produced results consistent with previous empirical evidence (Aufhaus et al., 2013; Kegeles et al., 2007; Rothman et al., 1993). Suppression of the 1.7 ppm MM resonance reduced the 3.0 ppm GABA peak by approximately 50% in relation to the peak resolved using the standard editing technique. A comparatively lower mean concentration in the AC is consistent with other studies showing differences in GABA levels in anterior and posterior cortical regions (Fahn and Côté, 1968; Veen and Shen, 2013); but as the voxels were not segmented to control for GM, WM and CSF composition, this cannot be confirmed.

The phantom experiments that were conducted yielded similar findings to Edden et al. (2012b). The authors observed a negligible decrease in modelled signal (~1%, with  $T_2$ -weighting) when modulating TE from 68 to 80 ms in vitro, while an increase of approximately 3% was seen here. Extrapolating from Edden et al.’s estimated signal loss in vivo (~7%), the present data suggests a signal loss of 4% would be expected in vivo. However, it appears that the frequency selectivity of editing pulses has a much larger effect. By increasing editing pulse duration from 16 to 20 ms, the editing pulse bandwidth was decreased, leading to improved efficiency of the GABA-editing experiment. Although both TE and editing pulse duration were manipulated in this experiment, the effect of TE is shown to be minimal and does not significantly contribute to the signal change.

As the focus on the relationships between endogenous GABA and cognitive-behavioural responses continues to grow, it is important to reiterate that the GABA concentration quantified with standard GABA-edited MRS contains an MM contribution. Whilst it is argued that MM are not likely to have any functional importance to such responses (Puts et al., 2011), the degree to which the MM contribution to the 3.0 ppm GABA signal differs within particular regions and across individuals is not fully known. This would be a significant issue only if the inter-individual variability of this contribution was large enough to drive correlations,

however, and it is still unclear whether this is the case. Nonetheless, quantification of GABA concentration in the AC in one symmetric suppression study showed that suppressing MM resulted in higher between-participant variability (~15%) compared to not suppressing MM (~10%) (Aufhaus et al., 2013). While a similar degree of inter-individual variability was seen in both the MM-suppressed and MM-contaminated AC concentrations from the current study, the findings from this previous study are reflected in the OCC data. However, any conclusions drawn about this variability are only speculative because of the difference in MM T<sub>2</sub> relaxation effects between the suppression and standard editing techniques caused by the increased TE used in the former method. That voxels were not segmented into different tissue components also prevents further conclusions on this. It should be additionally noted that the age range of participants in Aufhaus et al.'s study was larger compared to the current study, which may have contributed to the larger variability in the suppressed measurements.

When OCC GABA' and GABA'+MM concentrations were compared, only a weak association between the two was apparent. This finding was unexpected as the measurements would be thought to show a certain degree of correlation. Given the good reliability of both standard editing and symmetric suppression as demonstrated here, there are two possible explanations. Either one measurement is more sensitive to systematic effects (e.g., the effect of frequency drift on editing efficiency), or the inter-individual variability in the MM contribution to the GABA peak is large enough to affect the correlation. At this stage, this is only speculation and limited to the OCC data, necessitating further investigation.

A limitation of this study is that concentration measures were not corrected for tissue composition in each voxel. Whilst the scan-to-scan repeatability would not be affected by variation in tissue composition since participants were not repositioned during each scan session, it is still possible that between-participant variability could be influenced by tissue differences. GABA concentration has previously been reported to be higher in grey matter compared to white matter (Choi et al., 2007; I.-Y. Choi et al., 2006), which would affect the SNR of the GABA resonance and thus the reliability of the acquisition across participants.

Ultimately, what is desired is to be able to optimally detect pure GABA in vivo. Future spectroscopic studies, particularly those involving correlational designs, would benefit from employing symmetric editing to suppress MM. To

illustrate, whereas Gao et al. (2013) recently reported an age-related decline in GABA+MM concentration in a large healthy cohort, Aufhaus et al. (2013) showed that when MM is suppressed using symmetric editing the relationship between age and GABA concentration no longer holds. Suppression would also prove beneficial in clinical populations as differences in the MM baseline have been shown in at least neurological pathologies such as multiple sclerosis, stroke and tumours (Graham et al., 2001; Howe et al., 2003; Mader et al., 2001). What differences may occur in neuropsychiatric disorders, to which disruptions in GABAergic mechanisms have been tied, remains unknown. A further issue is the effect of motion-induced frequency drift, which may be especially problematic in patient populations. Negative drift, for example, will lead to more MM contamination in the GABA signal in standard editing (Harris et al., 2014), potentially impacting on the reproducibility of the technique. This is of particular concern in symmetric editing given the closer proximity of the OFF editing pulses to the MM resonance. All in all, these points highlight the need to account for the 1.7 ppm MM resonance in edited spectroscopy.

## 5.6 Conclusions

To conclude, symmetric editing-based MM suppression is shown to have comparable repeatability to that of standard GABA-editing. By slightly modifying the MEGA-PRESS sequence, this technique successfully attenuates a major limitation of GABA-edited MRS. A growing interest in measuring GABA concentration in vivo in both healthy and clinical populations is apparent. The need for both accurate and reliable quantification is therefore essential when attempting to draw conclusions between GABA measures, pathology and healthy behaviour. Here, it is shown that symmetric suppression produced higher ICCs in two regions and in two separate cohorts, suggesting that it is perhaps more sensitive to inter-individual differences in MRS-measured GABA.

# 6. Endogenous GABA Concentration and Individual Differences in Haemodynamic Contrast Tuning

## 6.1 Abstract

The inhibitory neurotransmitter  $\gamma$ -aminobutyric acid (GABA) has an integral role in neurovascular coupling. A relationship between simple task-induced haemodynamic responses and endogenous GABA concentration has previously been reported. This chapter describes a multimodal investigation of whether GABA levels are also associated with interindividual variability in response sensitivity as assessed with a graded visual contrast stimulus. Annular gratings displayed at five contrast levels were presented to 32 healthy volunteers. During stimulation, BOLD and CBF responses were measured simultaneously in the visual cortex. GABA-MRS was used to non-invasively quantify GABA concentration in the OCC. Both GABA'+MM and GABA' concentrations were measured. A power law contrast response function was used to model individual contrast tuning curves and the rate of response saturation was parameterised for each individual. Bayesian regression analysis showed that there was weak evidence supporting a model that did not include either GABA'+MM or GABA' as predictors of haemodynamic response saturation. However, exploratory analyses demonstrated that GABA'+MM was negatively associated with the rate of CBF saturation and displayed a similar but weaker effect with BOLD, such that participants with higher GABA'+MM levels showed a faster rate of response saturation to contrast. GABA' was not associated with rate of saturation. This study produced preliminary evidence that endogenous GABA'+MM concentration is associated with individual differences in haemodynamic contrast tuning and it is proposed that GABA may be a mediator of the dynamic range of CBF and the BOLD signal.

## 6.2 Introduction

The BOLD signal arises from a complex interplay between CBF, cerebral blood volume, neuronal firing and metabolic consumption of oxygen and glucose, collectively known as neurovascular coupling (Logothetis and Wandell, 2004; Logothetis, 2008; Viswanathan and Freeman, 2007). As described in Chapter 2, GABA has an integral role in the excitation–inhibition balance and consequently also on haemodynamic responses, such that it acts both indirectly as a mediator of synaptic transmission and directly as a vasomodulator (Cauli and Hamel, 2010; Lauritzen et al., 2012).

A number of studies have investigated the relationship between GABA, BOLD and CBF. (Chen et al., 2005) showed that by increasing GABA levels through pharmacological manipulation in rats, a corresponding decrease in the BOLD signal following somatosensory stimulation was observed. In human studies, an inverse association between endogenous GABA and measures of haemodynamics has been reported with respect to BOLD (Donahue et al., 2010; Muthukumaraswamy et al., 2012, 2009; Northoff et al., 2007; Stagg et al., 2011a; Stan et al., 2014; Violante et al., 2013), baseline CBF (Donahue et al., 2014; Krause et al., 2014) and task-related changes in CBF (Michels et al., 2012).

However, three issues remain unresolved in the literature. Firstly, some human studies have reported a positive association between GABA levels and haemodynamic measures, in contradiction to the negative relationship previously reported. For instance, (Wiebking et al., 2014) reported a positive correlation between GABA levels and BOLD in the insula while, in two other studies, baseline CBF correlated positively with GABA concentration (Donahue et al., 2010; Michels et al., 2012). In another recent case, the authors failed to replicate any association between GABA and BOLD in several cortical regions using a variety of tasks (Harris et al., 2015a). Muthukumaraswamy et al. (2012) also did not find an association between baseline CBF and GABA.

Secondly, the human studies mentioned above have only used standard GABA-MRS to non-invasively measure GABA concentration in localised regions of the cortex. The MM contamination that occurs using this technique confounds previously described associations between GABA and BOLD/CBF and has yet to be satisfactorily addressed. Removing this MM contamination from GABA

measurements would be an important step in providing a more accurate indication of the relationship between GABA and haemodynamic measures in humans.

Thirdly, past research examining task-induced haemodynamic responses has focused on characterising peak activation elicited by maximum-contrast stimuli (Harris et al., 2015a; Muthukumaraswamy et al., 2012, 2009; Violante et al., 2013). It is not yet known whether endogenous GABA plays a similar role in BOLD and CBF responses at lower grades of stimulation, and whether there are individual differences with respect to this. Indeed, it has recently been shown that the degree of coupling between CBF and the cerebral metabolic rate of oxygen varies with the strength of a stimulus (Liang et al., 2013). Keeping the role of GABAergic inhibition in neurovascular coupling in mind, differences in GABA concentration may predict the variation in interindividual sensitivity to a stimulus, in addition to being associated with individual variability of responses following maximal stimulation.

Given that neurons are known to selectively fire in response to specific properties of a stimulus, response sensitivity can be assessed by manipulating the strength of a stimulus over several grades. This tuning of neuronal responses can be represented as a transfer function from input to output. For instance, tuning using different grades of contrast results in characteristic neuronal responses in the visual cortex (Albrecht and Hamilton, 1982; Ohzawa et al., 1985). With respect to haemodynamics, a graded change in contrast has been shown to lead to a monotonic change in the BOLD signal (Boynton et al., 1996; Logothetis et al., 2001; Tootell et al., 1995), with a similar effect seen with CBF (Chiarelli et al., 2007; Hoge et al., 1999a, 1999b). Increases in stimulus contrast also result in a concomitant increase in the power of local field potentials and magnetoencephalographic activity in the high-frequency gamma band (Hall et al., 2005; Henrie and Shapley, 2005). The manifestation of these synchronous gamma oscillations has been demonstrated to arise from GABAergic inhibition (Bartos et al., 2007; Buzsáki and Wang, 2012). Measuring haemodynamic responses as visual contrast is modulated would therefore allow for the assessment of response sensitivity across individuals.

Using a graded visual contrast paradigm, BOLD and CBF responses were simultaneously measured in the visual cortex. GABA concentration in the occipital lobe was measured with GABA-edited MRS with and without symmetric MM suppression. It was hypothesised that GABA concentration would predict parameters characterising the properties of contrast tuning for BOLD and CBF

responses. It was also hypothesised that MM-suppressed GABA concentration would be a stronger predictor of these tuning properties than the MM-contaminated measure.

## 6.3 Methods

### 6.3.1 Participants

Thirty-two healthy volunteers (17 females; mean age  $\pm$  SD = 26.1  $\pm$  3.2 years) who were not on any psychiatric medication and who had not been diagnosed with a psychiatric or neurological disorder were recruited. Participants were asked to refrain from ingesting any alcohol 12 hours before the scan session. As a handful of studies have reported a differential effect of menstrual cycle on endogenous GABA concentration (Epperson et al., 2005; Harada et al., 2011a; Silveri et al., 2013), female participants were scanned in their luteal phase (cycle days ~15–28). None reported being a smoker. All participants gave consent before taking part in the study, which was approved by the local institutional ethics committee.

### 6.3.2 Visual Paradigm

A 20-min graded contrast visual stimulation paradigm was employed to examine contrast tuning of haemodynamic responses. Black and white gamma-corrected, square-wave, 1.2 cycles per degree (cpd) annular gratings ( $26^\circ \times 20^\circ$ ) reversing at 6 Hz were presented on a mean luminance background. Gratings were displayed at five Michelson contrast levels: 0%, 12.5%, 25%, 50% and 100%. A black fixation cross was presented within a small unfilled patch ( $1.7^\circ \times 1.7^\circ$ ) in the centre of the screen. Participants were instructed to fixate on this cross and press a button box with their right index finger whenever they saw the cross turn red; the cross changed colour for 1 s every 10–20 s throughout the entire paradigm. Visual presentation followed a block design: Gratings at each of the five contrast levels were shown once for 30 s, with 0% contrast (baseline) always presented first. This activation period (baseline + grating presentation; 150-s duration) was conducted six times (15 min total). The gratings were presented pseudorandomly to avoid order and adaptation effects. Additionally, a baseline block of 150 s was placed at the beginning and at the end of the paradigm to improve baseline haemodynamic measures. Stimuli were created in MATLAB using the Psychophysics Toolbox (Brainard, 1997; Pelli, 1997)

and presented via a Canon Xeed SX60 LCD projector (1024 × 768 display resolution, 60 Hz refresh rate).

### 6.3.3 Imaging Protocol

Imaging was conducted on a 3 T GE scanner with an eight-channel receive-only head coil and a body coil for transmit. Physiological monitoring was conducted during imaging acquisition where heart rate was recorded using a finger pulse oximeter, end-tidal CO<sub>2</sub> and O<sub>2</sub> traces were recorded via a nasal cannula and respiration was recorded via respiratory bellows.

#### 6.3.3.1 MRI

BOLD and CBF data were simultaneously acquired using a PICORE pulsed arterial spin labelling sequence with a QUIPSS II cut-off of the label (Wong et al., 1998) with a dual gradient-echo and spiral *k*-space acquisition (TE<sub>1</sub>/TE<sub>2</sub> = 2.9/30 ms, TI<sub>1</sub>/TI<sub>2</sub> = 700/1500 ms, TR = 2500 ms, 480 volumes, label thickness = 200 mm, 1-cm gap between label and imaging plane). Perfusion- and BOLD-weighted time series were obtained using the first and second echo, respectively. Twelve slices (voxel resolution = 3.5 × 3.5 × 5 mm<sup>3</sup>, 1-mm interslice gap, FOV = 22.4 cm, matrix size = 64 × 64) were prescribed axially such that the most inferior slice reached the most inferior edge of the occipital lobe. A separate calibration scan consisted of a single-shot *M*<sub>0</sub> acquisition (TR = 4000 ms, 30 slices) with the same parameters as the functional acquisition to measure the equilibrium brain tissue magnetisation for the purposes of quantifying CBF (Perthen et al., 2008). A *T*<sub>1</sub>-weighted 3D FSPGR structural image (TE/TI/TR = 3.0/450/7.9 ms, flip angle = 20°, voxel resolution = 1 mm<sup>3</sup>, FOV = 256 × 256 × 168 mm<sup>3</sup>, matrix size = 256 × 256) was also acquired for image registration and tissue segmentation.

#### 6.3.3.2 MRS

GABA-edited MRS with and without symmetric MM suppression was used to measure endogenous GABA concentration. Two 15-min acquisitions (512 averages) were employed using the same protocol as described in Experiment 2 in Chapter 5. The VOI was placed in the OCC as shown in Figure 6.1. The order of the MRS acquisitions was counterbalanced across participants. For two participants, MM-suppressed GABA-MRS scans were not able to be performed. Therefore, for any statistical comparisons between the two measures in the main analysis the MM-

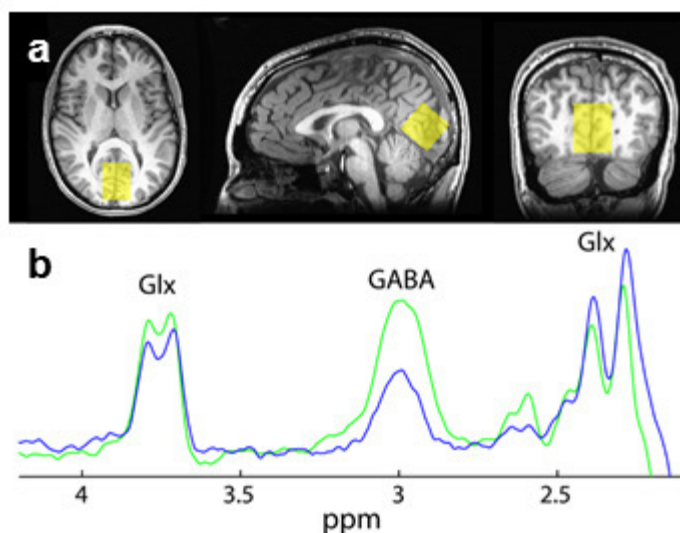


**Figure 6.1** *a: Representative placement of the MRS voxel in the occipital lobe. b: Sample difference spectra from one participant acquired using standard GABA-editing (green spectrum) and symmetric MM suppression (blue spectrum). The 3.0 ppm GABA peak is attenuated in the MM-suppressed spectrum. Composite glutamate + glutamine (Glx) peaks are also shown.*

contaminated measurements that were acquired for these particular participants were excluded.

### 6.3.4 MR Analysis

#### 6.3.4.1 MRI

Preprocessing and statistical analysis of functional imaging data were performed in AFNI (Cox, 1996). Registration and tissue segmentation were performed in FSL (Jenkinson et al., 2012).

To attain  $T_1$  equilibrium, the first four volumes of the acquisition were discarded. The raw data acquired from the first and second echo were first corrected for physiological noise. Cardiac, end-tidal  $\text{CO}_2$  and  $\text{O}_2$  partial pressure (Murphy et al., 2011), respiration volume per time (Birn et al., 2008) and RETROICOR (Glover et al., 2000) regressors were modelled from the physiological data and then used to remove variance attributed to physiological noise from each raw time series using a linear regression method in MATLAB (Murphy et al., 2013).

Each physiologically corrected time series was motion-corrected based on the transformation matrix of the second-echo BOLD-weighted time series. Interpolated surround subtraction of the first-echo tag and control image time series was performed to yield a perfusion-weighted time series. Interpolated surround averaging of the second-echo tag and control images was performed to yield a

BOLD-weighted time series (Liu and Wong, 2005). CBF images were calculated using the  $M_0$  of blood, estimated from the cerebrospinal fluid signal of the  $M_0$  image and the general kinetic model (Buxton et al., 1998).

Both the BOLD and CBF time series were analysed using a general linear model (GLM) in which stimulus regressors for each contrast level were convolved with a haemodynamic response function. Other regressors included motion parameters taken from the motion correction procedure and polynomial regressors to account for drift in the signal. In this experiment, baseline signal was taken to be the baseline regression coefficient, the constant term in the GLM. Each time series was converted into percent signal change by taking each stimulus-related regression coefficient per contrast level and dividing by the baseline coefficient. No other form of spatial or temporal filtering beyond surround subtraction/averaging was applied to the data.

An occipital lobe mask was selected from the MNI atlas, transformed into individual structural space and then transformed again into individual functional space for each time series through linear registration. The CBF occipital mask was multiplied by a grey matter mask based on each participant's tissue-segmented structural image. Separate BOLD and CBF activation regions of interest (ROI) were chosen based on voxels that were significantly activated to 100% contrast versus baseline (BOLD:  $t$ -score  $> 4.0$ , CBF:  $t$ -score  $> 1.6$ ; alpha level = 0.05, corrected for simultaneous comparisons). Finally, a single BOLD+CBF ROI was calculated by taking the intersection of these two activation ROI. Mean BOLD and CBF percent signal change at each contrast level was then determined within the BOLD+CBF ROI. One participant was removed from the dataset as their BOLD and CBF activation ROI did not intersect.

#### 6.3.4.2 MRS

Raw spectra were processed in Gannet following the same pipeline as used in Chapter 5. Fit errors ( $\epsilon_{\text{fit}}$ ) for the nonlinear least-squares model fits of the 3.0 ppm GABA peak were also calculated. GABA'+MM and GABA' concentration were quantified according to Eq. [3.16]. Using the tissue-segmented structural image, the

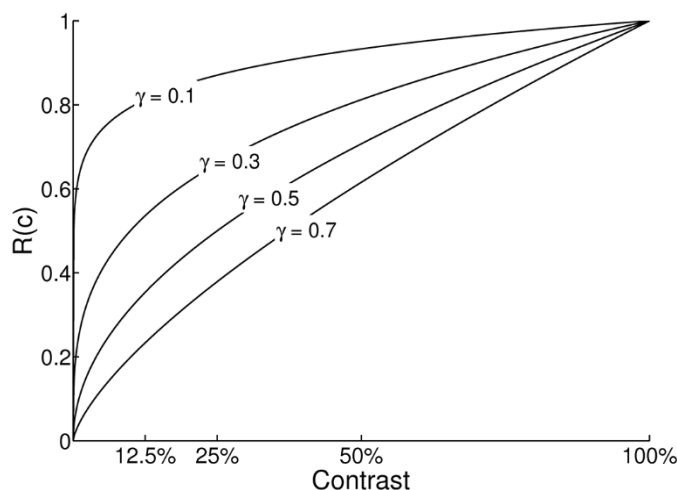


**Figure 6.2** Modelled power law contrast response functions with various assumptions of  $\gamma$  (rate of saturation of the response). A smaller  $\gamma$  value corresponds to faster saturation of the response to contrast,  $R(c)$ , whereas a larger value corresponds to slower saturation.  $R_{max}$  (modelled response at 100% contrast) is fixed at 1.

GABA integral was adjusted to account for the amount of CSF in the co-registered MRS voxel, with the water integral adjusted to account for tissue-dependent water visibility. In addition, the dependence of GABA concentration on GM was corrected using the method described in Chapter 3. The value of  $r_M$  was chosen based on the approach described in Section 3.4.3.3. In short, the 100 Brains cohort was used to choose the optimal  $r_M$  value by assessing 100 possible values linearly interpolated between the upper and lower bounds of the CI for the estimated  $r_M$  in that dataset (see Table 3.1). The optimal  $r_M$  was that which produced the smallest possible  $R^2$  when GABA concentration was regressed against  $t_{GM}$ . For the GABA'+MM dataset this was 1.53 and for the GABA' dataset this was 1.44.

### 6.3.5 Contrast Response Function

To characterise contrast tuning properties of the haemodynamic responses to graded contrast, a power law contrast response function (Legge, 1981) was used:

$$R(c) = R_{max}c^\gamma \quad [6.1]$$

where  $R_{max}$  is the modelled response at 100% contrast,  $c$  is contrast and  $\gamma$  is an exponent corresponding to the rate of saturation of the response. The rate of response change with contrast is slower when  $\gamma$  approaches 1 (i.e., linear, no saturation), signifying slower saturation; and faster when  $\gamma$  approaches 0, signifying faster saturation with increasing contrast. Predicted power law contrast response functions with assumed  $\gamma$  values are displayed in Figure 6.2. Contrast level (normalised to

100%) and percent signal change at each contrast level were converted into  $\log_{10}$  units. Eq. [6.1] was then fit to participants' BOLD and CBF tuning data in MATLAB with a least-squares fitting algorithm.

### 6.3.6 Statistical Analysis

For the primary analysis default Bayes factors ( $B_{10}$ ) for linear regression were calculated. As noted in Chapter 5, the Bayes factor is the ratio of the strength of evidence for one model (e.g., an alternative hypothesis) versus the strength of evidence for another model (e.g., a null hypothesis). Bayes factors were calculated according to the method described by Rouder and Morey (2012) using the freely available BayesFactor package (version 0.9.11-1). The prior probability was based on a Cauchy distribution of a continuous mixture of normals with scale factor ( $s$ ) set to  $\sqrt{2}/4$  (Liang et al., 2008; Rouder and Morey, 2012).

The BOLD signal arises following a complex cascade involving CBF and excitatory and inhibitory activity (Lauritzen et al., 2012; Sotero and Trujillo-Barreto, 2007). Therefore, regression models were examined to determine whether there was evidence to support that BOLD response saturation ( $\gamma_{\text{BOLD}}$ ) was better predicted by different combinations of relevant covariates: CBF response saturation ( $\gamma_{\text{CBF}}$ ), GABA'+MM and GABA'. Given the tight coupling between BOLD and CBF, the model that included  $\gamma_{\text{CBF}}$  was specifically compared against those that included  $\gamma_{\text{CBF}}$  and different combinations of the two GABA measures.

As an exploratory analysis, the individual correlations between contrast tuning parameters and GABA' and GABA'+MM in addition to the correlations between the GABA measures and BOLD/CBF responses at each contrast level are also reported. Due to the number of simultaneous comparisons made in the analysis, random permutation tests were performed on each correlational test within each family of comparisons. This nonparametric test controls for the familywise error rate while adaptively adjusting for the number of simultaneous comparisons that may or may not be dependent (Groppe et al., 2011). Thus, this method is similar to a Bonferroni correction in that it strongly controls for the probability of false discoveries within a family of comparisons but is more powerful as it accounts for the degree of correlation between tests. Based on the number of participants in this study, it would not have been feasible to compute all possible permutations (number of possible permutations = 31!); therefore, a random sample of 100,000 permutations

**Table 6.1** Mean ( $\pm$  SD) BOLD and CBF responses to graded visual contrast ( $n = 31$ ). Responses are represented as percent signal change from baseline (second and third columns) and as response normalised to percent change at 100% contrast (fourth and fifth columns).

Contrast	$\Delta$ BOLD (%)	$\Delta$ CBF (%)	Norm. $\Delta$ BOLD	Norm. $\Delta$ CBF
12.5%	0.96 $\pm$ 0.27	16.37 $\pm$ 5.29	0.41 $\pm$ 0.10	0.46 $\pm$ 0.16
25%	1.13 $\pm$ 0.29	19.01 $\pm$ 5.49	0.49 $\pm$ 0.11	0.53 $\pm$ 0.15
50%	1.54 $\pm$ 0.35	23.68 $\pm$ 5.02	0.66 $\pm$ 0.10	0.66 $\pm$ 0.13
100%	2.33 $\pm$ 0.41	36.27 $\pm$ 4.01	1.00	1.00

**Table 6.2** Mean ( $\pm$  SD) GABA concentration measured using standard GABA-editing ( $n = 31$ ) and symmetric MM suppression ( $n = 29$ ). The signal ratio represents the fraction of the signal retained following MM suppression (i.e.,  $[GABA'] / [GABA'+MM]$ ).

	GABA'+MM	GABA'
Concentration (i.u.)	1.56 $\pm$ 0.12	0.74 $\pm$ 0.15
$CV_{bs}$	7.80%	20.55%
Mean $\epsilon_{fit}$ ( $\pm$ SEM)	3.23 $\pm$ 0.09%	4.56 $\pm$ 0.20%
Signal ratio ( $\pm$ SD)	0.48 $\pm$ 0.09	

was generated per test. Both the uncorrected and corrected  $p$ -values (denoted  $p$  and  $p'$ , respectively) are reported when simultaneous comparisons were made. The robustness of correlation coefficients was assessed by calculating 95% CIs using a bootstrapping with replacement method. Iterations were performed 10,000 times. Bayes factors were also calculated for the individual correlational analyses comparing the relationship between BOLD and CBF response saturation and the two GABA measures.

## 6.4 Results

Mean BOLD and CBF percent signal change at each contrast level, including values normalised to response to 100% contrast, are given in Table 6.1. As expected, BOLD responses increased monotonically with contrast, with CBF showing the same trend. Paired  $t$ -tests showed that, for both BOLD and CBF, responses to contrast were significantly different from each other ( $p < 0.001$ ).

Table 6.2 shows the mean concentration of GABA'+MM and GABA'. Also shown is the between-subject coefficient of variation ( $CV_{bs}$ ). Mean GABA' concentration was approximately 50% that of mean GABA'+MM concentration.

**Table 6.3** Default Bayes factors for the linear regression model comparison. BOLD response saturation ( $\gamma_{BOLD}$ ) is the dependent variable and CBF response saturation ( $\gamma_{CBF}$ ), [GABA'+MM] and [GABA'] are treated as predictors.

	Model	$R^2$	$B_{m1}^a$	$B_{1m}^b$
M <sub>1</sub>	$\gamma_{CBF}$	0.32	1	1
M <sub>2</sub>	$\gamma_{CBF}$ , GABA'+MM, GABA'	0.33	0.16	6.30
M <sub>3</sub>	$\gamma_{CBF}$ , GABA'+MM	0.32	0.33	3.00
M <sub>4</sub>	$\gamma_{CBF}$ , GABA'	0.33	0.40	2.53

<sup>a</sup> Bayes factor of the comparison between each model and model M<sub>1</sub>.

<sup>b</sup> Bayes factor of the comparison between model M<sub>1</sub> and each model.

Two example spectra acquired using each acquisition are displayed in Figure 6.1b. The MM-suppressed values displayed about 2.5 times larger  $CV_{bs}$  (~21%) than the contaminated concentrations (~8%). While mean  $\epsilon_{fit}$  for the two acquisitions was significantly different ( $p < 0.001$ ), they were qualitatively low ( $< 5\%$ ). These results are similar to those reported in Chapter 5. The correlation coefficient between GABA'+MM and GABA' concentration was  $r = 0.43$  ( $p = 0.02$ ).

The results from the contrast response function fitting procedure were examined next. Mean ( $\pm$  SD)  $\gamma$  and  $R_{max}$  parameters for BOLD were  $0.44 \pm 0.16$  and  $2.20 \pm 0.42$ , respectively. For CBF, these were  $0.43 \pm 0.35$  and  $33.65 \pm 4.70$ , respectively (Table A.2). The mean  $\gamma$  for the BOLD data is similar to a previous contrast tuning fMRI study (Olman et al., 2004). The mean  $\gamma_{BOLD}$  and mean  $\gamma_{CBF}$  were not significantly different from each other ( $p = 0.72$ ).

Bayes factors for the compared linear regression models are displayed in Table 6.3. There was substantial evidence supporting the model including only  $\gamma_{CBF}$  versus the models including  $\gamma_{CBF}$ , [GABA'+MM] and [GABA'] ( $B_{01} = 6.30$ ). There was weak evidence supporting the model including only  $\gamma_{CBF}$  versus the models including  $\gamma_{CBF}$  and [GABA'+MM] ( $B_{01} = 3.00$ ) or  $\gamma_{CBF}$  and [GABA'] ( $B_{01} = 2.53$ ). The robustness of these Bayes factors was assessed by varying the scale factor of the Cauchy prior (Figure A.1). Additionally, the model including  $\gamma_{CBF}$  and [GABA'+MM] was compared against the model including  $\gamma_{CBF}$  and [GABA'] to determine which GABA measure better predicted  $\gamma_{BOLD}$  when  $\gamma_{CBF}$  was included as an additional covariate. There was weak evidence supporting the latter relative to the former model ( $B_{01} = 1.19$ ).

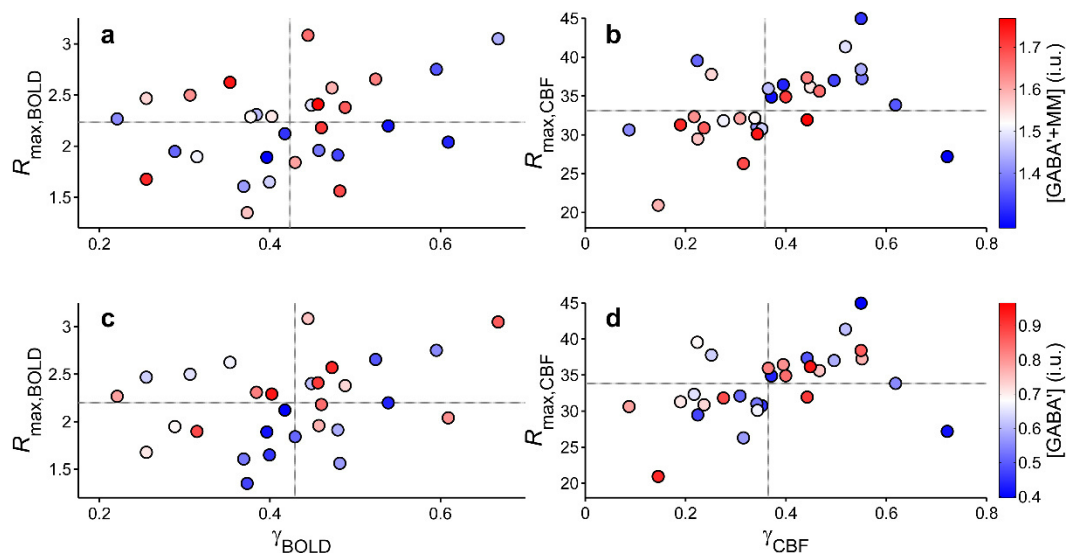


**Figure 6.3** Scatterplots of individual participants' response saturation parameter ( $\gamma$ ) as a function of their modelled maximum response to contrast ( $R_{max}$ ) for BOLD (a, c) and CBF (b, d). The colour bars indicate the amount of quantified GABA'+MM (top row) and GABA' concentration (bottom row), which is reflected by the colour of each individual point in the plots. The dashed lines show the median for each function parameter.

For the exploratory analysis, the association between contrast tuning parameters and endogenous GABA concentration was investigated. The  $\gamma$  parameter was negatively associated with [GABA'+MM] for CBF ( $r = -0.40$ ,  $p = 0.03$ ,  $p' = 0.10$ , CI:  $[-0.72, -0.09]$ ,  $B_{10} = 2.48$ ), such that participants with higher GABA levels had faster CBF response saturation to contrast. However, the significance of this relationship did not survive correction for simultaneous comparisons. For BOLD, this relationship was also negative but weaker and non-significant ( $r = -0.19$ ,  $p = 0.30$ ,  $p' = 0.73$ , CI:  $[-0.50, 0.14]$ ,  $B_{01} = 1.91$ ). GABA' measures did not correlate with the  $\gamma$  parameter for either BOLD ( $r = -0.07$ ,  $p = 0.71$ ,  $p' = 0.99$ ,  $B_{01} = 2.72$ ) or CBF ( $r = -0.31$ ,  $p = 0.10$ ,  $p' = 0.30$ ,  $B_{10} = 1.02$ ).

Neither [GABA'+MM] or [GABA'] were significantly related to  $R_{max}$ , the modelled haemodynamic response at 100% contrast, for BOLD ( $r = 0.15$ ,  $p = 0.42$ ;  $r = 0.36$ ,  $p = 0.05$ , respectively) or CBF ( $r = -0.26$ ,  $p = 0.17$ ;  $r = -0.12$ ,  $p = 0.55$ , respectively).

The inverse relationship between GABA'+MM levels and CBF response saturation suggest there may be a modulatory GABAergic effect on haemodynamic contrast tuning. To illustrate this, the derived  $\gamma$  parameters were plotted against individual  $R_{max}$  parameters for each participant and then individually stratified by their quantified GABA'+MM or GABA' concentration. As can be seen in Figure 6.3,

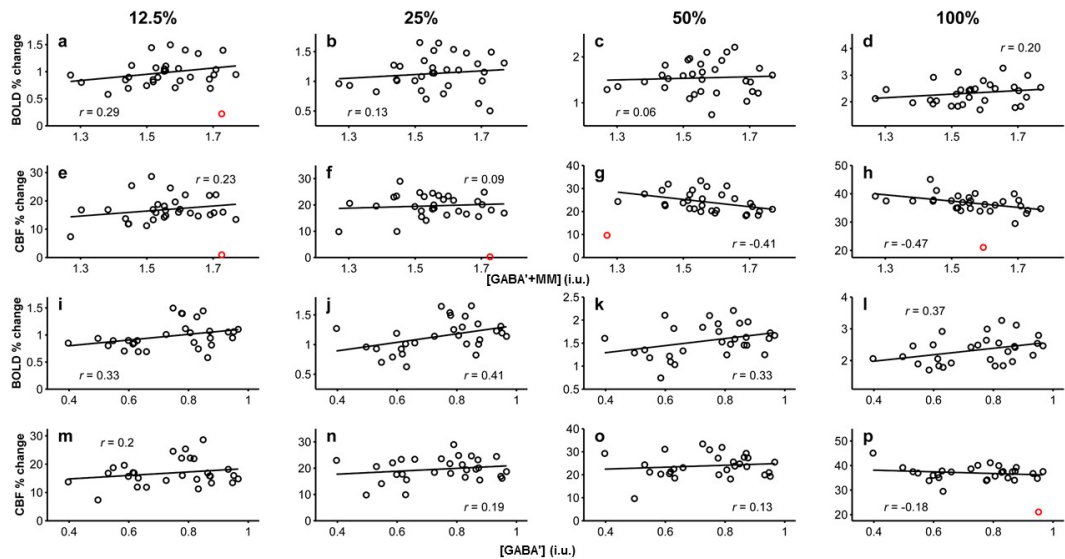


**Figure 6.4** Scatterplots of BOLD and CBF percent signal change at each contrast level as a function of GABA concentration. **a–h**:  $[GABA'+MM]$  versus BOLD (first row) and CBF (second row) responses. **i–p**:  $[GABA']$  versus BOLD (third row) and CBF (fourth row) responses. Red circles indicate outliers.

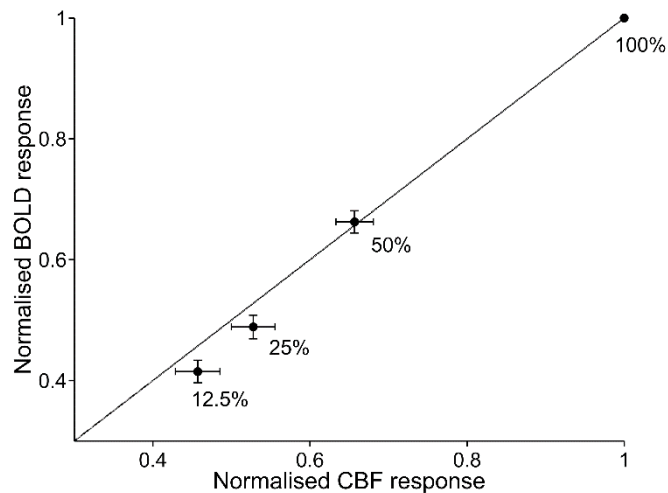


**Figure 6.5** Average BOLD and CBF percent signal change at each of the four contrasts normalised to responses to 100% contrast. BOLD displayed smaller response ratios at low contrast (12.5% and 25%) compared to CBF, indicated by the plotted points falling below the line of equality. Error bars are standard error of the mean. The solid line is the line of equality.

there is an observable bimodal distribution of response saturation parameters with respect to participants with high and low  $GABA'+MM$  levels for CBF. That is to say,  $GABA'+MM$  appears to mediate the degree of saturation of CBF at the least. This was not the case for BOLD or for  $GABA'$  for either haemodynamic response.

The relationships between GABA concentration and percent signal change at each contrast of the visual stimulus were also investigated.  $[GABA'+MM]$  was found to be negatively associated with CBF responses to 50% ( $r = -0.41$ ,  $p = 0.03$ ,

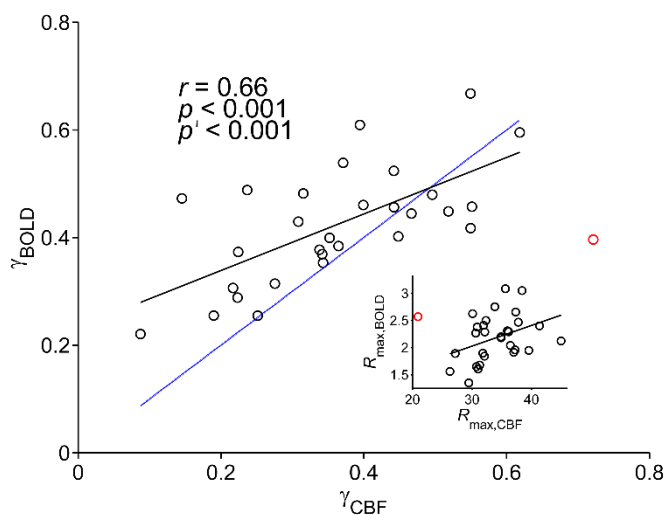


**Figure 6.6** The rate of response saturation ( $\gamma$ ) correlated between CBF and BOLD. A strong positive relationship was observed. The solid black line represents the best-fit line and the solid blue line represents the line of equality. That the majority of points are above the line of equality signifies that CBF generally showed faster saturation than BOLD. Both the uncorrected and corrected  $p$ -value is shown. The inset shows the scatterplot for modelled CBF and BOLD responses at 100% contrast ( $R_{max}$ ). These were also correlated ( $r = 0.38$ ,  $p = 0.04$ ,  $p' = 0.09$ ). Red circles indicate outliers.

CI:  $[-0.62, -0.13]$ ) and 100% contrast ( $r = -0.47$ ,  $p = 0.01$ , CI:  $[-0.63, -0.18]$ ). [GABA'] was positively associated with BOLD responses to 25% contrast ( $r = 0.41$ ,  $p = 0.03$ , CI:  $[0.09, 0.61]$ ). Given the large number of simultaneous comparisons, these correlations would not be expected to survive correction. Although some of the correlations uncharacteristically trended towards a positive relationship, none of these were significant (Figure 6.4). As previous studies have investigated the relationship between endogenous GABA levels and BOLD evoked by maximum-contrast visual stimuli (Harris et al., 2015a; Muthukumaraswamy et al., 2012, 2009; Violante et al., 2013), Bayes factors were calculated for the associations between BOLD responses at 100% contrast and both GABA measures. In both cases there was insufficient evidence to make a judgement:  $\Delta\text{BOLD}_{100}$  vs. [GABA'+MM]:  $B_{01} = 1.87$ ;  $\Delta\text{BOLD}_{100}$  vs. [GABA']:  $B_{10} = 1.60$ .

The simultaneous measurement of BOLD and CBF offers the opportunity to examine possible individual differences in the coupling between the two measures. Therefore, a second exploratory analysis of BOLD and CBF contrast tuning was carried out. Firstly, BOLD and CBF percent signal change were compared by normalising participants' responses to their response to 100% contrast. Figure 6.5 displays the response ratios for CBF against those for BOLD. The normalised percent signal change at 12.5% and 25% contrast was lower for BOLD than for CBF

but tended towards equality at 50%. Moreover, when the contrast tuning parameters were compared between fMRI signals, a strong positive correlation was revealed between  $\gamma_{\text{BOLD}}$  and  $\gamma_{\text{CBF}}$  ( $r = 0.66$ ,  $p < 0.001$ ,  $p' < 0.001$ , CI: [0.36, 0.83]).  $R_{\text{max,BOLD}}$  and  $R_{\text{max,CBF}}$  were also correlated ( $r = 0.38$ ,  $p = 0.04$ ,  $p' = 0.09$ , CI: [0.05, 0.62]) (Figure 6.6). For rate of response saturation, CBF displayed faster saturation than BOLD. This complements the finding showing that CBF response ratios were larger than BOLD response ratios at low contrast.

## 6.5 Discussion

Evidence has shown that GABA plays an important role in neurovascular coupling, with some in vivo investigations reporting an inverse relationship between GABA and BOLD- and perfusion-weighted fMRI measures (Donahue et al., 2014, 2010; Muthukumaraswamy et al., 2012, 2009; Northoff et al., 2007). However, there are discrepancies with respect to the direction of the relationship (Donahue et al., 2010; Wiebking et al., 2014), with some studies failing to reproduce an association (Harris et al., 2015a; Muthukumaraswamy et al., 2012). Here, GABA's potential role in contrast tuning properties of haemodynamic measures was examined. The primary finding, using Bayesian regression analysis, indicates that the most appropriate model to describe the behaviour of BOLD response saturation in the data was one that included CBF response saturation (as expected), but not GABA.

Nonetheless, exploratory analyses suggest that GABA'+MM concentration and the rate of CBF response saturation to graded contrast were associated, where increased endogenous GABA'+MM levels corresponded to faster saturation. Permutation tests showed that these correlations were not significant when accounting for simultaneous comparisons, however. Therefore, the results can only be taken to be preliminary evidence of a possible modulatory role of GABA'+MM concentration on haemodynamic response sensitivity to a visual stimulus.

It is also shown that GABA'+MM was negatively associated with CBF responses at higher contrast levels, but these would not be expected to survive correction for simultaneous comparisons given the large number of tests. Finally, to add to the understanding of how MRS-derived GABA concentration relates to fMRI measures, a symmetric MM suppression technique was employed in addition to standard MM-contaminated GABA-edited MRS. Contrary to the stated hypothesis,

GABA' was not a stronger predictor of haemodynamic response saturation or percent signal change to contrast compared to GABA'+MM.

Recent research by Katzner et al. (2011) has shown that pharmacological intervention of GABA<sub>A</sub> receptors of V1 neurons in cats modulates the response gain (an upward shift of the tuning curve) following stimulation by a contrast-graded visual stimulus. This effect on contrast gain control has been replicated in mice (Atallah et al., 2012), with a related effect having been observed with respect to adaptation to auditory stimuli in rats (Duque et al., 2014; Pérez-González et al., 2012). These studies demonstrate direct GABAergic control on response sensitivity to visual contrast. However, extrapolating the role of GABAergic inhibition from single-cell spiking activity to corresponding features of perfusion and the BOLD signal is very difficult given the highly complex network between activity at the vascular level and activity at the neuronal level (Singh, 2012). Moreover, the GABA concentration discussed in the present study is arguably a measure of total MR-visible GABA (intra- and extracellular), as opposed to exclusively synaptic GABA. Nonetheless, the link between endogenous GABA levels and haemodynamic contrast tuning provides a pathway to fill the gap between neurochemistry and imaging of neurovascular mechanisms.

GABA concentration was not related to BOLD or CBF responses to most contrasts. When a relationship was apparent, it was negative but only for CBF responses at higher contrast levels. This differs from the majority of studies that have found an inverse association between endogenous GABA concentration and BOLD responses (Donahue et al., 2010; Muthukumaraswamy et al., 2012, 2009; Northoff et al., 2007), but is consistent with a recent study that found no relationship between GABA and BOLD responses to a variety of stimuli (Harris et al., 2015a). Additionally, Bayes factors indicated there was insufficient evidence to favour an association between GABA and BOLD response at 100% contrast. It is possible that GABA's relationship with haemodynamics is more complex than a simple inverse relationship with peak signal change to a stimulus that maximally activates an area of the cortex. The fact that GABA'+MM measures did not correlate with BOLD responses at any contrast, but there was an association with CBF responses at high contrast, may suggest that GABAergic modulation of haemodynamics is different for stimuli applied at maximum strength compared to weaker stimuli. This proposition may not be true when endogenous GABA is related to steady-state

haemodynamic activity, such as resting-state BOLD and basal perfusion, where negative relationships have also been seen (Donahue et al., 2014; Kapogiannis et al., 2013); or when an activity-inducing task cannot intuitively be graded, such as with emotional stimuli (Northoff et al., 2007). It is also possible that the mechanisms behind GABA's relationship to the haemodynamic response is intrinsically different for BOLD and CBF. The complexity of the origin of the BOLD signal, and CBF's role in generating it, would make this likely.

Alternatively, GABA's role in observed BOLD and CBF responses may be more inherently related to their dynamic range. Albrecht and Hamilton (1982) seminally measured dynamic range in neurons in the striate cortex of the cat and monkey by measuring the contrast required for a neuron to produce 50% of its maximum firing rate (i.e., semi-saturation). Striate neurons displayed a large variation in dynamic range, and on average semi-saturation was reached at around 20% contrast. This finding has also been reported in fMRI studies, where semi-saturation occurs at around 10–20% contrast (Boynton et al., 1996; Gardner et al., 2005; Tootell et al., 1995). In this study, a power law function was used to characterise contrast tuning. A logical consequence of this model is a tight coupling between responses at low contrast and the saturation rate parameter (see Figure 6.2). Since some BOLD and CBF responses at low contrast trended towards a relationship with GABA'+MM concentration, and GABA'+MM concentration was inversely associated with CBF saturation rate, it is posited that endogenous GABA could be a marker of the dynamic range of haemodynamic responses. From this it can be argued that an association between GABA and task-related BOLD/CBF responses may not be necessarily evident if a stimulus is presented at maximal input and responses have reached their saturation point, or if the dynamic range of haemodynamic responses is not sufficiently wide.

One of the predictions was that GABA concentration derived from MM-suppressed GABA-editing would result in a stronger association with BOLD and CBF compared to the MM-contaminated measurements. Since the main advantage of symmetric suppression is that the 3.0 ppm MM peak that overlaps the 3.0 ppm GABA peak is removed, it provides a more specific measure of GABA. Indeed, the signal ratio of GABA' to GABA'+MM was approximately 0.50, which falls in line with empirical evidence (Aufhaus et al., 2013; Harris et al., 2015b; Rothman et al., 1993) and the study in Chapter 5. However, GABA' was not shown to be a stronger

predictor of BOLD and CBF response sensitivity. Moreover, there was only weak evidence in favour of the MM-suppressed GABA measure when compared to the MM-contaminated measure in the prediction of haemodynamic response saturation. This finding is difficult to explain as it is not clear how MM could contribute to perfusion and the BOLD signal. This would necessitate a more thorough investigation of the contaminating MM component. One explanation is that because the GABA' peak is effectively half of the GABA'+MM peak, the SNR will be lower, which would mean detecting any true relationships would require more statistical power in the experiment. Indeed, the  $\epsilon_{\text{fit}}$  between the two acquisitions was significantly different. Nonetheless, it was still qualitatively low ( $< 5\%$ ) in both cases. Given the novelty of using MM suppression in GABA-MRS research, and that very few studies have empirically compared the differences between symmetric suppression and standard editing, further work investigating the differences between the two acquisition techniques is required.

CBF displayed greater normalised responses to 12.5% and 25% contrast than BOLD. This mirrors a study by Liang et al. (2013) who used an experimental design similar to the one used here. They observed that BOLD had a greater dynamic range than CBF, reflected in the ratio between percent signal change at highest and lowest contrasts being greater for BOLD ( $\sim 4.3$ ) than CBF ( $\sim 2.4$ ). Indeed, in the data from the present study the dynamic range of BOLD was  $\sim 2.4$ , whereas for CBF it was  $\sim 2.2$ . Adding to that finding, participants' CBF responses demonstrated a faster degree of saturation than their corresponding BOLD responses. Taken together, these results contradict the commonly reported finding that CBF tends to increase linearly at higher grades of a stimulus whereas BOLD in turn tends to saturate (Chiarelli et al., 2007; Hoge et al., 1999b; Rees et al., 1997).

A limitation of this study is that the properties of the annular gratings differed somewhat from previous fMRI experiments using graded visual stimuli. For example, whereas BOLD and CBF responses appear to peak when stimuli are presented with a temporal frequency of 8 Hz (Kwong et al., 1992; Lin et al., 2008; Zhu et al., 1998), a temporal frequency of 6 Hz was used here. Although BOLD amplitudes evoked at 6 and 8 Hz may not be substantially different (Muthukumaraswamy and Singh, 2008), the choice of a specific temporal frequency may limit the extent to which the findings can be generalised. Additionally, studies have typically used high spatial frequencies (3+ cpd), whereas a comparatively

lower frequency (1.2 cpd) was used in this study. Nonetheless, previous studies suggest that primary visual cortex BOLD responses remain relatively stable as spatial frequency is modulated (Muthukumaraswamy and Singh, 2009; Singh et al., 2000; Swettenham et al., 2013). A second limitation is the intrinsically low SNR of the arterial spin labelling signal. This will contribute to poorer fitting of the tuning curves for the CBF data and thus poorer parameterisation of CBF response saturation.

Several avenues of future research are possible following the preliminary findings reported here. Firstly, given that the Bayes factors for the regression model comparison constituted weak, and therefore inconclusive, evidence against including GABA'+MM or GABA' in the model, a replication of this study is necessary with either a larger sample size or reduced comparisons. Secondly, the failure to find a relationship between GABA concentration measured using the symmetric suppression technique and contrast-tuning properties needs to be addressed, particularly as MM-contaminated GABA measures did show such a relationship. MM-suppressed GABA measures may show stronger differential effects following neurostimulation or pharmacological intervention compared to contaminated GABA measures, for instance. Thirdly, the use of calibrated fMRI techniques to non-invasively measure the cerebral metabolic rate of oxygen (Bulte et al., 2012; Davis et al., 1998; Wise et al., 2013) and  $^{13}\text{C}$  MRS to measure the cerebral metabolic rate of glucose (Hyder and Rothman, 2012; Patel et al., 2005) offer the possibility of better characterising the relationship between GABAergic inhibition, its role in response sensitivity and the underlying mechanisms of BOLD- and perfusion-weighted responses.

## 6.6 Conclusions

To conclude, BOLD and CBF were simultaneously measured as a contrast-graded visual stimulus was presented to participants. Additionally, endogenous GABA concentration was measured in the OCC using GABA-edited MRS with and without MM contamination. Using a Bayesian analysis, weak evidence was found against hypotheses that included GABA'+MM or GABA' in the prediction of response saturation. However, this did not pass the threshold to support a hypothesis that did not include GABA'+MM or GABA' in the model. Although the results of this study

are inconclusive, the possibility that the saturation of the BOLD or CBF signal may confound findings relating haemodynamic measures to GABA cannot be rejected.

# 7. Numerical Simulations of GABA-Editing Efficiency and the Impact of Frequency Drift<sup>††</sup>

## 7.1 Abstract

In this chapter, the editing efficiency of and impact of frequency drift on  $J$ -difference-edited MRS of GABA with and without symmetric MM suppression is investigated. GABA and MM multiplet patterns were simulated using density matrix formalism. Editing efficiency profiles were characterised with two editing pulses with different frequency bandwidths (95 and 76 Hz) and each at two echo times (68 and 80 ms). In a separate simulation, positive and negative linear frequency drift was induced in several experiments and the relative contribution of GABA and MM to the GABA+MM signal was compared. Both standard and symmetric editing schemes were simulated. Compared to standard editing, the lineshape of the 3.0 ppm GABA-H4 difference multiplet was markedly different when symmetric suppression was employed. The editing profile for the narrower bandwidth editing pulse produced a more frequency-selective efficiency profile and a negative difference integral at 1.5 ppm. Frequency drift had a greater impact on changes in the GABA signal in symmetric suppression. It is concluded that the proximity of the ON and OFF editing pulses in symmetric editing substantially affects the difference multiplet when drift is introduced into the experiment. Therefore, it is crucial to determine the editing efficiency of a given symmetric suppression experiment and to monitor shifts in centre frequency.

---

<sup>††</sup> The author is indebted to Dr. Jamie Near (McGill University) for providing the MATLAB software (FID-A, Simpson et al., 2015) used to perform the numerical simulations in this chapter as well as for providing advice and support with the modifications to the software's code.

## 7.2 Introduction

As discussed earlier in this thesis, spectral editing of GABA involves the subtraction of two scans each acquired at  $TE = 1/2J$ , one where the 3.0 ppm GABA-H4 resonance is refocused using  $180^\circ$  Gaussian frequency-selective refocusing pulses (ON scan) and one where the spin system is allowed to evolve freely (OFF scan). Shifts in centre frequency, and therefore in the frequency of the editing pulses, will have a detrimental effect on the resulting DIFF spectrum. For instance, when the frequency of each subspectrum of a MEGA-PRESS experiment is misaligned, residual Cr and Cho peaks that overlap with GABA will cause subtraction artefacts that distort the GABA DIFF peak (Evans et al., 2013), leading to signal loss and increased linewidth. Additionally, frequency drift will reduce the efficiency of spectral editing as the editing pulses move off resonance (Harris et al., 2014). The former effect can be typically rectified by correcting the centre frequency of each acquisition retrospectively (Evans et al., 2013; Near et al., 2015; Waddell et al., 2007). However, frequency drift affects the apparent position of the frequency selective RF pulse in the sequence, thus can only be prospectively corrected by real-time motion correction and frequency updating (Henry et al., 1999; Lange et al., 2011; Thiel et al., 2002; Zaitsev et al., 2010).

Harris et al. (2014) have recently reported the simulated and experimental impact of frequency drift on standard GABA-editing, where ON editing pulses are placed at 1.9 ppm and the OFF editing pulses are placed off resonance at 7.5 ppm. To replicate the protocol of a typical imaging study, BOLD-fMRI was conducted prior to three consecutive MEGA-PRESS acquisitions. The centre frequency drifted by an average of  $-7$  Hz during the MRS scans. This negative drift persisted up to 30 min after the fMRI scan. Although retrospective frequency correction led to an increased SNR and, consequently, greater quantified GABA concentration, total frequency drift was shown to impact on the degree of MM contamination in the resolved GABA signal.

Drift will be even more problematic in the symmetric editing scheme used to remove the MM contaminant given the close proximity of the OFF editing pulses to both the GABA-H3 resonance at 1.9 ppm and the M4 resonance at 1.7 ppm (Figure 7.1a). The editing efficiency of the GABA-H3 resonance in the OFF scan will

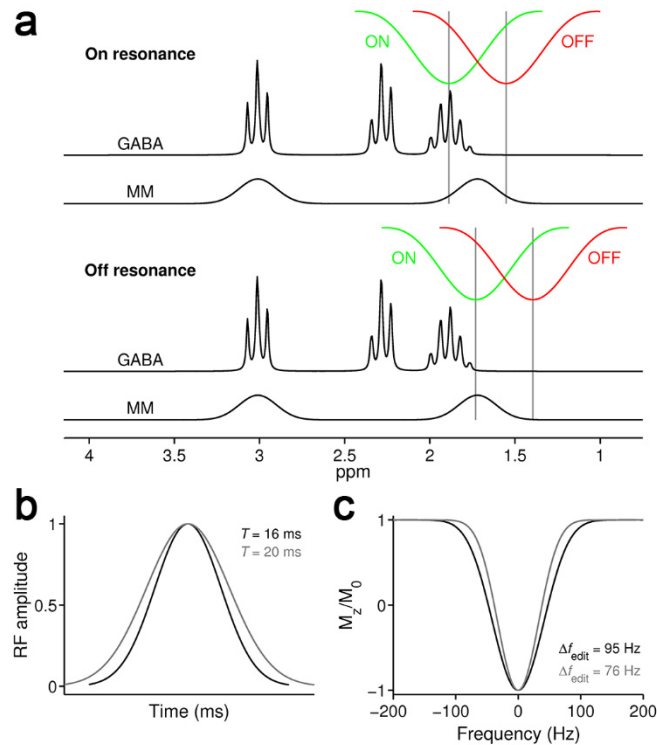


**Figure 7.1** a: Representations of the GABA and MM spin systems superimposed by inversion frequency profiles for representative Gaussian editing pulses offset according to the symmetric MM suppression editing scheme: ON = 1.9 ppm, OFF = 1.5 ppm. When on resonance, the editing pulses will lead to equal excitation of the MM resonance at 1.7 ppm (M4). The M4 resonance and the scalar-coupled M7 resonance at 3.0 ppm are then removed in the DIFF spectrum. Frequency drift moves the editing pulses off resonance, causing inefficient suppression of the M4 resonance and residual contamination of the 3.0 ppm GABA-H4 signal by the M7 resonance. b: Radiofrequency waveforms for two Gaussian editing pulses with 1% truncation. A longer pulse duration ( $T = 20$  ms) results in a narrower frequency bandwidth ( $\Delta f_{edit} = 76$  Hz) and better frequency selectivity, whereas a shorter pulse duration ( $T = 16$  ms) results in less frequency selectivity ( $\Delta f_{edit} = 95$  Hz). c: Inversion frequency profiles for the Gaussian editing pulses shown in b.

depend on the frequency selectivity of the editing pulse (Edden et al., 2012b; Harris et al., 2015b; Mikkelsen et al., 2016) and the degree of MM contamination will depend on the amount of frequency drift in the experiment (Harris et al., 2014).

Editing efficiency in the symmetric editing scheme, how it is affected by drift and how it compares to a standard editing scheme have yet to be described in detail. In this chapter, both the editing efficiency of the symmetric editing scheme and the impact of frequency drift on the resolved GABA signal in GABA-edited experiments were investigated by numerical simulation. This was compared against simulated experiments where a standard editing scheme was employed.

## 7.3 Methods

### 7.3.1 Simulations

Density matrix formalism was used to simulate the evolution of the GABA spin system at a  $B_0$  field strength of 3 T. Chemical shifts and coupling constants of the GABA spin system were taken from Near et al. (2013b) and are given in Table 2.1. MEGA-PRESS sequence parameters included ideal, instantaneous  $90^\circ$  excitation and  $180^\circ$  slice-selective refocusing pulses. Shaped editing pulses were simulated as Gaussian refocusing pulses with ideal  $180^\circ$  flip angles. To avoid transverse magnetisation artefacts, an eight-step phase cycle was employed with the following phase angles applied to the first and second editing pulses, respectively:  $[0^\circ, 90^\circ]$ ,  $[0^\circ, 90^\circ, 180^\circ, 270^\circ]$ . FIDs with 4096 data points were generated, apodized using an exponential filter corresponding to a linewidth of 2 Hz, zero-filled eight times and finally Fourier transformed into the frequency domain (spectral width = 5 kHz).

Two sets of simulated experiments were performed using the open-source MATLAB-based FID-A software toolkit (Simpson et al., 2015) to assess (i) the change in editing efficiency when editing pulse frequency bandwidth is modulated and (ii) the impact of frequency offsets as induced by drift in the  $B_0$  field in standard and symmetric editing. In the first set of simulations, the change in the GABA and MM integrals was examined by offsetting the ON editing pulse from 0 to  $-160$  Hz (1.89 to  $\sim 0.64$  ppm) in steps of 1.25 Hz ( $\sim 0.01$  ppm) in order to characterize editing efficiency profiles. The OFF editing pulse was fixed at 7.41 ppm. For MM, the spin system was assumed to be a  $A_2M_2X_2$  system with the same coupling constants and chemical shifts as GABA but with the M spins shifted to 1.72 ppm to match the M4 resonance of the MM baseline (Behar et al., 1994). The impact of frequency drift was simulated in the second set of simulations, whereby eleven difference-edited experiments were performed, each with 64 pairs of ON–OFF acquisitions. ON and OFF editing pulses were placed according to either a standard editing scheme (ON/OFF = 1.89/7.41 ppm) or a symmetric MM suppression scheme (ON/OFF = 1.89/1.55 ppm; i.e., symmetrical about the M4 resonance at 1.72 ppm). Various amounts of total frequency drift were induced in each experiment: 20, 16, 12, 8, 4, 0,  $-4$ ,  $-8$ ,  $-12$ ,  $-16$  or  $-20$  Hz. Editing pulse frequency was offset according to linear interpolation for each pair of intermediate ON/OFF scans in each experiment.

All simulations were performed either with editing pulse duration ( $T$ ) = 16 ms and TE = 68 ms or with  $T$  = 20 ms and TE = 80 ms in order to appraise the effect of increased frequency selectivity of editing pulses. This also allows a fair comparison with the in vivo experiments presented earlier in this thesis. The editing pulse had a Gaussian RF waveform with 1% truncation and a frequency bandwidth ( $\Delta f_{\text{edit}}$ ) at FWHM of 95 Hz for  $T$  = 16 ms and 76 Hz for  $T$  = 20 ms (Figure 7.1). The time-bandwidth product ( $R$ ) for this pulse was 1.53. Pulse timings ( $\tau_n$ ) of the MEGA-PRESS sequence (i.e., excitation –  $\tau_1$  – refocus –  $\tau_2$  – edit –  $\tau_3$  – refocus –  $\tau_4$  – edit –  $\tau_5$  – acquire) were 7, 13, 21, 13 and 14 ms for TE = 68 ms and 7, 16, 24, 16 and 17 ms for TE = 80 ms, respectively.

### 7.3.2 Phantom Experiments

Two phantom experiments were conducted on a 3 T GE scanner to determine the GABA DIFF multiplet lineshape in standard and symmetric GABA-edited spectroscopy. GABA was detected in a 20-mM phantom using two MEGA-PRESS acquisitions. In the first, a standard placement for the editing pulses was used: ON/OFF = 1.9/7.5 ppm. In the second, a symmetric editing scheme was employed: ON/OFF = 1.9/1.5 ppm. Other scan parameters were as follows: TE/TR = 80/1800 ms, voxel size =  $20 \times 20 \times 20$  mm<sup>3</sup>,  $T$  = 20 ms, 128 averages, 4096 data points, 5 kHz spectral width. The phantom was scanned at room temperature and the frequencies of the editing pulses were offset to account for temperature effects on chemical shift.

## 7.4 Results

### 7.4.1 Effect on Spectral Lineshape

GABA ON, OFF and DIFF multiplets for simulated standard and symmetric editing experiments are displayed in Figure 7.2a. These were simulated using the 76-Hz editing pulse. The lineshapes of all three spectra were experimentally replicated in

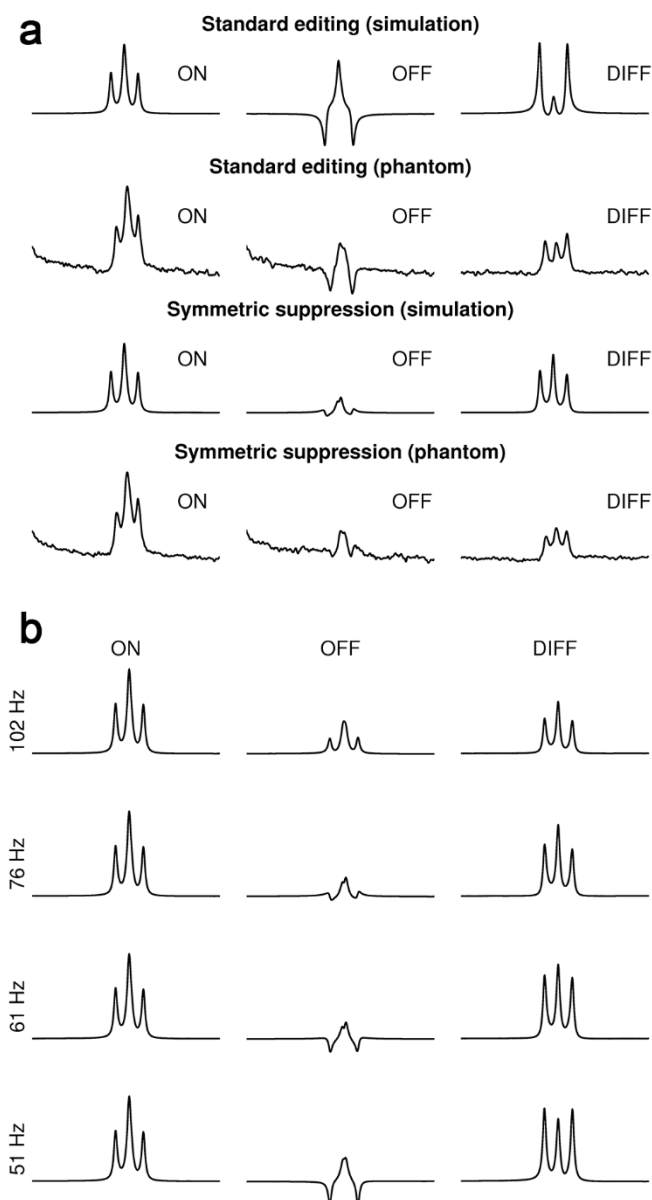


**Figure 7.2 a:** Simulated and experimental GABA-H4 ON, OFF and DIFF multiplets resolved by standard editing and symmetric MM suppression. The GABA resonance is partially refocused in the OFF scan in the symmetric editing scheme, leading to a prominent center peak and reduced intensities of the outer peaks in the DIFF multiplet. **b:** ON, OFF and DIFF multiplets from simulated symmetric editing experiments illustrating the effect of editing pulse frequency bandwidth on the GABA-H4 spectral lineshape (arranged in descending order according to increasing frequency selectivity).

vitro. The apparent center peak in the DIFF multiplet in the standard editing experimental data is a result of deviations in the flip angle of the slice-selective refocusing pulses from the ideal  $180^\circ$ . In the symmetric editing acquisition, both the simulated and experimental DIFF multiplets display a prominent center peak and outer peaks with reduced intensities. This is explained by partial refocusing of the GABA-H4 resonance in the OFF scan, a result of the bandwidth of the editing pulses

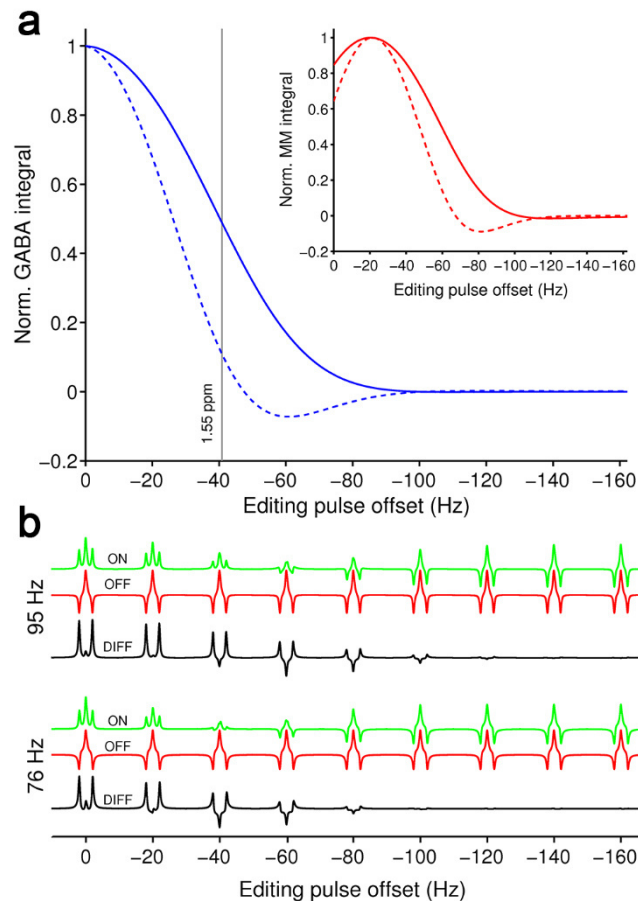


**Figure 7.3 a:** Editing efficiency profiles based on modulating the frequency bandwidth of the Gaussian editing pulse. The GABA (blue) and MM (red) integrals are normalised to maximal signal intensity and plotted as a function of ON editing pulse frequency offset. The editing efficiency profiles for the broader bandwidth, 95-Hz and narrower bandwidth, 76-Hz editing pulses are illustrated as solid and dashed lines, respectively. The grey line indicates the frequency offset of an OFF editing pulse in the symmetric editing scheme. **b:** Simulated GABA-H4 ON, OFF and DIFF multiplets at specified frequency offsets resolved by the 95- and 76-Hz editing pulses.

being insufficiently frequency-selective. This effect was confirmed by modulating editing pulse duration in the simulated symmetric editing experiment (Figure 7.2b). Increasing pulse duration, and thus narrowing the bandwidth, leads to improved frequency selectivity and less refocusing of the GABA-H4 resonance in the OFF scan.

#### 7.4.2 Editing Efficiency

The normalised GABA and MM integrals from the editing efficiency simulations are plotted as a function of ON editing pulse offset in Figure 7.3a. As expected, the broader bandwidth, 95-Hz editing pulse leads to a broader response in the integral as the ON pulse is shifted off resonance, whereas the narrower bandwidth, 76-Hz editing pulse leads to a narrower response and thus improved frequency selectivity.

**Table 7.1** Editing efficiency for standard editing and symmetric MM suppression

Technique	TE, $\Delta f_{\text{edit}}$	Editing efficiency
Standard editing	68 ms, 95 Hz	0.51
	80 ms, 76 Hz	0.47
Symmetric suppression	68 ms, 95 Hz	0.26
	80 ms, 76 Hz	0.42

The MM integrals behave in a similar fashion except with maximal signal attained at 1.72 ppm. For symmetric editing, it is crucial that the partial excitation of the GABA-H3 resonance at 1.89 ppm by the OFF pulse placed at 1.55 ppm is minimized. The efficiency profiles show that an OFF editing pulse with a broader bandwidth will lead to a larger degree of partial refocusing of the 3.01 ppm peak when the frequency is offset by approximately  $-40$  Hz (i.e., at 1.55 ppm), causing a loss in the signal in the DIFF multiplet. Interestingly, when using a 76-Hz pulse, the integral becomes negative between  $-40$  Hz and  $-90$  Hz offset. This is explained by the lineshape of the DIFF multiplet at these offsets (Figure 7.3b). The centre peak is inverted while the outer peaks are in phase but with an intensity comparatively lower than the absolute intensity of the anti-phase centre peak. The calculated integral for this lineshape is therefore below 0. The ON multiplets at  $-20$ ,  $-40$  and  $-60$  Hz offset resolved using the 95- and 76-Hz editing pulses mirror the lineshapes displayed in the OFF multiplets in Figure 7.2b.

A numerical estimate of editing efficiency can be derived by calculating the amount of GABA-H4 signal recovered in the DIFF spectrum as a fraction of the amount of total available signal in the experiment (estimated from the refocused GABA-H4 resonance in the ON scan). Editing efficiency estimates for the standard and symmetric editing techniques using the two editing pulses are given in Table 7.1. The editing efficiency for standard editing was  $\sim 0.50$ , as expected. The slightly lower ratio for the TE = 80 ms experiment is a result of  $J$ -evolution of the GABA spins. Conversely, there is a greater difference in ratios for symmetric suppression. The acquisition using the narrower bandwidth editing pulse was about 1.6 times more efficient than the acquisition with the broader bandwidth pulse when a symmetric editing scheme was used. This is due to differences in the degree of refocusing of the GABA-H4 resonance by the OFF editing pulse in either

experiment, which will lead to differences in the integral of the GABA DIFF multiplet.

### 7.4.3 Impact of Frequency Drift

The ON, OFF and DIFF multiplets for GABA and MM from the frequency drift simulations are shown in Figure 7.4 and Figure 7.5, respectively. The integrals of the GABA DIFF multiplet for each simulated experiment normalised to the integral at 0 Hz drift are plotted in Figure 7.6. Two characteristics can be discerned from this set of simulations. First, signal intensity is more sensitive to frequency drift when the frequency selectivity of the editing pulse is increased. This is demonstrated by the greater change in lineshape and amplitude the GABA and MM multiplets experience with frequency offset when the editing pulse is more frequency selective. Additionally, the rate of change of the integral as a result of drift is greater when  $\Delta f_{\text{edit}} = 76$  Hz (Figure 7.6). For instance, for  $-12$  Hz drift the GABA signal loss with

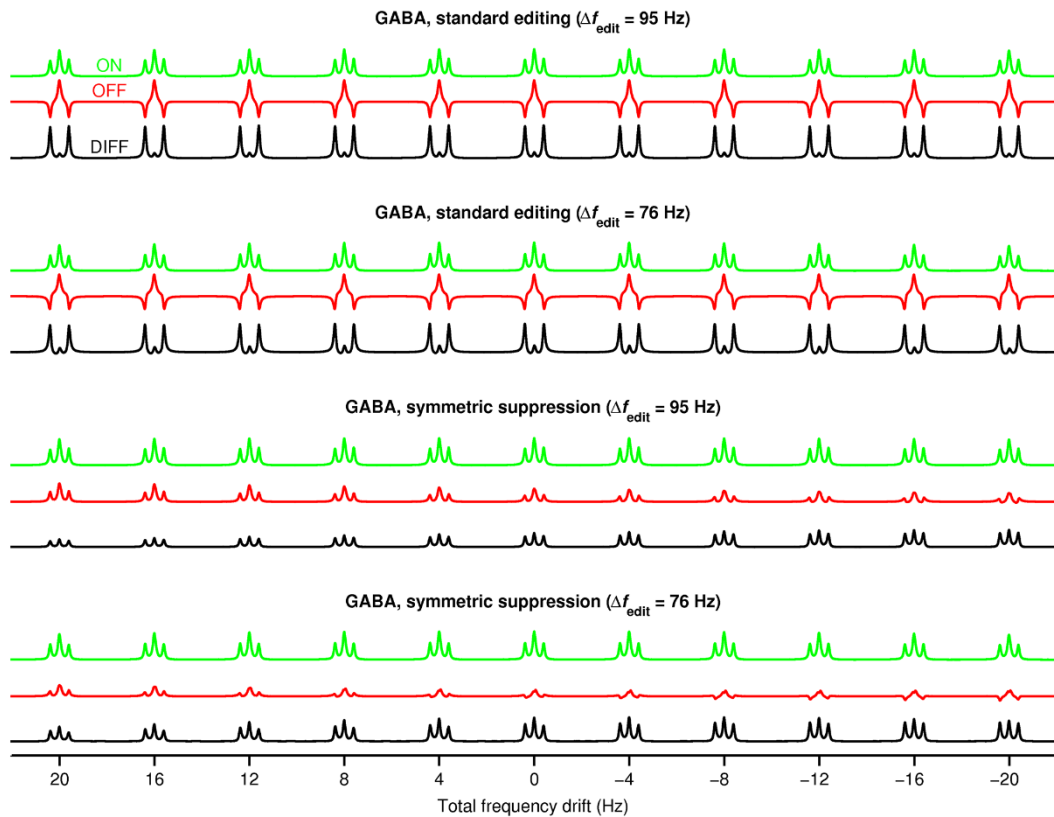


**Figure 7.4** ON, OFF and DIFF multiplets for the GABA-H4 resonance resolved by standard or symmetric editing with various amounts of total linear frequency drift (20 to  $-20$  Hz) induced in the simulated MEGA-PRESS experiment. The frequency bandwidth of the editing pulses ( $\Delta f_{\text{edit}}$ ) was either 95 or 76 Hz as shown. Number of ON–OFF pairs of acquisitions in each experiment = 64.

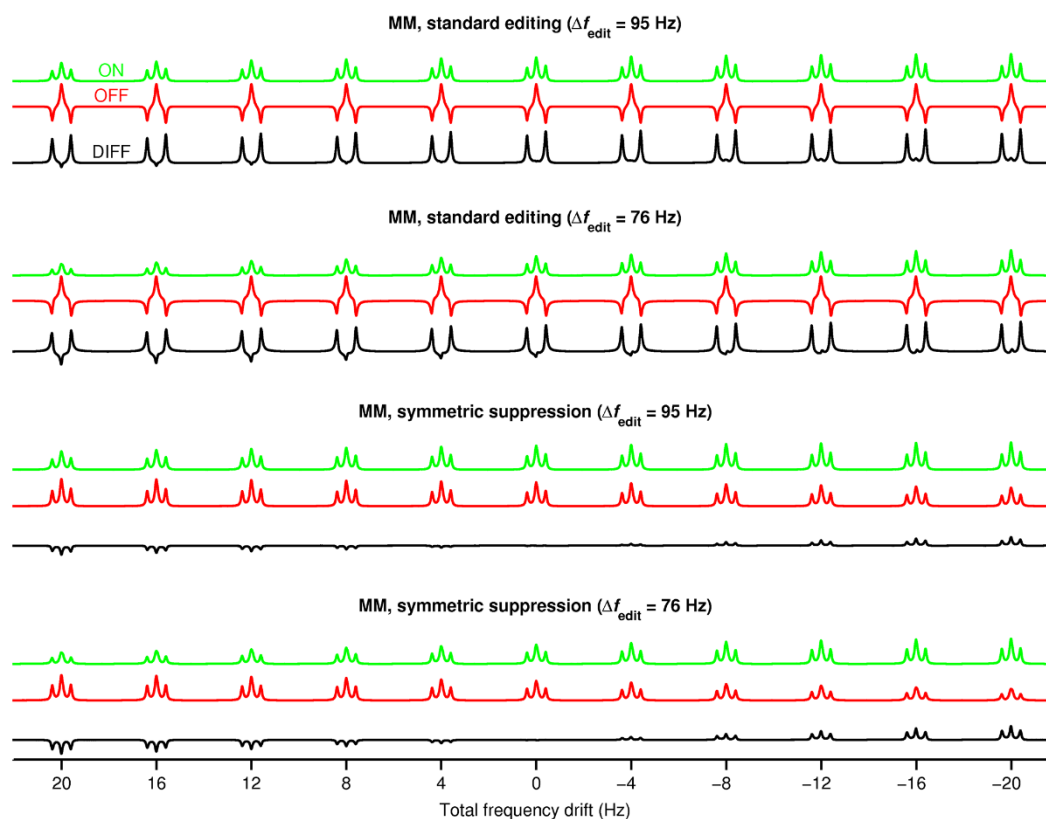
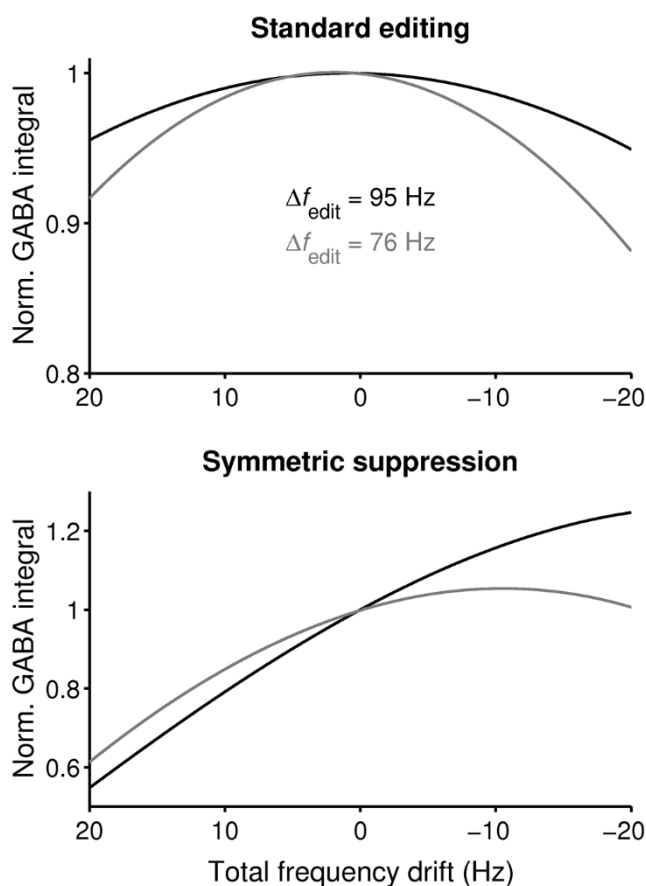


**Figure 7.5** ON, OFF and DIFF multiplets for the M7 macromolecule resonance resolved by standard or symmetric editing with various amounts of total linear frequency drift induced in the simulated MEGA-PRESS experiment. The MM spin system was assumed to mimic the GABA spin system but with the scalar-coupled M4 resonance set to 1.72 ppm in lieu of the GABA-H3 resonance at 1.89 ppm.

standard editing is 2% for the 95-Hz pulse but is nearly 2.5-times greater for the 76-Hz pulse (4.8% reduction).

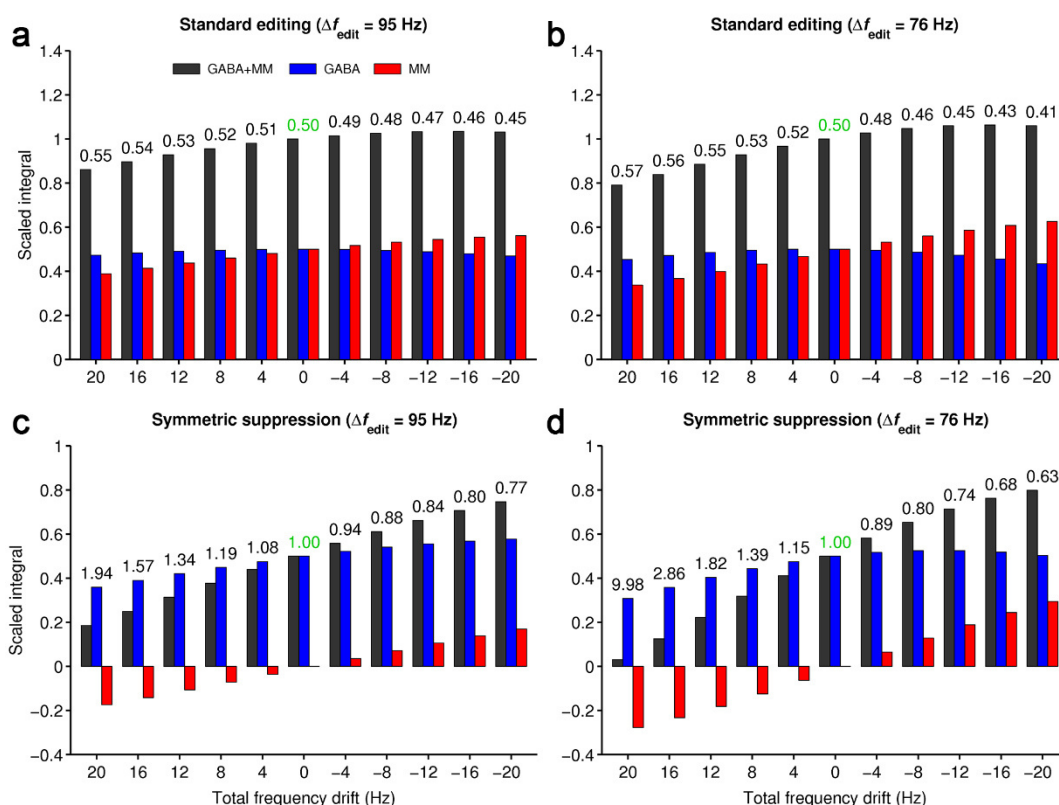
Second, the impact of frequency drift is more pronounced in the symmetric editing scheme than in the standard editing scheme. Similar to the more frequency-selective editing pulse, modulation of the GABA integral is greater with drift (Figure 7.6). Counterintuitively, for  $\Delta f_{\text{edit}} = 95$  Hz the GABA integral for symmetric editing increases when the editing pulse frequency is offset negatively, where the signal gain is 25% at  $-20$  Hz. When examining the ON and OFF GABA multiplets in Figure 7.4 for these particular simulations, it can be seen that at 0 Hz drift the OFF pulse partially refocuses the 3.0 ppm resonance. As the OFF pulse is offset negatively, the 3.0 ppm resonance is less refocused. Thus, when the two scans are subtracted there is greater signal in the DIFF scan at  $-20$  Hz than at 0 Hz.

Figure 7.7 displays the simulated GABA+MM integral as a function of drift. The integral was calculated from the respective GABA+MM DIFF multiplets that were resolved by adding together each GABA and MM FID for each corresponding



**Figure 7.6** The integral of the GABA-H4 DIFF multiplet as a function of total frequency drift in the MEGA-PRESS experiment normalised to the integral at 0 Hz drift. The impact of drift for the standard editing and symmetric suppression schemes using broader, 95-Hz (black) and narrower, 76-Hz (grey) editing pulses is illustrated.

drift-induced experiment. In addition, the relative contribution from GABA and MM to the total signal is shown, which for standard editing is typically assumed to be 50:50 in an ideal experiment. Consequently, the integrals were scaled such that at 0 Hz drift the GABA+MM integral equalled 1 and the GABA and MM integrals each equalled 0.5. For symmetric editing, the MM contribution will be nulled at 0 Hz drift, meaning that the GABA+MM integral will be equal to the GABA integral (i.e., 0.5). Thus, at 0 Hz drift the relative contribution of GABA to GABA+MM is 0.5 in the standard editing simulations and 1 in the symmetric editing simulations. As can be seen, this relative contribution changes with frequency drift. Compared to the 95-Hz editing pulse, the relative contribution changes more significantly with the 76-Hz pulse in standard editing. Moreover, negative drift (i.e., frequency shifts toward the MM peak at 1.72 ppm) will lead to greater MM contamination. The contribution of the MM signal is more complex when employing symmetric editing. Although with negative frequency offsets the GABA signal still accounts for the



**Figure 7.7** Relative contributions of GABA (blue) and MM (red) to the GABA+MM (black) integral in standard (a, b) and symmetric (c, d) editing as a function of total frequency drift. The effect of the 95- and 76-Hz editing pulses for each editing scheme is illustrated. The contributing fraction of GABA to the GABA+MM integral is indicated by the signal ratios placed at the top of each set of bars. At 0 Hz drift, GABA is assumed to account for 50% of the GABA+MM integral in standard editing and 100% in symmetric editing. Note that when the MM integral falls below 0 in symmetric editing as a result of positive frequency offsets of the editing pulse there is a loss in GABA+MM signal (c, d). The signal ratio then becomes greater than 1 and effectively indicates the units of signal needed to correct the GABA+MM integral for signal loss caused by MM contamination.

majority of the GABA+MM signal, when there is positive drift the MM integral becomes negative and leads to a loss in overall GABA+MM signal. The ratio of GABA to GABA+MM then becomes greater than 1, essentially equating to the factor needed to adjust the GABA+MM integral to a value that corresponds to a “pure” GABA signal if there were no MM contamination. It is also apparent that a greater change in relative contributions occurs with the more frequency-selective 76-Hz editing pulse.

## 7.5 Discussion

Numerical simulation of the GABA spin system using density matrix formalism has a multitude of applications. Here, this formalism was used to accurately describe and compare the quantum state of the GABA-H4 resonance resolved through standard

editing and symmetric MM suppression in GABA-edited experiments. From several simulations it was revealed that the GABA DIFF multiplet has a distinctive lineshape in symmetric suppression in comparison to standard editing. Moreover, by including shaped editing pulses with different frequency bandwidths in the numerical simulations it is demonstrated that the efficiency of spectral editing is not only dependent on the bandwidth of editing pulses, but when employing more frequency-selective pulses there is an uncharacteristic inversion of the editing profile between 1.6 and 1.2 ppm. This effect is a direct result of the lineshape of the partially refocused ON GABA multiplet that leads to minimal intensity of the outer GABA peaks in the GABA DIFF multiplet when the ON and OFF scans are subtracted. It has been demonstrated that when frequency drift is introduced into the MEGA-PRESS experiment, the symmetric suppression scheme is more sensitive than standard editing to editing pulse frequency offset, with increased frequency selectivity of editing pulses augmenting this sensitivity. Finally, drift modulates the relative contribution of GABA to the GABA+MM signal differently in symmetric suppression where positive frequency offsets lead to a negative MM DIFF multiplet consequently causing a substantial loss in overall GABA+MM signal.

Although it has been previously noted that, even in the absence of drift, the proximity of the 1.5 ppm OFF editing pulse in symmetric editing poses a significant issue when centre frequency shifts (Harris et al., 2015b, 2014; Henry et al., 2001; Terpstra et al., 2002), its exact effect on the GABA multiplet has not been described previously. It is shown that the GABA multiplet in the OFF scan has an important effect on the resulting DIFF integral such that the outer peaks of the DIFF multiplet have a lower amplitude compared to the centre peak. This arises from partial refocusing of the 3.0 ppm GABA-H4 spins as the 1.9 ppm GABA-H3 spins experience a low flip angle from the OFF editing pulse placed at 1.5 ppm, a consequence of insufficient frequency selectivity of the editing pulse. When the ON and OFF scans are subtracted the outer peaks are not completely in-phase/anti-phase as would be the case in standard editing. This then leads to a decrease in their intensity in the DIFF spectrum. A description of this effect is accurately derived through numerical simulation using product operator formalism.

The results of the numerical simulations have important implications for the quantification of GABA concentration. As the relative contributions of GABA and MM to the GABA+MM signal will vary with shifts in centre frequency, this will

add random variance to GABA data and will reduce the ability to observe true effects for a given experiment. This issue can be attenuated using techniques that prospectively correct for frequency drift at acquisition (Henry et al., 1999; Lange et al., 2011; Thiel et al., 2002; Zaitsev et al., 2010). In addition, a post-hoc correction for relative MM contamination could be calculated using the results from numerical simulations as demonstrated in this chapter. This would be a more accurate, experiment-dependent correction than the assumed 0.5 factor that is typically applied to standard GABA-edited concentrations (Harris et al., 2014; Mullins et al., 2014). To perform this correction properly GABA would need to be quantified from each difference subspectrum in a scan in order to correct for MM contamination that results from frequency offsets occurring at every other TR. The low SNR of each individual difference subspectrum would pose an obstacle to such a procedure, however. In terms of absolute quantification, it is also necessary to account for the efficiency of the editing technique itself (Edden et al., 2014; Mullins et al., 2014). The expected efficiency of standard editing (0.5) was confirmed in the numerical simulations. For symmetric MM suppression, the frequency selectivity of editing pulses has a substantial impact on the fraction of signal recovered in the difference scan. Decreasing the bandwidth of these pulses by ~20 Hz led to 1.6 times greater editing efficiency. Calculating the theoretical efficiency of symmetric editing prior to experimental studies is a recommended step in the absolute quantification procedure.

The distinct effects of editing pulse bandwidth and the placement of the OFF editing pulse in the symmetric editing scheme can be accurately described with density matrix formalism. Simulations of other important aspects of the *J*-difference editing experiment have previously been performed. For example, it is known that the parameters of slice-selective refocusing pulses used for volume localisation have an impact on the spatial profile of the GABA-H4 resonance (Edden and Barker, 2007; Kaiser et al., 2008; Near et al., 2013b). Additionally, pulse timings, particularly of the first spin echo ( $TE_1$ ) and the editing pulses, must be considered carefully to maximise the GABA signal intensity for a given PRESS acquisition (Gambarota et al., 2005; Napolitano et al., 2013). Numerical simulations also constitute an important step in the optimisation of both standard and novel MRS acquisition techniques that use either an unedited (Napolitano et al., 2013; Near et al., 2013a) or edited (Andreychenko et al., 2012; Near et al., 2011; Snyder et al.,

2009) approach. Thus, it would be possible to perform highly detailed and complex numerical simulations of *J*-difference editing of GABA that incorporate all parameters of the acquisition sequence in order to optimise in vivo experiments at different research sites and on different scanner platforms.

This study has some limitations, however. Firstly, the MM spin system was assumed to mimic the GABA  $A_2M_2X_2$  spin system, where the chemical shift of the M spin was offset to 1.7 ppm. This assumption was necessary given the paucity of knowledge surrounding both the exact molecules that contribute to the contaminating MM signal and their respective spin–spin coupling properties. The current understanding of these molecules with respect to  $^1\text{H}$  MRS is based on the seminal papers by Behar and Ogino (1993) and Behar et al. (1994) who reported that the 3.0 ppm M7 resonance in the MM baseline that is coupled to the 1.7 ppm M4 resonance is attributed to the amino acid lysine, which resolves as a triplet and has a coupling constant similar to GABA ( $\sim 7.6$  Hz). Although lysine has been used as a representative model for the MM contaminant (Henry et al., 2001), the M7 resonance is also attributed to other amino acids such as arginine and leucine (Behar and Ogino, 1993). Additionally, the long  $T_2$  and estimated concentration of the MM contaminant signifies that the signal originates in part from other mobile, possibly lysine-containing, amino acids and not solely from a bound MM pool (Choi et al., 2007). Secondly, when the relative contributions of GABA and MM to the GABA+MM integral were examined it was assumed that at 0 Hz drift the ratio was 50:50. However, empirically this ratio will be dependent on the intrinsic concentration of the contaminating MM, individual and regional differences, efficiency of the editing acquisition (itself dependent on sequence and pulse parameters), MR visibility and the *J*-evolution of the molecules in question. The multitude of uncertain variables pertinent to the MM spin system(s) makes it substantially difficult to provide an accurate numerical description of the effect of MM contamination on the *J*-edited GABA signal. As such, additional investigations of the MM resonances that contaminate the GABA signal in conventional spectral editing are necessary in order to extrapolate their effects in symmetric MM suppression.

## 7.6 Conclusions

Numerical simulations of standard and symmetric suppression *J*-difference editing demonstrate that the latter technique has a distinct effect on the GABA-H4 resonance compared to the former. The added complication of a contaminating MM resonance makes considering the efficiency of the symmetric suppression approach all the more important. The power of density matrix formalism is evident in the findings reported here, and it is only through simulations of the GABA spin system in the MEGA-PRESS experiment that a full description of standard and symmetric editing is possible. It can be concluded, then, that symmetric MM suppression is a technique that elegantly overcomes a significant disadvantage of standard GABA-MRS but that its implementation requires careful consideration of both acquisition parameters—particularly the frequency bandwidth of editing pulses—and offsets in centre frequency induced by heating of gradient coils or head motion.

# 8. General Discussion

## 8.1 Summary of Findings

The principal objective of carrying out the scientific research presented in this doctoral thesis was to further develop the modern methodology of  $^1\text{H}$  MRS of GABA, specifically that of *J*-difference GABA-editing. The findings of the work can be summarised into three general themes.

Firstly, that of the optimisation of absolute quantification. In Chapter 3, the unresolved issue of partial volume effects was addressed by the proposal of a new quantification procedure using internal tissue water as a concentration reference. The new method is a simple modification of the method first presented by Ernst et al. (1993) and refined by Gasparovic et al. (2006). It was shown that normalisation of MRS-derived GABA concentration based on the assumption of the ratio of the intrinsic concentration of GABA in GM and WM successfully removed the GM dependency from concentration measurements. Further understanding of the role of tissue segmentation on quantification error was presented in Chapter 4. Although error from tissue segmentation has been a concern, the findings showed that the contributed error is not substantial.

The second theme was that of the practical and applied implementation of symmetric MM suppression. The symmetric suppression approach to deal with MM contamination in GABA-MRS has not been widely adopted by the MRS community. It was shown, however, that the technique is reproducible when compared to standard GABA-editing, and that removing the MM contaminant may provide greater interindividual discrimination of GABA levels. This method was then applied in a multimodal study as presented in Chapter 6. This experiment sought to address outstanding uncertainties regarding the association between MRS-measured GABA and haemodynamic responses. Unfortunately, ambiguous results were found regarding the relationship between GABA and the rate of BOLD and CBF response saturation. In addition, MM-suppressed GABA concentration did not provide a better, or a less ambiguous, picture of this association.

The third and final theme was the critical importance of the editing efficiency of GABA-editing, particularly when the symmetric editing approach is employed. The numerical simulations described in Chapter 7 elegantly and accurately demonstrate the effect of the frequency-selectivity of editing pulses and of frequency offsets induced by  $B_0$  frequency drift in a given acquisition. Even though the concern regarding efficient editing has always been intuitively understood with respect to symmetric MM suppression, the numerical approach to investigating this known issue has not been conducted as rigorously as this before.

Taken as a whole, the empirical work of this thesis can be summarised into the following concluding statements: It is clear that there remain specific methodological limitations with the <sup>1</sup>H MRS of GABA with respect to accurate and reliable signal detection and quantification. The suppression of MM contamination by symmetric editing is a technique that holds great promise as a method to overcome a significant problem in GABA-MRS research, with the content of this thesis pushing its practical methodology forward. Nonetheless, this work also confirms that further implementation of symmetric MM suppression in applied studies is required in order to unequivocally demonstrate its true worth.

## 8.2 <sup>1</sup>H MRS of GABA: The Current and Future State of the Art

It should be clear from the topics discussed in Chapter 2 that in vivo measurement of GABA is currently an area of intense interest in modern neuroimaging. With this has come a steady stream of methodological development of <sup>1</sup>H MRS with the specific remit of optimally detecting and quantifying GABA. Furthermore, there have been some key milestones that nicely demonstrate just how much the field has pushed itself forward. For example, the development of Gannet (Edden et al., 2014) for easy and simple processing and quantification of GABA-edited data has opened up MRS to the wider imaging community, particularly to groups who may not have access to the technical expertise that would otherwise be necessary to implement GABA-MRS robustly. In addition, a recent consensus paper by Mullins et al. (2014) aimed to bring together various lab groups conducting GABA-MRS research in order to establish rules of best practice for GABA-edited spectroscopy. One of the important issues alluded to in the article is that of data acquisition on different

scanner platforms, highlighting that at present there is a drive towards more accurate and more reliable absolute quantification methods in the community.

Of course, it may be argued that the real scientific merit of a neuroimaging modality is not so much its methodological robustness but rather how its application can advance the wider field of neuroscience in a tangible manner. Again, the concise literature review presented in Chapter 2 aimed to illustrate that GABA-MRS has indeed brought a great deal of insight into GABA's role in brain function that would not be possible using conventional noninvasive imaging.

What of the future state of the art for the  $^1\text{H}$  MRS of GABA? Some prominent methodological issues (aside from those discussed in this thesis) still need to be satisfactorily addressed. The detrimental effects that head motion and  $B_0$  field drift have on MRS data greatly hamper empirical investigations, particularly in clinical or child populations where unfamiliarity or discomfort with the MRI setting will likely lead to an increased degree of such effects. An avenue for future optimisation, therefore, is the development of real-time motion correction and frequency updating. Although there are early examples of methods to achieve these (e.g., Henry et al., 1999; Thiel et al., 2002), more recent and advanced approaches show that their implementation is viable in GABA-MRS (Saleh et al., 2016). Prospective motion correction and frequency updating have not become mainstream, however. The benefits these methods could have for the field can be reasoned to be quite large.

Another possibility for advancing MRS of GABA is the use of truly functional approaches. A few studies have demonstrated that functional MRS (fMRS) is a viable technique that can aid in better understanding how stimuli modulate the biochemical concentration of specific metabolites. For instance, Apšvalka et al. (2015) were the first to have used an event-related design to investigate the neurometabolic effects of stimulus repetition suppression. Cleve et al. (2015) examined the dynamic changes of Glx and GABA in the presence of painful stimuli, while Bednařík et al. (2015) exploited the increased SNR of 7 T MRS to examine neurochemical responses to a simple visual stimulus with a large degree of success. If the basic methodology is improved and the practical challenges are addressed, fMRS possibly has the potential to provide just as much insight as pharmacological and neurostimulation interventions. One could even go so far as to say that fMRS would be more advantageous than these other approaches since its

temporal resolution would be much finer (seconds as opposed to minutes or hours) and its practical implementation far less complex. It is quite likely that in the next few years more groups will begin to use truly functional approaches in MRS studies.

Although nowhere near as common as 3 T, 7 T NMR holds significant promise for MRS given its greater SNR and, more importantly, greater spectral dispersion. The last few years have seen a surge of published methodological and applied studies of 7 T MRS to detect GABA, some with intriguing findings. Emir et al. (2012), for example, are only the second group to have attempted to detect *in vivo* GABA in Parkinson's disease patients in the basal ganglia, aided by the advantages of ultra-high field NMR. Marsman et al. (2014) in a study investigating neurochemical abnormalities in schizophrenia found that GABA in the medial prefrontal cortex was reduced compared to controls. This is noteworthy not only because it fits the GABAergic hypothesis of schizophrenia but because similar studies (at lower fields) have produced equivocal results. In another high-profile publication, Dou et al. (2013) were able to show regional variation in GABA concentration across the cingulate cortex, which closely matched GABA<sub>B</sub> receptor-architecture reported in an earlier post-mortem study (Palomero-Gallagher et al., 2009). Moreover, the application of symmetric editing at 7 T would greatly benefit from the increased frequency distance between the GABA and MM resonances, with initial investigations of its viability already having been demonstrated (Andreychenko et al., 2012; Terpstra et al., 2002; Wijtenburg et al., 2013). The continued installation of new 7 T scanners across the globe will mean that access to ultra-high field MRS will of course also increase, allowing researchers to tackle more difficult, more specific and more impactful research questions.

### **8.3 GABA Concentration as a Correlate: How Much Can Really Be Inferred?**

It was noted in Chapter 2 that GABA concentration has been shown to correlate with a host of different cognitive, behavioural, physiological and pathological measures. Providing evidence that GABA concentration can be confidently treated as a neurochemical predictor of these measures is quite important for neuroimaging and neuroscience as a whole. The issue, however, comes about when these associations are either not able to be replicated or are not as straightforward as a simple linear

relationship with a given direction. The multimodal study described in Chapter 6 is a perfect example of this problem. Its overarching aim was to provide an explanation for the equivocal findings surrounding the association between GABA concentration, the BOLD signal and CBF. Unfortunately, the results were themselves unclear. This is in spite of the fact that there is strong empirical evidence and theoretical understanding that GABAergic inhibition is a key component in neurovascular coupling (Lauritzen et al., 2012). Therefore, the prime criticism of multimodal MRS studies is that the GABA NMR signal is not a specific measure of GABAergic inhibition. Functions of the GABA system at the subnetwork neuronal level do not equate to GABA concentration on the macroscale (Singh, 2012). Going further, the utter complexity of the GABA system as described in Chapter 2 means that there are a variety of biological and chemical mechanisms in play, some of which may be independent of each other, that are captured by the NMR signal (and indeed some which are not). This is crucial to acknowledge as more often than not what researchers actually want to be measuring is GABA function as opposed to GABA content. The way GABA is detected—the averaging of several hundred FIDs acquired over a period of minutes—makes it quite difficult to make firm inferences about how an individual's GABA system is functioning with respect to, say, the amplitude of their BOLD signal. Therefore, any inferences made between observed correlations between GABA concentration and cognitive, behavioural, physiological and pathological measures should always be accompanied with the caveat that the GABA signal and GABA concentration represent measurements that are mechanistically distinct from GABAergic inhibition.

A second criticism of correlational studies in the field of MRS of GABA is that of small sample sizes. Although there are some notable exceptions (e.g., Gao et al., 2013; Rowland et al., 2016), for the most part studies do not tend to use more than 20 participants. While of course this criticism can be subjected to many areas of neuroimaging, it is a particular concern for MRS of GABA because of the aforementioned non-specificity of the GABA signal. Even discounting the contribution of measurement variance from the technical and physical attributes of MRS, the biochemical origin of the GABA signal will almost certainly add in a substantial proportion of variance to individual measures of GABA concentration.

What can be done to make the interpretations of associations between GABA and other variables more robust and theoretically plausible? This issue forms the

rationale for conducting GABA-MRS experiments alongside pharmacological and neurostimulation interventions whereby the GABA system can be perturbed with varying degrees of specificity. Alternatively, and as proposed in the previous section, functional approaches may bring a new level of interpretability to findings. For instance, the study conducted in Chapter 6 could be redesigned such that the contrast tuning paradigm would be applied as part of an fMRS acquisition. The rate of change in the GABA signal could then be correlated with the rate of haemodynamic response saturation. This experiment would likely only be viable at ultra-high field, however. Finally, it is worth noting that the necessity of large VOI in MRS could very well mean that the GABA of true interest is “hidden” by the GABA detected over a fairly diffuse portion of cortical tissue. This particular problem has always been known to spectroscopists and is unfortunately a compromise between VOI size and scan time, meaning it would be difficult to overcome it. Nevertheless, it is an issue that needs to be addressed. The obvious solution is to use higher field strengths to detect the GABA signal from smaller volumes. Future advancements may well come about within the next decade that could provide alternatives to the current poor spatial resolution of MRS. Reflection on these proposed solutions will lead one to a common conclusion: that of innovation in the methodological approaches in MRS and not in drastic changes regarding the use of an alternative, more specific, modality to assess in vivo GABA (such as positron emission tomography), nor indeed even in simply increasing sample sizes (and thereby increasing research costs). It is unquestionable that MRS is a technique currently without equal that exploits truly remarkable principles of quantum mechanics. It is therefore left to those who espouse its merits to push the envelope with respect to its implementation.

## 8.4 Closing Remarks

Did the research presented in this doctoral thesis achieve the aims that were set out in the Preface? In a sense, yes. The methodological refinements that have been developed have been shown to have a beneficial impact on the optimal acquisition and analysis of GABA-MRS data. Nonetheless, it is clear that some of the equivocal results in a few of the previous chapters demonstrate that there is still much work to be done if GABA-MRS is to flourish as a neuroimaging modality. Although this

doctoral research equates to a piecemeal scientific enterprise to achieve this grander goal, its defining distinction lies in its targeted approach at tackling some of the biggest problems that plague state-of-the-art  $^1\text{H}$  MRS of GABA. Foundations for future advancements have been laid and many new questions have arisen. The decision of where to progress to from here depends simply on which advances and questions are most interesting and relevant to engage with—and there are quite a few to choose from. All in all, however, the objective will remain the same: to utilise  $^1\text{H}$  MRS in a rigorous, sound and optimal manner to further elucidate how and why GABA is so highly important to the workings of the human brain.



## References

- Abdallah, C.G., Niciu, M.J., Fenton, L.R., Fasula, M.K., Jiang, L., Black, A., Rothman, D.L., Mason, G.F., Sanacora, G., 2014. Decreased Occipital Cortical Glutamate Levels in Response to Successful Cognitive-Behavioral Therapy and Pharmacotherapy for Major Depressive Disorder. *Psychother. Psychosom.* 83, 298–307. doi:10.1159/000361078
- Aguila, M.-E.R., Lagopoulos, J., Leaver, A.M., Rebeck, T., Hübscher, M., Brennan, P.C., Refshauge, K.M., 2015. Elevated levels of GABA<sup>+</sup> in migraine detected using <sup>1</sup>H-MRS. *NMR Biomed.* 28, 890–897. doi:10.1002/nbm.3321
- Albrecht, D.G., Hamilton, D.B., 1982. Striate cortex of monkey and cat: contrast response function. *J. Neurophysiol.* 48, 217–237.
- Alger, J.R., 2010. Quantitative proton magnetic resonance spectroscopy and spectroscopic imaging of the brain: A didactic review. *Top. Magn. Reson. Imaging* 21, 115–128. doi:10.1097/RMR.0b013e31821e568f
- Andreychenko, A., Boer, V.O., Arteaga De Castro, C.S., Luijten, P.R., Klomp, D.W.J., 2012. Efficient spectral editing at 7 T: GABA detection with MEGA-sLASER. *Magn. Reson. Med.* 68, 1018–1025. doi:10.1002/mrm.24131
- Apšvalka, D., Gadie, A., Clemence, M., Mullins, P.G., 2015. Event-related dynamics of glutamate and BOLD effects measured using functional magnetic resonance spectroscopy (fMRS) at 3T in a repetition suppression paradigm. *Neuroimage* 118, 292–300. doi:10.1016/j.neuroimage.2015.06.015
- Asada, H., Kawamura, Y., Maruyama, K., Kume, H., Ding, R., Ji, F.Y., Kanbara, N., Kuzume, H., Sanbo, M., Yagi, T., Obata, K., 1996. Mice Lacking the 65 kDa Isoform of Glutamic Acid Decarboxylase (GAD65) Maintain Normal Levels of GAD67 and GABA in Their Brains but Are Susceptible to Seizures. *Biochem. Biophys. Res. Commun.* 229, 891–895. doi:10.1006/bbrc.1996.1898
- Asada, H., Kawamura, Y., Maruyama, K., Kume, H., Ding, R.-G., Kanbara, N., Kuzume, H., Sanbo, M., Yagi, T., Obata, K., 1997. Cleft palate and decreased brain -aminobutyric acid in mice lacking the 67-kDa isoform of glutamic acid decarboxylase. *Proc. Natl. Acad. Sci. U. S. A.* 94, 6496–6499. doi:10.1073/pnas.94.12.6496
- Atallah, B. V., Bruns, W., Carandini, M., Scanziani, M., 2012. Parvalbumin-Expressing Interneurons Linearly Transform Cortical Responses to Visual Stimuli. *Neuron* 73, 159–170. doi:10.1016/j.neuron.2011.12.013
- Aufhaus, E., Weber-Fahr, W., Sack, M., Tunc-Skarka, N., Oberthuer, G., Hoerst, M., Meyer-Lindenberg, A., Boettcher, U., Ende, G., 2013. Absence of changes in GABA concentrations with age and gender in the human anterior cingulate cortex: A MEGA-PRESS study with symmetric editing pulse frequencies for macromolecule suppression. *Magn. Reson. Med.* 69, 317–320. doi:10.1002/mrm.24257
- Bai, X., Edden, R.A.E., Gao, F., Wang, G., Wu, L., Zhao, B., Wang, M., Chan, Q., Chen, W., Barker, P.B., 2015. Decreased  $\gamma$ -aminobutyric acid levels in the parietal region of patients with Alzheimer's disease. *J. Magn. Reson. Imaging* 41, 1326–1331. doi:10.1002/jmri.24665
- Balázs, R., Machiyama, Y., Hammond, B.J., Julian, T., Richter, D., 1970. The operation of the gamma-aminobutyrate bypath of the tricarboxylic acid cycle

- in brain tissue in vitro. *Biochem. J.* 116, 445–461.
- Barker, P.B., Soher, B.J., Blackband, S.J., Chatham, J.C., Mathews, V.P., Bryan, R.N., 1993. Quantitation of proton NMR spectra of the human brain using tissue water as an internal concentration reference. *NMR Biomed.* 6, 89–94. doi:10.1002/nbm.1940060114
- Bartos, M., Vida, I., Jonas, P., 2007. Synaptic mechanisms of synchronized gamma oscillations in inhibitory interneuron networks. *Nat. Rev. Neurosci.* 8, 45–56. doi:10.1038/nrn2044
- Battaglioli, G., Liu, H., Martin, D.L., 2003. Kinetic differences between the isoforms of glutamate decarboxylase: implications for the regulation of GABA synthesis. *J. Neurochem.* 86, 879–887. doi:10.1046/j.1471-4159.2003.01910.x
- Bednařík, P., Tkáč, I., Giove, F., DiNuzzo, M., Deelchand, D.K., Emir, U.E., Eberly, L.E., Mangia, S., 2015. Neurochemical and BOLD responses during neuronal activation measured in the human visual cortex at 7 Tesla. *J. Cereb. Blood Flow Metab.* 35, 601–610. doi:10.1038/jcbfm.2014.233
- Behar, K.L., Ogino, T., 1993. Characterization of macromolecule resonances in the <sup>1</sup>H NMR spectrum of rat brain. *Magn. Reson. Med.* 30, 38–44. doi:10.1002/mrm.1910300107
- Behar, K.L., Rothman, D.L., Spencer, D.D., Petroff, O.A.C., 1994. Analysis of macromolecule resonances in <sup>1</sup>H NMR spectra of human brain. *Magn. Reson. Med.* 32, 294–302. doi:10.1002/mrm.1910320304
- Belelli, D., Harrison, N.L., Maguire, J., Macdonald, R.L., Walker, M.C., Cope, D.W., 2009. Extrasynaptic GABA<sub>A</sub> Receptors: Form, Pharmacology, and Function. *J. Neurosci.* 29, 12757–12763. doi:10.1523/JNEUROSCI.3340-09.2009
- Benes, F.M., Berretta, S., 2001. GABAergic interneurons: Implications for understanding schizophrenia and bipolar disorder. *Neuropsychopharmacology.* doi:10.1016/S0893-133X(01)00225-1
- Bernard, C., Cossart, R., Hirsch, J.C., Esclapez, M., Ben-Ari, Y., 2000. What is GABAergic Inhibition? How Is it Modified in Epilepsy? *Epilepsia* 41, S90–S95. doi:10.1111/j.1528-1157.2000.tb01564.x
- Bernstein, E.M., Quick, M.W., 1999. Regulation of  $\gamma$ -Aminobutyric Acid (GABA) Transporters by Extracellular GABA. *J. Biol. Chem.* 274, 889–895. doi:10.1074/jbc.274.2.889
- Bhagwagar, Z., Wylezinska, M., Jezzard, P., Evans, J., Ashworth, F., Sule, A., Matthews, P.M., Cowen, P.J., 2007. Reduction in Occipital Cortex  $\gamma$ -Aminobutyric Acid Concentrations in Medication-Free Recovered Unipolar Depressed and Bipolar Subjects. *Biol. Psychiatry* 61, 806–812. doi:10.1016/j.biopsych.2006.08.048
- Bhagwagar, Z., Wylezinska, M., Jezzard, P., Evans, J., Boorman, E., M. Matthews, P., J. Cowen, P., 2008. Low GABA concentrations in occipital cortex and anterior cingulate cortex in medication-free, recovered depressed patients. *Int. J. Neuropsychopharmacol.* 11, 255–260. doi:10.1017/S1461145707007924
- Bhagwagar, Z., Wylezinska, M., Taylor, M., Jezzard, P., Matthews, P.M., Cowen, P.J., 2004. Increased Brain GABA Concentrations Following Acute Administration of a Selective Serotonin Reuptake Inhibitor. *Am. J. Psychiatry* 161, 368–370. doi:10.1176/appi.ajp.161.2.368
- Bhattacharyya, P.K., Phillips, M.D., Stone, L.A., Bermel, R.A., Lowe, M.J., 2013. Sensorimotor Cortex Gamma-Aminobutyric Acid Concentration Correlates with Impaired Performance in Patients with MS. *Am. J. Neuroradiol.* 34, 1733–

1739. doi:10.3174/ajnr.A3483
- Bhattacharyya, P.K., Phillips, M.D., Stone, L.A., Lowe, M.J., 2011. In vivo magnetic resonance spectroscopy measurement of gray-matter and white-matter gamma-aminobutyric acid concentration in sensorimotor cortex using a motion-controlled MEGA point-resolved spectroscopy sequence. *Magn. Reson. Imaging* 29, 374–379. doi:10.1016/j.mri.2010.10.009
- Bigal, M.E., Hetherington, H., Pan, J., Tsang, A., Grosberg, B., Avdievich, N., Friedman, B., Lipton, R.B., 2008. Occipital levels of GABA are related to severe headaches in migraine. *Neurology* 70, 2078–2080. doi:10.1212/01.wnl.0000313376.07248.28
- Birn, R.M., Smith, M.A., Jones, T.B., Bandettini, P.A., 2008. The respiration response function: The temporal dynamics of fMRI signal fluctuations related to changes in respiration. *Neuroimage* 40, 644–654. doi:10.1016/j.neuroimage.2007.11.059
- Bloch, F., 1946. Nuclear Induction. *Phys. Rev.* 70, 460–474. doi:10.1103/PhysRev.70.460
- Bogner, W., Gruber, S., Doelken, M., Stadlbauer, A., Ganslandt, O., Boettcher, U., Trattning, S., Doerfler, A., Stefan, H., Hammen, T., 2010. In vivo quantification of intracerebral GABA by single-voxel 1H-MRS—How reproducible are the results? *Eur. J. Radiol.* 73, 526–531. doi:10.1016/j.ejrad.2009.01.014
- Bolvig, T., Larsson, O.M., Pickering, D.S., Nelson, N., Falch, E., Krosgaard-Larsen, P., Schousboe, A., 1999. Action of bicyclic isoxazole GABA analogues on GABA transporters and its relation to anticonvulsant activity. *Eur. J. Pharmacol.* 375, 367–374. doi:10.1016/S0014-2999(99)00263-0
- Borden, L.A., 1996. GABA transporter heterogeneity: Pharmacology and cellular localization. *Neurochem. Int.* 29, 335–356. doi:10.1016/0197-0186(95)00158-1
- Bottomley, P.A., 1987. Spatial Localization in NMR Spectroscopy in Vivo. *Ann. N. Y. Acad. Sci.* 508, 333–348. doi:10.1111/j.1749-6632.1987.tb32915.x
- Boy, F., Evans, C.J., Edden, R.A.E., Lawrence, A.D., Singh, K.D., Husain, M., Sumner, P., 2011. Dorsolateral Prefrontal  $\gamma$ -Aminobutyric Acid in Men Predicts Individual Differences in Rash Impulsivity. *Biol. Psychiatry* 70, 866–872. doi:10.1016/j.biopsych.2011.05.030
- Boy, F., Evans, C.J., Edden, R.A.E., Singh, K.D., Husain, M., Sumner, P., 2010. Individual Differences in Subconscious Motor Control Predicted by GABA Concentration in SMA. *Curr. Biol.* 20, 1779–1785. doi:10.1016/j.cub.2010.09.003
- Boynton, G.M., Engel, S.A., Glover, G.H., Heeger, D.J., 1996. Linear systems analysis of functional magnetic resonance imaging in human V1. *J. Neurosci.* 16, 4207–21.
- Bradford, H., 1995. Glutamate, GABA and epilepsy. *Prog. Neurobiol.* 47, 477–511. doi:10.1016/0301-0082(95)00030-5
- Brady, R.O., McCarthy, J.M., Prescot, A.P., Jensen, J.E., Cooper, A.J., Cohen, B.M., Renshaw, P.F., Öngür, D., 2013. Brain gamma-aminobutyric acid (GABA) abnormalities in bipolar disorder. *Bipolar Disord.* 15, 434–439. doi:10.1111/bdi.12074
- Brainard, D.H., 1997. The Psychophysics Toolbox. *Spat. Vis.* 10, 433–436. doi:10.1163/156856897X00357
- Brickley, S.G., Cull-Candy, S.G., Farrant, M., 1996. Development of a tonic form of synaptic inhibition in rat cerebellar granule cells resulting from persistent

- activation of GABAA receptors. *J. Physiol.* 497, 753–759. doi:10.1113/jphysiol.1996.sp021806
- Brunel, N., Wang, X.-J., 2003. What determines the frequency of fast network oscillations with irregular neural discharges? I. Synaptic dynamics and excitation-inhibition balance. *J. Neurophysiol.* 90, 415–430. doi:10.1152/jn.01095.2002
- Bulte, D.P., Kelly, M., Germuska, M., Xie, J., Chappell, M.A., Okell, T.W., Bright, M.G., Jezzard, P., 2012. Quantitative measurement of cerebral physiology using respiratory-calibrated MRI. *Neuroimage* 60, 582–591. doi:10.1016/j.neuroimage.2011.12.017
- Buxton, R.B., Frank, L.R., Wong, E.C., Siewert, B., Warach, S., Edelman, R.R., 1998. A general kinetic model for quantitative perfusion imaging with arterial spin labeling. *Magn. Reson. Med.* 40, 383–396. doi:10.1002/mrm.1910400308
- Buxton, R.B., Uludağ, K., Dubowitz, D.J., Liu, T.T., 2004. Modeling the hemodynamic response to brain activation. *Neuroimage* 23, S220–S233. doi:10.1016/j.neuroimage.2004.07.013
- Buzsáki, G., Kaila, K., Raichle, M., 2007. Inhibition and Brain Work. *Neuron* 56, 771–783. doi:10.1016/j.neuron.2007.11.008
- Buzsáki, G., Wang, X.-J., 2012. Mechanisms of Gamma Oscillations. *Annu. Rev. Neurosci.* 35, 203–225. doi:10.1146/annurev-neuro-062111-150444
- Cabanes, E., Confort-Gouny, S., Le Fur, Y., Simond, G., Cozzone, P.J., 2001. Optimization of Residual Water Signal Removal by HLSVD on Simulated Short Echo Time Proton MR Spectra of the Human Brain. *J. Magn. Reson.* 150, 116–125. doi:10.1006/jmre.2001.2318
- Cai, K., Nanga, R.P., Lamprou, L., Schinstine, C., Elliott, M., Hariharan, H., Reddy, R., Epperson, C.N., 2012. The Impact of Gabapentin Administration on Brain GABA and Glutamate Concentrations: A 7T <sup>1</sup>H-MRS Study. *Neuropsychopharmacology* 37, 2764–2771. doi:10.1038/npp.2012.142
- Calabresi, P., Picconi, B., Tozzi, A., Ghiglieri, V., Di Filippo, M., 2014. Direct and indirect pathways of basal ganglia: a critical reappraisal. *Nat. Neurosci.* 17, 1022–1030. doi:10.1038/nn.3743
- Carlsson, A., Waters, N., Holm-Waters, S., Tedroff, J., Nilsson, M., Carlsson, M.L., 2001. Interactions between monoamines, glutamate, and GABA in schizophrenia: new evidence. *Annu. Rev. Pharmacol. Toxicol.* 41, 237–60. doi:10.1146/annurev.pharmtox.41.1.237
- Cauli, B., Hamel, E., 2010. Revisiting the role of neurons in neurovascular coupling. *Front. Neuroenergetics* 2, 9. doi:10.3389/fnene.2010.00009
- Cawley, N., Solanky, B.S., Muhlert, N., Tur, C., Edden, R. a. E., Wheeler-Kingshott, C. a. M., Miller, D.H., Thompson, A.J., Ciccarelli, O., 2015. Reduced gamma-aminobutyric acid concentration is associated with physical disability in progressive multiple sclerosis. *Brain* 138, 2584–2595. doi:10.1093/brain/awv209
- Chadderton, P., Margrie, T.W., Häusser, M., 2004. Integration of quanta in cerebellar granule cells during sensory processing. *Nature* 428, 856–860. doi:10.1038/nature02442
- Chalifoux, J.R., Carter, A.G., 2011. GABAB receptor modulation of synaptic function. *Curr. Opin. Neurobiol.* 21, 339–344. doi:10.1016/j.conb.2011.02.004
- Chance, F.S., Abbott, L., Reyes, A.D., 2002. Gain Modulation from Background Synaptic Input. *Neuron* 35, 773–782. doi:10.1016/S0896-6273(02)00820-6
- Chang, L., Cloak, C.C., Ernst, T., 2003. Magnetic resonance spectroscopy studies of

- GABA in neuropsychiatric disorders. *J. Clin. Psychiatry* 64 Suppl 3, 7–14.
- Chatton, J.-Y., Pellerin, L., Magistretti, P.J., 2003. GABA uptake into astrocytes is not associated with significant metabolic cost: Implications for brain imaging of inhibitory transmission. *Proc. Natl. Acad. Sci. U. S. A.* 100, 12456–12461. doi:10.1073/pnas.2132096100
- Chen, C.-M.A., Stanford, A.D., Mao, X., Abi-Dargham, A., Shungu, D.C., Lisanby, S.H., Schroeder, C.E., Kegeles, L.S., 2014. GABA level, gamma oscillation, and working memory performance in schizophrenia. *NeuroImage Clin.* 4, 531–539. doi:10.1016/j.nicl.2014.03.007
- Chen, Z., Silva, A.C., Yang, J., Shen, J., 2005. Elevated endogenous GABA level correlates with decreased fMRI signals in the rat brain during acute inhibition of GABA transaminase. *J. Neurosci. Res.* 79, 383–391. doi:10.1002/jnr.20364
- Chiarelli, P.A., Bulte, D.P., Gallichan, D., Piechnik, S.K., Wise, R., Jezzard, P., 2007. Flow-metabolism coupling in human visual, motor, and supplementary motor areas assessed by magnetic resonance imaging. *Magn. Reson. Med.* 57, 538–547. doi:10.1002/mrm.21171
- Choi, C., Bhardwaj, P.P., Kalra, S., Casault, C.A., Yasmin, U.S., Allen, P.S., Coupland, N.J., 2007. Measurement of GABA and contaminants in gray and white matter in human brain in vivo. *Magn. Reson. Med.* 58, 27–33. doi:10.1002/mrm.21275
- Choi, C., Coupland, N.J., Bhardwaj, P.P., Kalra, S., Casault, C.A., Reid, K., Allen, P.S., 2006. T2 measurement and quantification of glutamate in human brain in vivo. *Magn. Reson. Med.* 56, 971–977. doi:10.1002/mrm.21055
- Choi, I.-Y., Lee, S.-P., Merkle, H., Shen, J., 2006. In vivo detection of gray and white matter differences in GABA concentration in the human brain. *Neuroimage* 33, 85–93. doi:10.1016/j.neuroimage.2006.06.016
- Chowdhury, F.A., O’Gorman, R.L., Nashef, L., Elwes, R.D., Edden, R.A., Murdoch, J.B., Barker, G.J., Richardson, M.P., 2015. Investigation of glutamine and GABA levels in patients with idiopathic generalized epilepsy using MEGAPRESS. *J. Magn. Reson. Imaging* 41, 694–699. doi:10.1002/jmri.24611
- Christiansen, P., Henriksen, O., Stubgaard, M., Gideon, P., Larsson, H.B.W., 1993. In vivo quantification of brain metabolites by 1H-MRS using water as an internal standard. *Magn. Reson. Imaging* 11, 107–118. doi:10.1016/0730-725X(93)90418-D
- Christiansen, P., Toft, P.B., Gideon, P., Danielsen, E.R., Ring, P., Henriksen, O., 1997. MR-visible water content in human brain: A proton MRS study. *Magn. Reson. Imaging* 12, 1237–1244.
- Clark, K.A., Woods, R.P., Rottenberg, D.A., Toga, A.W., Mazziotta, J.C., 2006. Impact of acquisition protocols and processing streams on tissue segmentation of T1 weighted MR images. *Neuroimage* 29, 185–202. doi:10.1016/j.neuroimage.2005.07.035
- Cleve, M., Gussew, A., Reichenbach, J.R., 2015. In vivo detection of acute pain-induced changes of GABA+ and Glx in the human brain by using functional 1H MEGA-PRESS MR spectroscopy. *Neuroimage* 105, 67–75. doi:10.1016/j.neuroimage.2014.10.042
- Cobb, S.R., Buhl, E.H., Halasy, K., Paulsen, O., Somogyi, P., 1995. Synchronization of neuronal activity in hippocampus by individual GABAergic interneurons. *Nature* 378, 75–8. doi:10.1038/378075a0
- Cox, R.W., 1996. AFNI: Software for Analysis and Visualization of Functional Magnetic Resonance Neuroimages. *Comput. Biomed. Res.* 29, 162–173.

- doi:10.1006/cbmr.1996.0014
- Curthoys, N.P., Watford, M., 1995. Regulation of Glutaminase Activity and Glutamine Metabolism. *Annu. Rev. Nutr.* 15, 133–159. doi:10.1146/annurev.nutr.15.1.133
- Davis, T.L., Kwong, K.K., Weisskoff, R.M., Rosen, B.R., 1998. Calibrated functional MRI: Mapping the dynamics of oxidative metabolism. *Proc. Natl. Acad. Sci. U. S. A.* 95, 1834–1839. doi:10.1073/pnas.95.4.1834
- de Graaf, R.A., 2007. *In Vivo NMR Spectroscopy: Principles and Techniques*, 2nd ed. John Wiley & Sons, Ltd.
- de Graaf, R.A., Brown, P.B., McIntyre, S., Nixon, T.W., Behar, K.L., Rothman, D.L., 2006. High magnetic field water and metabolite proton T1 and T2 relaxation in rat brain in vivo. *Magn. Reson. Med.* 56, 386–394. doi:10.1002/mrm.20946
- de Graaf, R.A., Rothman, D.L., 2001. In vivo detection and quantification of scalar coupled <sup>1</sup>H NMR resonances. *Concepts Magn. Reson.* 13, 32–76. doi:10.1002/1099-0534(2001)13:1<32::AID-CMR4>3.0.CO;2-J
- de Graaf, R.A., van Kranenburg, A., Nicolay, K., 1999. Off-resonance metabolite magnetization transfer measurements on rat brain in situ. *Magn. Reson. Med.* 41, 1136–1144. doi:10.1002/(SICI)1522-2594(199906)41:6<1136::AID-MRM9>3.0.CO;2-G
- de la Fuente-Sandoval, C., Reyes-Madrigal, F., Mao, X., León-Ortiz, P., Rodríguez-Mayoral, O., Solís-Vivanco, R., Favila, R., Graff-Guerrero, A., Shungu, D.C., 2015. Cortico-Striatal GABAergic and Glutamatergic Dysregulations in Subjects at Ultra-High Risk for Psychosis Investigated with Proton Magnetic Resonance Spectroscopy. *Int. J. Neuropsychopharmacol.* pyv105. doi:10.1093/ijnp/pyv105
- de la Vega, A., Brown, M.S., Snyder, H.R., Singel, D., Munakata, Y., Banich, M.T., 2014. Individual Differences in the Balance of GABA to Glutamate in pFC Predict the Ability to Select among Competing Options. *J. Cogn. Neurosci.* 26, 2490–2502. doi:10.1162/jocn\_a\_00655
- Dericioglu, N., Garganta, C.L., Petroff, O.A., Mendelsohn, D., Williamson, A., 2008. Blockade of GABA synthesis only affects neural excitability under activated conditions in rat hippocampal slices. *Neurochem. Int.* 53, 22–32. doi:10.1016/j.neuint.2008.04.006
- Dickinson, W.C., 1950. Dependence of the F19 Nuclear Resonance Position on Chemical Compound. *Phys. Rev.* 77, 736–737. doi:10.1103/PhysRev.77.736.2
- Dienes, Z., 2011. Bayesian Versus Orthodox Statistics: Which Side Are You On? *Perspect. Psychol. Sci.* 6, 274–290. doi:10.1177/1745691611406920
- Doelken, M.T., Hammen, T., Bogner, W., Mennecke, A., Stadlbauer, A., Boettcher, U., Doerfler, A., Stefan, H., 2010. Alterations of intracerebral  $\gamma$ -aminobutyric acid (GABA) levels by titration with levetiracetam in patients with focal epilepsies. *Epilepsia* 51, 1477–1482. doi:10.1111/j.1528-1167.2010.02544.x
- Donahue, M.J., Near, J., Blicher, J.U., Jezard, P., 2010. Baseline GABA concentration and fMRI response. *Neuroimage* 53, 392–398. doi:10.1016/j.neuroimage.2010.07.017
- Donahue, M.J., Rane, S., Hussey, E., Mason, E., Pradhan, S., Waddell, K.W., Ally, B.A., 2014.  $\gamma$ -Aminobutyric acid (GABA) concentration inversely correlates with basal perfusion in human occipital lobe. *J. Cereb. Blood Flow Metab.* 34, 532–541. doi:10.1038/jcbfm.2013.231
- Dou, W., Palomero-Gallagher, N., van Tol, M.-J., Kaufmann, J., Zhong, K.,

- Bernstein, H.-G., Heinze, H.-J., Speck, O., Walter, M., 2013. Systematic regional variations of GABA, glutamine, and glutamate concentrations follow receptor fingerprints of human cingulate cortex. *J. Neurosci.* 33, 12698–12704. doi:10.1523/JNEUROSCI.1758-13.2013
- Draper, A., Stephenson, M.C., Jackson, G.M., Pépés, S., Morgan, P.S., Morris, P.G., Jackson, S.R., 2014. Increased GABA Contributes to Enhanced Control over Motor Excitability in Tourette Syndrome. *Curr. Biol.* 2343–2347. doi:10.1016/j.cub.2014.08.038
- Duarte, J.M.N., Lei, H., Mlynárik, V., Gruetter, R., 2012. The neurochemical profile quantified by in vivo 1H NMR spectroscopy. *Neuroimage* 61, 342–362. doi:10.1016/j.neuroimage.2011.12.038
- Duque, D., Malmierca, M.S., Caspary, D.M., 2014. Modulation of stimulus-specific adaptation by GABA<sub>A</sub> receptor activation or blockade in the medial geniculate body of the anaesthetized rat. *J. Physiol.* 592, 729–743. doi:10.1113/jphysiol.2013.261941
- Durst, C.R., Michael, N., Tustison, N.J., Patrie, J.T., Raghavan, P., Wintermark, M., Sendhil Velan, S., 2015. Noninvasive evaluation of the regional variations of GABA using magnetic resonance spectroscopy at 3 Tesla. *Magn. Reson. Imaging* 33, 611–617. doi:10.1016/j.mri.2015.02.015
- Edden, R.A.E., Barker, P.B., 2007. Spatial effects in the detection of  $\gamma$ -aminobutyric acid: Improved sensitivity at high fields using inner volume saturation. *Magn. Reson. Med.* 58, 1276–1282. doi:10.1002/mrm.21383
- Edden, R.A.E., Crocetti, D., Zhu, H., Gilbert, D.L., Mostofsky, S.H., 2012a. Reduced GABA Concentration in Attention-Deficit/Hyperactivity Disorder. *Arch. Gen. Psychiatry* 69, 750–3. doi:10.1001/archgenpsychiatry.2011.2280
- Edden, R.A.E., Muthukumaraswamy, S.D., Freeman, T.C.A., Singh, K.D., 2009. Orientation Discrimination Performance Is Predicted by GABA Concentration and Gamma Oscillation Frequency in Human Primary Visual Cortex. *J. Neurosci.* 29, 15721–15726. doi:10.1523/JNEUROSCI.4426-09.2009
- Edden, R.A.E., Puts, N.A.J., Barker, P.B., 2012b. Macromolecule-suppressed GABA-edited magnetic resonance spectroscopy at 3T. *Magn. Reson. Med.* 68, 657–661. doi:10.1002/mrm.24391
- Edden, R.A.E., Puts, N.A.J., Harris, A.D., Barker, P.B., Evans, C.J., 2014. Gannet: A batch-processing tool for the quantitative analysis of gamma-aminobutyric acid-edited MR spectroscopy spectra. *J. Magn. Reson. Imaging* 40, 1445–1452. doi:10.1002/jmri.24478
- Edwards, F.A., Konnerth, A., Sakmann, B., 1990. Quantal analysis of inhibitory synaptic transmission in the dentate gyrus of rat hippocampal slices: a patch-clamp study. *J. Physiol.* 430, 213–249. doi:10.1113/jphysiol.1990.sp018289
- Eggert, L.D., Sommer, J., Jansen, A., Kircher, T., Konrad, C., 2012. Accuracy and Reliability of Automated Gray Matter Segmentation Pathways on Real and Simulated Structural Magnetic Resonance Images of the Human Brain. *PLoS One* 7. doi:10.1371/journal.pone.0045081
- Emir, U.E., Tuite, P.J., Öz, G., 2012. Elevated Pontine and Putamenal GABA Levels in Mild-Moderate Parkinson Disease Detected by 7 Tesla Proton MRS. *PLoS One* 7, e30918. doi:10.1371/journal.pone.0030918
- Ende, G., Cackowski, S., Van Eijk, J., Sack, M., Demirakca, T., Kleindienst, N., Bohus, M., Sobanski, E., Krause-Utz, A., Schmahl, C., 2016. Impulsivity and Aggression in Female BPD and ADHD Patients: Association with ACC Glutamate and GABA Concentrations. *Neuropsychopharmacology* 41, 410–

418. doi:10.1038/npp.2015.153
- Epperson, C.N., Haga, K., Mason, G.F., Sellers, E., Gueorguieva, R., Zhang, W., Weiss, E., Rothman, D.L., Krystal, J.H., 2002. Cortical  $\gamma$ -Aminobutyric Acid Levels Across the Menstrual Cycle in Healthy Women and Those With Premenstrual Dysphoric Disorder: A Proton Magnetic Resonance Spectroscopy Study. *Arch. Gen. Psychiatry* 59, 851–858. doi:10.1001/archpsyc.59.9.851
- Epperson, C.N., O'Malley, S., Czarkowski, K.A., Gueorguieva, R., Jatlow, P., Sanacora, G., Rothman, D.L., Krystal, J.H., Mason, G.F., 2005. Sex, GABA, and nicotine: The impact of smoking on cortical GABA levels across the menstrual cycle as measured with proton magnetic resonance spectroscopy. *Biol. Psychiatry* 57, 44–48. doi:10.1016/j.biopsych.2004.09.021
- Erlander, M.G., Tillakaratne, N.J.K., Feldblum, S., Patel, N., Tobin, A.J., 1991. Two genes encode distinct glutamate decarboxylases. *Neuron* 7, 91–100. doi:10.1016/0896-6273(91)90077-D
- Ernst, T., Kreis, R., Ross, B.D., 1993. Absolute quantitation of water and metabolites in the human brain. I. Compartments and water. *J. Magn. Reson. Ser. B* 102, 1–8. doi:10.1006/jmrb.1993.1055
- Errante, L.D., Williamson, A., Spencer, D.D., Petroff, O.A., 2002. Gabapentin and vigabatrin increase GABA in the human neocortical slice. *Epilepsy Res.* 49, 203–210. doi:10.1016/S0920-1211(02)00034-7
- Esclapez, M., Tillakaratne, N.J., Kaufman, D.L., Tobin, a J., Houser, C.R., 1994. Comparative localization of two forms of glutamic acid decarboxylase and their mRNAs in rat brain supports the concept of functional differences between the forms. *J. Neurosci.* 14, 1834–1855.
- Ethofer, T., Mader, I., Seeger, U., Helms, G., Erb, M., Grodd, W., Ludolph, A., Klose, U., 2003. Comparison of longitudinal metabolite relaxation times in different regions of the human brain at 1.5 and 3 Tesla. *Magn. Reson. Med.* 50, 1296–1301. doi:10.1002/mrm.10640
- Evans, C.J., Boy, F., Edden, R.A., Singh, K.D., Sumner, P., 2011. Regional variations in GABA measured with MEGA-PRESS, in: *Proc. Intl. Soc. Mag. Reson. Med.* p. 3473.
- Evans, C.J., McGonigle, D.J., Edden, R.A.E., 2010. Diurnal stability of  $\gamma$ -aminobutyric acid concentration in visual and sensorimotor cortex. *J. Magn. Reson. Imaging* 31, 204–209. doi:10.1002/jmri.21996
- Evans, C.J., Puts, N.A.J., Robson, S.E., Boy, F., McGonigle, D.J., Sumner, P., Singh, K.D., Edden, R.A.E., 2013. Subtraction artifacts and frequency (mis-)alignment in J-difference GABA editing. *J. Magn. Reson. Imaging* 38, 970–975. doi:10.1002/jmri.23923
- Fahn, S., Côté, L.J., 1968. Regional distribution of  $\gamma$ -aminobutyric acid (GABA) in brain of the rhesus monkey. *J. Neurochem.* 15, 209–13.
- Farrant, M., Nusser, Z., 2005. Variations on an inhibitory theme: phasic and tonic activation of GABA receptors. *Nat. Rev. Neurosci.* 6, 215–229. doi:10.1038/nrn1625
- Floyer-Lea, A., Wylezinska, M., Kincses, T., Matthews, P.M., 2006. Rapid modulation of GABA concentration in human sensorimotor cortex during motor learning. *J. Neurophysiol.* 95, 1639–1644. doi:10.1152/jn.00346.2005
- Foerster, B.R., Carlos, R.C., Dwamena, B.A., Callaghan, B.C., Petrou, M., Edden, R.A.E., Mohamed, M.A., Welsh, R.C., Barker, P.B., Feldman, E.L., Pomper, M.G., 2014. Multimodal MRI as a diagnostic biomarker for amyotrophic lateral

- sclerosis. *Ann. Clin. Transl. Neurol.* 1, 107–114. doi:10.1002/acn3.30
- Foerster, B.R., Petrou, M., Edden, R.A.E., Sundgren, P.C., Schmidt-Wilcke, T., Lowe, S.E., Harte, S.E., Clauw, D.J., Harris, R.E., 2012. Reduced insular  $\gamma$ -aminobutyric acid in fibromyalgia. *Arthritis Rheum.* 64, 579–583. doi:10.1002/art.33339
- Frahm, J., Merboldt, K.-D., Hänicke, W., 1987. Localized proton spectroscopy using stimulated echoes. *J. Magn. Reson.* 72, 502–508. doi:10.1016/0022-2364(87)90154-5
- Froestl, W., 2011. An historical perspective on GABAergic drugs. *Future Med. Chem.* 3, 163–175. doi:10.4155/fmc.10.285
- Fujihara, K., Narita, K., Suzuki, Y., Takei, Y., Suda, M., Tagawa, M., Ujita, K., Sakai, Y., Narumoto, J., Near, J., Fukuda, M., 2015. Relationship of  $\gamma$ -aminobutyric acid and glutamate+glutamine concentrations in the perigenual anterior cingulate cortex with performance of Cambridge Gambling Task. *Neuroimage* 109, 102–108. doi:10.1016/j.neuroimage.2015.01.014
- Gabbay, V., Mao, X., Klein, R.G., Ely, B.A., Babb, J.S., Panzer, A.M., Alonso, C.M., Shungu, D.C., 2012. Anterior cingulate cortex  $\gamma$ -aminobutyric acid in depressed adolescents: Relationship to anhedonia. *Arch. Gen. Psychiatry* 69, 139–49. doi:10.1001/archgenpsychiatry.2011.131
- Gaetz, W., Bloy, L., Wang, D.J., Port, R.G., Blaskey, L., Levy, S.E., Roberts, T.P.L., 2014. GABA estimation in the brains of children on the autism spectrum: Measurement precision and regional cortical variation. *Neuroimage* 86, 1–9. doi:10.1016/j.neuroimage.2013.05.068
- Gähwiler, B.H., Brown, D.A., 1985. GABAB-receptor-activated  $K^+$  current in voltage-clamped CA3 pyramidal cells in hippocampal cultures. *Proc. Natl. Acad. Sci. U. S. A.* 82, 1558–1562. doi:10.1073/pnas.82.5.1558
- Gambarota, G., Van Der Graaf, M., Klomp, D., Mulkern, R. V., Heerschap, a., 2005. Echo-time independent signal modulations using PRESS sequences: A new approach to spectral editing of strongly coupled AB spin systems. *J. Magn. Reson.* 177, 299–306. doi:10.1016/j.jmr.2005.08.006
- Ganji, S.K., An, Z., Banerjee, A., Madan, A., Hulsey, K.M., Choi, C., 2014. Measurement of regional variation of GABA in the human brain by optimized point-resolved spectroscopy at 7 T in vivo. *NMR Biomed.* 27, 1167–1175. doi:10.1002/nbm.3170
- Gao, F., Edden, R.A.E., Li, M., Puts, N.A.J., Wang, G., Liu, C., Zhao, B., Wang, H., Bai, X., Zhao, C., Wang, X., Barker, P.B., 2013. Edited magnetic resonance spectroscopy detects an age-related decline in brain GABA levels. *Neuroimage* 78, 75–82. doi:10.1016/j.neuroimage.2013.04.012
- Gao, F., Wang, G., Ma, W., Ren, F., Li, M., Dong, Y., Liu, C., Liu, B., Bai, X., Zhao, B., Edden, R.A.E., 2015. Decreased auditory GABA+ concentrations in presbycusis demonstrated by edited magnetic resonance spectroscopy. *Neuroimage* 106, 311–316. doi:10.1016/j.neuroimage.2014.11.023
- Gardner, J.L., Sun, P., Waggoner, R.A., Ueno, K., Tanaka, K., Cheng, K., 2005. Contrast adaptation and representation in human early visual cortex. *Neuron* 47, 607–20. doi:10.1016/j.neuron.2005.07.016
- Garwood, M., DelaBarre, L., 2001. The Return of the Frequency Sweep: Designing Adiabatic Pulses for Contemporary NMR. *J. Magn. Reson.* 153, 155–177. doi:10.1006/jmre.2001.2340
- Gasparovic, C., Bedrick, E.J., Mayer, A.R., Yeo, R.A., Chen, H., Damaraju, E., Calhoun, V.D., Jung, R.E., 2011. Test-retest reliability and reproducibility of

- short-echo-time spectroscopic imaging of human brain at 3T. *Magn. Reson. Med.* 66, 324–332. doi:10.1002/mrm.22858
- Gasparovic, C., Neeb, H., Feis, D.L., Damaraju, E., Chen, H., Doty, M.J., South, D.M., Mullins, P.G., Bockholt, H.J., Shah, N.J., 2009. Quantitative spectroscopic imaging with in situ measurements of tissue water T1, T2, and density. *Magn. Reson. Med.* 62, 583–590. doi:10.1002/mrm.22060
- Gasparovic, C., Song, T., Devier, D., Bockholt, H.J., Caprihan, A., Mullins, P.G., Posse, S., Jung, R.E., Morrison, L.A., 2006. Use of tissue water as a concentration reference for proton spectroscopic imaging. *Magn. Reson. Med.* 55, 1219–1226. doi:10.1002/mrm.20901
- Geramita, M., van der Veen, J.W., Barnett, A.S., Savostyanova, A.A., Shen, J., Weinberger, D.R., Marengo, S., 2011. Reproducibility of prefrontal  $\gamma$ -aminobutyric acid measurements with J-edited spectroscopy. *NMR Biomed.* 24, 1089–1098. doi:10.1002/nbm.1662
- Glaeser, B.S., Hare, T.A., 1975. Measurement of GABA in human cerebrospinal fluid. *Biochem. Med.* 12, 274–282. doi:10.1016/0006-2944(75)90129-5
- Glover, G.H., Li, T.-Q., Ress, D., 2000. Image-based method for retrospective correction of physiological motion effects in fMRI: RETROICOR. *Magn. Reson. Med.* 44, 162–167. doi:10.1002/1522-2594(200007)44:1<162::AID-MRM23>3.0.CO;2-E
- Goddard, A.W., Mason, G.F., Almai, A., Rothman, D.L., Behar, K.L., Petroff, O.A.C., Charney, D.S., Krystal, J.H., 2001. Reductions in Occipital Cortex GABA Levels in Panic Disorder Detected With <sup>1</sup>H-Magnetic Resonance Spectroscopy. *Arch. Gen. Psychiatry* 58, 556. doi:10.1001/archpsyc.58.6.556
- Goddard, A.W., Mason, G.F., Appel, M., Rothman, D.L., Gueorguieva, R., Behar, K.L., Krystal, J.H., 2004. Impaired GABA Neuronal Response to Acute Benzodiazepine Administration in Panic Disorder. *Am. J. Psychiatry* 161, 2186–2193. doi:10.1176/appi.ajp.161.12.2186
- Godlewska, B.R., Near, J., Cowen, P.J., 2015. Neurochemistry of major depression: a study using magnetic resonance spectroscopy. *Psychopharmacology (Berl)*. 232, 501–507. doi:10.1007/s00213-014-3687-y
- Godlewska, B.R., Yip, S.W., Near, J., Goodwin, G.M., Cowen, P.J., 2014. Cortical glutathione levels in young people with bipolar disorder: a pilot study using magnetic resonance spectroscopy. *Psychopharmacology (Berl)*. 231, 327–332. doi:10.1007/s00213-013-3244-0
- Gonzalez-Burgos, G., Lewis, D.A., 2008. GABA Neurons and the Mechanisms of Network Oscillations: Implications for Understanding Cortical Dysfunction in Schizophrenia. *Schizophr. Bull.* 34, 944–961. doi:10.1093/schbul/sbn070
- Goto, N., Yoshimura, R., Kakeda, S., Moriya, J., Hori, H., Hayashi, K., Ikenouchi-Sugita, A., Nakano-Umene, W., Katsuki, A., Nishimura, J., Korogi, Y., Nakamura, J., 2010a. No alterations of brain GABA after 6 months of treatment with atypical antipsychotic drugs in early-stage first-episode schizophrenia. *Prog. Neuro-Psychopharmacology Biol. Psychiatry* 34, 1480–1483. doi:10.1016/j.pnpbp.2010.08.007
- Goto, N., Yoshimura, R., Moriya, J., Kakeda, S., Hayashi, K., Ueda, N., Ikenouchi-Sugita, A., Umene-Nakano, W., Oonari, N., Korogi, Y., Nakamura, J., 2010b. Critical examination of a correlation between brain gamma-aminobutyric acid (GABA) concentrations and a personality trait of extroversion in healthy volunteers as measured by a 3 Tesla proton magnetic resonance spectroscopy study. *Psychiatry Res. Neuroimaging* 182, 53–57.

- doi:10.1016/j.psychresns.2009.11.002
- Goto, N., Yoshimura, R., Moriya, J., Kakeda, S., Ueda, N., Ikenouchi-Sugita, A., Umene-Nakano, W., Hayashi, K., Oonari, N., Korogi, Y., Nakamura, J., 2009. Reduction of brain  $\gamma$ -aminobutyric acid (GABA) concentrations in early-stage schizophrenia patients: 3T Proton MRS study. *Schizophr. Res.* doi:10.1016/j.schres.2009.04.026
- Graham, G.D., Hwang, J.-H., Rothman, D.L., Prichard, J.W., 2001. Spectroscopic Assessment of Alterations in Macromolecule and Small-Molecule Metabolites in Human Brain After Stroke. *Stroke* 32, 2797–2802. doi:10.1161/hs1201.099414
- Groppe, D.M., Urbach, T.P., Kutas, M., 2011. Mass univariate analysis of event-related brain potentials/fields I: A critical tutorial review. *Psychophysiology*. doi:10.1111/j.1469-8986.2011.01273.x
- Guastella, J., Nelson, N., Nelson, H., Czyzyk, L., Keynan, S., Miedel, M., Davidson, N., Lester, H., Kanner, B., 1990. Cloning and expression of a rat brain GABA transporter. *Science* (80-. ). 249, 1303–1306. doi:10.1126/science.1975955
- Gulledge, A.T., Stuart, G.J., 2003. Excitatory Actions of GABA in the Cortex. *Neuron* 37, 299–309. doi:10.1016/S0896-6273(02)01146-7
- Gupta, A., Wang, Y., Markram, H., 2000. Organizing principles for a diversity of GABAergic interneurons and synapses in the neocortex. *Science* (80-. ). 287, 273–8.
- Gussev, A., Erdtel, M., Hiepe, P., Rzanny, R., Reichenbach, J.R., 2012. Absolute quantitation of brain metabolites with respect to heterogeneous tissue compositions in 1H-MR spectroscopic volumes. *Magn. Reson. Mater. Physics, Biol. Med.* 25, 321–333. doi:10.1007/s10334-012-0305-z
- Haag, L., Quetscher, C., Dharmadhikari, S., Dydak, U., Schmidt-Wilcke, T., Beste, C., 2015. Interrelation of resting state functional connectivity, striatal GABA levels, and cognitive control processes. *Hum. Brain Mapp.* 36, 4383–4393. doi:10.1002/hbm.22920
- Hall, S.D., Holliday, I.E., Hillebrand, A., Singh, K.D., Furlong, P.L., Hadjipapas, A., Barnes, G.R., 2005. The missing link: analogous human and primate cortical gamma oscillations. *Neuroimage* 26, 13–17. doi:10.1016/j.neuroimage.2005.01.009
- Ham, B.-J., Sung, Y., Kim, N., Kim, S.J., Kim, J.E., Kim, D.J., Lee, J.Y., Kim, J.H., Yoon, S.J., Lyoo, I.K., 2007. Decreased GABA levels in anterior cingulate and basal ganglia in medicated subjects with panic disorder: A proton magnetic resonance spectroscopy (1H-MRS) study. *Prog. Neuro-Psychopharmacology Biol. Psychiatry* 31, 403–411. doi:10.1016/j.pnpbp.2006.10.011
- Hamann, M., Rossi, D.J., Attwell, D., 2002. Tonic and Spillover Inhibition of Granule Cells Control Information Flow through Cerebellar Cortex. *Neuron* 33, 625–633. doi:10.1016/S0896-6273(02)00593-7
- Hanstock, C.C., Coupland, N.J., Allen, P.S., 2002. GABA X2 multiplet measured pre- and post-administration of vigabatrin in human brain. *Magn. Reson. Med.* 48, 617–623. doi:10.1002/mrm.10265
- Harada, M., Kubo, H., Nose, A., Nishitani, H., Matsuda, T., 2011a. Measurement of variation in the human cerebral GABA level by in vivo MEGA-editing proton MR spectroscopy using a clinical 3 T instrument and its dependence on brain region and the female menstrual cycle. *Hum. Brain Mapp.* 32, 828–833. doi:10.1002/hbm.21086
- Harada, M., Taki, M.M., Nose, A., Kubo, H., Mori, K., Nishitani, H., Matsuda, T.,

- 2011b. Non-invasive evaluation of the GABAergic/glutamatergic system in autistic patients observed by MEGA-editing proton MR spectroscopy using a clinical 3 Tesla instrument. *J. Autism Dev. Disord.* 41, 447–454. doi:10.1007/s10803-010-1065-0
- Harris, A.D., Glaubitz, B., Near, J., John Evans, C., Puts, N.A.J., Schmidt-Wilcke, T., Tegenthoff, M., Barker, P.B., Edden, R.A.E., 2014. Impact of frequency drift on gamma-aminobutyric acid-edited MR spectroscopy. *Magn. Reson. Med.* 72, 941–8. doi:10.1002/mrm.25009
- Harris, A.D., Puts, N.A.J., Anderson, B.A., Yantis, S., Pekar, J.J., Barker, P.B., Edden, R.A.E., 2015a. Multi-Regional Investigation of the Relationship between Functional MRI Blood Oxygenation Level Dependent (BOLD) Activation and GABA Concentration. *PLoS One* 10, e0117531. doi:10.1371/journal.pone.0117531
- Harris, A.D., Puts, N.A.J., Barker, P.B., Edden, R.A.E., 2015b. Spectral-editing measurements of GABA in the human brain with and without macromolecule suppression. *Magn. Reson. Med.* 74, 1523–1529. doi:10.1002/mrm.25549
- Harris, A.D., Puts, N.A.J., Edden, R.A.E., 2015c. Tissue correction for GABA-edited MRS: Considerations of voxel composition, tissue segmentation, and tissue relaxations. *J. Magn. Reson. Imaging* 42, 1431–1440. doi:10.1002/jmri.24903
- Harris, A.D., Singer, H.S., Horska, A., Kline, T., Ryan, M., Edden, R.A.E., Mahone, E.M., 2015d. GABA and Glutamate in Children with Primary Complex Motor Stereotypies: An 1H-MRS Study at 7T. *Am. J. Neuroradiol.* 1–6. doi:10.3174/ajnr.A4547
- Hasler, G., Neumeister, A., van der Veen, J.W., Tumonis, T., Bain, E.E., Shen, J., Drevets, W.C., Charney, D.S., 2005. Normal Prefrontal Gamma-Aminobutyric Acid Levels in Remitted Depressed Subjects Determined by Proton Magnetic Resonance Spectroscopy. *Biol. Psychiatry* 58, 969–973. doi:10.1016/j.biopsych.2005.05.017
- Hasler, G., van der Veen, J.W., Geraci, M., Shen, J., Pine, D., Drevets, W.C., 2009. Prefrontal Cortical Gamma-Aminobutyric Acid Levels in Panic Disorder Determined by Proton Magnetic Resonance Spectroscopy. *Biol. Psychiatry* 65, 273–275. doi:10.1016/j.biopsych.2008.06.023
- Hasler, G., van der Veen, J.W., Grillon, C., Drevets, W.C., Shen, J., 2010. Effect of Acute Psychological Stress on Prefrontal GABA Concentration Determined by Proton Magnetic Resonance Spectroscopy. *Am. J. Psychiatry* 167, 1226–1231. doi:10.1176/appi.ajp.2010.09070994
- Hasler, G., van der Veen, J.W., Tumonis, T., Meyers, N., Shen, J., Drevets, W.C., 2007. Reduced Prefrontal Glutamate/Glutamine and  $\gamma$ -Aminobutyric Acid Levels in Major Depression Determined Using Proton Magnetic Resonance Spectroscopy. *Arch. Gen. Psychiatry* 64, 193. doi:10.1001/archpsyc.64.2.193
- Heba, S., Puts, N.A.J., Kalisch, T., Glaubitz, B., Haag, L.M., Lenz, M., Dinse, H.R., Edden, R.A.E., Tegenthoff, M., Schmidt-Wilcke, T., 2016. Local GABA Concentration Predicts Perceptual Improvements After Repetitive Sensory Stimulation in Humans. *Cereb. Cortex* 26, 1295–1301. doi:10.1093/cercor/bhv296
- Helms, G., Piringer, A., 2001. Restoration of motion-related signal loss and line-shape deterioration of proton MR spectra using the residual water as intrinsic reference. *Magn. Reson. Med.* 46, 395–400. doi:10.1002/mrm.1203
- Henrie, J.A., Shapley, R., 2005. LFP Power Spectra in V1 Cortex: The Graded Effect

- of Stimulus Contrast. *J. Neurophysiol.* 94, 479–490. doi:10.1152/jn.00919.2004
- Henry, P.-G., Dautry, C., Hantraye, P., Bloch, G., 2001. Brain GABA editing without macromolecule contamination. *Magn. Reson. Med.* 45, 517–520. doi:10.1002/1522-2594(200103)45:3<517::AID-MRM1068>3.0.CO;2-6
- Henry, P.-G., van de Moortele, P.-F., Giacomini, E., Nauwerth, A., Bloch, G., 1999. Field-frequency locked in vivo proton MRS on a whole-body spectrometer. *Magn. Reson. Med.* 42, 636–642. doi:10.1002/(SICI)1522-2594(199910)42:4<636::AID-MRM4>3.0.CO;2-I
- Hetherington, H.P., Pan, J.W., Mason, G.F., Adams, D., Vaughn, M.J., Twieg, D.B., Pohost, G.M., 1996. Quantitative <sup>1</sup>H spectroscopic imaging of human brain at 4.1 T using image segmentation. *Magn. Reson. Med.* 36, 21–29. doi:10.1002/mrm.1910360106
- Hofmann, L., Slotboom, J., Boesch, C., Kreis, R., 2001. Characterization of the macromolecule baseline in localized <sup>1</sup>H-MR spectra of human brain. *Magn. Reson. Med.* 46, 855–863. doi:10.1002/mrm.1269
- Hofmann, L., Slotboom, J., Jung, B., Maloca, P., Boesch, C., Kreis, R., 2002. Quantitative <sup>1</sup>H-magnetic resonance spectroscopy of human brain: Influence of composition and parameterization of the basis set in linear combination model-fitting. *Magn. Reson. Med.* 48, 440–453. doi:10.1002/mrm.10246
- Hoge, R.D., Atkinson, J., Gill, B., Crelier, G.R., Marrett, S., Pike, G.B., 1999a. Investigation of BOLD signal dependence on cerebral blood flow and oxygen consumption: The deoxyhemoglobin dilution model. *Magn. Reson. Med.* 42, 849–863. doi:10.1002/(SICI)1522-2594(199911)42:5<849::AID-MRM4>3.0.CO;2-Z
- Hoge, R.D., Atkinson, J., Gill, B., Crelier, G.R., Marrett, S., Pike, G.B., 1999b. Linear coupling between cerebral blood flow and oxygen consumption in activated human cortex. *Proc. Natl. Acad. Sci. U. S. A.* 96, 9403–9408. doi:10.1073/pnas.96.16.9403
- Hong, S.-T., Balla, D.Z., Pohmann, R., 2011. Determination of regional variations and reproducibility in in vivo <sup>1</sup>H NMR spectroscopy of the rat brain at 16.4 T. *Magn. Reson. Med.* 66, 11–17. doi:10.1002/mrm.22943
- Howe, F.A., Barton, S.J., Cudlip, S.A., Stubbs, M., Saunders, D.E., Murphy, M., Wilkins, P., Opstad, K.S., Doyle, V.L., McLean, M.A., Bell, B.A., Griffiths, J.R., 2003. Metabolic profiles of human brain tumors using quantitative in vivo <sup>1</sup>H magnetic resonance spectroscopy. *Magn. Reson. Med.* 49, 223–232. doi:10.1002/mrm.10367
- Huppertz, H.J., Kröll-Seger, J., Klöppel, S., Ganz, R.E., Kassubek, J., 2010. Intra- and interscanner variability of automated voxel-based volumetry based on a 3D probabilistic atlas of human cerebral structures. *Neuroimage* 49, 2216–2224. doi:10.1016/j.neuroimage.2009.10.066
- Hyder, F., Patel, A.B., Gjedde, A., Rothman, D.L., Behar, K.L., Shulman, R.G., 2006. Neuronal–glial glucose oxidation and glutamatergic–GABAergic function. *J. Cereb. Blood Flow Metab.* 26, 865–877. doi:10.1038/sj.jcbfm.9600263
- Hyder, F., Rothman, D.L., 2012. Quantitative fMRI and oxidative neuroenergetics. *Neuroimage* 62, 985–994. doi:10.1016/j.neuroimage.2012.04.027
- Isaacson, J.S., Scanziani, M., 2011. How inhibition shapes cortical activity. *Neuron* 72, 231–43. doi:10.1016/j.neuron.2011.09.027
- Jenkinson, M., Bannister, P., Brady, M., Smith, S., 2002. Improved optimization for

- the robust and accurate linear registration and motion correction of brain images. *Neuroimage* 17, 825–841. doi:10.1016/S1053-8119(02)91132-8
- Jenkinson, M., Beckmann, C.F., Behrens, T.E.J., Woolrich, M.W., Smith, S.M., 2012. FSL. *Neuroimage* 62, 782–90. doi:10.1016/j.neuroimage.2011.09.015
- Jenkinson, M., Smith, S., 2001. A global optimisation method for robust affine registration of brain images. *Med. Image Anal.* 5, 143–156. doi:10.1016/S1361-8415(01)00036-6
- Jensen, J.E., de B. Frederick, B., Renshaw, P.F., 2005. Grey and white matter GABA level differences in the human brain using two-dimensional, J-resolved spectroscopic imaging. *NMR Biomed.* 18, 570–576. doi:10.1002/nbm.994
- Jin, H., Wu, H., Osterhaus, G., Wei, J., Davis, K., Sha, D., Floor, E., Hsu, C.-C., Kopke, R.D., Wu, J.-Y., 2003. Demonstration of functional coupling between  $\gamma$ -aminobutyric acid (GABA) synthesis and vesicular GABA transport into synaptic vesicles. *Proc. Natl. Acad. Sci. U. S. A.* 100, 4293–4298. doi:10.1073/pnas.0730698100
- Jocham, G., Hunt, L.T., Near, J., Behrens, T.E.J., 2012. A mechanism for value-guided choice based on the excitation-inhibition balance in prefrontal cortex. *Nat. Neurosci.* 15, 960–961. doi:10.1038/nn.3140
- Jonas, P., Bischofberger, J., Fricker, D., Miles, R., 2004. Interneuron Diversity series: Fast in, fast out - Temporal and spatial signal processing in hippocampal interneurons. *Trends Neurosci.* 27, 30–40. doi:10.1016/j.tins.2003.10.010
- Jung, W.-I., 1996. Localized double spin echo proton spectroscopy. Part I: Basic concepts. *Concepts Magn. Reson.* 8, 1–15. doi:10.1002/(SICI)1099-0534(1996)8:1<1::AID-CMR1>3.0.CO;2-2
- Kaiser, L.G., Young, K., Meyerhoff, D.J., Mueller, S.G., Matson, G.B., 2008. A detailed analysis of localized J-difference GABA editing: theoretical and experimental study at 4T. *NMR Biomed.* 21, 22–32. doi:10.1002/nbm.1150
- Kalueff, A. V, Nutt, D.J., 2007. Role of GABA in anxiety and depression. *Depress. Anxiety* 24, 495–517. doi:10.1002/da.20262
- Kapogiannis, D., Reiter, D.A., Willette, A.A., Mattson, M.P., 2013. Posteromedial cortex glutamate and GABA predict intrinsic functional connectivity of the default mode network. *Neuroimage* 64, 112–119. doi:10.1016/j.neuroimage.2012.09.029
- Katzner, S., Busse, L., Carandini, M., 2011. GABA Inhibition Controls Response Gain in Visual Cortex. *J. Neurosci.* 31, 5931–5941. doi:10.1523/JNEUROSCI.5753-10.2011
- Kaufman, D.L., Houser, C.R., Tobin, A.J., 1991. Two Forms of the  $\gamma$ -Aminobutyric Acid Synthetic Enzyme Glutamate Decarboxylase Have Distinct Intraneuronal Distributions and Cofactor Interactions. *J. Neurochem.* 56, 720–723. doi:10.1111/j.1471-4159.1991.tb08211.x
- Kaufman, R.E., Ostacher, M.J., Marks, E.H., Simon, N.M., Sachs, G.S., Jensen, J.E., Renshaw, P.F., Pollack, M.H., 2009. Brain GABA levels in patients with bipolar disorder. *Prog. Neuro-Psychopharmacology Biol. Psychiatry* 33, 427–434. doi:10.1016/j.pnpbp.2008.12.025
- Kaupmann, K., Malitschek, B., Schuler, V., Heid, J., Froestl, W., Beck, P., Mosbacher, J., Bischoff, S., Kulik, A., Shigemoto, R., Karschin, A., Bettler, B., 1998. GABAB-receptor subtypes assemble into functional heteromeric complexes. *Nature* 396, 683–7. doi:10.1038/25360
- Kegeles, L.S., Mao, X., Gonzalez, R., Shungu, D.C., 2007. Evaluation of anatomic variation in macromolecule contribution to the GABA signal using metabolite

- nulling and the J-editing technique at 3.0 T, in: *Proc. Intl. Soc. Mag. Reson. Med.* p. 1391.
- Kegeles, L.S., Mao, X., Stanford, A.D., Girgis, R., Ojeil, N., Xu, X., Gil, R., Slifstein, M., Abi-Dargham, A., Lisanby, S.H., Shungu, D.C., 2012. Elevated Prefrontal Cortex  $\gamma$ -Aminobutyric Acid and Glutamate-Glutamine Levels in Schizophrenia Measured In Vivo With Proton Magnetic Resonance Spectroscopy. *Arch. Gen. Psychiatry.* doi:10.1001/archgenpsychiatry.2011.1519
- Kelemen, O., Kiss, I., Benedek, G., Kéri, S., 2013. Perceptual and cognitive effects of antipsychotics in first-episode schizophrenia: The potential impact of GABA concentration in the visual cortex. *Prog. Neuro-Psychopharmacology Biol. Psychiatry* 47, 13–19. doi:10.1016/j.pnpbp.2013.07.024
- Kim, H.J., Kim, J.E., Cho, G., Song, I.C., Bae, S., Hong, S.J., Yoon, S.J., Lyoo, I.K., Kim, T.S., 2009. Associations between anterior cingulate cortex glutamate and  $\gamma$ -aminobutyric acid concentrations and the harm avoidance temperament. *Neurosci. Lett.* 464, 103–107. doi:10.1016/j.neulet.2009.07.087
- Kim, S., Stephenson, M.C., Morris, P.G., Jackson, S.R., 2014. tDCS-induced alterations in GABA concentration within primary motor cortex predict motor learning and motor memory: A 7T magnetic resonance spectroscopy study. *Neuroimage* 99, 237–243. doi:10.1016/j.neuroimage.2014.05.070
- Klauschen, F., Goldman, A., Barra, V., Meyer-Lindenberg, A., Lundervold, A., 2009. Evaluation of automated brain MR image segmentation and volumetry methods. *Hum. Brain Mapp.* 30, 1310–1327. doi:10.1002/hbm.20599
- Knight-Scott, J., Haley, A.P., Rossmiller, S.R., Farace, E., Mai, V.M., Christopher, J.M., Manning, C. a., Simnad, V.I., Siragy, H.M., 2003. Molality as a unit of measure for expressing  $^1\text{H}$  MRS brain metabolite concentrations in vivo. *Magn. Reson. Imaging* 21, 787–797. doi:10.1016/S0730-725X(03)00179-6
- Krause, B.W., Wijtenburg, S.A., Holcomb, H.H., Kochunov, P., Wang, D.J.J., Hong, L.E., Rowland, L.M., 2014. Anterior cingulate GABA levels predict whole-brain cerebral blood flow. *Neurosci. Lett.* 561, 188–191. doi:10.1016/j.neulet.2013.12.062
- Kreis, R., Bolliger, C.S., 2012. The need for updates of spin system parameters, illustrated for the case of  $\gamma$ -aminobutyric acid. *NMR Biomed.* 25, 1401–1403. doi:10.1002/nbm.2810
- Kreis, R., Ernst, T., Ross, B.D., 1993. Absolute quantitation of water and metabolites in the human brain. II. Metabolite concentrations. *J. Magn. Reson. Ser. B* 102, 9–19. doi:10.1006/jmrb.1993.1056
- Kubas, B., Kułak, W., Sobaniec, W., Tarasow, E., Łebkowska, U., Walecki, J., 2012. Metabolite alterations in autistic children: a  $^1\text{H}$  MR spectroscopy study. *Adv. Med. Sci.* 57, 152–156. doi:10.2478/v10039-012-0014-x
- Kühn, S., Schubert, F., Mекle, R., Wenger, E., Ittermann, B., Lindenberger, U., Gallinat, J., 2015. Neurotransmitter changes during interference task in anterior cingulate cortex: evidence from fMRI-guided functional MRS at 3 T. *Brain Struct. Funct.* doi:10.1007/s00429-015-1057-0
- Kuzniecky, R., Hetherington, H., Ho, S., Pan, J., Martin, R., Gilliam, F., Hugg, J., Faught, E., 1998. Topiramate increases cerebral GABA in healthy humans. *Neurology* 51, 627–629. doi:10.1212/WNL.51.2.627
- Kuzniecky, R., Ho, S., Pan, J., Martin, R., Gilliam, F., Faught, E., Hetherington, H., 2002. Modulation of cerebral GABA by topiramate, lamotrigine, and gabapentin in healthy adults. *Neurology* 58, 368–372.

doi:10.1212/WNL.58.3.368

- Kwong, K.K., Belliveau, J.W., Chesler, D.A., Goldberg, I.E., Weisskoff, R.M., Poncelet, B.P., Kennedy, D.N., Hoppel, B.E., Cohen, M.S., Turner, R., Cheng, H.M., Brady, T.J., Rosen, B.R., 1992. Dynamic magnetic resonance imaging of human brain activity during primary sensory stimulation. *Proc. Natl. Acad. Sci. U. S. A.* 89, 5675–9.
- Lange, T., Zaitsev, M., Buechert, M., 2011. Correction of frequency drifts induced by gradient heating in 1H spectra using interleaved reference spectroscopy. *J. Magn. Reson. Imaging* 33, 748–754. doi:10.1002/jmri.22471
- Lauritzen, M., Mathiesen, C., Schaefer, K., Thomsen, K.J., 2012. Neuronal inhibition and excitation, and the dichotomic control of brain hemodynamic and oxygen responses. *Neuroimage* 62, 1040–1050. doi:10.1016/j.neuroimage.2012.01.040
- Lauterbur, P.C., 1973. Image Formation by Induced Local Interactions: Examples Employing Nuclear Magnetic Resonance. *Nature* 242, 190–191. doi:10.1038/242190a0
- Lecocq, A., Le Fur, Y., Amadon, A., Vignaud, A., Cozzone, P.J., Guye, M., Ranjeva, J.-P., 2015. Fast water concentration mapping to normalize 1H MR spectroscopic imaging. *Magn. Reson. Mater. Physics, Biol. Med.* 28, 87–100. doi:10.1007/s10334-014-0451-6
- Lecrux, C., Hamel, E., 2011. The neurovascular unit in brain function and disease. *Acta Physiol.* 203, 47–59. doi:10.1111/j.1748-1716.2011.02256.x
- Legge, G.E., 1981. A power law for contrast discrimination. *Vision Res.* 21, 457–467. doi:10.1016/0042-6989(81)90092-4
- Leibfritz, D., Dreher, W., 2001. Magnetization transfer MRS. *NMR Biomed.* 14, 65–76. doi:10.1002/nbm.681
- Lerma, J., Herranz, A.S., Herreras, O., Abaira, V., del Rio, R.M., 1986. In vivo determination of extracellular concentration of amino acids in the rat hippocampus. A method based on brain dialysis and computerized analysis. *Brain Res.* 384, 145–155. doi:10.1016/0006-8993(86)91230-8
- Lewis, D.A., Hashimoto, T., Volk, D.W., 2005. Cortical inhibitory neurons and schizophrenia. *Nat. Rev. Neurosci.* 6, 312–324. doi:10.1038/nrn1648
- Lewis, D.A., Pierri, J.N., Volk, D.W., Melchitzky, D.S., Woo, T.-U.W., 1999. Altered GABA neurotransmission and prefrontal cortical dysfunction in schizophrenia. *Biol. Psychiatry* 46, 616–626. doi:10.1016/S0006-3223(99)00061-X
- Liang, C.L., Ances, B.M., Perthen, J.E., Moradi, F., Liao, J., Buracas, G.T., Hopkins, S.R., Buxton, R.B., 2013. Luminance contrast of a visual stimulus modulates the BOLD response more than the cerebral blood flow response in the human brain. *Neuroimage* 64, 104–111. doi:10.1016/j.neuroimage.2012.08.077
- Liang, F., Paulo, R., Molina, G., Clyde, M.A., Berger, J.O., 2008. Mixtures of g Priors for Bayesian Variable Selection. *J. Am. Stat. Assoc.* 103, 410–423. doi:10.1198/016214507000001337
- Licata, S.C., Jensen, J.E., Conn, N. a., Winer, J.P., Lukas, S.E., 2014. Zolpidem increases GABA in depressed volunteers maintained on SSRIs. *Psychiatry Res. Neuroimaging* 224, 28–33. doi:10.1016/j.psychresns.2014.05.009
- Licata, S.C., Jensen, J.E., Penetar, D.M., Prescott, A.P., Lukas, S.E., Renshaw, P.F., 2009. A therapeutic dose of zolpidem reduces thalamic GABA in healthy volunteers: a proton MRS study at 4 T. *Psychopharmacology (Berl.)* 203, 819–829. doi:10.1007/s00213-008-1431-1

- Lin, A.L., Fox, P.T., Yang, Y., Lu, H., Tan, L.H., Gao, J.H., 2008. Evaluation of MRI models in the measurement of CMRO<sub>2</sub> and its relationship with CBF. *Magn. Reson. Med.* 60, 380–389. doi:10.1002/mrm.21655
- Liu, B., Wang, G., Gao, D., Gao, F., Zhao, B., Qiao, M., Yang, H., Yu, Y., Ren, F., Yang, P., Chen, W., Rae, C.D., 2015. Alterations of GABA and glutamate–glutamine levels in premenstrual dysphoric disorder: A 3T proton magnetic resonance spectroscopy study. *Psychiatry Res. Neuroimaging* 231, 64–70. doi:10.1016/j.psychres.2014.10.020
- Liu, T.T., Wong, E.C., 2005. A signal processing model for arterial spin labeling functional MRI. *Neuroimage* 24, 207–215. doi:10.1016/j.neuroimage.2004.09.047
- Logothetis, N.K., 2008. What we can do and what we cannot do with fMRI. *Nature* 453, 869–878. doi:10.1038/nature06976
- Logothetis, N.K., Pauls, J., Augath, M., Trinath, T., Oeltermann, A., 2001. Neurophysiological investigation of the basis of the fMRI signal. *Nature* 412, 150–157. doi:10.1038/35084005
- Logothetis, N.K., Wandell, B.A., 2004. Interpreting the BOLD Signal. *Annu. Rev. Physiol.* 66, 735–769. doi:10.1146/annurev.physiol.66.082602.092845
- Long, Z., Li, X.-R., Xu, J., Edden, R.A.E., Qin, W.-P., Long, L.-L., Murdoch, J.B., Zheng, W., Jiang, Y.-M., Dydak, U., 2014. Thalamic GABA Predicts Fine Motor Performance in Manganese-Exposed Smelter Workers. *PLoS One* 9, e88220. doi:10.1371/journal.pone.0088220
- Long, Z., Medlock, C., Dzemidzic, M., Shin, Y.-W., Goddard, A.W., Dydak, U., 2013. Decreased GABA levels in anterior cingulate cortex/medial prefrontal cortex in panic disorder. *Prog. Neuro-Psychopharmacology Biol. Psychiatry* 44, 131–135. doi:10.1016/j.pnpbp.2013.01.020
- Lu, H., Nagae-Poetscher, L.M., Golay, X., Lin, D., Pomper, M., van Zijl, P.C.M., 2005. Routine clinical brain MRI sequences for use at 3.0 Tesla. *J. Magn. Reson. Imaging* 22, 13–22. doi:10.1002/jmri.20356
- Mader, I., Seeger, U., Weissert, R., Klose, U., Naegele, T., Melms, A., Grodd, W., 2001. Proton MR spectroscopy with metabolite-nulling reveals elevated macromolecules in acute multiple sclerosis. *Brain* 124, 953–61. doi:10.1093/brain/124.5.953
- Mandal, P.K., 2007. Magnetic resonance spectroscopy (MRS) and its application in Alzheimer’s disease. *Concepts Magn. Reson. Part A* 30A, 40–64. doi:10.1002/cmr.a.20072
- Mann, E.O., Kohl, M.M., Paulsen, O., 2009. Distinct Roles of GABAA and GABAB Receptors in Balancing and Terminating Persistent Cortical Activity. *J. Neurosci.* 29, 7513–7518. doi:10.1523/JNEUROSCI.6162-08.2009
- Mann, E.O., Mody, I., 2010. Control of hippocampal gamma oscillation frequency by tonic inhibition and excitation of interneurons. *Nat. Neurosci.* 13, 205–212. doi:10.1038/nn.2464
- Mann, E.O., Paulsen, O., 2007. Role of GABAergic inhibition in hippocampal network oscillations. *Trends Neurosci.* 30, 343–349. doi:10.1016/j.tins.2007.05.003
- Mansfield, P., Grannell, P.K., 1973. NMR “diffraction” in solids? *J. Phys. C Solid State Phys.* 6, L422–L426. doi:10.1088/0022-3719/6/22/007
- Marengo, S., Meyer, C., Kuo, S., van der Veen, J.W., Shen, J., DeJong, K., Barnett, A.S., Apud, J.A., Dickinson, D., Weinberger, D.R., Berman, K.F., 2016. Prefrontal GABA Levels Measured With Magnetic Resonance Spectroscopy in

- Patients With Psychosis and Unaffected Siblings. *Am. J. Psychiatry* appi.ajp.2015.1. doi:10.1176/appi.ajp.2015.15020190
- Markram, H., Toledo-Rodriguez, M., Wang, Y., Gupta, A., Silberberg, G., Wu, C., 2004. Interneurons of the neocortical inhibitory system. *Nat. Rev. Neurosci.* 5, 793–807. doi:10.1038/nrn1519
- Marsman, A., Mandl, R.C.W., Klomp, D.W.J., Bohlken, M.M., Boer, V.O., Andreychenko, A., Cahn, W., Kahn, R.S., Luijten, P.R., Hulshoff Pol, H.E., 2014. GABA and glutamate in schizophrenia: A 7 T 1H-MRS study. *NeuroImage Clin.* 6, 398–407. doi:10.1016/j.nicl.2014.10.005
- Martin, D.L., Rimvall, K., 1993. Regulation of gamma-aminobutyric acid synthesis in the brain. *J. Neurochem.* 60, 395–407.
- Martinez-Hernandez, A., Bell, K., Norenberg, M., 1977. Glutamine synthetase: glial localization in brain. *Science* (80- ). 195, 1356–1358. doi:10.1126/science.14400
- Marty, A., Llano, I., 2005. Excitatory effects of GABA in established brain networks. *Trends Neurosci.* 28, 284–289. doi:10.1016/j.tins.2005.04.003
- Mason, G.F., Martin, D.L., Martin, S.B., Manor, D., Sibson, N.R., Patel, A., Rothman, D.L., Behar, K.L., 2001. Decrease in GABA synthesis rate in rat cortex following GABA-transaminase inhibition correlates with the decrease in GAD67 protein. *Brain Res.* 914, 81–91. doi:10.1016/S0006-8993(01)02778-0
- Mazziotta, J., Toga, A., Evans, A., Fox, P., Lancaster, J., Zilles, K., Woods, R., Paus, T., Simpson, G., Pike, B., Holmes, C., Collins, L., Thompson, P., MacDonald, D., Iacoboni, M., Schormann, T., Amunts, K., Palomero-Gallagher, N., Geyer, S., Parsons, L., Narr, K., Kabani, N., Goualher, G.L., Boomsma, D., Cannon, T., Kawashima, R., Mazoyer, B., 2001. A probabilistic atlas and reference system for the human brain: International Consortium for Brain Mapping (ICBM). *Philos. Trans. R. Soc. B Biol. Sci.* 356, 1293–1322. doi:10.1098/rstb.2001.0915
- McCormick, D.A., 1989. GABA as an inhibitory neurotransmitter in human cerebral cortex. *J. Neurophysiol.* 62, 1018–1027.
- McIntire, S.L., Reimer, R.J., Schuske, K., Edwards, R.H., Jorgensen, E.M., 1997. Identification and characterization of the vesicular GABA transporter. *Nature* 389, 870–6. doi:10.1038/39908
- McLean, M.A., Barker, G.J., 2006. Concentrations and magnetization transfer ratios of metabolites in gray and white matter. *Magn. Reson. Med.* 56, 1365–1370. doi:10.1002/mrm.21070
- McLean, M.A., Simister, R.J., Barker, G.J., Duncan, J.S., 2004. Discrimination between neurochemical and macromolecular signals in human frontal lobes using short echo time proton magnetic resonance spectroscopy. *Faraday Discuss.* 126, 93–102. doi:10.1039/b304938h
- Mescher, M., Merkle, H., Kirsch, J., Garwood, M., Gruetter, R., 1998. Simultaneous in vivo spectral editing and water suppression. *NMR Biomed.* 11, 266–272. doi:10.1002/(SICI)1099-1492(199810)11:6<266::AID-NBM530>3.0.CO;2-J
- Mescher, M., Tannus, A., Johnson, M.O., Garwood, M., 1996. Solvent Suppression Using Selective Echo Dephasing. *J. Magn. Reson. Ser. A* 123, 226–229. doi:10.1006/jmra.1996.0242
- Meyerhoff, D.J., Mon, A., Metzler, T., Neylan, T.C., 2014. Cortical Gamma-Aminobutyric Acid and Glutamate in Posttraumatic Stress Disorder and Their Relationships to Self-Reported Sleep Quality. *Sleep* 37, 893–900. doi:10.5665/sleep.3654

- Michels, L., Martin, E., Klaver, P., Edden, R., Zelaya, F., Lythgoe, D.J., Lüchinger, R., Brandeis, D., O’Gorman, R.L., 2012. Frontal GABA Levels Change during Working Memory. *PLoS One* 7, e31933. doi:10.1371/journal.pone.0031933
- Michels, L., Schulte-Vels, T., Schick, M., O’Gorman, R.L., Zeffiro, T., Hasler, G., Mueller-Pfeiffer, C., 2014. Prefrontal GABA and glutathione imbalance in posttraumatic stress disorder: Preliminary findings. *Psychiatry Res. Neuroimaging* 224, 288–295. doi:10.1016/j.psychres.2014.09.007
- Mierisová, Š., van den Boogaart, A., Tkáč, I., Van Hecke, P., Vanhamme, L., Liptaj, T., 1998. New approach for quantitation of short echo time in vivo 1H MR spectra of brain using AMARES. *NMR Biomed.* 11, 32–39. doi:10.1002/(SICI)1099-1492(199802)11:1<32::AID-NBM501>3.0.CO;2-#
- Mikkelsen, M., Singh, K.D., Sumner, P., Evans, C.J., 2016. Comparison of the repeatability of GABA-edited magnetic resonance spectroscopy with and without macromolecule suppression. *Magn. Reson. Med.* 75, 946–53. doi:10.1002/mrm.25699
- Milak, M.S., Proper, C.J., Mulhern, S.T., Parter, a L., Kegeles, L.S., Ogden, R.T., Mao, X., Rodriguez, C.I., Oquendo, M. a, Suckow, R.F., Cooper, T.B., Keilp, J.G., Shungu, D.C., Mann, J.J., 2015. A pilot in vivo proton magnetic resonance spectroscopy study of amino acid neurotransmitter response to ketamine treatment of major depressive disorder. *Mol. Psychiatry* 1–8. doi:10.1038/mp.2015.83
- Miller, G.A., Chapman, J.P., 2001. Misunderstanding analysis of covariance. *J. Abnorm. Psychol.* 110, 40–48. doi:10.1037/0021-843X.110.1.40
- Mintz, I.M., Bean, B.P., 1993. GABAB receptor inhibition of P-type Ca<sup>2+</sup> channels in central neurons. *Neuron* 10, 889–898. doi:0896-6273(93)90204-5 [pii]
- Mitchell, S.J., Silver, R.A., 2003. Shunting Inhibition Modulates Neuronal Gain during Synaptic Excitation. *Neuron* 38, 433–445. doi:10.1016/S0896-6273(03)00200-9
- Mlynárik, V., Gambarota, G., Frenkel, H., Gruetter, R., 2006. Localized short-echo-time proton MR spectroscopy with full signal-intensity acquisition. *Magn. Reson. Med.* 56, 965–970. doi:10.1002/mrm.21043
- Mlynárik, V., Gruber, S., Moser, E., 2001. Proton T1 and T2 relaxation times of human brain metabolites at 3 Tesla. *NMR Biomed.* 14, 325–331. doi:10.1002/nbm.713
- Mody, I., 2001. Distinguishing between GABA(A) receptors responsible for tonic and phasic conductances. *Neurochem. Res.* 26, 907–13. doi:10.1023/A:1012376215967
- Mody, I., De Koninck, Y., Otis, T.S., Soltesz, I., 1994. Bridging the cleft at GABA synapses in the brain. *Trends Neurosci.* 17, 517–525. doi:10.1016/0166-2236(94)90155-4
- Morgan, P.T., Pace-Schott, E.F., Mason, G.F., Forselius, E., Fasula, M., Valentine, G.W., Sanacora, G., 2012. Cortical GABA Levels in Primary Insomnia. *Sleep* 35, 807–814. doi:10.5665/sleep.1880
- Mozzrymas, J.W., 2004. Dynamism of GABAA receptor activation shapes the “personality” of inhibitory synapses. *Neuropharmacology* 47, 945–960. doi:10.1016/j.neuropharm.2004.07.003
- Mozzrymas, J.W., Zarnowska, E.D., Pytel, M., Mercik, K., 2003. Modulation of GABA(A) receptors by hydrogen ions reveals synaptic GABA transient and a crucial role of the desensitization process. *J. Neurosci.* 23, 7981–7992.
- Mueller, S.G., Weber, O.M., Duc, C.O., Weber, B., Meier, D., Russ, W., Boesiger,

- P., Wieser, H.G., 2008. Effects of Vigabatrin on Brain GABA+/CR Signals in Patients with Epilepsy Monitored by 1H-NMR-Spectroscopy: Responder Characteristics. *Epilepsia* 42, 29–40. doi:10.1046/j.1528-1157.2001.077889.x
- Mullins, P.G., McGonigle, D.J., O’Gorman, R.L., Puts, N.A.J., Vidyasagar, R., Evans, C.J., Edden, R.A.E., 2014. Current practice in the use of MEGA-PRESS spectroscopy for the detection of GABA. *Neuroimage* 86, 43–52. doi:10.1016/j.neuroimage.2012.12.004
- Murphy, K., Birn, R.M., Bandettini, P.A., 2013. Resting-state fMRI confounds and cleanup. *Neuroimage* 80, 349–359. doi:10.1016/j.neuroimage.2013.04.001
- Murphy, K., Harris, A.D., Wise, R.G., 2011. Robustly measuring vascular reactivity differences with breath-hold: Normalising stimulus-evoked and resting state BOLD fMRI data. *Neuroimage* 54, 369–379. doi:10.1016/j.neuroimage.2010.07.059
- Muthukumaraswamy, S.D., Edden, R.A.E., Jones, D.K., Swettenham, J.B., Singh, K.D., 2009. Resting GABA concentration predicts peak gamma frequency and fMRI amplitude in response to visual stimulation in humans. *Proc. Natl. Acad. Sci. U. S. A.* 106, 8356–8361. doi:10.1073/pnas.0900728106
- Muthukumaraswamy, S.D., Evans, C.J., Edden, R.A.E., Wise, R.G., Singh, K.D., 2012. Individual variability in the shape and amplitude of the BOLD-HRF correlates with endogenous GABAergic inhibition. *Hum. Brain Mapp.* 33, 455–465. doi:10.1002/hbm.21223
- Muthukumaraswamy, S.D., Singh, K.D., 2009. Functional decoupling of BOLD and gamma-band amplitudes in human primary visual cortex. *Hum. Brain Mapp.* 30, 2000–2007. doi:10.1002/hbm.20644
- Muthukumaraswamy, S.D., Singh, K.D., 2008. Spatiotemporal frequency tuning of BOLD and gamma band MEG responses compared in primary visual cortex. *Neuroimage* 40, 1552–1560. doi:10.1016/j.neuroimage.2008.01.052
- Myers, J.F.M., Evans, C.J., Kalk, N.J., Edden, R.A.E., Lingford-Hughes, A.R., 2014. Measurement of GABA using J-difference edited 1H-MRS following modulation of synaptic GABA concentration with tiagabine. *Synapse* 68, 355–362. doi:10.1002/syn.21747
- Napolitano, A., Kockenberger, W., Auer, D.P., 2013. Reliable gamma aminobutyric acid measurement using optimized PRESS at 3 T. *Magn. Reson. Med.* 69, 1528–1533. doi:10.1002/mrm.24397
- Near, J., Andersson, J., Maron, E., Mekle, R., Gruetter, R., Cowen, P., Jezzard, P., 2013a. Unedited in vivo detection and quantification of  $\gamma$ -aminobutyric acid in the occipital cortex using short-TE MRS at 3 T. *NMR Biomed.* 26, 1353–1362. doi:10.1002/nbm.2960
- Near, J., Edden, R., Evans, C.J., Paquin, R., Harris, A., Jezzard, P., 2015. Frequency and phase drift correction of magnetic resonance spectroscopy data by spectral registration in the time domain. *Magn. Reson. Med.* 73, 44–50. doi:10.1002/mrm.25094
- Near, J., Evans, C.J., Puts, N.A.J., Barker, P.B., Edden, R.A.E., 2013b. J-difference editing of gamma-aminobutyric acid (GABA): Simulated and experimental multiplet patterns. *Magn. Reson. Med.* 70, 1183–1191. doi:10.1002/mrm.24572
- Near, J., Leung, I., Claridge, T., Cowen, P., Jezzard, P., 2012. Chemical shifts and coupling constants of the GABA spin system, in: *Proc. Intl. Soc. Mag. Reson. Med.* p. 4386.
- Near, J., Simpson, R., Cowen, P., Jezzard, P., 2011. Efficient  $\gamma$ -aminobutyric acid

- editing at 3T without macromolecule contamination: MEGA-SPECIAL. *NMR Biomed.* 24, 1277–1285. doi:10.1002/nbm.1688
- Norenberg, M.D., Martinez-Hernandez, A., 1979. Fine structural localization of glutamine synthetase in astrocytes of rat brain. *Brain Res.* 161, 303–310. doi:10.1016/0006-8993(79)90071-4
- Northoff, G., Walter, M., Schulte, R.F., Beck, J., Dydak, U., Henning, A., Boeker, H., Grimm, S., Boesiger, P., 2007. GABA concentrations in the human anterior cingulate cortex predict negative BOLD responses in fMRI. *Nat. Neurosci.* 10, 1515–1517. doi:10.1038/nn2001
- Nutt, D.J., Malizia, A.L., 2001. New insights into the role of the GABAA-benzodiazepine receptor in psychiatric disorder. *Br. J. Psychiatry* 179, 390–396. doi:10.1192/bjp.179.5.390
- O’Gorman, R.L., Michels, L., Edden, R.A., Murdoch, J.B., Martin, E., 2011. In vivo detection of GABA and glutamate with MEGA-PRESS: Reproducibility and gender effects. *J. Magn. Reson. Imaging* 33, 1262–1267. doi:10.1002/jmri.22520
- Oeltzschner, G., Bhattacharyya, P.K., 2015. Editing efficiency for macromolecule-suppressed and unsuppressed J-edited GABA spectroscopy, in: *Proc. Intl. Soc. Mag. Reson. Med.* p. 1957.
- Ohzawa, I., Sclar, G., Freeman, R.D., 1985. Contrast gain control in the cat’s visual system. *J. Neurophysiol.* 54, 651–667.
- Olman, C.A., Ugurbil, K., Schrater, P., Kersten, D., 2004. BOLD fMRI and psychophysical measurements of contrast response to broadband images. *Vision Res.* 44, 669–683. doi:10.1016/j.visres.2003.10.022
- Olsen, R.W., 2002. GABA, in: *Neuropsychopharmacology: The Fifth Generation of Progress.* Lippincott, Williams, & Wilkins, pp. 159–168.
- Olsen, R.W., 1982. Drug Interactions at the GABA Receptor-Ionophore Complex. *Annu. Rev. Pharmacol. Toxicol.* 22, 245–277. doi:10.1146/annurev.pa.22.040182.001333
- Öngür, D., Prescott, A.P., McCarthy, J., Cohen, B.M., Renshaw, P.F., 2010. Elevated gamma-aminobutyric acid levels in chronic schizophrenia. *Biol. Psychiatry* 68, 667–670. doi:10.1016/j.biopsych.2010.05.016
- Öz, G., Terpstra, M., Tkáč, I., Aia, P., Lowary, J., Tuite, P.J., Gruetter, R., 2006. Proton MRS of the unilateral substantia nigra in the human brain at 4 Tesla: Detection of high GABA concentrations. *Magn. Reson. Med.* 55, 296–301. doi:10.1002/mrm.20761
- Palomero-Gallagher, N., Vogt, B.A., Schleicher, A., Mayberg, H.S., Zilles, K., 2009. Receptor architecture of human cingulate cortex: Evaluation of the four-region neurobiological model. *Hum. Brain Mapp.* 30, 2336–2355. doi:10.1002/hbm.20667
- Patel, A.B., de Graaf, R.A., Martin, D.L., Battaglioli, G., Behar, K.L., 2006. Evidence that GAD65 mediates increased GABA synthesis during intense neuronal activity in vivo. *J. Neurochem.* 97, 385–396. doi:10.1111/j.1471-4159.2006.03741.x
- Patel, A.B., de Graaf, R.A., Mason, G.F., Rothman, D.L., Shulman, R.G., Behar, K.L., 2005. The contribution of GABA to glutamate/glutamine cycling and energy metabolism in the rat cortex in vivo. *Proc. Natl. Acad. Sci. U. S. A.* 102, 5588–5593. doi:10.1073/pnas.0501703102
- Patel, A.B., de Graaf, R.A., Rothman, D.L., Behar, K.L., 2015. Effects of  $\gamma$ -Aminobutyric acid transporter 1 inhibition by tiagabine on brain glutamate and

- $\gamma$ -Aminobutyric acid metabolism in the anesthetized rat In vivo. *J. Neurosci. Res.* 93, 1101–1108. doi:10.1002/jnr.23548
- Pelli, D.G., 1997. The VideoToolbox software for visual psychophysics: transforming numbers into movies. *Spat. Vis.* 10, 437–442. doi:10.1163/156856897X00366
- Pennington, D.L., Abé, C., Batki, S.L., Johannes Meyerhoff, D., 2014. A preliminary examination of cortical neurotransmitter levels associated with heavy drinking in posttraumatic stress disorder. *Psychiatry Res. Neuroimaging* 224, 281–287. doi:10.1016/j.psychresns.2014.09.004
- Pérez-González, D., Hernández, O., Covey, E., Malmierca, M.S., 2012. GABAA-Mediated Inhibition Modulates Stimulus-Specific Adaptation in the Inferior Colliculus. *PLoS One* 7, e34297. doi:10.1371/journal.pone.0034297
- Perrine, S.A., Ghoddoussi, F., Michaels, M.S., Sheikh, I.S., McKelvey, G., Galloway, M.P., 2014. Ketamine reverses stress-induced depression-like behavior and increased GABA levels in the anterior cingulate: An 11.7T 1H-MRS study in rats. *Prog. Neuro-Psychopharmacology Biol. Psychiatry* 51, 9–15. doi:10.1016/j.pnpbp.2013.11.003
- Perthen, J.E., Lansing, A.E., Liao, J., Liu, T.T., Buxton, R.B., 2008. Caffeine-induced uncoupling of cerebral blood flow and oxygen metabolism: a calibrated BOLD fMRI study. *Neuroimage* 40, 237–47. doi:10.1016/j.neuroimage.2007.10.049
- Petroff, O.A.C., Hyder, F., Collins, T., Mattson, R.H., Rothman, D.L., 1999. Acute Effects of Vigabatrin on Brain GABA and Homocarnosine in Patients with Complex Partial Seizures. *Epilepsia* 40, 958–964. doi:10.1111/j.1528-1157.1999.tb00803.x
- Petroff, O.A.C., Hyder, F., Rothman, D.L., Mattson, R.H., 2001a. Homocarnosine and seizure control in juvenile myoclonic epilepsy and complex partial seizures. *Neurology* 56, 709–715. doi:10.1212/WNL.56.6.709
- Petroff, O.A.C., Hyder, F., Rothman, D.L., Mattson, R.H., 2001b. Topiramate Rapidly Raises Brain GABA in Epilepsy Patients. *Epilepsia* 42, 543–548. doi:10.1046/j.1528-1157.2001.18800.x
- Petroff, O.A.C., Hyder, F., Rothman, D.L., Mattson, R.H., 2000. Effects of Gabapentin on Brain GABA, Homocarnosine, and Pyrrolidinone in Epilepsy Patients. *Epilepsia* 41, 675–680. doi:10.1111/j.1528-1157.2000.tb00227.x
- Petroff, O.A.C., Mattson, R.H., Behar, K.L., Hyder, F., Rothman, D.L., 1998. Vigabatrin increases human brain homocarnosine and improves seizure control. *Ann. Neurol.* 44, 948–952. doi:10.1002/ana.410440614
- Petroff, O.A.C., Ogino, T., Alger, J.R., 1988. High-resolution proton magnetic resonance spectroscopy of rabbit brain: Regional metabolite levels and postmortem changes. *J. Neurochem.* 51, 163–171. doi:10.1111/j.1471-4159.1988.tb04850.x
- Petroff, O.A.C., Rothman, D.L., Behar, K.L., Collins, T.L., Mattson, R.H., 1996a. Human brain GABA levels rise rapidly after initiation of vigabatrin therapy. *Neurology* 47, 1567–1571. doi:10.1212/WNL.47.6.1567
- Petroff, O.A.C., Rothman, D.L., Behar, K.L., Lamoureux, D., Mattson, R.H., 1996b. The effect of gabapentin on brain gamma-aminobutyric acid in patients with epilepsy. *Ann. Neurol.* 39, 95–99. doi:10.1002/ana.410390114
- Petroff, O.A.C., Rothman, D.L., Behar, K.L., Mattson, R.H., 1996c. Low brain GABA level is associated with poor seizure control. *Ann. Neurol.* 40, 908–911. doi:10.1002/ana.410400613

- Petroff, O.A.C., Rothman, D.L., Behar, K.L., Mattson, R.H., 1996d. Human brain GABA levels rise after initiation of vigabatrin therapy but fail to rise further with increasing dose. *Neurology* 46, 1459–1459. doi:10.1212/WNL.46.5.1459
- Petroff, O.A.C., Yu, R.K., Ogino, T., 2006. High-resolution proton magnetic resonance analysis of human cerebrospinal fluid. *J. Neurochem.* 47, 1270–1276. doi:10.1111/j.1471-4159.1986.tb00750.x
- Piechnik, S.K., Evans, J., Bary, L.H., Wise, R.G., Jezzard, P., 2009. Functional changes in CSF volume estimated using measurement of water T2 relaxation. *Magn. Reson. Med.* 61, 579–586. doi:10.1002/mrm.21897
- Pizzarelli, R., Cherubini, E., 2011. Alterations of GABAergic signaling in autism spectrum disorders. *Neural Plast.* 2011. doi:10.1155/2011/297153
- Pollack, M.H., Jensen, J.E., Simon, N.M., Kaufman, R.E., Renshaw, P.F., 2008. High-field MRS study of GABA, glutamate and glutamine in social anxiety disorder: Response to treatment with levetiracetam. *Prog. Neuro-Psychopharmacology Biol. Psychiatry* 32, 739–743. doi:10.1016/j.pnpbp.2007.11.023
- Preuss, N., van der Veen, J.W., Carlson, P.J., Shen, J., Hasler, G., 2013. Low single dose gabapentin does not affect prefrontal and occipital gamma-aminobutyric acid concentrations. *Eur. Neuropsychopharmacol.* 23, 1708–1713. doi:10.1016/j.euroneuro.2013.08.006
- Price, R.B., Shungu, D.C., Mao, X., Nestadt, P., Kelly, C., Collins, K.A., Murrugh, J.W., Charney, D.S., Mathew, S.J., 2009. Amino Acid Neurotransmitters Assessed by Proton Magnetic Resonance Spectroscopy: Relationship to Treatment Resistance in Major Depressive Disorder. *Biol. Psychiatry* 65, 792–800. doi:10.1016/j.biopsych.2008.10.025
- Proctor, W.G., Yu, F.C., 1950. The Dependence of a Nuclear Magnetic Resonance Frequency upon Chemical Compound. *Phys. Rev.* 77, 717–717. doi:10.1103/PhysRev.77.717
- Purcell, E.M., Torrey, H.C., Pound, R. V., 1946. Resonance Absorption by Nuclear Magnetic Moments in a Solid. *Phys. Rev.* 69, 37–38. doi:10.1103/PhysRev.69.37
- Puts, N.A.J., Edden, R.A.E., 2012. In vivo magnetic resonance spectroscopy of GABA: A methodological review. *Prog. Nucl. Magn. Reson. Spectrosc.* 60, 29–41. doi:10.1016/j.pnmrs.2011.06.001
- Puts, N.A.J., Edden, R.A.E., Evans, C.J., McGlone, F., McGonigle, D.J., 2011. Regionally Specific Human GABA Concentration Correlates with Tactile Discrimination Thresholds. *J. Neurosci.* 31, 16556–16560. doi:10.1523/JNEUROSCI.4489-11.2011
- Puts, N.A.J., Harris, A.D., Crocetti, D., Nettles, C., Singer, H.S., Tommerdahl, M., Edden, R.A.E., Mostofsky, S.H., 2015. Reduced GABAergic inhibition and abnormal sensory symptoms in children with Tourette syndrome. *J. Neurophysiol.* 114, 808–817. doi:10.1152/jn.00060.2015
- Quetscher, C., Yildiz, A., Dharmadhikari, S., Glaubitz, B., Schmidt-Wilcke, T., Dydak, U., Beste, C., 2014. Striatal GABA-MRS predicts response inhibition performance and its cortical electrophysiological correlates. *Brain Struct. Funct.* doi:10.1007/s00429-014-0873-y
- Rabi, I.I., 1937. Space Quantization in a Gyration Magnetic Field. *Phys. Rev.* 51, 652–654. doi:10.1103/PhysRev.51.652
- Rae, C., Nasrallah, F.A., Griffin, J.L., Balcar, V.J., 2009. Now I know my ABC. A systems neurochemistry and functional metabolomic approach to

- understanding the GABAergic system. *J. Neurochem.* 109, 109–116. doi:10.1111/j.1471-4159.2009.05803.x
- Rae, C.D., 2014. A Guide to the Metabolic Pathways and Function of Metabolites Observed in Human Brain 1H Magnetic Resonance Spectra. *Neurochem. Res.* 39, 1–36. doi:10.1007/s11064-013-1199-5
- Raichle, M.E., Mintun, M.A., 2006. Brain Work and Brain Imaging. *Annu. Rev. Neurosci.* 29, 449–476. doi:10.1146/annurev.neuro.29.051605.112819
- Ratney, H., Sdika, M., Coenradie, Y., Cavassila, S., van Ormondt, D., Graveron-Demilly, D., 2005. Time-domain semi-parametric estimation based on a metabolite basis set. *NMR Biomed.* 18, 1–13. doi:10.1002/nbm.895
- Rees, G., Howseman, A., Josephs, O., Frith, C.D., Friston, K.J., Frackowiak, R.S.J., Turner, R., 1997. Characterizing the Relationship between BOLD Contrast and Regional Cerebral Blood Flow Measurements by Varying the Stimulus Presentation Rate. *Neuroimage* 6, 270–278. doi:10.1006/nimg.1997.0300
- Ribeiro, M.J., Violante, I.R., Bernardino, I., Edden, R.A.E., Castelo-Branco, M., 2015. Abnormal relationship between GABA, neurophysiology and impulsive behavior in neurofibromatosis type 1. *Cortex* 64, 194–208. doi:10.1016/j.cortex.2014.10.019
- Richerson, G.B., Wu, Y., 2003. Dynamic Equilibrium of Neurotransmitter Transporters: Not Just for Reuptake Anymore. *J. Neurophysiol.* 90, 1363–1374. doi:10.1152/jn.00317.2003
- Riese, F., Gietl, A., Zölch, N., Henning, A., O’Gorman, R., Kälin, A.M., Leh, S.E., Buck, A., Warnock, G., Edden, R.A.E., Luechinger, R., Hock, C., Kollias, S., Michels, L., 2015. Posterior cingulate  $\gamma$ -aminobutyric acid and glutamate/glutamine are reduced in amnesic mild cognitive impairment and are unrelated to amyloid deposition and apolipoprotein E genotype. *Neurobiol. Aging* 36, 53–59. doi:10.1016/j.neurobiolaging.2014.07.030
- Roberts, E., Frankel, S., 1950.  $\gamma$ -Aminobutyric acid in brain: Its formation from glutamic acid. *J. Biol. Chem.* 187, 55–63.
- Robertson, C.E., Ratai, E., Kanwisher, N., 2016. Reduced GABAergic Action in the Autistic Brain. *Curr. Biol.* 26, 80–85. doi:10.1016/j.cub.2015.11.019
- Rodriguez, C.I., Kegeles, L.S., Levinson, A., Ogden, R.T., Mao, X., Milak, M.S., Vermes, D., Xie, S., Hunter, L., Flood, P., Moore, H., Shungu, D.C., Simpson, H.B., 2015. In vivo effects of ketamine on glutamate-glutamine and gamma-aminobutyric acid in obsessive-compulsive disorder: Proof of concept. *Psychiatry Res. Neuroimaging* 233, 141–147. doi:10.1016/j.psychres.2015.06.001
- Rojas, D.C., Singel, D., Steinmetz, S., Hepburn, S., Brown, M.S., 2014. Decreased left perisylvian GABA concentration in children with autism and unaffected siblings. *Neuroimage* 86, 28–34. doi:10.1016/j.neuroimage.2013.01.045
- Rossi, D.J., Hamann, M., 1998. Spillover-mediated transmission at inhibitory synapses promoted by high affinity  $\alpha 6$  subunit GABAA receptors and glomerular geometry. *Neuron* 20, 783–795. doi:10.1016/S0896-6273(00)81016-8
- Rosso, I.M., Weiner, M.R., Crowley, D.J., Silveri, M.M., Rauch, S.L., Jensen, J.E., 2014. Insula and anterior cingulate GABA levels in posttraumatic stress disorder: Preliminary findings using magnetic resonance spectroscopy. *Depress. Anxiety* 31, 115–123. doi:10.1002/da.22155
- Rothman, D.L., Petroff, O.A., Behar, K.L., Mattson, R.H., 1993. Localized 1H NMR measurements of gamma-aminobutyric acid in human brain in vivo. *Proc. Natl.*

- Acad. Sci. U. S. A. 90, 5662–5666.
- Rouder, J.N., Morey, R.D., 2012. Default Bayes Factors for Model Selection in Regression. *Multivariate Behav. Res.* 47, 877–903. doi:10.1080/00273171.2012.734737
- Rowland, L.M., Edden, R.A.E., Kontson, K., Zhu, H., Barker, P.B., Hong, L.E., 2013a. GABA Predicts Inhibition of Frequency-Specific Oscillations in Schizophrenia. *J. Neuropsychiatry Clin. Neurosci.* 25, 83–87. doi:10.1176/appi.neuropsych.11120368
- Rowland, L.M., Kontson, K., West, J., Edden, R. a, Zhu, H., Wijtenburg, S.A., Holcomb, H.H., Barker, P.B., 2013b. In Vivo Measurements of Glutamate, GABA, and NAAG in Schizophrenia. *Schizophr. Bull.* 39, 1096–1104. doi:10.1093/schbul/sbs092
- Rowland, L.M., Krause, B.W., Wijtenburg, S. a, McMahon, R.P., Chiappelli, J., Nugent, K.L., Nisonger, S.J., Korenic, S. a, Kochunov, P., Hong, L.E., 2016. Medial frontal GABA is lower in older schizophrenia: a MEGA-PRESS with macromolecule suppression study. *Mol. Psychiatry* 21, 198–204. doi:10.1038/mp.2015.34
- Rubenstein, J.L.R., Merzenich, M.M., 2003. Model of autism: increased ratio of excitation/inhibition in key neural systems. *Genes, Brain Behav.* 2, 255–267. doi:10.1034/j.1601-183X.2003.00037.x
- Saleh, M.G., Alhamud, A., Near, J., van der Kouwe, A.J.W., Meintjes, E.M., 2016. Volumetric navigated MEGA-SPECIAL for real-time motion and shim corrected GABA editing. *NMR Biomed.* 29, 248–255. doi:10.1002/nbm.3454
- Sampaio-Baptista, C., Filippini, N., Stagg, C.J., Near, J., Scholz, J., Johansen-Berg, H., 2015. Changes in functional connectivity and GABA levels with long-term motor learning. *Neuroimage* 106, 15–20. doi:10.1016/j.neuroimage.2014.11.032
- Sanacora, G., Fenton, L.R., Fasula, M.K., Rothman, D.L., Levin, Y., Krystal, J.H., Mason, G.F., 2006. Cortical  $\gamma$ -Aminobutyric Acid Concentrations in Depressed Patients Receiving Cognitive Behavioral Therapy. *Biol. Psychiatry* 59, 284–286. doi:10.1016/j.biopsych.2005.07.015
- Sanacora, G., Gueorguieva, R., Epperson, C.N., Wu, Y.-T., Appel, M., Rothman, D.L., Krystal, J.H., Mason, G.F., 2004. Subtype-Specific Alterations of  $\gamma$ -Aminobutyric Acid and Glutamate in Patients With Major Depression. *Arch. Gen. Psychiatry* 61, 705. doi:10.1001/archpsyc.61.7.705
- Sanacora, G., Mason, G.F., Rothman, D.L., Behar, K.L., Hyder, F., Petroff, O.A.C., Berman, R.M., Charney, D.S., Krystal, J.H., 1999. Reduced Cortical  $\gamma$ -Aminobutyric Acid Levels in Depressed Patients Determined by Proton Magnetic Resonance Spectroscopy. *Arch. Gen. Psychiatry* 56, 1043. doi:10.1001/archpsyc.56.11.1043
- Sanacora, G., Mason, G.F., Rothman, D.L., Hyder, F., Ciarcia, J.J., Ostroff, R.B., Berman, R.M., Krystal, J.H., 2003. Increased Cortical GABA Concentrations in Depressed Patients Receiving ECT. *Am. J. Psychiatry* 160, 577–579. doi:10.1176/appi.ajp.160.3.577
- Sanacora, G., Mason, G.F., Rothman, D.L., Krystal, J.H., 2002. Increased Occipital Cortex GABA Concentrations in Depressed Patients After Therapy With Selective Serotonin Reuptake Inhibitors. *Am. J. Psychiatry* 159, 663–665. doi:10.1176/appi.ajp.159.4.663
- Sandberg, K., Blicher, J.U., Dong, M.Y., Rees, G., Near, J., Kanai, R., 2014. Occipital GABA correlates with cognitive failures in daily life. *Neuroimage* 87,

- 55–60. doi:10.1016/j.neuroimage.2013.10.059
- Schirmer, T., Auer, D.P., 2000. On the reliability of quantitative clinical magnetic resonance spectroscopy of the human brain. *NMR Biomed.* 13, 28–36. doi:10.1002/(SICI)1099-1492(200002)13:1<28::AID-NBM606>3.0.CO;2-L
- Sedley, W., Parikh, J., Edden, R.A.E., Tait, V., Blamire, A., Griffiths, T.D., 2015. Human Auditory Cortex Neurochemistry Reflects the Presence and Severity of Tinnitus. *J. Neurosci.* 35, 14822–14828. doi:10.1523/JNEUROSCI.2695-15.2015
- Semyanov, A. V., 2002. GABA-ergic Inhibition in the CNS: Types of GABA Receptors and Mechanisms of Tonic GABA-Mediated Inhibitory Action. *Neurophysiology* 34, 71–80. doi:10.1023/A:1020274226515
- Semyanov, A., Walker, M.C., Kullmann, D.M., Silver, R.A., 2004. Tonically active GABAA receptors: modulating gain and maintaining the tone. *Trends Neurosci.* 27, 262–269. doi:10.1016/j.tins.2004.03.005
- Shaw, A., Brealy, J., Richardson, H., Muthukumaraswamy, S.D., Edden, R.A., John Evans, C., Puts, N.A.J., Singh, K.D., Keedwell, P.A., 2013. Marked Reductions in Visual Evoked Responses But Not  $\gamma$ -Aminobutyric Acid Concentrations or  $\gamma$ -Band Measures in Remitted Depression. *Biol. Psychiatry* 73, 691–698. doi:10.1016/j.biopsych.2012.09.032
- Silveri, M.M., Sneider, J.T., Crowley, D.J., Covell, M.J., Acharya, D., Rosso, I.M., Jensen, J.E., 2013. Frontal Lobe  $\gamma$ -Aminobutyric Acid Levels During Adolescence: Associations with Impulsivity and Response Inhibition. *Biol. Psychiatry* 74, 296–304. doi:10.1016/j.biopsych.2013.01.033
- Simister, R.J., McLean, M.A., Barker, G.J., Duncan, J.S., 2009. Proton MR spectroscopy of metabolite concentrations in temporal lobe epilepsy and effect of temporal lobe resection. *Epilepsy Res.* 83, 168–176. doi:10.1016/j.epilepsyres.2008.11.006
- Simister, R.J., McLean, M.A., Barker, G.J., Duncan, J.S., 2007. Proton magnetic resonance spectroscopy of malformations of cortical development causing epilepsy. *Epilepsy Res.* 74, 107–115. doi:10.1016/j.epilepsyres.2007.02.002
- Simister, R.J., McLean, M.A., Barker, G.J., Duncan, J.S., 2003a. Proton MRS reveals frontal lobe metabolite abnormalities in idiopathic generalized epilepsy. *Neurology* 61, 897–902. doi:10.1212/01.WNL.0000086903.69738.DC
- Simister, R.J., McLean, M.A., Barker, G.J., Duncan, J.S., 2003b. A Proton Magnetic Resonance Spectroscopy Study of Metabolites in the Occipital Lobes in Epilepsy. *Epilepsia* 44, 550–558. doi:10.1046/j.1528-1157.2003.19102.x
- Simpson, H.B., Shungu, D.C., Bender, J., Mao, X., Xu, X., Slifstein, M., Kegeles, L.S., 2012. Investigation of Cortical Glutamate–Glutamine and  $\gamma$ -Aminobutyric Acid in Obsessive–Compulsive Disorder by Proton Magnetic Resonance Spectroscopy. *Neuropsychopharmacology* 37, 2684–2692. doi:10.1038/npp.2012.132
- Simpson, R., Devenyi, G.A., Jezzard, P., Hennessy, T.J., Near, J., 2015. Advanced processing and simulation of MRS data using the FID appliance (FID-A)—An open source, MATLAB-based toolkit. *Magn. Reson. Med.* 00, n/a–n/a. doi:10.1002/mrm.26091
- Singer, W., 1996. Neurophysiology: The changing face of inhibition. *Curr. Biol.* 6, 395–397. doi:10.1016/S0960-9822(02)00505-5
- Singh, K.D., 2012. Which “neural activity” do you mean? fMRI, MEG, oscillations and neurotransmitters. *Neuroimage* 62, 1121–1130. doi:10.1016/j.neuroimage.2012.01.028

- Singh, K.D., Smith, A.T., Greenlee, M.W., 2000. Spatiotemporal Frequency and Direction Sensitivities of Human Visual Areas Measured Using fMRI. *Neuroimage* 12, 550–564. doi:10.1006/nimg.2000.0642
- Sivilotti, L., Nistri, A., 1991. GABA receptor mechanisms in the central nervous system. *Prog. Neurobiol.* 36, 35–92. doi:10.1016/0301-0082(91)90036-Z
- Slotboom, J., Boesch, C., Kreis, R., 1998. Versatile frequency domain fitting using time domain models and prior knowledge. *Magn. Reson. Med.* 39, 899–911. doi:10.1002/mrm.1910390607
- Śmigielka-Kuzia, J., Boćkowski, L., Sobaniec, W., Kułak, W., Sendrowski, K., 2010. Amino acid metabolic processes in the temporal lobes assessed by proton magnetic resonance spectroscopy (1H MRS) in children with Down syndrome. *Pharmacol. Reports* 62, 1070–1077. doi:10.1016/S1734-1140(10)70369-8
- Smith, S.A., Levante, T.O., Meier, B.H., Ernst, R.R., 1994. Computer Simulations in Magnetic Resonance. An Object-Oriented Programming Approach. *J. Magn. Reson. Ser. A* 106, 75–105. doi:10.1006/jmra.1994.1008
- Smith, S.M., 2002. Fast robust automated brain extraction. *Hum. Brain Mapp.* 17, 143–155. doi:10.1002/hbm.10062
- Snyder, J., Hanstock, C.C., Wilman, A.H., 2009. Spectral editing of weakly coupled spins using variable flip angles in PRESS constant echo time difference spectroscopy: Application to GABA. *J. Magn. Reson.* 200, 245–250. doi:10.1016/j.jmr.2009.07.010
- Soeiro-de-Souza, M.G., Henning, A., Machado-Vieira, R., Moreno, R.A., Pastorello, B.F., da Costa Leite, C., Vallada, H., Otaduy, M.C.G., 2015. Anterior cingulate Glutamate–Glutamine cycle metabolites are altered in euthymic bipolar I disorder. *Eur. Neuropsychopharmacol.* 25, 2221–2229. doi:10.1016/j.euroneuro.2015.09.020
- Soghomonian, J.-J., Martin, D.L., 1998. Two isoforms of glutamate decarboxylase: why? *Trends Pharmacol. Sci.* 19, 500–505. doi:10.1016/S0165-6147(98)01270-X
- Somogyi, P., Klausberger, T., 2005. Defined types of cortical interneurone structure space and spike timing in the hippocampus. *J. Physiol.* 562, 9–26. doi:10.1113/jphysiol.2004.078915
- Sørensen, O.W., Eich, G.W., Levitt, M.H., Bodenhausen, G., Ernst, R.R., 1984. Product operator formalism for the description of NMR pulse experiments. *Prog. Nucl. Magn. Reson. Spectrosc.* 16, 163–192. doi:10.1016/0079-6565(84)80005-9
- Sotero, R.C., Trujillo-Barreto, N.J., 2007. Modelling the role of excitatory and inhibitory neuronal activity in the generation of the BOLD signal. *Neuroimage* 35, 149–165. doi:10.1016/j.neuroimage.2006.10.027
- Stagg, C.J., 2014. Magnetic Resonance Spectroscopy as a tool to study the role of GABA in motor-cortical plasticity. *Neuroimage* 86, 19–27. doi:10.1016/j.neuroimage.2013.01.009
- Stagg, C.J., Bachtiar, V., Johansen-Berg, H., 2011a. The Role of GABA in Human Motor Learning. *Curr. Biol.* 21, 480–484. doi:10.1016/j.cub.2011.01.069
- Stagg, C.J., Bachtiar, V., Johansen-Berg, H., 2011b. What are we measuring with GABA magnetic resonance spectroscopy? *Commun. Integr. Biol.* 4, 573–5. doi:10.4161/cib.4.5.16213
- Stan, A.D., Ghose, S., Zhao, C., Hulse, K., Mihalakos, P., Yanagi, M., Morris, S.U., Bartko, J.J., Choi, C., Tamminga, C. a, 2015. Magnetic resonance spectroscopy and tissue protein concentrations together suggest lower glutamate signaling in

- dentate gyrus in schizophrenia. *Mol. Psychiatry* 20, 433–439. doi:10.1038/mp.2014.54
- Stan, A.D., Schirda, C. V, Bertocci, M.A., Bebko, G.M., Kronhaus, D.M., Aslam, H.A., LaBarbara, E.J., Tanase, C., Lockovich, J.C., Pollock, M.H., Stiffler, R.S., Phillips, M.L., 2014. Glutamate and GABA contributions to medial prefrontal cortical activity to emotion: Implications for mood disorders. *Psychiatry Res. Neuroimaging* 223, 253–260. doi:10.1016/j.psychres.2014.05.016
- Stanisz, G.J., Odobina, E.E., Pun, J., Escaravage, M., Graham, S.J., Bronskill, M.J., Henkelman, R.M., 2005. T1, T2 relaxation and magnetization transfer in tissue at 3T. *Magn. Reson. Med.* 54, 507–512. doi:10.1002/mrm.20605
- Star-Lack, J., Adalsteinsson, E., Gold, G.E., Ikeda, D.M., Spielman, D.M., 2000. Motion correction and lipid suppression for 1H magnetic resonance spectroscopy. *Magn. Reson. Med.* 43, 325–330. doi:10.1002/(SICI)1522-2594(200003)43:3<325::AID-MRM1>3.0.CO;2-8
- Stein, V., Nicoll, R.A., 2003. GABA Generates Excitement. *Neuron* 37, 375–378. doi:10.1016/S0896-6273(03)00056-4
- Stokes, P.R.A., Myers, J.F., Kalk, N.J., Watson, B.J., Erritzoe, D., Wilson, S.J., Cunningham, V.J., Barros, D.R., Hammers, A., Turkheimer, F.E., Nutt, D.J., Lingford-Hughes, A.R., 2014. Acute increases in synaptic GABA detectable in the living human brain: A [<sup>11</sup>C]Ro15-4513 PET study. *Neuroimage* 99, 158–165. doi:10.1016/j.neuroimage.2014.05.035
- Stone, J.M., Dietrich, C., Edden, R., Mehta, M.A., De Simoni, S., Reed, L.J., Krystal, J.H., Nutt, D., Barker, G.J., 2012. Ketamine effects on brain GABA and glutamate levels with 1H-MRS: relationship to ketamine-induced psychopathology. *Mol. Psychiatry* 17, 664–665. doi:10.1038/mp.2011.171
- Streeter, C.C., Whitfield, T.H., Owen, L., Rein, T., Karri, S.K., Yakhkind, A., Perlmutter, R., Prescott, A., Renshaw, P.F., Ciraulo, D. a, Jensen, J.E., 2010. Effects of Yoga Versus Walking on Mood, Anxiety, and Brain GABA Levels: A Randomized Controlled MRS Study. *J. Altern. Complement. Med.* 16, 1145–1152. doi:10.1089/acm.2010.0007
- Sumner, P., Edden, R.A.E., Bompas, A., Evans, C.J., Singh, K.D., 2010. More GABA, less distraction: a neurochemical predictor of motor decision speed. *Nat. Neurosci.* 13, 825–827. doi:10.1038/nn.2559
- Swettenham, J.B., Muthukumaraswamy, S.D., Singh, K.D., 2013. BOLD Responses in Human Primary Visual Cortex are Insensitive to Substantial Changes in Neural Activity. *Front. Hum. Neurosci.* 7. doi:10.3389/fnhum.2013.00076
- Sytinsky, I.A., Soldatenkov, A.T., Lajtha, A., 1978. Neurochemical basis of the therapeutic effect of  $\gamma$ -aminobutyric acid and its derivatives. *Prog. Neurobiol.* 10, 89–133. doi:10.1016/0301-0082(78)90009-6
- Sytinsky, I.A., Thinh, N.T., 1964. The distribution of  $\gamma$ -aminobutyric acid in the monkey brain during picrotoxin-induced seizures. *J. Neurochem.* 11, 551–556. doi:10.1111/j.1471-4159.1964.tb07506.x
- Tayoshi, S., Nakataki, M., Sumitani, S., Taniguchi, K., Shibuya-Tayoshi, S., Numata, S., Iga, J.I., Ueno, S.I., Harada, M., Ohmori, T., 2010. GABA concentration in schizophrenia patients and the effects of antipsychotic medication: A proton magnetic resonance spectroscopy study. *Schizophr. Res.* 117, 83–91. doi:10.1016/j.schres.2009.11.011
- Telgkamp, P., Padgett, D.E., Ledoux, V.A., Woolley, C.S., Raman, I.M., 2004. Maintenance of High-Frequency Transmission at Purkinje to Cerebellar

- Nuclear Synapses by Spillover from Boutons with Multiple Release Sites. *Neuron* 41, 113–126. doi:10.1016/S0896-6273(03)00802-X
- Tepper, J.M., Koós, T., Wilson, C.J., 2004. GABAergic microcircuits in the neostriatum. *Trends Neurosci.* 27, 662–669. doi:10.1016/j.tins.2004.08.007
- Tepper, J.M., Wilson, C.J., Koós, T., 2008. Feedforward and feedback inhibition in neostriatal GABAergic spiny neurons. *Brain Res. Rev.* 58, 272–281. doi:10.1016/j.brainresrev.2007.10.008
- Terhune, D.B., Russo, S., Near, J., Stagg, C.J., Cohen Kadosh, R., 2014. GABA Predicts Time Perception. *J. Neurosci.* 34, 4364–4370. doi:10.1523/JNEUROSCI.3972-13.2014
- Terpstra, M., Ugurbil, K., Gruetter, R., 2002. Direct in vivo measurement of human cerebral GABA concentration using MEGA-editing at 7 Tesla. *Magn. Reson. Med.* 47, 1009–1012. doi:10.1002/mrm.10146
- Thiel, T., Czisch, M., Elbel, G.K., Hennig, J., 2002. Phase coherent averaging in magnetic resonance spectroscopy using interleaved navigator scans: Compensation of motion artifacts and magnetic field instabilities. *Magn. Reson. Med.* 47, 1077–1082. doi:10.1002/mrm.10174
- Tillakaratne, N.J.K., Medina-Kauwe, L., Gibson, K.M., 1995. Gamma-aminobutyric acid (GABA) metabolism in mammalian neural and nonneural tissues. *Comp. Biochem. Physiol. Part A Physiol.* 112, 247–263. doi:10.1016/0300-9629(95)00099-2
- Tinaz, S., Belluscio, B. a, Malone, P., van der Veen, J.W., Hallett, M., Horowitz, S.G., 2014. Role of the sensorimotor cortex in Tourette syndrome using multimodal imaging. *Hum. Brain Mapp.* 35, 5834–5846. doi:10.1002/hbm.22588
- Tkáč, I., Starčuk, Z., Choi, I.-Y., Gruetter, R., 1999. In vivo <sup>1</sup>H NMR spectroscopy of rat brain at 1 ms echo time. *Magn. Reson. Med.* 41, 649–656. doi:10.1002/(SICI)1522-2594(199904)41:4<649::AID-MRM2>3.0.CO;2-G
- Tootell, R.B., Reppas, J.B., Kwong, K.K., Malach, R., Born, R.T., Brady, T.J., Rosen, B.R., Belliveau, J.W., 1995. Functional analysis of human MT and related visual cortical areas using magnetic resonance imaging. *J. Neurosci.* 15, 3215–3230.
- Träber, F., Block, W., Lamerichs, R., Gieseke, J., Schild, H.H., 2004. <sup>1</sup>H metabolite relaxation times at 3.0 Tesla: Measurements of T1 and T2 values in normal brain and determination of regional differences in transverse relaxation. *J. Magn. Reson. Imaging* 19, 537–545. doi:10.1002/jmri.20053
- Traub, R.D., Cunningham, M.O., Gloveli, T., LeBeau, F.E.N., Bibbig, A., Buhl, E.H., Whittington, M. a, 2003. GABA-enhanced collective behavior in neuronal axons underlies persistent gamma-frequency oscillations. *Proc. Natl. Acad. Sci. U. S. A.* 100, 11047–52. doi:10.1073/pnas.1934854100
- Tsang, O., Gholipour, A., Kehtarnavaz, N., Gopinath, K., Briggs, R., Panahi, I., 2008. Comparison of tissue segmentation algorithms in neuroimage analysis software tools, in: 2008 30th Annual International Conference of the IEEE Engineering in Medicine and Biology Society. IEEE, pp. 3924–3928. doi:10.1109/IEMBS.2008.4650068
- Valentine, G.W., Mason, G.F., Gomez, R., Fasula, M., Watzl, J., Pittman, B., Krystal, J.H., Sanacora, G., 2011. The antidepressant effect of ketamine is not associated with changes in occipital amino acid neurotransmitter content as measured by [<sup>1</sup>H]-MRS. *Psychiatry Res. Neuroimaging* 191, 122–127. doi:10.1016/j.psychresns.2010.10.009

- van Loon, A.M., Knapen, T., Scholte, H.S., St. John-Saaltink, E., Donner, T.H., Lamme, V.A.F., 2013. GABA Shapes the Dynamics of Bistable Perception. *Curr. Biol.* 23, 823–827. doi:10.1016/j.cub.2013.03.067
- Vanhamme, L., van den Boogaart, A., Van Huffel, S., 1997. Improved Method for Accurate and Efficient Quantification of MRS Data with Use of Prior Knowledge. *J. Magn. Reson.* 129, 35–43. doi:10.1006/jmre.1997.1244
- Veen, J.W. van der, Shen, J., 2013. Regional difference in GABA levels between medial prefrontal and occipital cortices. *J. Magn. Reson. Imaging* 38, 745–750. doi:10.1002/jmri.24009
- Verhoeff, N.P.L.G., Petroff, O.A.C., Hyder, F., Zoghbi, S.S., Fujita, M., Rajeevan, N., Rothman, D.L., Seibyl, J.P., Mattson, R.H., Innis, R.B., 1999. Effects of Vigabatrin on the GABAergic System as Determined by [123I]Iomazenil SPECT and GABA MRS. *Epilepsia* 40, 1433–1438. doi:10.1111/j.1528-1157.1999.tb02016.x
- Vida, I., Bartos, M., Jonas, P., 2006. Shunting Inhibition Improves Robustness of Gamma Oscillations in Hippocampal Interneuron Networks by Homogenizing Firing Rates. *Neuron* 49, 107–117. doi:10.1016/j.neuron.2005.11.036
- Violante, I.R., Ribeiro, M.J., Edden, R.A.E., Guimarães, P., Bernardino, I., Rebola, J., Cunha, G., Silva, E., Castelo-Branco, M., 2013. GABA deficit in the visual cortex of patients with neurofibromatosis type 1: Genotype-phenotype correlations and functional impact. *Brain* 136, 918–925. doi:10.1093/brain/aws368
- Viswanathan, A., Freeman, R.D., 2007. Neurometabolic coupling in cerebral cortex reflects synaptic more than spiking activity. *Nat. Neurosci.* 10, 1308–1312. doi:10.1038/nn1977
- Vul, E., Harris, C., Winkielman, P., Pashler, H., 2009. Puzzlingly High Correlations in fMRI Studies of Emotion, Personality, and Social Cognition. *Perspect. Psychol. Sci.* 4, 274–290. doi:10.1111/j.1745-6924.2009.01125.x
- Waddell, K.W., Avison, M.J., Joers, J.M., Gore, J.C., 2007. A practical guide to robust detection of GABA in human brain by J-difference spectroscopy at 3 T using a standard volume coil. *Magn. Reson. Imaging* 25, 1032–1038. doi:10.1016/j.mri.2006.11.026
- Waddell, K.W., Zanjani, P., Pradhan, S., Xu, L., Welch, E.B., Joers, J.M., Martin, P.R., Avison, M.J., Gore, J.C., 2011. Anterior cingulate and cerebellar GABA and Glu correlations measured by <sup>1</sup>H J-difference spectroscopy. *Magn. Reson. Imaging* 29, 19–24. doi:10.1016/j.mri.2010.07.005
- Wall, M.J., Usowicz, M.M., 1997. Development of action potential-dependent and independent spontaneous GABA(A) receptor-mediated currents in granule cells of postnatal rat cerebellum. *Eur. J. Neurosci.* 9, 533–548. doi:10.1111/j.1460-9568.1997.tb01630.x
- Wang, P.W., Sailasuta, N., Chandler, R.A., Ketter, T.A., 2006. Magnetic resonance spectroscopic measurement of cerebral gamma-aminobutyric acid concentrations in patients with bipolar disorders. *Acta Neuropsychiatr.* 18, 120–126. doi:10.1111/j.1601-5215.2006.00132.x
- Wang, Q., Zhang, Z., Dong, F., Chen, L., Zheng, L., Guo, X., Li, J., 2014. Anterior Insula GABA Levels Correlate with Emotional Aspects of Empathy: A Proton Magnetic Resonance Spectroscopy Study. *PLoS One* 9, e113845. doi:10.1371/journal.pone.0113845
- Wang, Y., Li, S.J., 1998. Differentiation of metabolic concentrations between gray matter and white matter of human brain by in vivo <sup>1</sup>H magnetic resonance

- spectroscopy. *Magn. Reson. Med.* 39, 28–33. doi:10.1002/mrm.1910390107
- Wansapura, J.P., Holland, S.K., Dunn, R.S., Ball, W.S., 1999. NMR relaxation times in the human brain at 3.0 Tesla. *J. Magn. Reson. Imaging* 9, 531–538. doi:10.1002/(SICI)1522-2586(199904)9:4<531::AID-JMRI4>3.0.CO;2-L
- Waschkies, C.F., Bruns, A., Müller, S., Kapps, M., Borroni, E., von Kienlin, M., Rudin, M., Künnecke, B., 2014. Neuropharmacological and Neurobiological Relevance of In vivo <sup>1</sup>H-MRS of GABA and Glutamate for Preclinical Drug Discovery in Mental Disorders. *Neuropsychopharmacology* 39, 2331–2339. doi:10.1038/npp.2014.79
- Weber, O.M., Verhagen, A., Duc, C.O., Meier, D., Leenders, K.L., Boesiger, P., 1999. Effects of vigabatrin intake on brain GABA activity as monitored by spectrally edited magnetic resonance spectroscopy and positron emission tomography. *Magn. Reson. Imaging* 17, 417–425. doi:10.1016/S0730-725X(98)00184-2
- Wiebking, C., Duncan, N.W., Tiret, B., Hayes, D.J., Marjańska, M., Doyon, J., Bajbouj, M., Northoff, G., 2014. GABA in the insula - a predictor of the neural response to interoceptive awareness. *Neuroimage*. doi:10.1016/j.neuroimage.2013.04.042
- Wijtenburg, S.A., Rowland, L.M., Edden, R.A.E., Barker, P.B., 2013. Reproducibility of brain spectroscopy at 7T using conventional localization and spectral editing techniques. *J. Magn. Reson. Imaging* 38, 460–467. doi:10.1002/jmri.23997
- Wijtenburg, S.A., Yang, S., Fischer, B.A., Rowland, L.M., 2015. In vivo assessment of neurotransmitters and modulators with magnetic resonance spectroscopy: Application to schizophrenia. *Neurosci. Biobehav. Rev.* 51, 276–295. doi:10.1016/j.neubiorev.2015.01.007
- Winkelman, J.W., Buxton, O.M., Jensen, J.E., Benson, K.L., O'Connor, S.P., Wang, W., Renshaw, P.F., 2008. Reduced brain GABA in primary insomnia: preliminary data from 4T proton magnetic resonance spectroscopy (1H-MRS). *Sleep* 31, 1499–506.
- Wise, R.G., Harris, A.D., Stone, A.J., Murphy, K., 2013. Measurement of OEF and absolute CMRO<sub>2</sub>: MRI-based methods using interleaved and combined hypercapnia and hyperoxia. *Neuroimage* 83, 135–147. doi:10.1016/j.neuroimage.2013.06.008
- Wong, E.C., Buxton, R.B., Frank, L.R., 1998. Quantitative imaging of perfusion using a single subtraction (QUIPSS and QUIPSS II). *Magn. Reson. Med.* 39, 702–708. doi:10.1002/mrm.1910390506
- Wu, H., Jin, Y., Buddhala, C., Osterhaus, G., Cohen, E., Jin, H., Wei, J., Davis, K., Obata, K., Wu, J.-Y., 2007. Role of glutamate decarboxylase (GAD) isoform, GAD65, in GABA synthesis and transport into synaptic vesicles—Evidence from GAD65-knockout mice studies. *Brain Res.* 1154, 80–83. doi:10.1016/j.brainres.2007.04.008
- Wu, Y., Wang, W., Díez-Sampedro, A., Richerson, G.B., 2007. Nonvesicular Inhibitory Neurotransmission via Reversal of the GABA Transporter GAT-1. *Neuron* 56, 851–865. doi:10.1016/j.neuron.2007.10.021
- Wu, Y., Wang, W., Richerson, G.B., 2003. Vigabatrin induces tonic inhibition via GABA transporter reversal without increasing vesicular GABA release. *J. Neurophysiol.* 89, 2021–34. doi:10.1152/jn.00856.2002
- Yamamoto, T., Isobe, T., Akutsu, H., Masumoto, T., Ando, H., Sato, E., Takada, K., Anno, I., Matsumura, A., 2015. Influence of echo time in quantitative proton

- MR spectroscopy using LCModel. *Magn. Reson. Imaging* 33, 644–648. doi:10.1016/j.mri.2015.01.015
- Yoon, J.H., Maddock, R.J., Rokem, A., Silver, M. a, Minzenberg, M.J., Ragland, J.D., Carter, C.S., 2010. GABA Concentration Is Reduced in Visual Cortex in Schizophrenia and Correlates with Orientation-Specific Surround Suppression. *J. Neurosci.* 30, 3777–3781. doi:10.1523/JNEUROSCI.6158-09.2010
- Zaitsev, M., Speck, O., Hennig, J., Büchert, M., 2010. Single-voxel MRS with prospective motion correction and retrospective frequency correction. *NMR Biomed.* 23, 325–332. doi:10.1002/nbm.1469
- Zhang, Y., Brady, M., Smith, S., 2001. Segmentation of brain MR images through a hidden Markov random field model and the expectation-maximization algorithm. *IEEE Trans. Med. Imaging* 20, 45–57. doi:10.1109/42.906424
- Zhu, H., Edden, R.A.E., Ouwerkerk, R., Barker, P.B., 2011. High resolution spectroscopic imaging of GABA at 3 Tesla. *Magn. Reson. Med.* 65, 603–609. doi:10.1002/mrm.22671
- Zhu, X.H., Kim, S.G., Andersen, P., Ogawa, S., Uğurbil, K., Chen, W., 1998. Simultaneous oxygenation and perfusion imaging study of functional activity in primary visual cortex at different visual stimulation frequency: Quantitative correlation between BOLD and CBF changes. *Magn. Reson. Med.* 40, 703–711. doi:10.1002/mrm.1910400510

## Appendix A: Supplementary Material

**Table A.1** Individual theoretical tissue-corrected [GABA] ( $C_{G,corr}$ ) for each participant with corresponding means ( $\pm$  SD) and coefficients of variation.

	G_1	G_2	G_3	G_4	G_5			
S01	0.74	0.73	0.74	0.73	0.70			
S02	0.70	0.70	0.70	0.70	0.70			
S03	0.70	0.69	0.71	0.71	0.71			
S04	0.71	0.70	0.70	0.70	0.70			
S05	0.70	0.70	0.70	0.70	0.70			
S06	0.69	0.69	0.70	0.70	0.70			
S07	0.69	0.69	0.71	0.69	0.68			
S08	0.70	0.69	0.70	0.70	0.70			
S09	0.70	0.70	0.70	0.69	0.70			
S10	0.70	0.70	0.70	0.70	0.70			
G_6	G_7	G_8	G_9	G_10	Mean	SD	CV	
0.72	0.72	0.73	0.75	0.74	0.73	0.011	1.57%	
0.70	0.72	0.71	0.72	0.72	0.71	0.007	1.05%	
0.71	0.71	0.71	0.71	0.71	0.71	0.005	0.74%	
0.71	0.71	0.70	0.70	0.70	0.70	0.004	0.51%	
0.71	0.70	0.70	0.71	0.71	0.70	0.006	0.79%	
0.70	0.70	0.70	0.70	0.72	0.70	0.008	1.09%	
0.70	0.69	0.71	0.70	0.71	0.70	0.012	1.65%	
0.70	0.69	0.70	0.70	0.70	0.70	0.004	0.62%	
0.71	0.72	0.70	0.70	0.71	0.70	0.008	1.11%	
0.70	0.71	0.71	0.71	0.71	0.70	0.003	0.46%	

**Table A.2** Tuning parameters from the power law contrast response function fit to BOLD and CBF response data for each participant. Rate of response saturation is represented by  $\gamma$  and the modelled response at 100% contrast is represented by  $R_{\max}$ .

Participant	BOLD		CBF	
	$\gamma$	$R_{\max}$	$\gamma$	$R_{\max}$
S01	0.26	1.68	0.19	31.29
S02	0.67	3.05	0.55	38.41
S04	0.45	2.40	0.52	41.34
S05	0.43	1.84	0.31	32.11
S06	0.48	1.91	0.50	37.01
S07	0.52	2.65	0.44	37.34
S08	0.40	2.29	0.45	36.15
S09	0.46	1.96	0.55	37.24
S10	0.38	2.31	0.36	35.95
S11	0.31	2.50	0.22	32.33
S12	0.47	2.57	0.15	20.94
S13	0.61	2.04	0.39	36.45
S14	0.49	2.38	0.24	30.87
S15	0.60	2.75	0.62	33.84
S16	0.46	2.41	0.44	31.94
S17	0.44	3.08	0.47	35.62
S18	0.35	2.62	0.34	30.10
S19	0.22	2.27	0.09	30.63
S20	0.25	2.47	0.25	37.78
S21	0.42	2.12	0.55	44.96
S22	0.40	1.89	0.72	27.19
S23	0.46	2.18	0.40	34.90
S24	0.48	1.56	0.32	26.29
S25 <sup>a</sup>	1.11	2.35	2.13	32.96
S26	0.38	2.29	0.34	32.15
S27	0.29	1.95	0.22	39.54
S28	0.37	1.61	0.34	31.03
S29	0.54	2.20	0.37	34.87
S30	0.37	1.35	0.22	29.47

S31	0.40	1.65	0.35	30.75
S32	0.31	1.90	0.28	31.82
Mean $\pm$ SD	$0.44 \pm 0.16$	$2.20 \pm 0.42$	$0.43 \pm 0.35$	$33.65 \pm 4.70$

<sup>a</sup> This participant's  $\gamma$  values were treated as outliers and excluded from the main analysis.

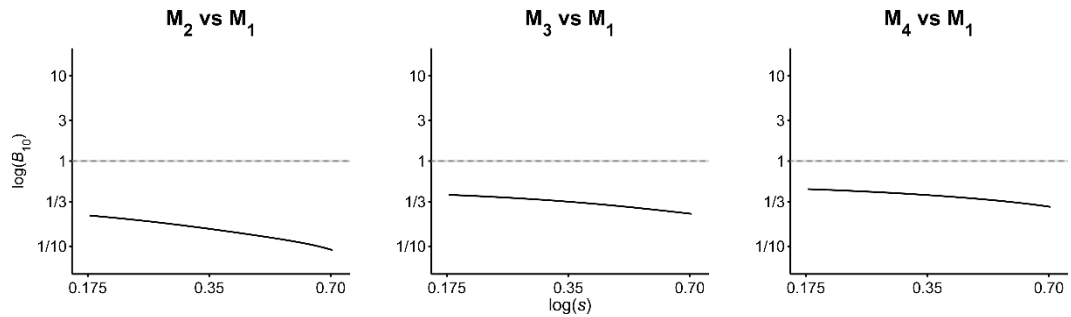


**Figure A.1** Robustness plots displaying calculated Bayes factors ( $B_{10}$ ) for each regression model compared against model  $M_1$  as function of scale factor ( $s$ ) for the distribution of the Cauchy prior. (Refer to Table 6.3 for model details). The default scale factor used in the analysis was set to  $\sqrt{2}/4$  (i.e.,  $\sim 0.35$ ). Axes are scaled logarithmically.





$I_x, I_y, S_x, S_y$	In-phase x and y coherence of spins I and S (transverse magnetisation)
$2I_xS_z, 2I_yS_z$	Anti-phase x and y coherence of spin I with respect to spin S
$2I_xS_x, 2I_xS_y, 2I_yS_x, 2I_yS_y$	Two-spin coherence of spins I and S
$2I_zS_z$	Longitudinal two-spin order of spins I and S

The basis set also includes the unity operator 1.

Product operator formalism can be used to describe the  $J$ -evolution of coupled systems. For instance, an IS spin system is characterised by two forms of coherence: in-phase and anti-phase coherence. For the in-phase coherences ( $I_x$ ) the resonances of a doublet are in the same phase (e.g., along the x axis), while for the anti-phase coherences ( $2I_yS_z$ ) the same resonances are along opposite axes and 90° out of phase with the in-phase coherences. Using the product operators listed above, the evolution of the in-phase  $I_x$  coherences can be numerically represented as

$$I_x \rightarrow [I_x \cos(\pi J\tau) + 2I_yS_z \sin(\pi J\tau)]e^{-\tau/T_2} \quad [\text{B.1}]$$

where  $J$  is the scalar coupling constant  $J_{IS}$ ,  $\tau$  is the echo time of the NMR experiment and  $T_2$  is the transverse relaxation time of the nuclear spins. Similarly, the anti-phase coherences  $2I_yS_z$  are described by

$$2I_yS_z \rightarrow [2I_yS_z \cos(\pi J\tau) + I_x \sin(\pi J\tau)]e^{-\tau/T_2} \quad [\text{B.2}]$$

For the purpose of visualisation, both coherences can be plotted as a function of signal across time (Figure B.1a).

The above equations can be taken further to simulate more complex spin systems. For an  $IS_2$  or  $I_2S_2$  spin system (e.g., the GABA H4–H3 system), the evolution of the  $I_x$  coherences is described by

$$I_x \rightarrow [I_x \cos(\pi J\tau)^2 + 2I_y(S_{1z} + S_{2z}) \sin(\pi J\tau) \cos(\pi J\tau) - 4I_xS_{1z}S_{2z} \sin(\pi J\tau)^2] \times e^{-\tau/T_2} \quad [\text{B.3}]$$

the evolution of the  $2I_y(S_{1z} + S_{2z})$  coherences by

$$2I_y(S_{1z} + S_{2z}) \rightarrow [2I_y(S_{1z} + S_{2z}) \cos(\pi J\tau)^2 + I_x \sin(\pi J\tau) \cos(\pi J\tau) - 4I_xS_{1z}S_{2z} \sin(\pi J\tau)^2]e^{-\tau/T_2} \quad [\text{B.4}]$$

and the evolution of the  $4I_xS_{1z}S_{2z}$  coherences by

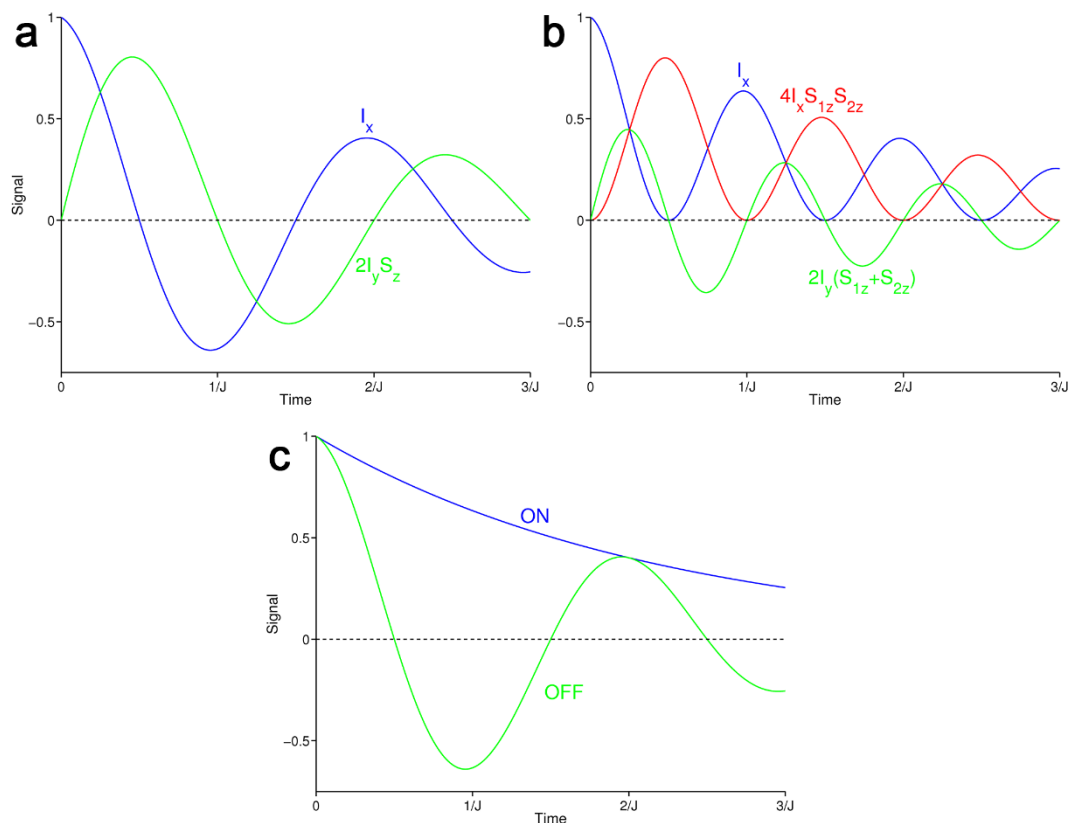


**Figure B.1** **a:** Graphical representation of the scalar evolution of an IS spin system in a theoretical spin echo NMR experiment. The in-phase coherence  $I_x$  (blue) and anti-phase coherence  $2I_y S_z$  (green) display a complex evolution as a result of  $J$ -coupling. **b:** The evolution of coherences for an  $IS_2$  spin system showing the in-phase coherence  $I_x$  (blue) and the anti-phase coherences  $2I_y(S_{1z} + S_{2z})$  (green) and  $4I_x S_{1z} S_{2z}$  (red). **c:** The evolution of the  $I_y$  coherence of an IS spin system in a spectral editing experiment. The selective inversion of S spins (ON, blue) leads to in-phase refocusing of the I spin and thus a monoexponential evolution. In the experiment where the editing pulses do not invert the S spin, the  $I_y$  coherence evolves as normal (OFF, green). For all experiments, the assumed  $J$ -coupling constant was 7.3 Hz and the assumed  $T_2$  relaxation time was 300 ms.

$$4I_x S_{1z} S_{2z} \rightarrow [4I_x S_{1z} S_{2z} \cos(\pi J \tau)^2 + 2I_y (S_{1z} + S_{2z}) \sin(\pi J \tau) \cos(\pi J \tau) + I_x \sin(\pi J \tau)^2] e^{-\tau/T_2} \quad [\text{B.5}]$$

The graphical representation of these evolutions is given in Figure B.1b.

Given these equations, product operator formalism can be employed to adequately describe a  $J$ -difference-edited experiment. Spectral editing is defined as any NMR technique that exploits the spin–spin couplings of a spin system in order to distinguish it from all other uncoupled resonances. In a straightforward  $J$ -editing spin echo experiment, two  $180^\circ$  frequency-selective editing pulses are placed symmetrical about a  $180^\circ$  broadband slice-selective pulse (positioned in time at  $TE/2$ ). The editing pulses selectively invert the S spins such that the rotation of the I spins are reversed in the spin echo (ON scan). The result is that the I-spin

coherences are completely in phase after delays that are multiples of  $TE/2$ . In a second acquisition the refocusing pulses do not invert the S spins and thus the I spins evolve as normal (OFF scan). As before, the evolution of the coherences in these two experiments can be represented in a simple manner by product operators for the ON scan by

$$I_y \rightarrow I_y e^{-\tau/T_2} \quad [\text{B.6}]$$

and for the OFF scan by

$$I_y \rightarrow I_y \cos(\pi J\tau) e^{-\tau/T_2} \quad [\text{B.7}]$$

These transformations can then be graphically illustrated as time-by-signal functions (Figure B.1c). Subtraction of the two scans will lead to removal of all uncoupled resonances, allowing for optimal detection of resonances that overlap with other, larger signals.

It should now be apparent that product operator formalism is a powerful and flexible mathematical tool that can be utilised to numerically simulate the  $J$ -difference-edited experiment of GABA when combined with prior knowledge of  $J$ -coupling constants and chemical shifts, and inclusion of appropriate acquisition sequence parameters. (Although not discussed here, product operators can also accurately describe transformations induced by chemical shifts and external RF fields since these properties of NMR modulate the quantum states of nuclear spins.)

## Appendix C: Published Work

This publication is copyrighted. It can be found at its original source:

DOI: [10.1002/mrm.25699](https://doi.org/10.1002/mrm.25699)

This publication is copyrighted. It can be found at its original source:

DOI: [10.1002/mrm.25699](https://doi.org/10.1002/mrm.25699)

This publication is copyrighted. It can be found at its original source:

DOI: [10.1002/mrm.25699](https://doi.org/10.1002/mrm.25699)

This publication is copyrighted. It can be found at its original source:

DOI: [10.1002/mrm.25699](https://doi.org/10.1002/mrm.25699)

This publication is copyrighted. It can be found at its original source:

DOI: [10.1002/mrm.25699](https://doi.org/10.1002/mrm.25699)

This publication is copyrighted. It can be found at its original source:

DOI: [10.1002/mrm.25699](https://doi.org/10.1002/mrm.25699)

This publication is copyrighted. It can be found at its original source:

DOI: [10.1002/mrm.25699](https://doi.org/10.1002/mrm.25699)

This publication is copyrighted. It can be found at its original source:

DOI: [10.1002/mrm.25699](https://doi.org/10.1002/mrm.25699)